VANILLIN HYDRODEOXYGENATION REACTION KINETICS OVER SUPPORTED MONOMETALLIC AND BIMETALLIC Pd-BASED CATALYSTS IN DIFFERENT SOLVENTS AND BINARY ENVIRONMENTS.

BY

ELIAS ALIU

A Thesis Submitted on February 2020 to School of Chemical Engineering, University of Birmingham, UK in Partial Fulfilment of the Requirements for the Degree of Doctor of Philosophy.

Abstract

In this thesis, the kinetics of hydrodeoxygenation (HDO) reaction over commercial monometallic and synthesised bimetallic Pd-based catalysts was investigated using vanillin as the representative model of oxygenates present in bio-oils. Prior to the kinetic studies, preliminary experiments were carried out to investigate non-catalytic effect, solvent effect, role of catalytic supports and active elements in HDO reaction of vanillin. It was found that non-catalytic effect contributed less than 1% in conversion, while contribution from catalytic supports was no more than 4% in conversion. In contrast, the amount of vanillin converted varies remarkably from 99% under Pd-based catalysts to 21% under Rh-based catalyst. Likewise, the amount of vanillin converted changes significantly from 100% under 2-propanol to 70% with toluene as the reaction solvent. Consequently, it was concluded that the reaction is severely affected by the choice of solvent and catalytic active element. In addition, from the preliminary studies completed it was found that the selectivity toward the deoxygenated product creosol varies significantly with the processing condition. Within the range of processing conditions investigated, the combination of processing parameters that maximises selectivity toward creosol and conversion include 338 K temperature, 3.0 MPa hydrogen gas partial pressure, 0.5 kg/m^3 catalyst loading, and 500 rpm agitation speed. From vanillin HDO reactions over Pd/C, Pd/Al$_2$O$_3$, and PdRh/Al$_2$O$_3$ catalyst using ethylacetate as the solvent, it was found that nonfirst-order kinetics reliably describes the initial reaction rate dependence on starting vanillin concentration and hydrogen gas partial pressure. More importantly, a derived Langmuir – Hinshelwood – Hougen – Watson (LHHW) expression was

successfully used to reliably model the kinetics of the reaction over the various catalysts. Interestingly, at 95% confidence level the estimated intrinsic activation energy for the reaction varies from 24.10 kJ/mol under PdRh/Al$_2$O$_3$ to 64.08 kJ/mol under Pd/Al$_2$O$_3$ catalyst. Additional experiments performed using 2-propanol, tetrahydrofuran, and toluene as the reaction solvent with bimetallic PdRh/Al$_2$O$_3$ particles as the catalyst reaffirms the nonfirst-order dependence of the initial reaction rate on starting vanillin concentration and hydrogen gas partial pressure. Nonetheless, at 95% confidence level the estimated intrinsic activation energy for the reaction varies from 23.60 kJ/mol in 2-propanol to 56.30 kJ/mol in toluene. The observed variation in the intrinsic activation energies for the reaction thus possibly explains the changes in performance (i.e. conversion and selectivity toward creosol) under different catalysts and solvents. In order to examine the impact of other prominent compounds present in bio-oil, vanillin HDO reaction was conducted in binary environments using the prepared bimetallic PdRh/Al$_2$O$_3$ particles as the catalyst and ethylacetate as the solvent. The secondary components in the binary environments were acetic acid and guaiacol. In both vanillin – acetic acid and vanillin – guaiacol environments, nonfirst-order kinetics still best describes the initial reaction rate dependence on starting vanillin concentration and hydrogen gas partial pressure. However, the order of reaction with respect to hydrogen gas partial pressure changes from 0.4 in vanillin-only environment to 0.6 in the binary environments. Notably, the presence of guaiacol or acetic acid in the starting mixture caused significant change in intrinsic activation energy of the reaction. At 95% confidence level, the estimated intrinsic activation energy of the reaction changes from 24.10 kJ/mol in vanillin-only environment to 51.00 kJ/mol in vanillin – acetic acid and 34.10 kJ/mol in vanillin – guaiacol environment. Hence, the studies completed in this thesis suggest the energy barrier to vanillin HDO reaction is strongly affected by the presence of other bio-oil model compounds, solvent and catalyst type.

Dedication

The author would like to dedicate the present work to Abiodun Nasiru Aliu (Father), Abosede Ayodele Aliu (Mother), Osikueme Dolapo Akinfenwa (Sister), Adams Adedapo Aliu (Brother), and Adekunbi Idayat Adepoju (Spouse).

Acknowledgement

List of Publications & Conference Contributions

This thesis is based on the following submitted manuscript and publications:

I. Aliu, E., Hart, A., Wood, J., (2019). Kinetics of Vanillin Hydrodeoxygenation Reaction in an Organic Solvent Using a Pd/C catalyst, *Ind Eng Chem Res*., 58, 15162–15172.

II. Aliu, E., Hart, A., Wood, J., (2019). Reaction Kinetics of Vanillin Hydrodeoxygenation in Acidic and Nonacidic Environments Using Bimetallic $PdRh/Al_2O_3$ Catalyst, *Energy Fuels*., 33, 11712–11723.

III. Aliu, E., Hart, A., Wood, J., (2020). Mild-Temperature Hydrodeoxygenation of Vanillin a Typical Bio-Oil Model Compound to Creosol, Accepted for Publication in *Catal. Today*.

Oral Conference Contributions

Aliu, E., Hart, A., Wood, J., (2019). Catalytic Conversion of Vanillin a Bio-Oil Model Compound to Creosol a Potential Future Fuel, Presented at the Fifth International Conference Catalysis for Renewable Sources: Fuel, Energy, and Chemicals, Crete, Greece.

Poster Conference Contributions

Aliu, E., Hart, A., Wood, J., (2018). Hydrodeoxygenation of Vanillin as a Model Bio-Oil Compound and Kinetic Studies, Presented at ChemEngDayUK: Molecules to Manufacturing, Leeds, England.

Aliu, E., Hart, A., Wood, J., (2017). Kinetic Studies on Bio-Oil and Related Model Compounds HDO Reaction, Presented at Catalysis and Reaction Engineering Symposium, Sheffield, England.

Table of Contents

List of Figures

List of Tables

Nomenclature

Abbreviation	Meaning
FGBs	First generation biofuels
SGBs	Second generation biofuels
TGBs	Third generation biofuels
FGBs	Fourth generation biofuels
HV	Heating Value
HDO	Hydrodeoxygenation
HDN	Hydrodenitration
HDS	Hydrodesulphurisation
Y_{oil}	Yield of oil
$Y_{waterphase}$	Yield of water phase
Y_{gas}	Yield of gas
Y_{carbon}	Yield of carbon
DDO	Direct deoxygenation
HYD	Hydrogenation
DOD	Degree of deoxygenation
w_{oxy}	Ratio of oxygen mass in product to the mass in bio-oil
μ_{50}	Measured viscosity at fixed temperature of 50 °C
ρ	Density
α	Hydrogen bond donor capability
β	Hydrogen bond acceptor capability
ε	Dielectric constant
μ	Dipole moment
ppm	ppm
S/N	Signal to Noise Ratio
X_{VL}	Conversion of vanillin
S_{VA}	Selectivity toward vanillyl alcohol
S_{CR}	Selectivity toward creosol
Y	Yield
VL	Vanillin
VA	Vanillyl Alcohol
CR	Creosol
GUA	Guaiacol
AA	Acetic Acid

Abbreviation	Meaning
ACET	Acetaldehyde
C_{VL0}	Starting concentration of vanillin
FUR	Furfural
C_{VL}	Final concentration of vanillin
C_{VA}	Concentration of vanillyl alcohol formed
C_{CR}	Concentration of creosol formed
D_{ei}	Effective diffusivity of species i
E_A	Activation energy of the reaction
ΔH_H	Change in enthalpy of adsorption for hydrogen
ΔH_{VL}	Change in enthalpy of adsorption for vanillin
ΔH_A	Change in enthalpy of adsorption for acetic acid
ΔH_G	Change in enthalpy of adsorption for guaiacol
K_H	Adsorption equilibrium constant for hydrogen gas
K_S	Surface reaction rate constant
ΔS_H	Change in entropy of hydrogen
ΔS_{VL}	Change in entropy of vanillin
K_{S1}	Rate constant at temperature 1
K_{S2}	Rate constant at temperature 2
T1	Temperature 1
T2	Temperature 2
K_{VL}	Adsorption equilibrium constant for vanillin
K_A	Adsorption equilibrium constant for acetic acid
K_G	Adsorption equilibrium constant for guaiacol
ΔH_{ads}	Change in enthalpy due to adsorption
ΔS	Change in system entropy
K_{ads}	Adsorption equilibrium constant
R	Universal gas constant
L	Characteristic length of catalyst particle
LHHW	Langmuir – Hinshelwood – Hougen –Watson
P_H	Hydrogen gas partial pressure
r_0	Initial reaction rate
rpm	revolutions per minute
r^{EXP}	Experimental values of reaction rates
r^{MOD}	Reaction rates predicted from LHHW models
R^2	Coefficient of determination
S_i	Active site i on the catalyst surface

Abbreviation	Meaning
RSS	Residual sum of squares
T	Reaction temperature
t	Reaction time
ω	Weight of catalyst in kg per unit volume of solvent in m^3
Φ	Thiele Modulus
η	Effectiveness Factor
$\eta\Phi_i^2$	Observable modulus for species i
θ_V	Vacant site fractional coverage
θ_{VL}	Fractional coverage of vanillin
θ_A	Fractional coverage of acetic acid
θ_G	Fractional coverage of guaiacol
θ_H	Fractional coverage of hydrogen
TOF	Turnover Frequency of catalyst
P	Total hydrogen gas pressure
P_0	Saturation pressure
V_m	Monolayer capacity
S	Slope of the line
i	Intercept of the line
θ	Contact angle between mercury and the surface
γ	Surface tension of mercury
a_m	Cross-sectional area occupied by adsorbate molecule at 77 K
m_V	Volume of one mole of an ideal gas at STP
STP	Standard temperature and pressure
V	Total specific pore volume
d_{AVG}	Average pore size
D_p	Pore size
V_{gas}	Measured amount of adsorbed gas at maximum equilibrium relative pressure
V_{liq}	Volume of liquid nitrogen
V_N	Molar volume of liquid nitrogen
S_{BET}	Specific surface area of catalyst measured
n_a	Avogadro's number
$C_{VL,F}$	Concentration of vanillin in feed
C_{AA}	Concentration of acetic acid in feed
C_{FUR}	Concentration of furfural in feed
C_{ACET}	Concentration of acetaldehyde in feed

Abbreviation	Meaning
C_{GUA}	Concentration of guaiacol in feed
C_{AA0}	Starting concentration of acetic acid
C_{GUA0}	Starting concentration of guaiacol
W_S	Weight of the sample
V_b	Bulk volume of the sample
ρ_s	Apparent catalyst density
V_S	Skeletal volume of the sample
V_{tot}	Total intrusion volume
P_{PC}	Porosity of catalyst
n_{VL}	Number of moles of vanillin converted
n_H	Number of moles of hydrogen consumed
n_{CR}	Number of moles of creosol formed
S_{BET}	Specific surface area from BET analysis
BET	Brunauer – Emmett – Teller
S*	Commercial catalysts surface areas from strem manufacturer's guide
V*	Commercial catalysts pore volumes from strem manufacturer's guide
C	BET constant
PSD	Pore size distribution
SEM	Scanning Electron Microscopy
EDX	Energy Dispersive X-Ray
XRD	X-Ray Diffraction
XRF	X-Ray Fluorescence

Chapter 1

Introduction.

1.1. Background and Motivation

For many years fossil derived fuels have been the major source of energy to the world.[1] Consequently, the capacity of the limited individual reserves responsible for producing fossil fuels have been in constant decline over the past decades. Despite the decline, and the forecast of complete depletion in 2112, fossil fuels are expected to remain the leading source of energy to homes and businesses around the world for at least the next 10 years.[2] Massive consumption of fossil fuels through combustion to generate energy poses significant threats to the environment and human lives because toxic gases such as CO_2, NO_x, etc., and very harmful particulate matter such as heavy metals, arsenic, mercury, etc., generated during the process are released into the atmosphere.[3–6] As a result of the identified concerns on widespread application of fossil fuels, stringent legislation has been passed in most countries around the world to encourage production of energy and other valuable chemicals from alternative renewable and sustainable resources such as wind, solar, hydrogen fuel cell, and biomass.[7] Moreover, the expected surge in world energy demand by 20 – 30% from 2019 to 2040 due to increase in global population and rapid economic developments in countries such as China, and India escalate interest in energy production from renewable and sustainable sources.[8] Currently, plant biomass is the most abundant and promising renewable carbon source for producing liquid hydrocarbon fuels, otherwise known as biofuels.[9–12] The little amount of CO_2 gases emitted during combustion of plant biomass are offset by the

amount of CO_2 gases absorbed from the atmosphere during photosynthesis.[13,14] Biofuels can be classified into four different categories depending on the feedstock and production technologies. This include first generation biofuels (FGBs), second generation biofuels (SGBs), ,third generation biofuels (TGBs), and fourth generation biofuels.[15,16] FGBs which include bioethanol and biodiesel are generally produced via relatively simple process like fermentation and transesterification from food crops such as grains, sugars, seeds, vegetable oils, or animal fats, and starch. They have been produced in significant quantities in countries like Malaysia, US, Germany, and Brazil.[16, 17] Nonetheless, the long term viability of FGBs is questionable because they threaten the food supply chain and reduces land use efficiency. Moreover, constant production of FGBs will adversely affect the prices of food crops.[18] Based on the identified limitations, research attention drifted toward SGBs which are generally produced from non-edible residue of food crops like cereal straw, corn cobs, rice husk, e.t.c. or non-edible whole plant biomass such as grasses or trees through either biochemical or thermochemical techniques. The use of SGBs reduces the food versus fuel competition associated with FGBs, improves land use efficiency, and potentially offers significant cost reduction in the long term. Interestingly, the lignin fraction of plant biomass traditionally regarded as wastes are now widely perceived as valuable sources for manufacturing liquid biofuels better known as bio-oils because they contain approximately 40% of the possible energy of the biomass.[1, 19] The production of bio-oil from the lignin fraction of plant biomass has increasingly become an area of strong interest in renewable and sustainable energy research field. Fast pyrolysis is the preferred technology for converting the lignin fraction of plant biomass to bio-oils because it offers economic advantages over competing technology like liquefaction.[20–22] As a result of the rapid processing condition used during fast pyrolysis, bio-oils usually contain large amount of water and thermodynamically unstable oxygenated compounds such as cresols, anisoles,

syringols, carboxylic acids, ketones, and aldehydes.[23–26] Table 1.1 summarises the percentage weight of the major oxygenated compounds present in a typical bio-oil. In comparison to conventional fuels with less than 1 wt % oxygen content and water content of 0.1 wt %, bio-oils usually have oxygen content of 20 wt % to 50 wt % and water content of 30 wt % to 50 wt %.[1,27–29]

Table 1.1. Chemical Composition of Bio-oil.[30]

Compounds	Weight Percentage (%)
Carboxylic Acids	4 – 6
Carbonyl	15 – 20
Sugars	25 – 35
Water	30 – 50
Water Insoluble Lignin Derivatives	20 – 25

Table 1.2 shows the differences in properties of typical bio-oils compared to conventional fuels. The high oxygen and water content of bio-oil lead to undesirable effects such as low heating value, poor volatility, poor chemical and thermal stability, high viscosity and corrosiveness. These undesirable characteristics of bio-oils resulted in problems such as blocked filters, excessive corrosion and pump breakdown during initial attempts to substitute conventional fuels with bio-oils in operation of furnaces, gas turbines, boilers and space heaters. Hence, bio-oils must be upgraded to fulfil their potential as liquid fuels and chemical feedstocks to other processes.[31–34] Among the various methods for upgrading bio-oils, hydrodeoxygenation (HDO) is widely considered as the most suitable technique to reduce the oxygen content of bio-oils to levels close to the 1 wt % in conventional fuels because it ensures high selectivity to the desired liquid product at the expense of coke and gas formation.[35–38]

Table 1.2. Comparison between Typical Bio-oil and Conventional Fuels Properties.[39]

Property	Bio-Oil	Gasoline	Diesel	Heating Oil
Heating value (MJ/kg)	18 – 20	44	42	45.5
Density at 15°C (kg/m³)	1200	737	820 – 950	865
Flash Point (°C)	48 – 55	40	42	38
Pour Point (K)	258	213	244	267
Viscosity at 40°C [cP]	40 – 100	0.37 – 0.44	2.4	1.8 – 3.4
pH	2.0 – 3.0	–	–	–
Solids (%wt)	0.2 – 1.0	0	0	–
Elemental Analysis (%wt)				
Carbon	42 – 47	84.9	87.4	86.4
Hydrogen	6.0 – 8.0	14.76	12.1	12.7
Nitrogen	< 0.1	0.08	< 0.4	0.006
Sulfur	< 0.02	-	1.39	0.2 – 0.7
Oxygen	46 – 51			0.04
Ash	< 0.02			< 0.01

Hydrodeoxygenation is similar to conventional hydrotreating processes such as hydrodesulphurisation (HDS) and hydrodenitration (HDN) frequently employed in the petroleum industry. It involves selective removal of oxygen as water from the oxygenated compounds in bio-oil through the use of hydrogen and a heterogeneous catalyst.[40–42] However, the complexity of bio-oil composition and other possible side reactions during the HDO process such as cracking, hydrogenation, hydrocracking, decarbonylation, decarboxylation etc., compelled most laboratory scale studies to model oxygenates or their mixtures primarily to improve the design of HDO catalyst, understand the mechanisms and kinetics of HDO reaction.[7,32,43–47] Guaiacyl species such as guaiacols, cresols, and anisoles have received significant attention because they represent the primary structure of lignin. Additionally, these compounds are often preferred as model of bio-oil because they contain specific functional group of interest.[48–50] The most utilised compounds among the guaiacyl species are guaiacols since they contain methoxy ($-OCH_3$) and hydroxyl ($-OH$) groups

which are typical functional groups found in lignin derived phenolic monomers.[34–51] However, vanillin, which is a less reported member of the guaiacyl species, is the compound of interest in this research project. This compound is attractive as a model of bio-oil because it contains the carbonyl functional group which is largely responsible for thermodynamic instability of actual bio-oil.[52–56] Vanillin is an aromatic aldehyde containing two additional functional groups, namely ether and hydroxyl groups. Up to four different analytical studies confirmed vanillin as a prominent component in real bio-oil. In the work of Qi et al[14] it was reported that vanillin represents 6.35% of the main organic compounds detected in GC-MS analysis of bio-oil produced from P. indicus. On industrial scale, vanillin is produced through depolymerisation of lignin.[57] Past studies on HDO of vanillin over different catalysts reported vanillyl alcohol and creosol as the major products. In general, catalysts used in past studies on HDO of lignin model compounds include Mo-based sulfides, base metals, noble metals, metal phosphides, carbides, supported noble metals, and bifunctional catalysts.[26,58–61] Interestingly, noble metals which comprises ruthenium (Ru), palladium (Pd), platinum (Pt), and rhodium (Rh) appear to be the most promising group of metal catalyst for lignin model compound and actual bio-oil HDO reaction because they are active at mild temperatures.[62–64] Nonetheless, large scale application of noble metals in HDO processes is not economically feasible without improvement in catalyst design to minimise hydrogen consumption, increase robustness and selectivity toward the deoxygenated liquid products.[65] These objectives can be achieved through improved understanding on the mechanism for catalyst deactivation and the kinetics of HDO reaction.[58,66,67] According to the literature, bimetallic catalyst comprising of a noble metal and another metal often demonstrates better resistance against poisoning agents and higher selectivity toward the deoxygenated liquid products compared to supported mono-metal catalysts.[68] Notably, the majority of past studies on reaction kinetics of

vanillin HDO utilised Ru-based catalyst. For instance, Bindwal et al[69] used Ru/C catalyst to investigate the reaction kinetics of mild aqueous-phase hydrogenation of vanillin. While in the work of Mahfud et al., [70] Huang et al., [71] and Bussetto et al.[72] homogeneous Ru-based catalysts were used to investigate the kinetics of vanillin hydrodeoxygenation reaction. Although, Pd-based catalysts are widely recommended for catalytic upgrading of bio-oil and model compounds, information on reaction kinetics of vanillin hydrodeoxygenation over supported Pd-based catalysts are limited.[73] In fact, information on the kinetics of vanillin hydrodeoxygenation reaction over non Ru-based supported noble metal catalysts was missing in the literature until recent publications by Santos et al.,[74] Sulman et al.,[75] and Hao et al.[76] Sulman and co-workers [75] investigated vanillin hydrodeoxygenation reaction in different solvents; their results suggested the rate of vanillin hydrodeoxygenation reaction increases as the polarity of the solvent increases. In a similar study by Nie and co-workers [64], it was reported that vanillin conversion varies with the solvent type because hydrophobic and hydrophilic properties affects the dispersion of catalysts in various solvents. Remarkably, past studies on the effect of solvent on vanillin hydrodeoxygenation focused only on changes in the rate of reaction. Hence, one of the objectives in the present work is to determine the variation in intrinsic kinetic parameters such as intrinsic activation energy, enthalpy of adsorption for the reactants, and rate constants following changes in the solvent for vanillin hydrodeoxygenation reaction.

1.2. Knowledge Gaps

On the basis of literature survey on vanillin hydrodeoxygenation reaction, the gaps in knowledge identified include:

➢ Insufficient information on kinetics of the reaction over Pd-based catalysts.

➢ Lack of information on kinetics of the reaction over bimetallic catalysts.

- Lack of information on changes in intrinsic kinetic parameters following changes in the reaction solvent.

- Lack of information on model describing the reaction kinetics of vanillin hydrodeoxygenation in the presence of other compounds such as acetic acid or guaiacol.

1.3. **Hypotheses**

Based on the identified gaps in knowledge on vanillin hydrodeoxygenation reaction, hypotheses of this research work are as follows:

- Intrinsic kinetic parameters for the reaction over Pd-based catalysts will be different from those reported for Ru-based catalysts because different reaction rates were reported in the literature on HDO of vanillin over Pd-based catalyst and Ru-based catalyst.

- Energy barrier for the reaction in the presence of bimetallic catalyst will be lower compared to mono-metal catalysts counterparts since bimetallic catalysts are known to have superior activity and selectivity toward deoxygenated products.

- Changes in solvent will alter the reactants adsorption enthalpy and activation energy for the reaction due to expected differences in the interaction of the catalyst, substrate, and products under the various solvents.

- In the presence of other model compounds, the competition for adsorption onto active sites on the catalyst will most likely be higher. As a result, it is assumed that the energy barrier for the reaction in binary and pure environments will be different, with the former higher than the latter.

1.4. Aim and Objectives

The overall aim of this research work is to determine changes in product selectivity and kinetics of vanillin hydrodeoxygenation reaction following changes in catalyst, and the reaction environment. To fulfil this aim, specific objectives that must be accomplished include:

1) To establish the best condition for the reaction and the influence of processing parameters by;

    a) Using Taguchi method to design a suitable orthogonal array of experiments.

    b) Isolating the effect of each processing parameter on conversion and selectivity toward the desired deoxygenated product.

    c) Determining the configuration of processing parameters that optimises conversion and selectivity toward the deoxygenated product.

2) To design and prepare a suitable bimetallic Pd-based catalyst for vanillin hydrodeoxygenation reaction by;

    a) Investigating performance under different commercial noble metal catalysts using criteria such as hydrogen consumption, conversion, and product selectivity.

    b) Investigating the influence of commercial catalyst supports such as alumina (Al_2O_3), silica (SiO_2), and carbon (C) on the reaction.

3) To establish changes in kinetics of the reaction over monometallic and bimetallic Pd-based catalysts by;

    a) Investigating the effect of changes in hydrogen gas partial pressure, temperature, and starting concentration of vanillin on the rate of reaction in the presence of monometallic and bimetallic Pd-based catalysts.

b) Developing models to describe the reaction kinetics of vanillin hydrodeoxygenation under the different catalysts.

4) To establish changes in kinetics of the reaction under different solvents by;

a) Investigating the effect of changes in solvent on conversion, selectivity toward the deoxygenated product, and hydrogen consumption.

b) Investigating the effect of changes in starting concentration of vanillin, temperature, and hydrogen gas partial pressure on the rate of reaction in different solvents.

c) Developing models to describe the kinetics of vanillin hydrodeoxygenation reaction under the various solvents.

5) To establish the effect of other model compounds presence on the kinetics of vanillin hydrodeoxygenation reaction by;

a) Investigating the effect of changes in temperature, starting vanillin concentration, and hydrogen gas partial pressure on the rate of reaction in vanillin – acetic acid and vanillin – guaiacol environments.

b) Developing models to describe kinetics of vanillin hydrodeoxygenation reaction in vanillin – acetic acid and vanillin – guaiacol environments.

1.5. Thesis Outline

This thesis contain seven chapters in total. The first chapter provides the background to the research work through discussion on the need for bio-oil upgrading via hydrodeoxygenation, the role of model compound studies in designing efficient HDO catalyst and understanding kinetics of hydrodeoxygenation reaction. In addition, this chapter present the gaps in knowledge, the research hypotheses, specific aim and objectives of the research project. The second chapter reviews the present state of bio-oil and model compounds upgrading through hydrodeoxygenation. In the third chapter, details on the analytical tools, experimental set-up and procedures used in the research are presented. The results of standalone model compound hydrodeoxygenation experiments to investigate the effect of catalyst, support, heat, solvent and operating condition on conversion, hydrogen consumption, and product selectivity are presented in Chapter 4. While Chapter 5 details the kinetics of the model compound hydrodeoxygenation over monometallic and bimetallic Pd-based catalysts. Chapter 6 present the kinetics of the model compound hydrodeoxygenation reaction in different solvents and binary environments to illustrate the impact of solvent and other compounds on kinetics of the reaction. The last chapter of the thesis summarises the conclusions from the various studies conducted and recommends possible areas for future research work.

Chapter 2

Literature Review

2.1. Introduction

Fossil-based resources such as coal, oil and natural gas have been the dominant route of energy to homes and businesses around the world for several years. Figure 2.1 illustrate changes in the global energy consumption between 2007 and 2017.[77] It indicates approximately 2% per annum increase in the global energy consumption.[2] Plausible reasons for the observed increase in global energy consumption includes rapid development in improving economies like China and India and growth in world population.[78] Infact, it has been predicted that in the next 25 yrs the world population will increase by 30%.   Figure 2.2 shows the energy consumption by source for the last 20 yrs and forecast for the next 20 yrs. It clearly shows that in the last 20 yrs fossil derived fuels have been the major source of energy to the world and likely to remain the dominant source of energy to the world over the next 20 yrs.[79] However, proven reserves responsible for producing these fuels are concentrated in few countries. Moreover, these reserves are expected to fluctuate with price and other economic conditions. The identified uncertainties around proven reserves combined with the expected growth in energy consumption puts security of the global energy supply in jeopardy.[80] In addition, campaigns against the use of fossil resources has grown over the last decade mainly because burning of these resources to generate energy adversely affects the environment.[5,6] The drive to become less reliant on fossil resources and increase security on energy

supply compelled many countries around the world, in particular members of the European Union (EU) to set specific renewable energy targets.
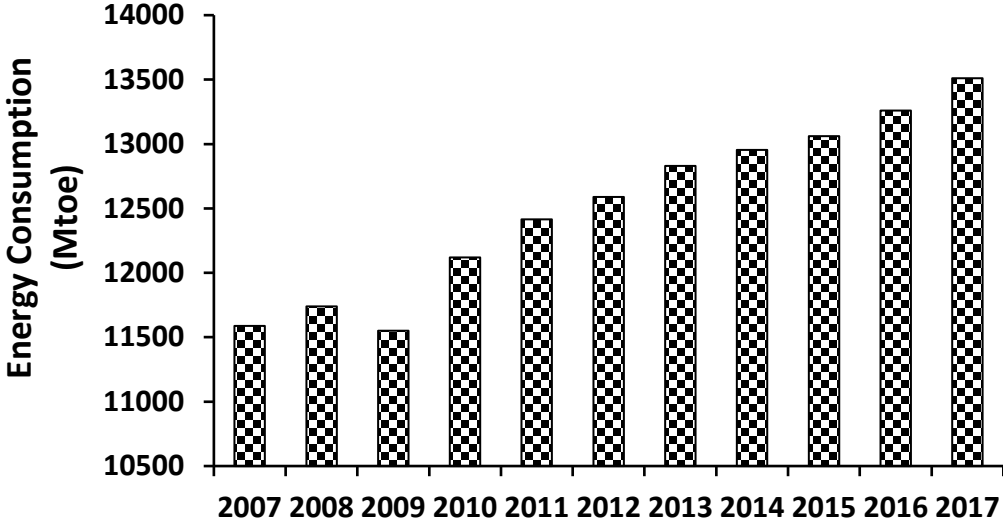
Fig. 2.1. Annual world energy supply between 2007 and 2017.[77]
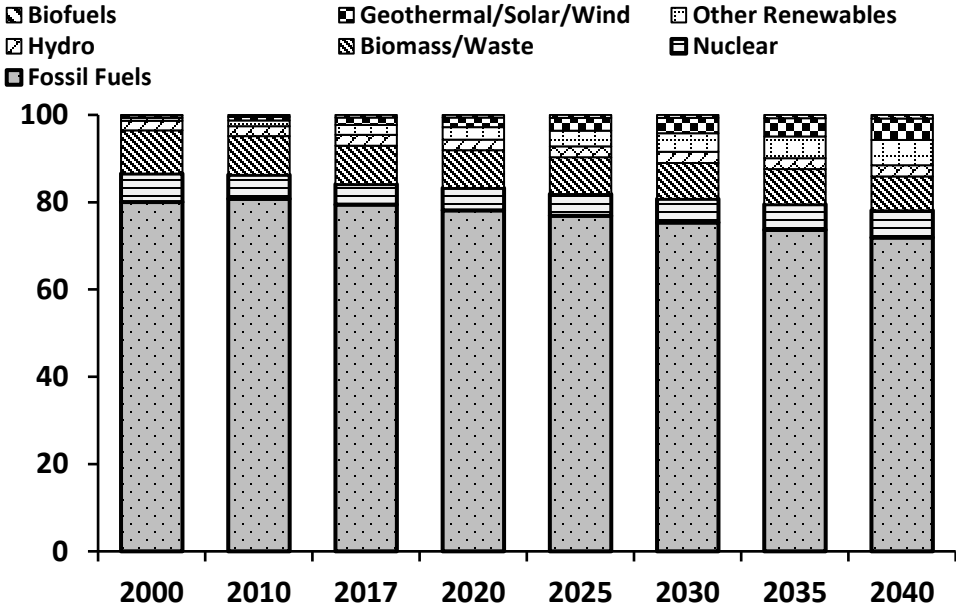
Fig. 2.2. Shares of Global Primary Energy Consumption by Fuel.[78]

EU members are committed to national renewable targets ranging from a low target of 10% in Malta to a high target of 49% in Sweden and at least 10% of transport fuels from renewable sources by 2020.[81] Despite the United Kingdom (UK) plans to exit the EU, UK government remain keen on increasing renewable consumption from 1.5% in 2005 to 15% by 2020.[82] The sustained interest in renewable energy consumption by the UK government is affiliated to the increase security of energy supplies and opportunities for investment. To achieve this national renewable target of 15%, it has been estimated that around 30% of electricity demand, 12% of heating demand and 10% of transport demand must come from renewable sources.[82] Significant progress has been made in the use of renewable sources for electricity, in contrast progress in the use of renewables to provide heat and transport has been very slow. The present rate of uptake means greater effort is required from the UK to meet the 2032 binding EU renewable energy target of at least 32%.[83] This motivates the development of renewable fuels compatible with existing infrastructures for heating and transport in the UK. Renewables such as wind, solar and hydrogen fuel cells are all promising alternatives to fossil resources. Nonetheless, the wide-spread application of these renewables will require time to become economically and technically viable. Moreover, majority of the present infrastructures around the world operates on liquid hydrocarbon fuels.[84, 85] Currently, plant biomass is the only renewable and sustainable source of carbon that can be used to produce liquid fuels and valuable chemicals that can fit directly into nowadays infrastructures with little or no modification.[10–12,86] Besides, plant biomass contains tiny amounts of sulphur, nitrogen and other heavy metals compared to fossil feedstocks. Hence, fuels from plant biomass (i.e. biofuels), when burnt, produce negligible amounts of toxic gases such as SO_2 and NO_x. The net emission of CO_2 from combustion of biofuels are insignificant since the CO_2 absorbed from the atmosphere during photosynthesis balances the emitted CO_2.[13, 87–89] Based on the identified benefits, biofuel

production has received great attention over the past decade. Nonetheless, issues such as rapid catalyst deactivation, and low yields need to be resolved before biofuels can fulfil their potential as substitute for fossil derived fuels.

2.2. Biomass Feedstocks

In general, feedstocks derived from biomass can be grouped into three categories. This include starchy feedstocks, triglyceride feedstocks, and lignocellulosic feedstocks. Biofuels derived from the different feedstocks are presented in Figure 2.3. Starchy feedstocks are from food crops such as corn, beets, sugarcane etc. which are limited resources. They usually contain network of glucose polysaccharides that are linked together by α-glycosidic bonds such as amylase and amylopectin.[85] Although, α-glycosidic bonds can be hydrolysed easily into sugar monomers, the production of biofuels from starchy feedstocks received less attention because they are widely perceived as highly valuable resources for human consumption as food not as fuel nor feedstock to other processes.[90] Triglyceride feedstocks which contain fatty acids and glycerol are derived from plant and animal sources such as soyabeans, algae, vegetable oils etc.[11] Unlike starch and triglycerides which are found in limited number of plants, an integral part of plant biomass are lignocellulosic feedstocks. Lignocellulosic feedstocks are the cheapest and most available source of biomass for biofuel production.[47, 91] Examples of lignocellulosic feedstocks include switchgrass, waste from wood processing, municipal wastes, miscanthus and agricultural residues.[85]
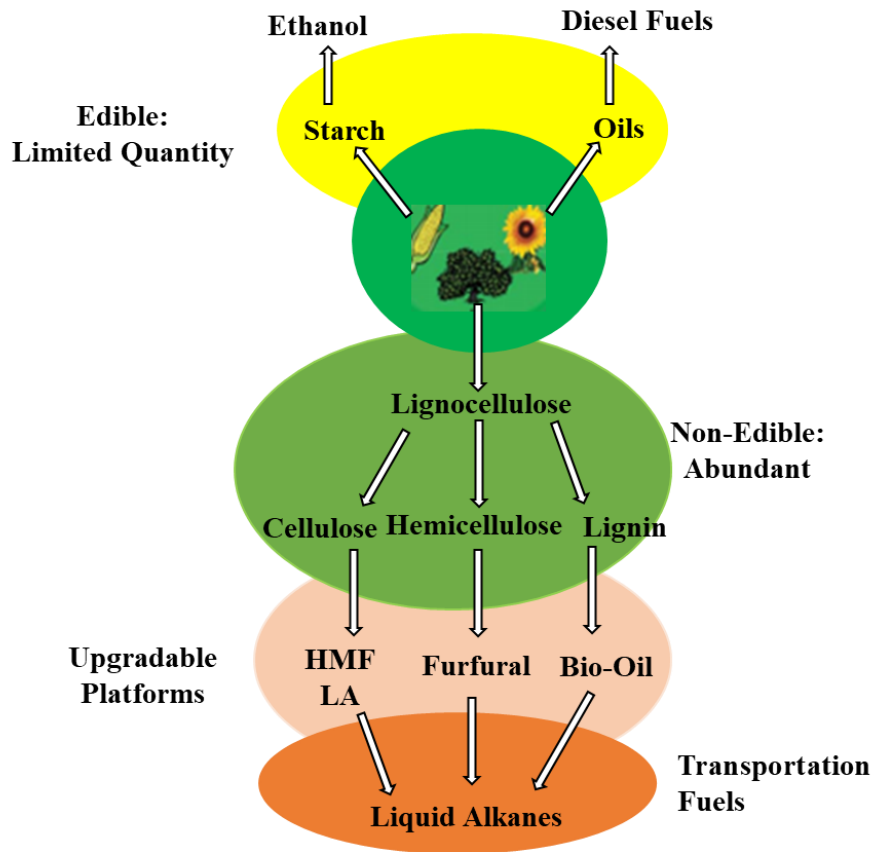
Fig. 2.3. Biofuels from Biomass Feedstocks.[85]

2.2.1. Lignocellulosic Biomass Composition

Lignocellulosic biomass is primarily made up of oxygen containing organic polymers (i.e. biopolymers), which include cellulose, hemicellulose and lignin.[92] The percentage weight of these biopolymers varies appreciably with the type of feedstock, as illustrated in Table 2.1. The secondary components found in lignocellulosic feedstocks include inorganic minerals (e.g. potassium, calcium, sodium, chlorine, phosphorus etc.) and organic extractives.[92, 93]

Table 2.1. Composition of Three Lignocellulosic Biomass feedstocks.[92]

Biomass Species	Lignocellulosic Composition (wt %)		
	Cellulose	Hemicellulose	Lignin
Poplar	50.8 – 53.3	26.2 – 28.7	15.5 – 16.3
Oak	40.4	35.9	24.1
Eucalyptus	54.1	18.4	21.5
Pine	42.0 – 50.0	24.0 – 27.0	20.0
Douglas fir	44.0	11.0	27.0
Spruce	45.5	22.9	27.9
Wheat Straw	35.0 – 39.0	23.0 – 30.0	12.0 – 16.0
Grasses	25.0 – 40.0	25.0 – 50.0	10.0 – 30.0
Switchgrass	35.0 – 40.0	25.0 – 30.0	15.0 – 20.0
Rice Straw	29.2 – 34.7	23.0 – 25.9	17.0 – 19.0
Corn Cobs	33.7 – 41.2	31.9 – 36.0	6.1–15.9

2.2.2. Cellulose

Cellulose is the main component in the cell wall of plants, and therefore the largest fraction in lignocellulosic biomass. This fraction of the lignocellulosic biomass contains 50 wt % carbon and 50 wt % oxygen.[93] Cellulose is a high molecular weight linear polymer formed from the polymerisation of 10 units to 15,000 units of β-D-anhydoglucopyranose (AGUs).[93] The repeated units found in cellulose illustrated in Figure 2.4 are called cellobiose, it contain two AGUs.[94] These units lie parallel to each other within the cellulose structure and are held together by hydrogen bonds. As a result, cellulose decomposes at ~ 573 K to levoglucosan and other anhydrocellulose.[95]
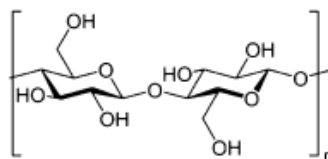
Fig. 2.4. Cellobiose unit of Cellulose.[93, 94]

2.2.3. Hemicellulose

Hemicellulose is formed from polymerisation of glucose and other sugars that are highly substituted with acetic acids e.g. xylose, mannose, galactose and arabinose.[93] As a result, the decomposition of hemicellulose at 473 K – 533 K produces acetic acid and anhydrocellulose.[20, 96] Hemicellulose contain up to 200 monomeric units of shorter and branched chain sugars.[97] Figure 2.5 illustrates the main constituents of hemicellulose. Normally, this fraction contains 50 wt % carbon and 50 wt % oxygen.[93]
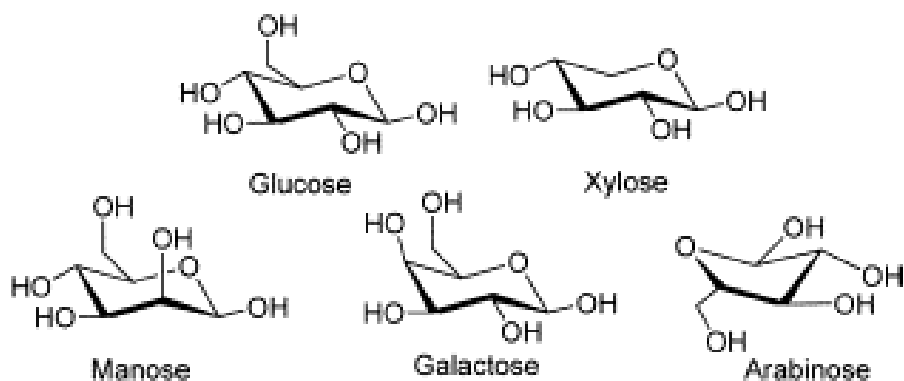
Fig. 2.5. Main components in Hemicellulose.[93]

2.2.4. Lignin

The lignin fraction plays an extremely important role in the structure of lignocellulosic biomass.[98] It fills the gap between the cellulose and hemicellulose as illustrated in Figure 2.6, thereby holds the plant cell wall structure together.[99] The structure and properties of lignin varies with the biomass feedstock. However, in general it is a highly branched, amorphous and substituted polymer of hydroxyl and methoxyl substituted phenylpropane units.[100] The representative units within the lignin structure include p-coumaryl, coniferyl, and sinapyl.[20] Lignin fraction varies

appreciably with the feedstock. Nonetheless, the proportion of lignin is generally higher in woody biomass compared to other feedstocks.[101]
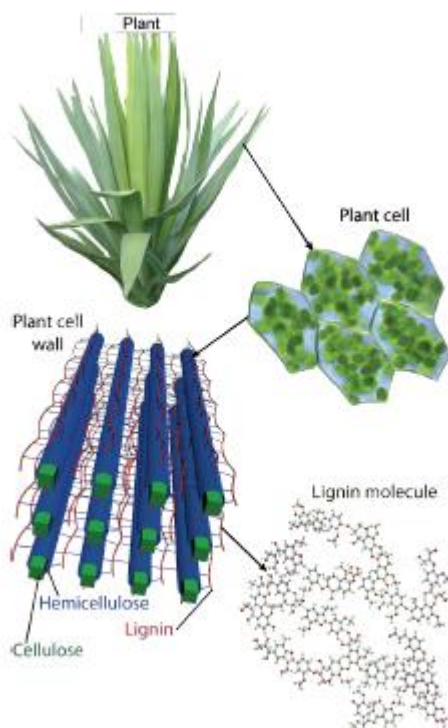
Fig. 2.6. Location and molecular structure of lignin in lignocellulosic biomass.[99]

The elemental composition of lignin fraction usually is 60 wt % carbon and 30 wt % oxygen.[93] As a result, the lignin fraction which is characterised with low O/C ratio is a more valuable source for fuel production since the other two fractions have higher O/C ratio. Moreover, breaking down the lignin fraction enables access to other components of the lignocellulosic biomass. Lignin degrades at 553 K – 773 K through cleavage of the C–C bonds and ether to form a mixture of monomeric polysubstituted phenols and oligomers.[93, 101]

2.3. Conversion of lignocellulosic Biomass to liquid fuel

The methods used to transform lignocellulosic biomass into fuels and other valuable fine chemicals are presented in Figure 2.7. They involve either a thermochemical or hydrolysis route.[85] The hydrolysis route requires separation of the lignin and sugars from the lignocellulosic biomass to permit selective processing into the desired product via either catalytic or biochemical method. As shown in Figure 2.7, the possible products from catalytic-hydrolysis route include gasoline, diesel, esters and MTHF, while the biochemical-hydrolysis route produces only ethanol. On this basis, hydrolysis routes can be used to produce liquid hydrocarbon fuels and valuable chemicals.[12] However, the thermochemical routes are generally preferred to the complex and costly hydrolysis routes.[85, 91] Besides, liquid hydrocarbon fuels are the only possible products from processing via the thermochemical routes.
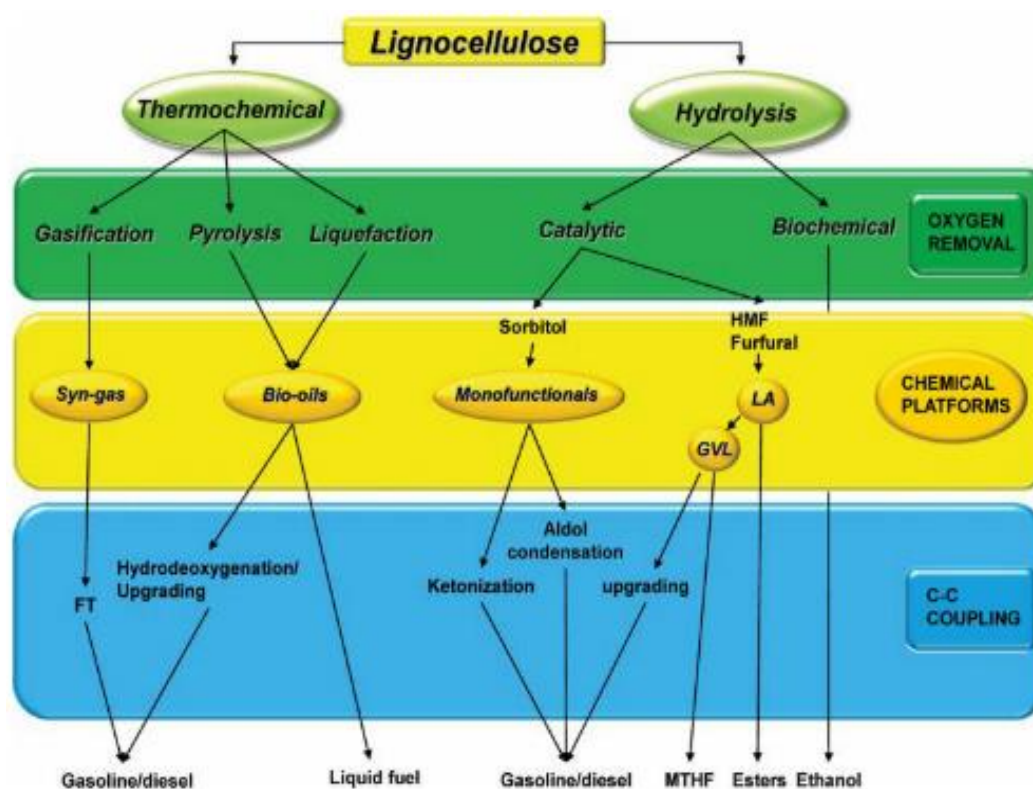
Fig. 2.7. Methods for converting lignocellulosic biomass to fuels and valuable chemicals.[85]

Thermochemical routes comprising gasification, pyrolysis and liquefaction involves processing of the whole lignocellulosic biomass under high temperatures and/or pressures. The refining of lignocellulosic biomass via gasification produces synthesis gases (i.e. mixture of CO and H_2 gases, abbreviated as syngas). As a result, further processing of the syngas via Fischer-Tropsch (FT) synthesis or hydrodeoxygenation (HDO) is required to produce liquid hydrocarbon fuels such as diesel and gasoline.[102] In contrast, pyrolysis and liquefaction directly produce liquid hydrocarbon fuel known as bio-oils. Hence, the economic disadvantage of gasification makes pyrolysis and liquefaction attractive platforms for transforming lignocellulosic biomass into liquid fuel.[85, 103,104] Liquefaction requires working pressures of 5 MPa – 20 MPa, while working pressures of 0.1 MPa – 0.5 MPa are used in pyrolysis. The huge difference in working pressures translate to significant reduction in capital cost, and thus account for the general preference of pyrolysis over liquefaction.[86] Other benefits of pyrolysis include simplicity and ability to handle different feedstocks.[21] Besides, different pyrolysis technologies are presently used commercially, while liquefaction processes are still at laboratory to pilot scale level.[20]

2.3.1. Pyrolysis Technologies

The term "pyrolysis" refers to thermal anaerobic decomposition of biomass at elevated temperatures to produce gaseous products, subsequently these products react and condense to a complex liquid mixture known as "bio-oil".[90] Table 2.2 summarises typical operating conditions for different pyrolysis technology and associated primary products. Slow pyrolysis process such as carbonization with longer residence times favours the production of solid fuel (i.e. charcoal) that can be used to generate energy through combustion. Whereas fast and flash liquid pyrolysis which

are normally operated for short duration favours bio-oil production.[87, 105,106] The stoichiometric

empirical formula for biomass conversion to bio-oil via pyrolysis is presented in equation 2.1.[90]

$$CH_{1.46}O_{0.67} \rightarrow 0.71\ CH_{1.98}O_{0.76} + 0.21CH_{0.1}O_{0.15} + 0.08CH_{0.44}O_{1.23} \qquad (2.1)$$
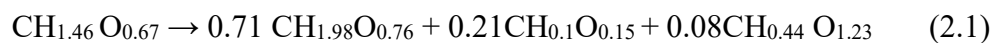
Biomass   Bio-oil   Char   Gas

Table 2.2. Operating conditions for different pyrolysis technology and the primary products.[105]

Pyrolysis Technology	Residence Time	Heating Rate	Temperature (K)	Products
Carbonization	days	very low	673	Charcoal
conventional	5 – 30 min	low	873	oil,gas,char
fast	0.5 – 5 s	very high	923	bio-oil
flash-liquid	< 1 s	high	< 923	bio-oil
flash-gas	< 1 s	high	< 923	chemicals, gas
ultra	< 0.5 s	very high	1273	chemicals, gas
vacuum	2 – 30 s	medium	673	bio-oil
hydro-pyrolysis	< 10 s	high	< 773	bio-oil
methano-pyrolysis	< 10 s	high	> 973	chemicals

Yield of bio-oil up to 80 wt % of the dry feed has been reported for fast pyrolysis, therefore it is

the preferred pyrolysis technology for bio-oil production.[80, 88] A schematic diagram of fast

pyrolysis process is presented in Figure 2.8.
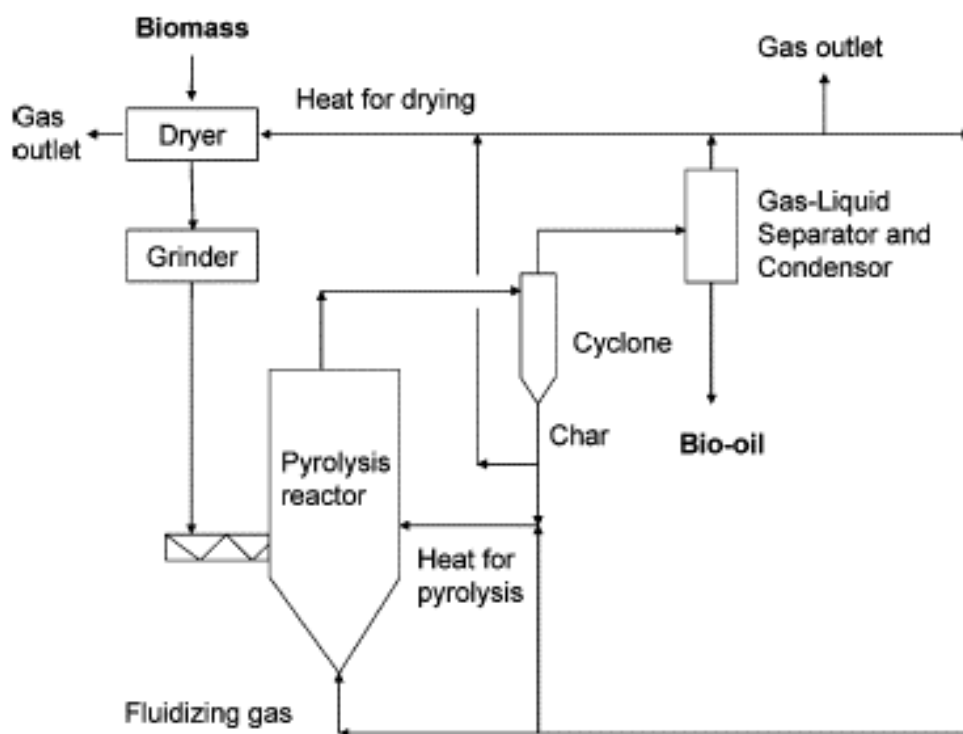
Fig. 2.8. Schematic of biomass Fast Pyrolysis Process.[9, 107]

2.4. Bio-Oil Composition

The bio-oil produced from fast pyrolysis of biomass is a complex mixture of highly oxygenated compounds with the composition dependent on initial biomass feedstock, processing conditions (i.e. temperature, residence time, heating rate etc.) and efficiency of the product removal system.[108,109] Table 2.3 illustrates variation in the composition of bio-oil produced from different biomass feedstocks.

Table 2.3. Chemical Composition of Bio-oil from different Biomass Sources.

Feedstock	Hardwood (wt %)	Softwood (wt %)	Pine (wt %)	Corn Stover (wt %)
Temperature (K)	733	783	793	773
Phenols	1.40 – 3.90	1.40 – 3.90	-	2.39
Ketones	0.08 – 0.96	0.02 – 0.73	5.36	0.20
Aldehydes	1.03 – 14.36	0.52 – 0.70	9.73	4.00
Acids	3.30 – 21.50	2.20 – 19.00	5.60	6.26
Esters	–	–	–	–
Furans	0.20 – 1.93	0.39 – 1.83	4.47	0.71
Ethers	–	–	–	–
Alcohols	6.41–7.82	1.78 – 3.17	2.90	7.12
Others	49.53 – 87.58	70.67 – 94.21	71.94	79.32
Reference	110	110	111, 112	113

The observed variation in composition of bio-oils can be attributed to the noticeable differences in relative proportion of the building blocks of lignocellulosic biomass feedstocks as highlighted in Section 2.2.1. In fact, the pyrolysis of biomass feedstock containing high lignin fraction produces bio-oil rich in phenolic compounds. While in contrast, the pyrolysis of biomass feedstock rich in cellulose or hemicellulose produces lower molecular weight oxygenated compounds.[114] Despite the expected differences in the composition of bio-oils, they generally contain significant moisture content ranging from 30 wt % to 50 wt % and high oxygen content within the interval of 20 wt % and 50 wt %.[28, 29] Due to the heterogeneity of biomass, over 400 different compounds have been found in bio-oils. Interestingly, up to 300 of these compounds contain oxygen.[32,46,115] The oxygenated compounds present in bio-oil are formed from depolymerisation, re-polymerisation, dehydration, rearrangement and fragmentation of the complex biomass building blocks.[115,116] Oligomeric species with molecular weight ranging from several hundreds to 5000 or more formed mostly from the lignin fraction of the biomass are also present in bio-oil.

Consequently, complete characterisation of the bio-oil is very challenging and almost impossible.[20] Analytical techniques that have been used to characterise bio-oil include High Pressure Liquid Chromatography (HPLC), Gel Permeation Chromatography (GPC), Gas Chromatography-Mass Spectroscopy (GC-MS), Nuclear Magnetic Resonance (NMR), Fourier Transform Infrared (FTIR) spectroscopy and HPLC with electrospray Mass spectroscopy. Among the listed techniques for characterising bio-oil, GC-MS is the most adopted method. However, the GC-MS method is only capable of detecting the volatile components of bio-oil. The volatile components accounts for 25% – 40% of the bio-oil, the non-volatile components are analysed by Fourier Transform-Ion Cyclotron Resonance (FT-ICR).[20] Table 2.3 shows the prevalent organic compounds detected in bio-oil. Broadly, these compounds can be grouped into either water soluble (aqueous) or water insoluble (organic) fractions depending on their affinity for water.[9] GC-MS analysis of bio-oils have shown that the less polar compounds such as acetic acids and hydroxyacetone are concentrated in the aqueous fraction, while the more polar compounds, less aliphatic and aromatic hydrocarbons (such as vanillin, levoglucosan, furfural, phenols and benzaldehyde) are concentrated in the organic fraction.[117]

2.4.1 Bio-Oil Properties

As mentioned previously in Section 2.4, the composition of bio-oil varies with factors such as processing conditions, feedstocks etc. However, in general they are described as a dark free flowing liquids with very pungent smell.[20,118] Bio-oils are normally produced via a rapid fast pyrolysis process that takes 1 to 2 s.[119] Consequently, bio-oils are typically a mixture of unstable oxygenated compounds that naturally strive to attain chemical equilibria by reacting with neighbouring species. These inherent reactions within the bio-oils inhibit their functionality as

fuels in existing vehicles or as platform chemicals.[120–123] For instance, the composition of bio-oil changes over time during storage. The technical term used to describe this phenomenon is "aging". Aging occurs because the unstable oxygenated compounds within the bio-oil undergo different reactions at typical storage temperature to produce stable products.[124] Model compounds of bio-oil belonging to the carboxylic group react with neighbouring alcohols to form esters, while model compounds with the carbonyl functional group react with neighbouring alcohols to form acetals or hemiacetals.[9,108] Other reactions which take place during storage of bio-oil involve homopolymerisation of olefins to form stable network of compounds. Hence, bio-oils can separate into phases during storage and their viscosity increases over time.[117] In addition to the aging property described, bio-oils usually have a pH value of 2.8 – 3.8 because they contain significant amount of carboxylic acids (e.g. formic acid and acetic acid).[125,126] The actual pH value of bio-oil varies considerably with the biomass feedstock. For example, bio-oils derived from hardwood and rice husk have pH values of 2.8 and 3.23 respectively.[127,128] However, regardless of the starting biomass feedstock, bio-oils are generally acidic. This makes it difficult to store and transport bio-oil in vessels made from conventional materials of construction. The corrosive problem of bio-oil is intensified by the presence of ash, especially at elevated temperatures.[32, 117,129,130] Since bio-oils contain significant amounts of oxygen trapped in the form of water and other oxygenates, they usually exhibit hydrophilic properties. As a result, bio-oils are immiscible with other liquid hydrocarbon fuels.[93,117] In addition, due to the high O_2 content in bio-oils, they generally have energy density that is 50% lower than that of conventional fuels.[29,117] Table 2.4 summarises the differences in elemental composition and properties of a typical bio-oil and conventional liquid fuels.

Table 2.4. Comparison between Bio-oil and Conventional Fuels Properties.[39]

Property	Bio-Oil	Gasoline	Diesel	Heating Oil
Heating value (MJ/kg)	18 – 20	44	42	45.5
Density at 15°C (kg/m^3)	1200	737	820 – 950	865
Flash Point (°C)	4855	40	42	38
Pour Point (K)	258	213	244	267
Viscosity at 40°C [cP]	40 – 100	0.37 – 0.44	2.4	1.8 – 3.4
pH	2.0 – 3.0	–	–	–
Solids (% wt)	0.2 – 1.0	0	0	–
Elemental Analysis (% wt)				
Carbon	42 – 47	84.9	87.4	86.4
Hydrogen	6.0 – 8.0	14.76	12.1	12.7
Nitrogen	< 0.1	0.08	< 0.4	0.006
Sulfur	< 0.02	–	1.39	0.2 – 0.7
Oxygen	46 – 51			0.04
Ash	< 0.02			< 0.01

2.4.2. Methods for Upgrading Bio-Oil

Due to the aforementioned undesirable properties of bio-oils, problems such as blocked filters, excessive corrosion, breakdown of pumps etc. have all been encountered during attempts to substitute conventional fuels with bio-oils in the operation of furnaces, gas turbines, boilers and space heaters.[131, 132] As highlighted in Section 2.4.1, the high O_2 content is primarily responsible for the numerous undesirable properties of bio-oil. Hence, bio-oils must be upgraded through either pre-pyrolysis or post-pyrolysis treatment to fulfil their potential as fuel or valuable chemical feedstock.[40] Pre-pyrolysis treatments such as hot gas filtering are used to eliminate the inorganic chemicals such as alkali metals found in bio-oil. Although, these treatments effectively address concerns on bio-oil stability, they cannot be used to eliminate other defects preventing the integration of bio-oil into existing petroleum refineries and end-use infrastructure.[114,133] On the other hand, post-pyrolysis treatments which include aqueous phase reforming (APR),

emulsification, hydrodeoxygenation and zeolite cracking are all promising methods that can be used to upgrade bio-oil to fuel.[134–138] APR produces syngas, which must be converted to liquid fuels through FT synthesis. Moreover, only the water-soluble fraction of the bio-oil is used in this upgrading method. Ideally the APR process should be used to supply hydrogen externally for bio-oil hydrotreating.[117] The simplest way to improve ignition characteristics of bio-oil is through emulsification. Emulsification involves the use of surfactant to create a stable microemulsion of bio-oil in diesel. However, the high energy input and cost makes emulsification less attractive. Besides, engines with emulsified diesel have demonstrated more severe corrosion/erosion when compared to those running on pure diesel.[9, 139–141] Following the identified shortcomings of APR and emulsification, catalytic upgrading routes which include hydrodeoxygenation and zeolite cracking have received greater attention over the years.[118, 125,130] Both zeolite cracking and hydrodeoxygenation have similarities with conventional processes used in the petroleum refinery. Zeolite cracking (ZC), which is analogous to Fluidised Catalytic Cracking (FCC), involves the use of zeolite catalysts such as ZSM-5 at atmospheric pressure and high temperatures (623 K – 923 K) in the absence of H_2 gas to induce C–C bond cracking, methyl transfer, isomerization, dehydration, decarboxylation and dehydration reactions.[93,115,129] These reactions lead to rejection of oxygen from the bio-oil as either carbon monoxide (CO) or carbon dioxide (CO_2), both gases are harmful to the environment.[9,40,142–148] In addition, loss of carbon during the process reduces the quality of the upgraded bio-oil and often results in significant deactivation of the catalyst.[129] Although ZC method is effective at upgrading small oxygenates within the bio-oil such as aldehydes and ketones, it struggles to deoxygenate higher phenolic compounds due to their small pore openings.[118,149–152] In addition, the high temperature used in ZC method results in severe catalyst deactivation from the high amount of coke formed through cracking reactions.[115,130] Of course, deactivation as a

result of coking could be addressed by oxidising the coke formed during ZC process in a fluidised catalytic cracking system to regenerate the catalysts. However, this introduces additional cost, which may render the produced bio-oil less competitive compared to conventional fuels.[117] Hydrodeoxygenation which is a form of hydrotreating, is the most promising post-pyrolysis treatment for upgrading bio-oil to liquid fuel.[126,153,154] As the name suggests, it involves hydrogenation and deoxygenation of different classes of compounds within the bio-oil.[118] This is because polycyclic aliphatic, aromatic structures and oxygen atoms are common features of model compounds within the bio-oil. Hence, the HDO process is used to saturate the unstable unsaturated bonds and reduce the oxygen content.[93, 155] Table 2.5 compares the quality and properties of upgraded bio-oil via HDO and ZC to crude oil. It shows that properties of upgraded bio-oil via HDO are closely aligned with crude oil properties. While in contrast, the properties of upgraded bio-oil via ZC differed remarkably from crude oil properties. Moreover, higher oil yield can be achieved from the HDO process as shown in Table 2.5. All these reasons justify the preference of HDO over ZC as post-pyrolysis treatment of bio-oil. Detailed review on bio-oil upgrading through HDO and ZC was carried out by Mortensen et al.[130] The subject of interest in this research project is upgrading of a typical bio-oil model compound via HDO.

Table 2.5. Comparison of Upgraded Bio-Oil via HDO and ZC to Crude Oil.[130]

	HDO	Zeolite Cracking	Crude Oil
Upgraded bio-oil			
Y_{oil} [wt %]	21 – 65	21 – 28	–
$Y_{waterphase}$ [wt %]	13 – 49	24 – 28	–
Y_{gas} [wt %]	3 – 15	6 – 13	
Y_{carbon} [wt %]	4 – 26	26 – 39	
Oil Characteristics			
Water [wt %]	1.5	–	0.1
pH	5.8	–	–
ρ [kg/l]	1.2	–	0.86
$\mu_{50^{\circ}c}$ [cP]	1 – 5	–	180
HHV [MJ/kg]	42 – 45	21 – 36	44
C [wt %]	85 – 89	61 – 79	83 – 86
O [wt %]	< 5	13 – 24	< 1
H [wt %]	10 – 14	2 – 8	11 – 14
S [wt %]	< 0.005	–	< 4
N [wt %]	–	–	< 1
Ash [wt %]	–	–	0.1
H/C	1.3 – 2.0	0.3 – 1.8	1.5 – 2.0
O/C	< 0.1	0.1 – 0.3	≈ 0

2.5. Hydrodeoxygenation

Hydrodeoxygenation (HDO) is a special form of hydrotreating often used to reject oxygen from bio-oil as water. The process normally takes place in the presence of a suitable catalyst under high hydrogen gas pressures. Hence, compared to ZC method, this method of bio-oil upgrading is considerably more expensive. However, it is a very promising method for upgrading bio-oils to liquid hydrocarbon fuel because it maximises selectivity toward liquid product by minimising formation of coke and other light gases.[37, 38,129,155]

$$CH_{1.4}O_{0.4} + 0.7\,H_2 \rightarrow \quad \text{-}CH_2\text{-} \quad + \quad 0.4\,H_2O \qquad\qquad (2.2) \quad \text{Hydrodeoxygenation}$$

Bio-oil   Upgraded Bio-Oil   water
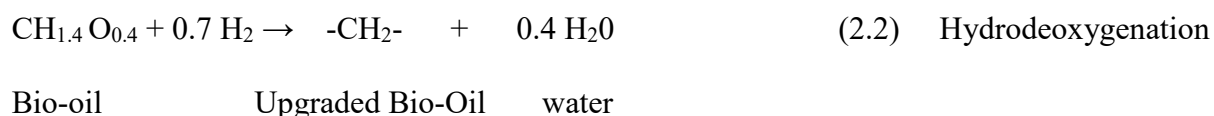
The conceptual overall reaction of the HDO process shown in equation 2.2 illustrates the role of hydrogen as the reducing agent.[80] In addition, hydrogen is used in the process to saturate different polycyclic aliphatic and aromatic hydrocarbons present in bio-oils. Since the reactivity of these compounds varies significantly, the degree of deoxygenation and saturation via HDO depends on the type of catalyst and operating conditions.[93] For instance, C=C bonds in olefins with a bond dissociation energy (BDE) of 614 kJ/mol and C=O bonds in aldehydes and ketones with BDE of 749 kJ/mol are the most reactive groups in bio-oil, these bonds undergo hydrogenation at temperatures between 423 K and 473 K. While in contrast, C–O bond present in phenols, dibenzofuran and diphenyl ether with BDE of 1076.5 kJ/mol is the least reactive group and therefore requires temperatures between 573 K and 673 K to react.[93, 117,129] In practice, different side reactions occur simultaneously during the HDO process. These side reactions, described conceptually in equations 2.3 to 2.7, must be inhibited to effectively manage H_2 consumption.[37,115,130] In particular, it is highly desirable to prevent hydrogenation of aromatic rings because this not only affects the H_2 consumption but octane number of the produced bio-oil.[93,125] Other side reactions such as decarboxylation and decarbonylation are not desirable because they lead to formation of harmful gases (i.e. CO and CO_2) as shown in equations 2.6 and 2.7.

$$R'C_4H_8R'' \rightarrow R'C_2H_3 + C_2H_3R'' \qquad\qquad (2.3) \qquad \text{Cracking}$$

$$R'C_2H_4R'' + H_2 \rightarrow R'H + CO \qquad\qquad (2.4) \qquad \text{Hydrocracking}$$

$$R'C_2H_4R'' + H_2 \rightarrow R'C_2H_4R'' + H_2O \qquad\qquad (2.5) \qquad \text{Hydrogenation}$$

$$R'COOH \rightarrow R'H + CO_2 \qquad\qquad (2.6) \qquad \text{Decarboxylation}$$

$$R'CHO \rightarrow R'H + CO \qquad\qquad (2.7) \qquad \text{Decarbonylation}$$
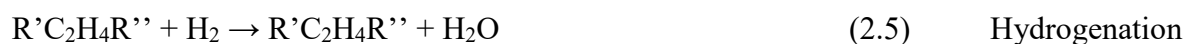
To minimise the overall H_2 consumption, side reactions and emission of harmful gases, the prerequisites for an efficient HDO process include suitable operating conditions and choice of suitable catalyst (metal and support). Table 2.6 summarises the operating conditions and catalyst used in previous works on bio-oil upgrading via HDO. It shows considerable variation in the quantity and quality of produced oil following changes in the operating conditions and catalyst. According to the investigation by Elliot and Hart[156], the yield of oil from HDO of a wood based bio-oil over Pd/C catalyst in a fixed bed reactor decreased from 75% at 583 K to 56% at 633 K. Conversely, it was found that the degree of deoxygenation increased from 65% at 583 K to 70% at 613 K. These observations from the work of Elliot et al., [156] indicate an interesting trend between the operating temperature, quantity and quality of the produced oil. It shows that higher operating temperature favours the removal of oxygen but leads to increase formation of gases due to extensive cracking reaction as opposed to HDO. As a result, bio-oil HDO normally requires minimum of two stages.[68,93] This includes a mild temperature stage (473 K – 523 K) to stabilise the oil and high temperature stage (623 K – 723 K) to deoxygenate the more difficult model compounds.[40,93,156] Moreover, cascade HDO treatment minimises reactor plugging and catalyst deactivation as a result of heavy coking.

Table 2.6. Operating Conditions and Catalysts used in previous works on Bio-Oil HDO.[129]

Catalyst	Reactor Type	Yield of Oil (wt %) Dry feed basis	Deoxyge nation (wt %) Dry feed basis	Temperature (K)	Pressure (MPa)	Time (h)
NiMoS/Al$_2$O$_3$	Batch	30	36	523	10	4
Pd/C	Batch	43	56	523	10	4
CoMoS/Al$_2$O$_3$	Batch	27	41	523	10	4
Ru/C	Batch	35	45	523	10	4
NiMoS/Al$_2$O$_3$	Batch	27	74	623	10	4
Pd/C	Batch	65	85	623	10	4
CoMoS/Al$_2$O$_3$	Batch	25	82	623	10	4
Ru/C	Batch	53	86	623	10	4
Pd/C	Continuous	62	71	613	13.5	4
Pd/C	Continuous	45	75	616	13.5	4
Proprietary	Continuous	61	98.8	678	10.2	5
Proprietary	Continuous	81	98.7	678	10.2	5
Pd/C & Proprietary	Continuous	50	98.4	523/683	13.5	6.67
Pd/C & Proprietary	Continuous	54	99	523/683	13.5	6.67
Pd/C & Proprietary	Continuous	37	99.3	523/683	13.5	-
Ru/C	Continuous	63	26.9	573	25	0.1
Ru/C	Continuous	95	16.9	448	20	0.1
Ru/C	Continuous	50	35.4	498	20	0.18
Ru/C	Continuous	54	44.7	448/498/648/673	24.1	0.45
Ru/C	Continuous	52	64.1	623/648/673/673	23	5.26
RuS/C-NiMoS	Continuous	45	99	443/663	13.5	5.26
RuS/C-NiMoS/C	Continuous	37	94	443/663	13.5	5.26
RuS/C-NiMoS/C	Continuous	43	95	443/663	13.5	4
Ru/C	Batch	53	31	493	19	4
Ru/C	Batch	58	40.8	543	19	4
Ru/C	Batch	56	59.7	583	19	4
Ru/C	Batch	15	43.4	493	19	4

Ru/C	Batch	30	43.4	543	19	4
Ru/C	Batch	31	51.7	583	19	4
Ru/C	Batch	83	38	493	19	4
Ru/C	Batch	74	41.9	543	19	4
Ru/C	Batch	70	64.9	583	16	4
NiCu/TiO$_2$	Batch	45.5	62.3	423/623	20	1/3
NiCu/Sibunite	Batch	35.9	86.5	423/623	20	1/3
NiCu/δ-Al$_2$O$_3$	Batch	42.2	57.4	423/623	20	1/3

Normally HDO processes are operated at 7.5 MPa – 30 MPa to ensure sufficient hydrogen is transferred to the catalyst surface, reduce the possibility of coking and increase reaction rate.[157, 158] The effect of hydrogen gas pressure on quantity and quality of upgraded bio-oil from HDO was examined by Venderbosch et al., [159] findings from the investigation showed that it is possible to achieve high deoxygenation level under hydrogen gas pressure within the typical range of 7.5 MPa – 30 MPa. From the investigation carried out by Elliot et al.,[156] it was established that longer residence time favours high degree of deoxygenation, with the O$_2$ content in the upgraded oil decreasing from 21 wt % to 10 wt % as residence time increased from 1.4 h to 4 h. This justifies the 3 h – 4 h reaction time used in past batch and continuous operation of bio-oil HDO.

2.5.1. Model Compounds in HDO

As mentioned earlier in Section 2.4, bio-oils contain more than 400 different organic compounds.[32, 46,115] Consequently, the complexity of bio-oil and possibility of multiple side reactions compelled HDO studies at research scale to model compounds instead. According to Ahmad et al., [38] most studies in the literature on HDO are on specific model compounds or mixtures of oxygenates to simulate real bio-oil. This approach is particularly useful because it simplifies the reactions that take place, highlight structure – reactivity of bio-oil components, analysis required and tracking of products formed. In addition, it provides valuable information on specific

steps involved in the transformation process. Model compound studies have been used at research scale to evaluate performance of different synthesised catalysts, and improve the design of catalyst for bio-oil upgrading. These studies have especially proven beneficial in understanding the mechanism and kinetics of HDO reaction.[125] However, volatile compounds detectable by GC-MS are often used in these studies. It is worth mentioning that findings from model compounds studies may not necessarily depicts behaviour in real bio-oil environment which contain additional interactions from neighbouring compounds. In addition, catalysts showing excellent stability in model compound studies, may undergo significant deactivation when placed in real bio-oil environment. Despite the drawbacks in specific model compound studies, they provide valuable information on the best approach to selectively hydrogenate the targeted C–O bonds and minimise cleavage of C–C or C–O bonds.[160]

GC-MS analysis of bio-oils from seven studies confirmed the presence of phenol in the structure of compounds detected.[161–167] Interestingly, in more than four of these references phenol, catechol, cresols, syringaldehyde, guaiacol, 4-methylguaiacol, 3-methylcatechol, vanillin, eugenol, syringol, acetovanillone, isoeugenol, 4-vinylguaiacol, 4-ethylphenol, and acetosyringone were reported.[52–56] Consequently, any of these compounds could be used as representative model of bio-oil in HDO studies. Nonetheless, guaiacol, cresols and anisole shown in Figure 2.9 are the most frequently used compounds to represent bio-oil in past HDO studies. These compounds are usually employed as base model of bio-oil because they contain multiple functional groups. Besides, the development of catalysts efficient in converting lignin derived phenolics is essential to bio-oil upgrading, since phenolics are primarily responsible for coke formation which leads to catalyst deactivation. Furthermore, these compounds are the most difficult to upgrade among the components present in bio-oils.[125] Nonetheless, the diversity of functional groups present in bio-oil necessitate extension

of studies on specific model compounds to less reported compounds such as vanillin, eugenol, syringol, isoeugenol, acetic acid etc. This will help bridge the knowledge gap on mechanism and reaction pathways of less popular functional groups within the bio-oil. Moreover, the behaviour of these less famous compounds during upgrading of the actual bio-oil could be different from the common model compounds shown in Figure 2.9. In fact, double oxygenated phenolic compounds such as guaiacols are reported to have greater poisoning effect than single oxygenated phenolic compounds like phenol.[168]

Cresol   **Guaiacol**   **Anisole**
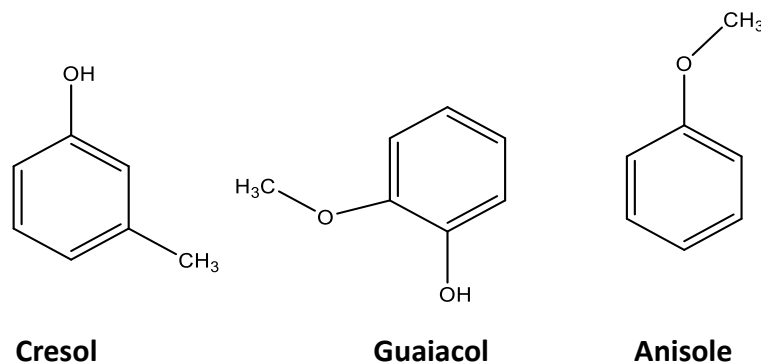
Fig. 2.9. Structure of common lignin derived phenolics employed in HDO studies.

In this research work, the base model compound of interest is vanillin, a commonly reported component from analytical studies on bio-oil.[64] It is currently the most available pure monoaromatic phenol produced at commercial scale. Annually up to 20,000 tons of vanillin is produced, and about 15% of this annual production comes from depolymerisation of lignin.[169–171] As shown in Figure 2.10, vanillin contain three different functional groups. This include a hydroxyl, methoxy, and aldehyde group.[172] Nonetheless, vanillin can be classified as a bifunctional compound since the aldehyde and hydroxyl groups are far more reactive than the methoxy group.[57] In the literature [57], the bond dissociation energies specified include 380.7 kJ/mol for the aldehyde group, 468.6 kJ/mol for the hydroxyl group, and 426.8 kJ/mol for the methoxyl group. As a result

of the identified differences in reactivity of the functional groups in vanillin, past studies on HDO reaction of vanillin confirmed the aldehyde group as the preferential site of attack. Vanillin is partially soluble in both the organic and aqueous phases, therefore it can be combined easily with components from either phases of bio-oil to mimic real bio-oil behaviour. As previously mentioned in Section 2.4.1, bio-oils are generally not very stable because they contain compounds with very reactive functional groups, such as the aldehyde group present in vanillin.
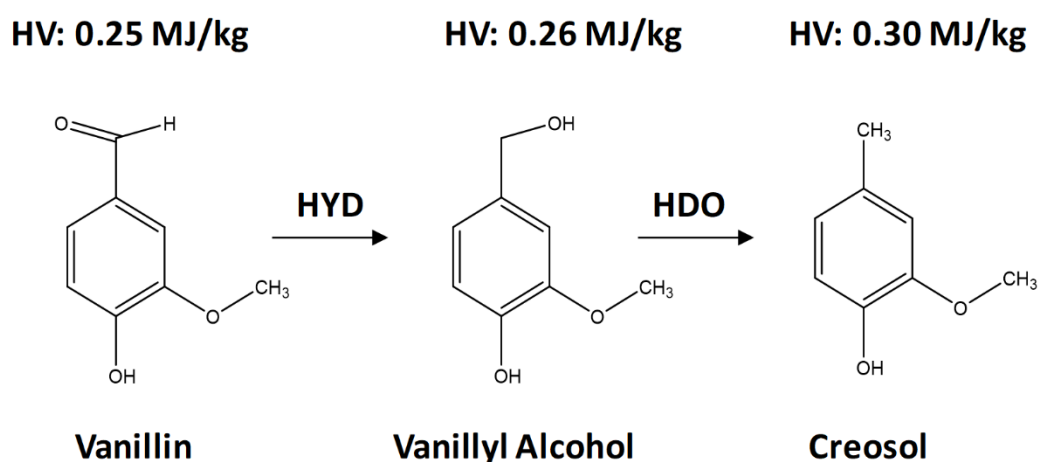
Fig. 2.10. Reaction Scheme for Vanillin (VL) HDO Reaction. HV represent the heating value estimated from Channiwala's and Parikh's correlation.[155]

In theory, the HDO of an aldehyde group can proceed via one of four possible routes which include: i) direct hydrogenolysis of C=O bond; ii) hydrogenation of the C=O bond to form alcohol and then hydrogenolysis of the C–O bond; iii) hydrogenation of C=O bond to form alcohol followed by dehydration and finally rehydrogenation of C=C bond; iv) decarbonylation of C=O bond to form CO and alkane. However, findings from past studies on vanillin (VL) HDO indicates the reaction often proceeds via route ii in two steps as shown in Figure 2.10.[64,74,173] The first step involves hydrogenation (HYD) of the aldehyde group to form vanillyl alcohol (VA), while the final step

involves hydrodeoxygenation (HDO) of the vanillyl alcohol to creosol (CR).[64,173] VL upgrading sometimes proceeds through direct deoxygenation (DDO) to produce CR. Applying the Channiwala's and Parikh's correlation,[155] Figure 2.10 shows that conversion of VL to CR leads to approximately 20% increase in the heating value. Likewise, CR is a more stable compound than VL because it contains the unreactive methyl group instead of the highly reactive C=O bond in VL. As a result of the improved heating value and stability, CR is widely reported as the desired product from VL HDO reaction at mild conditions. Nonetheless, under very harsh conditions identical to those used in real bio-oil HDO, guaiacol (GUA) and other hydrocarbons have been reported as byproducts from VL HDO reaction.[174,175] Both homogeneous and heterogeneous catalysts have been used to investigate VL HDO reaction.[71,72,176] Table 2.7 summarises the conditions and results from previous studies on VL HDO reaction. It shows that HDO reactions of VL have been performed in the temperature range of 328 K to 573 K and pressure range of 1 MPa to 5 MPa in different reaction media.

Table 2.7. Operating Conditions used to Investigate VL HDO Reaction in Literature and their results.

Catalyst	Reaction Conditions (Temperature, Pressure, Solvent)	Conversion (%), Time (h)	Main Product	Selectivity (%)	Ref.
Ni/SiO$_2$–ZrO$_2$	573 K, 5 MPa, Octane	100 (16h)	Hydrocarbons	54	174
Co/N–C	453 K, 1 MPa, 2-propanol	95 (4h)	Creosol	96	177
Co/N–C	423 K, 1 MPa N2 , 2-propanol	98 (4h)	Creosol	85	74
CoMo / Al$_2$O$_3$	573 K, 5 MPa, Dodecane	53 (4h)	Guaiacol	23	175
Mo$_2$C	453 K, 1 MPa, Water	100 (3h)	Creosol	78	63
Pd/C	373 K, 1 MPa, Octane-Water	> 99 (3h)	Creosol	94	178
Pd/CN	343 K, 1 MPa, Water	99 (1h)	Creosol	98	173
Ru/CNT	423 K, 1 MPa, Decalin - Water	100 (3h)	Creosol	96	179
Ru/C	328 K, 1.38 MPa, Water	95 (1h)	Vanillyl Alcohol	91	160
Au/CNT	423 K, 1 MPa, Decalin	94 (6h)	Creosol	100	172
RuCl$_3$/TPPTS	343 K, 4.5 MPa, Water - n-hexane	84 (3h)	Creosol	95	176
RuCl$_2$(PPh$_3$)$_3$	363 K, 3.3 MPa, Ethyl Acetate	91 (6h)	Vanillyl Alcohol	72	70
Ru-Based Shvo	418 K, 1 MPa, Toluene	98 (1h)	Vanillyl Alcohol	91	72
Cu–Ni/CeO$_2$–SiO$_2$	433 K, 2.5 MPa, Water	96(12h)	Creosol	82	180
Cu$_3$Pd@BBA–1	413 K, 1.0 MPa, 2-propanol	99(8h)	Creosol	94	73
Co$_x$P@POP	423 K,4.0 MPa, 2-propanol	100(5h)	Creosol	65	181

2.5.2. <u>Solvent Effect on VL HDO Reaction</u>

The role of solvents in heterogeneous catalysed reactions such as VL HDO cannot be overlooked because possible solvent – substrate interaction, solvent – product interaction, and solvent – catalyst interaction can affect product selectivity and reaction rates. In the work of Dyson et al[182],

solvent properties which include polarity, hydrogen bond donating capability, and hydrogen bond accepting capability are reported to have strong influence on catalytic performance. However, differences in polarity has been used in most studies to explain the changes in VL HDO performance under different solvents.[64,75,183–186] Although, the influence of solvent polarity on reaction kinetics cannot be undermine, more in-depth studies are required to understand the effect of solvent on HDO reaction. Isolating the effect of solvent is particularly difficult in reactions catalysed by supported metal catalysts because interaction between the solvent and support is also a possibility. In terms of polarity, it has been established that polar solvents enhances the adsorption of non-polar reactants. While in contrast, non-polar solvents enhances the adsorption of polar reactants.[187,188] Notably, water which is a highly polar solvent and present in significant quantities in bio-oil, is the most common media used in past HDO studies on VL and other model compounds. However, from Table 2.7 it can be seen that excellent vanillin conversion and selectivity toward CR were achieved in other reaction media such as n-hexane, decalin and 2-propanol. According to He et al.,[189] the ideal solvent for the HDO reaction must: (i) be able to hold the reactants and intermediates in solution, (ii) dissipate heat generated from the reaction, (iii) dissolve and transport H_2, and (iv) be stable under the processing conditions i.e. temperature, pressure etc. The effect of solvents on HDO reaction of vanillin over different heterogeneous catalysts have been investigated under various conditions. Sulman et al.,[75] evaluated VL HDO performance in tetrahydrofuran (THF), 2-propanol and water, the observed reaction rate increased with solvent polarity as follows: THF < 2-propanol < water. An identical study by Nie et al.,[64] using water, cyclohexane, ethyl acetate and THF as solvent for VL HDO reaction showed that VL conversion decreased as follows: water > cyclohexane > ethyl acetate > THF. The findings from both studies conformed to the previously mentioned effect of solvent polarity, since the highest

conversion and reaction rate were observed in the most polar solvent (i.e. water). However, most studies on the effect of solvent on VL HDO reaction only reported the rate of reaction in different solvents. This thesis investigate the kinetics of VL HDO reaction in different solvents to gain better insight into changes in intrinsic parameters such as activation energy, reactants enthalpy of adsorption, and rate constants.

2.6. Heterogeneous Catalysis in HDO of Bio-oil and Model Compounds.

Hydrodeoxygenation (HDO) of bio-oil and specific model compounds have been investigated using both heterogeneous and homogeneous catalysts.[71, 72, 74,176] However, the former are more promising as catalyst for industrial applications because they are less expensive and easily separated from the reactants and/or products for catalyst regeneration and reuse.[74,190] Consequently, different heterogeneous catalysts have been tested in past HDO studies on bio-oils and related model compounds. Heterogeneous catalysts normally contain active sites at the solid surface, promoters and are usually supported on inorganic porous materials.[93] Materials commonly used as support for these catalysts include Zirconia (ZrO_2), Titania (TiO_2), amorphous Silica-Alumina (SiO_2-Al_2O_3), alumina (Al_2O_3), carbon (C) and zeolites. Nonetheless, recent studies by Shit and co-workers suggest porous organic polymers can effectively act as support for catalysts in HDO reaction of VL.[73,181] In general, heterogeneous HDO catalysts can be grouped into six classes.[125] These includes: transition metal sulfides, noble or precious metals, base metals, transition metal phosphides/carbides/nitrides, other metal catalysts, and bifunctional catalysts.

2.6.1. Transition Metal Sulfided (TMS) Catalysts

The oldest type of heterogeneous catalyst used in HDO experiments of bio-oil are transition metal sulfided catalysts (TMS), they have been used for decades.[40,130,191] The first application of this type of catalyst in bio-oil upgrading via HDO was in 1970.[118] Since then, they have been used in many bio-oil HDO experiments. These catalysts are widely used in the refining of petroleum because they have excellent hydrogenation and heteroatom removal capabilities. Based on materials processed per year, TMS catalysts are the most used catalysts in the industry.[125] These group of catalysts usually contain sulfided molybdenum on an alumina support promoted with either Cobalt (Co) or Nickel (Ni). On rare occasions, base metals and promoters such as tungsten, phosphorous, fluorine, rhenium, rhodium, palladium and ruthenium are used. Among HDO catalysts, the chemistry of Mo-based catalysts is the most understood.[93, 192] Proposed mechanisms in the literature for deoxygenation of bio-oil on TMS catalysts include hydrodeoxygenation (HDO), direct deoxygenation (DDO) and decarbonylation/decarboxylation (DCO).[125] However, DDO is the most desired mechanism because it minimises overall H_2 consumption and maintain integrity of the aromatic rings. In the petroleum refinery, conventional hydrotreating process involves reaction at moderate temperatures (473 K – 698 K) with feeding of H_2 at high pressure (7–30 MPa) and H_2S at appropriate concentrations to maintain activity of the sulfided catalyst.[93,193] TMS catalysts are thermally stable, tolerant of most heteroatoms and their products provided they are appropriately sulfided. At low temperatures and sufficient sulfur environment, sulfided $NiMo/Al_2O_3$ favours the HDO route. While in contrast, sulfided $CoMo/Al_2O_3$ favours the DDO route at high temperature when reaction inhibition is not limiting and the reactant stream is not rich in hydrogen sulphide and ammonia.[125] Over the last decades, TMS catalysts have been tuned to

optimise petroleum refining hydrotreating processes such as hydrodesulphurisation (HDS), hydrodenitrogenation (HDN), and hydrodeoxygenation (HDO). However, optimised TMS catalysts for the refining of petroleum may be unsuitable for bio-oil HDO, since bio-oil contain up to 500,000 ppm oxygen and petroleum feedstock contain no more than 3000 ppm oxygen.[125] The high amount of oxygen in bio-oil can lead to rapid deactivation of the catalyst during HDO.[118,194] Besides, the water present in bio-oil potentially deactivates TMS catalyst since it encourages sulfur leaching.[195] The addition of sulfur to maintain activity of TMS catalysts weakens the advantage of bio-oil as fuel with low sulfur content. Moreover, the conventional support (i.e. ɣ-alumina) used in TMS catalysts promotes coking which causes deactivation. Losses in activity of TMS catalysts under conditions used for HDO have also been linked to compositional changes in the support to a new compound called boehmite.[196, 197] As a result of the documented drawbacks in TMS catalysts, alternative catalysts for HDO gained attention over the years.

2.6.2. Noble or Precious Metal Catalysts

Supported noble metal catalysts (e.g., Pt, Pd, Rh and Ru) are promising alternative catalyst for HDO because they are renowned for their excellent hydrogenation capabilities even at low temperatures.[198, 199] In contrast to TMS catalysts which degrade and deactivate during HDO processes, supported noble metal catalysts do not require co-feeding with a sulfur source and are less susceptible to deactivation by water. Hence, this group of catalysts have great potential to exhibit longer lifetimes and yield better HDO performance.[125] Historically, supported noble metal catalysts were used in APR processes to convert polyols and sugars to syngas, light alkanes, hydrogen, and monofunctional compounds.[85] However, most of the studies on efficacy of supported noble metal catalysts for HDO reaction have been carried out using model compounds

of bio-oil.[93] Table 2.8 summarises the findings from recent studies on bio-oil model compounds upgrading via HDO over supported noble metal catalysts. Among the noble metals, Ru catalysts have been used in majority of the previous HDO studies on vanillin (VL) the model compound of interest in this research project.[71,72,160] However, the few studies on VL HDO reactions over supported Pd based catalysts showed excellent conversion of 99% or more and selectivity to the desired deoxygenated product creosol greater than or equal to 94%.[74,173] Despite the promising prospect of Ru catalysts in HDO reactions, other noble metals with great potential such as Pd need to be tested more thoroughly. From results on model compounds past HDO studies displayed in Table 2.8, it is clear that Pt-based catalysts demonstrates the least effective performance. Interestingly, this conclusion conflicts findings from past HDO studies on the whole bio-oil. Bio-oils from different feedstocks were used by Elkasabi et al.,[109] to compare the HDO performance of Pt/C, Ru/C and Pd/C at 593 K under 14.5 MPa pressure. The optimal catalyst in terms of deoxygenation efficiency, H_2 consumed and upgraded compounds was Pt/C. Conversely, HDO screening test by Wildschut et al.,[200] among Ru/C, Ru/TiO_2, Ru/Al_2O_3, Pt/C, and Pd/C at 523 K and 623 K under 10 MPa and 20 MPa using beech wood fast pyrolysis oil showed that Ru/C is the optimal catalyst in terms of oil yield and extent of deoxygenation. Ardiyanti et al.,[201] compared the HDO performance of zirconia supported monometallic and bimetallic catalysts of Pd, Rh and Pt in a batch reactor using fast pyrolysis oil from pinewood. The upgraded bio-oil from Rh/ZrO_2 catalysed HDO reaction had the lowest thermogravimetric (TG) residue and consequently emerged as the most suitable co-feed to existing oil refineries. However, based on activity which was measured as the ratio of H_2 uptake to product of the metal intake and reaction time, Pd/ZrO_2 catalyst demonstrated superior performance. On the basis of conclusions from the different screening tests in past HDO studies, the performance of noble metal catalysts seems to be affected by the

feedstocks from which bio-oils are derived.[115] Furthermore, the observed differences in conclusion on optimal noble metal catalyst for HDO reaction highlights potential drawbacks in findings from model compound studies.

Table 2.8. Summary of recent HDO studies on model compounds of Bio-oil over supported noble metal catalysts.[125]

Catalyst	Catalyst Loading (wt %)	S_{BET} (m²/g)	Model Compound	Reaction Conditions	Main Product(s)	Conversion (%)	Reaction Pathway
Pd/C	5	845	2-methoxy-4-n-propylphenol	H_3PO_4-H_2O, 523 K, 5 MPa H_2	n-Propylcyclohexane	100	HDO
Pd/C	5	845	Phenol	H_2O, 473 K, 5 MPa H_2	Cyclohexanol	100	HYD
Pd/C	5	845	Phenol	H_3PO_4-H_2O, 523 K, 5 MPa H_2	Cyclohexane	100	HDO
			4-n-Propylphenol		n-Propylcyclohexane	100	HDO
			Catechol		Cyclohexane	100	HDO
			4-Methyl-2-methoxyphenol		Methylcyclohexane	100	HDO
			4-Ethyl-2-methoxyphenol		Ethylcyclohexane	100	HDO
			4-Propyl-2-methoxyphenol		Propylcyclohexane	100	HDO
			4-(2-Propenyl)-2,6-dimethoxyphenol		Propylcyclohexane	92	HDO
Ru/C	7.8	-	Guaiacol	H_2O, 473 K, 13.8 MPa H_2	2-Methoxycyclohexanol	100	HYD,DDO
				H_2O, 523 K, 13.8 MPa H_2	Cyclohexane	100	HDO
				H_2O, 573 K, 13.8 MPa H_2	Phenol, cresols	100	DMO,MT

Table 2.8. (Cont.)

Catalyst	Catalyst Loading (wt %)	SBET (m²/g)	Model Compound	Reaction Conditions	Main Product(s)	Conversion (%)	Reaction Pathway
Pd/C	3	-	Guaiacol	H_2O, 473 K, 13.8 MPa H_2	2-Methoxycyclohexanol	66	HYD,DDO
				H_2O, 573 K, 13.8 MPa H_2	Cyclohexane	99	HDO
Rh/ZrO$_2$	0.39	20	Guaiacol	n-hexadecane, 373 K, 8 MPa H_2	1-Methyl-1,2-cyclohexanediol	99	HYD,MT
				n-hexadecane, 573 K, 8 MPa H_2	Benzene	100	DDO,DMO
RhPt/ZrO$_2$	0.25Rh 0.25Pt	23	Guaiacol	n-hexadecane, 373 K, 8 MPa H_2	1-Methyl-1,2-cyclohexanediol	99	MT,HYD
				n-hexadecane, 573 K, 8 MPa H_2	Benzene	100	DDO, DMO
Rh/ZrO$_2$	3	4.72	Guaiacol	n-Decane, 523 K, 4 MPa H_2	2-Methoxycyclohexanol	95	HYD
Rh/ZrO$_2$+ SiO$_2$-Al$_2$O$_3$	3	4.72			2-Methoxycyclohexanol, cyclohexane	38	HYD,HDO
Rh/ SiO$_2$-Al$_2$O$_3$	3	569			Cyclohexane	57	HDO
Rh/C	3	238			2-Methoxycyclohexanol, cyclohexane	68	HYD,HDO
Rh/Al$_2$O$_3$	3	122			2-Methoxycyclohexanol, cyclohexane	43	HYD,HDO,DMO

Table 2.8. (Cont.)

Catalyst	Catalyst Loading (wt %)	S_{BET} (m^2/g)	Model Compound	Reaction Conditions	Main Product(s)	Conversion (%)	Reaction Pathway
Ru/C	5.7	730	p-cresol	CH$_3$COOH-H$_2$0, 573 K, 4.8 MPa H$_2$	Methylcyclohexane	67	HDO
Rh/ZrO$_2$	1	6.6	Guaiacol	n-Tetradecane,673 K, 5 MPa H$_2$	Cyclohexane	100	HDO
PtRh/ZrO$_2$	1Rh 1Pt	7.0	Guaiacol		2-Methoxycyclohexanol	100	HYD
PdRh/ZrO$_2$	1Rh 1Pd	5.9	Guaiacol		2-Methoxycyclohexanol	100	HYD
Pt/Al$_2$O$_3$	1.7	87	m-cresol	533 K,50.5 kPa H$_2$	Toluene, Methylcyclohexane	38	DDO,HDO
				533 K,0.10 MPa H$_2$	Toluene, Methylcyclohexane	74	DDO,HDO
Pt/Al$_2$O$_3$	1.6	87	m-cresol	533 K,50.5 kPa H$_2$	Toluene, Methylcyclohexane	38	DDO,HDO
PtCo/Al$_2$O$_3$	1.3 Pt 4.3Co				Methylcyclohexane, toluene	57	
PtNi/Al$_2$O$_3$	1.5 Pt 4.9Ni				Methylcyclohexane, toluene	63	
Pt/Al$_2$O$_3$	1	206	Anisole	573 K, 42 kPa H$_2$	Phenol, cresols	7	DME, MT
			4-Methylanisole		Cresols	6	
Pt/Al$_2$O$_3$	1	206	Guaiacol		Phenol, Catechol	8	DDO, DME
Pt/MgO	1	100	Guaiacol		Phenol, Catechol	8	DDO, DME
Pt/HBEA	1 / 0.2	710	Anisole	673 K,0.10 MPa H$_2$	Benzene, toluene, xylenes	30	DME, MT, DDO

Generally, the yield of hydrocarbon and deoxygenation level seems to be better in HDO reactions catalysed by noble metals. Wildschut et al., [200] compared the performance of supported Ru, Pd, and Pt catalysts against conventional TMS catalysts (i.e. $NiMo/Al_2O_3$ and $CoMo/Al_2O_3$) using actual bio-oil. In terms of oil yield and degree of deoxygenation, Pd/C and Ru/C catalysts performed better than conventional TMS catalysts at the two conditions considered. In addition to the superior HDO performance, operational issues such as reactor plugging and deactivation as a result of excess coking are less likely when noble metal catalysts are used since operation at high temperatures is no longer a necessity.[93, 118] HDO reaction over supported noble metal catalysts proceed through the mechanisms shown in Figure 2.11a and 2.11b.
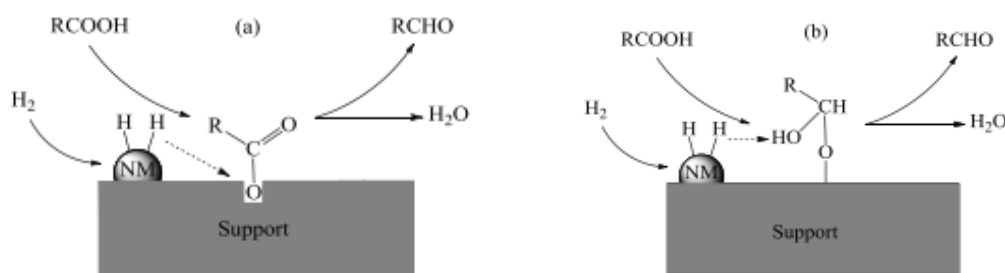
Fig. 2.11. Mechanisms for HDO reaction over supported noble metal catalysts.[155]

Figure 2.11a represents the mechanism for HDO reaction over noble metal catalysts on non-reducible metal oxide supports. It involves adsorption and activation of H_2 on sites of the noble metal, while the oxygenated compounds becomes adsorbed and activated on either sites of the noble metal or at the metal-support interface.[202, 203] Intermediates of the adsorbed oxygenated compounds will then react with spilled over H atoms, resulting in scission of C–O bond and subsequently formation of water and deoxygenated products. Conversely, the mechanism for HDO reaction over noble metal catalysts on reducible metal oxide supports such as MoO_3, WO_3,

Fe$_2$O$_3$ and SnO$_2$ described in Figure 2.11b involves reaction of H$_2$ with lattice oxygen to create oxygen vacancies which are then refilled by oxygen from the oxygenated compounds. Through cleavage of C–O bonds in the intermediate species the final products are formed.[155, 204] In common both mechanisms followed a hydrogenation-dehydration-hydrogenation sequence. Thus indicates that HDO reaction over supported noble metal catalysts usually requires a site for hydrogenation and another site for dehydration.[125] In contrast, HDO studies on model compounds using TMS catalysts often favours direct deoxygenation. Thereby suggesting that H$_2$ consumption may be higher in HDO reactions catalysed by noble metals.[93, 118] The use of noble metal catalysts on industrial scale has been severely hampered by price and availability. Besides, they are prone to deactivation through sintering and particularly poisoning by substances (e.g., sulfur and nitrogen) present in bio-oil.[115, 155] Most of the concerns on suitability of noble metal catalysts for HDO reaction are insignificant in model compound studies since contamination by foreign substances and coking are less likely to occur. Undoubtedly despite the potential drawbacks in the use of noble metal catalysts, they remain the leading candidates for HDO reaction.[64]

2.6.3. Base or Non-Precious Metal catalysts

Non-sulfided base metals (e.g., Ni, Cu, Fe and their alloys) are another attractive group of catalysts for HDO reactions. These group of catalysts are relatively cheap and have demonstrated excellent catalytic activity. As a result, they are perceived as promising substitute to TMS and noble metal catalysts.[205] Cheng et al.,[31] investigated HDO activity of monometallic (Ni) and bimetallic (Ni doped with Fe, Mo and Cu) catalysts supported on activated carbon using prairie cordgrass bio-oil under mild operating conditions of 3.47 MPag and 623 K. The results showed that all the catalysts significantly improved the bio-oil physicochemical properties (i.e. chemical composition, HHV, pH, O$_2$ and H$_2$O content). However, upgraded

bio-oil from the Ni/AC catalysed reaction contained the highest fraction of gasoline range hydrocarbons. Notably the reactions with bimetallic catalysts produced upgraded bio-oils rich in alkyl-phenols, with upgraded bio-oil from the NiMo/AC catalysed reaction containing the highest amount of alkyl-phenols. Furthermore, it was found that the addition of a second metal reduced the amount of coke formed and increased activity of the catalyst.[31] The HDO efficacy of monometallic (Ni and Cu) and bimetallic (Ni doped in Cu) catalysts supported on δ-Al$_2$O$_3$ were compared to commercial Ru/C catalyst by Ardiyanti et al.[206] It was found that the bimetallic Ni$_x$Cu$_y$/ δ-Al$_2$O$_3$ catalyst outperformed monometallic Ni/ δ-Al$_2$O$_3$ and Cu/ δ-Al$_2$O$_3$ catalysts. However, activity of the best bimetallic (i.e., Ni$_{16}$Cu$_2$/ δ-Al$_2$O$_3$) catalyst was still less than the benchmark commercial Ru/C catalyst. Interestingly, findings from the study supported Cheng et al.,[31] claim that addition of a second metal increases resistance to coking. As it showed that the bimetallic catalyst with maximum nickel loading (16 wt %) experienced the least amount of leaching and coking. In a parallel study of three bio-oil model compounds (i.e., furfuryl, alcohol, benzene alcohol and ethyloenanthate) and actual bio-oil HDO reactions over NiFe/ γ-Al$_2$O$_3$ by Leng et al.[207] excellent conversions and yields were achieved from the model studies. Notably the conversions achieved were higher than those achieved under rival HDO catalysts which includes sulfided CoMo, Ru-based and Cu-based. In addition, the heating value of the bio-oil increased from 37.8 MJ/kg to 43.9 MJ/kg and the pH changed from 6.65 to 7.50. These results from Leng et al.,[207] studies reinforces the potential of bifunctional base metals as catalysts for bio-oil and model compounds HDO reaction. According to the literature,[208, 209] properties of bimetallic catalysts are different from monometallic counterparts because of the following reasons:

- Dilution effect: The presence of a second metal changes the geometry or dilutes the active metal site (ensemble).

- Ligand or electronic effect: The presence of a second metal changes the active metal site electronic configuration through transfer of electron.

- Stabilisation effect: The presence of a second metal stabilises the metal active sites by preventing sintering and coke formation.

- Synergistic effect: The different metals participate in the catalytic process by stabilizing the transition state via chemical bonding.

- Bi-functional effect: Both metals catalyse different reactions e.g. one metal facilitate hydrogenation reaction and the other metal catalyse hydrogenolysis reaction.

From the above listed reasons, it is clear that structural properties of bimetallic catalysts strongly influence their catalytic properties. Most bimetallic catalysts contain an oxophilic metal (i.e. Co, Cr, Fe, W, Mo, and Re) which modifies the hydrogenating metal (i.e. Ni, Pt, Pd, and Rh). Figure 2.12 depicts proposed mechanism in the literature [208] for HDO reaction over bimetallic catalyst.
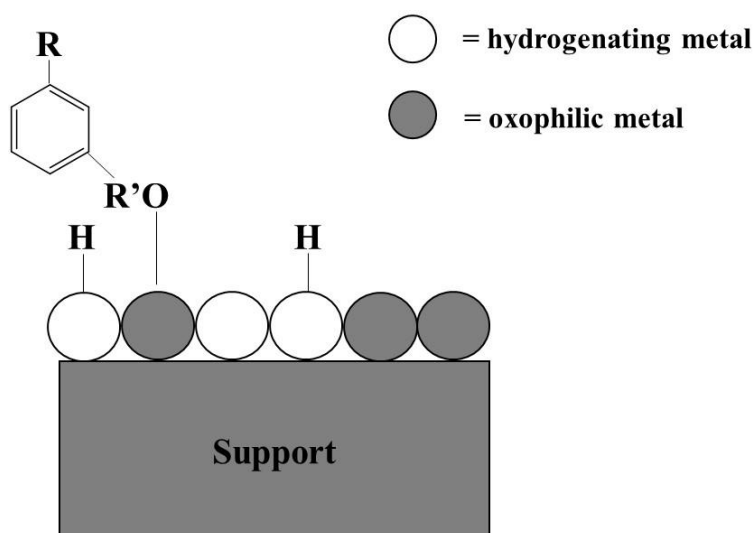
Fig. 2.12. Mechanism for HDO reaction over bimetallic catalysts.[208]

The mechanism for HDO reaction over bimetallic catalyst presented in Figure 2.12 shows that the hydrogenating metal provides hydrogen, while the oxophilic metal strongly binds the

model oxygenate to the surface through the oxygen functionality. As a result, C–O scission occurs easily and new pathways unavailable on a monometallic catalyst are probably created. Yang et al., [177] investigated the effectiveness of low cost nitrogen-doped carbon encapsulated Cobalt catalyst for vanillin HDO reaction at 453 K for 4 h in the presence of formic acid as a redundant. Excellent conversion and selectivity toward the deoxygenated product creosol was achieved. Despite the promising potential of base metal catalysts, they are not as active as noble metals. Hence, longer reaction times, higher catalyst loading and temperatures are required to use base metals as HDO catalyst. Besides, they deactivate easily under acidic environment which is typical of real bio-oils.[31, 147] As a result of these drawbacks, transition metal phosphides, carbides and nitrides received attention as alternatives to base metal catalysts.

2.6.4. Transition Metal Phosphides/Nitrides and Carbides

Over the last decade, transition metal phosphides (TMPs) have gained attention as low cost, readily available and environmentally friendly source of catalysts for bio-oil HDO reaction. This attention stems from proven history of iron, cobalt, nickel, molybdenum and tungsten phosphides as active catalysts for HDN and HDS reactions.[93,130,210] Whiffen et al.,[211] investigated the performance of unsupported molybdenum phosphides (MoP), oxides (MoO$_x$), and sulfides (MoS$_2$) catalysts in HDO of a bio-model compound p-cresol. MoP emerged as the best in terms of activity and selectivity toward hydrogenated products. However, in the work of Li et al., [26] on deoxygenation of anisole over Ni$_2$P/SiO$_2$, MoP/SiO$_2$, and Ni$_x$Mo$_y$P/SiO$_2$ catalyst, Ni$_2$P was the most active phase. Zhao et al., [212] probed the HDO of guaiacol over Ni$_2$P/SiO$_2$, Fe$_2$P/SiO$_2$, MoP/SiO$_2$, Co$_2$P/ SiO$_2$, WP/ SiO$_2$, Pd/ Al$_2$O$_3$ and CoMoS/Al$_2$O$_3$ catalyst. Interestingly, the superior active phase was again Ni$_2$P. It is believed that the superior activity and selectivity of Ni$_2$P was down to the inherent properties (i.e., ligand effect and electron

density) and crystal structure (i.e., type of surface sites).[125] Figure 2.13 represents the proposed mechanism in the literature for HDO reaction over TMP catalysts.
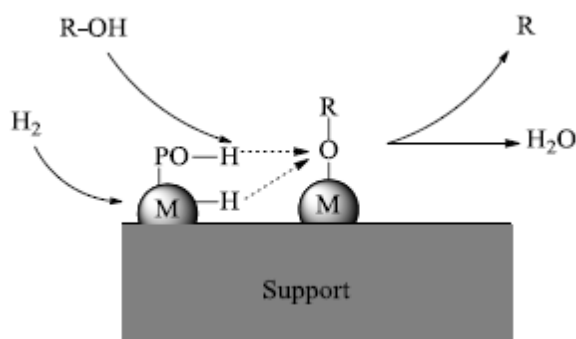
Fig. 2.13. Mechanism for HDO reaction over TMP catalysts.[155]

Despite the promising potential of TMPs as catalyst for HDO reaction, they are not very stable under the typical condition for HDO.[125] Under this condition, they are oxidised by the water present in bio-oil into a phosphate group, this group adheres strongly to the active sites and thereby leads to deactivation. Other peculiar problems with noble metal and TMS catalysts such as leaching and sintering have been reported for TMPs under conditions that are not even representative of real bio-oil HDO.[125] Transition metal carbides (TMCs) and nitrides (TMNs) have recently gained attention as catalysts for HDO because they demonstrated noble metal like property and activity.[213] HDO of anisole over molybdenum carbide (Mo$_2$C) in the vapor phase was investigated by Lee et al.,[214] at 420 K – 520 K under ambient pressure, 90% selectivity toward benzene and less than 9% selectivity toward cyclohexane was achieved. Lu et al., [215] conducted a parallel study using Mo$_2$C and tungsten carbide (W$_2$C) at 423 K – 443 K, the highest benzene selectivity of 96% to date was achieved when the anisole HDO reaction was catalysed by W$_2$C. He et al., [63] investigated the reusability and HDO activity of Mo$_2$C at 373 K, 2.0 MPa and 3 h in a batch reactor using vanillin. The results showed excellent yield of creosol and conversion, thereby indicating that Mo$_2$C catalyst exhibited good resistance against deactivation. The HDO performance of different molybdenum nitride catalysts were

investigated by Ghampson et al.,[7] using guaiacol at 573 K and 5 MPa in a batch reactor. Mo_2N emerged as the most active among the tested molybdenum nitride catalysts. Although, transition metal nitrides and carbides have shown excellent potential as catalysts for individual model compound HDO reactions. They have not been sufficiently tested in real bio-oil environment and HDO condition to ascertain their effectiveness. In general the major challenges to commercial viability of these new group of catalysts include: scalable and reproducible synthesis method, understanding the active sites and composition of the surfaces under reaction conditions.[125, 210,213]

2.6.5. Other Catalysts

Recently the HDO performance of amorphous catalysts (e.g. Ni–Mo–B, Co–Mo–B, Co–Ni–Mo–B, Ni–W–P–B etc.,) renowned for high concentration of coordinated unsaturated sites and unique isotropic property were investigated by Wang et al., [216] using bio-oil model compounds. Notably these catalysts demonstrated high catalytic activity and deoxygenation rates. However, more tuning in compositional ratio of these catalysts are required to further improve their stability and activity.[115, 217]

2.7. Challenges to Bio-oil Upgrading via HDO

2.7.1. Catalyst Deactivation

Catalyst deactivation is one of the most challenging issues hindering continuous upgrading of bio-oil via HDO.[93, 117,125,130] The different mechanisms responsible for deactivation are illustrated in Figure 2.14. Notably, the formation of coke on catalyst surfaces as a result of polymerisation and polycondensation reaction is widely perceived as the leading cause of deactivation.[20,115] Coke formed on the surface of catalysts deny reactants access into the active sites, this translates to reduced activity over time.[80] The acidity of catalyst has been heavily

linked to severe deactivation, with catalysts on highly acidic alumina support deactivating faster than those on inert materials (i.e. carbon, silica, e.t.c.).[40] Nonetheless, presence of acidic sites on the catalyst surface is a pre-requisite for good activity. Polyaromatic species with more than two oxygen atoms such as vanillin, guaiacol, eugenol, etc., present in bio-oil promotes coking because they easily polymerise under typical HDO condition.[147, 195, 218]
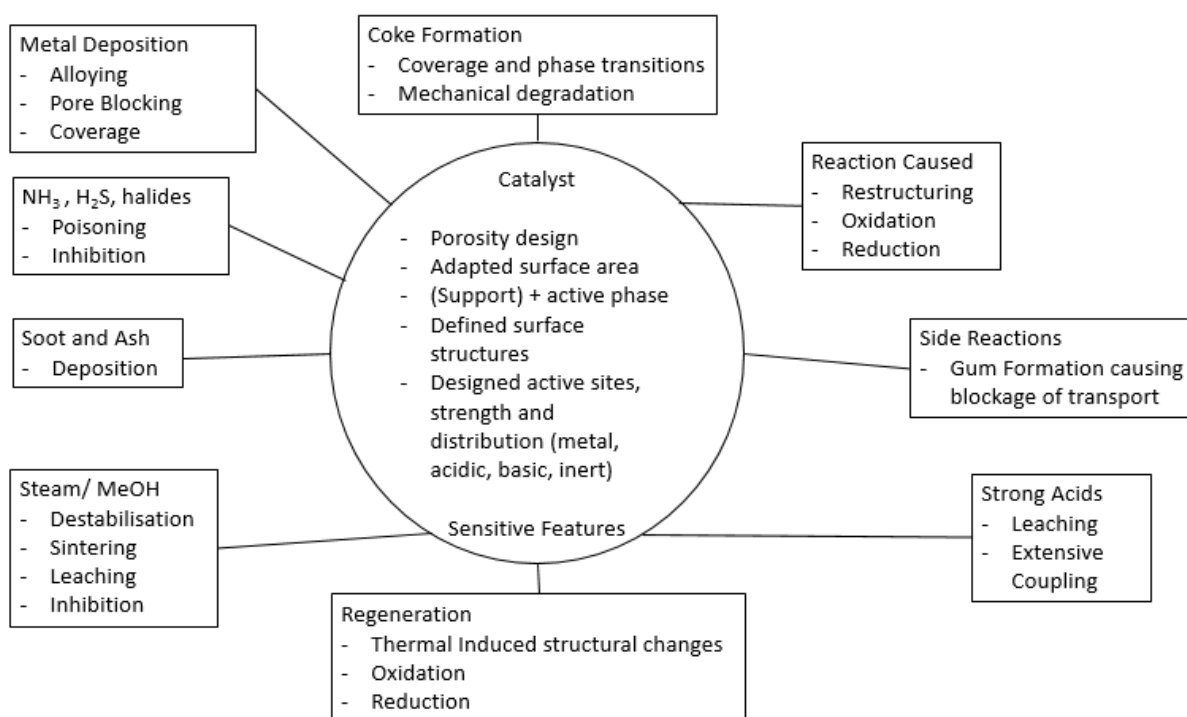
Fig. 2.14. Mechanisms for Catalyst Deactivation in Bio-Oil HDO treatment.[117]

The invention of integrated HDO systems have proved effective in reducing coking issues from polyaromatic species. A 2-stage HDO treatment was operated for up to 700 h under single catalyst loading for the first time in 2012, while in 2013 the runtime was extended to 1440 h through a 3-stage treatment.[68] As noted in Section 2.5, high temperature and hydrogen gas pressure are required to achieve excellent deoxygenation. However, increase in the reaction temperature escalates the amount of coke formed. Fortunately, noble metal catalysts have proven useful in permitting HDO operation at moderate to low temperatures. The requirement

of high hydrogen gas pressure normally raises concerns of cost and safety. But high H_2 gas pressure help prevents coke formation through hydrogenation of carbon precursors. Some researchers suggested using steam or aqueous phase reforming to meet the high hydrogen gas demand.[130] Other considerations involve the use of hydrogen donating solvents such as tetralin, cyclohexane, 1-butanol, etc., to minimise the amount of fresh hydrogen gas required for HDO reaction. Lee et al., [219] highlighted the important roles hydrogen donating solvents play in minimising catalyst deactivation during bio-oil HDO. Controlled addition of hydrogen as the reaction temperature increases using multi-port injections have also been explored.[68] Clearly significant efforts have been made to minimise catalyst deactivation and develop more promising catalyst for HDO reaction.

2.7.2 Modelling HDO Reaction Kinetics

The mandatory requirement for the design of any process that involves multiple reaction pathways is excellent knowledge of the overall reaction kinetics. Having such knowledge is particularly important to control the reactions occurring and maximise selectivity toward the desired product. Consequently, developing an accurate kinetic model is critical to the commercial viability of bio-oil upgrade through HDO. The task of developing kinetic model for bio-oil HDO reaction has been difficult because of the complex nature of bio-oils.[93, 125] Most of the developed kinetic expressions describing HDO reactions are for specific model compounds, and they are often based on Langmuir – Hinshelwood – Hougen – Watson (LHHW) kinetic models.[160, 220–225] Bindwal et al., [160,221] used LHHW models to describe the HDO reaction of vanillin and levoglucosan over Ru/C catalyst at mild operating conditions. However, Sulman et al[75].used a different approach based on fundamental mass balances to develop kinetic models for vanillin HDO reaction over Pt/C catalyst in different solvent at 353 K to 473 K under 3 MPa hydrogen gas pressure. Nie et al., [222] successfully used the LHHW

model to investigate the mechanism of m-cresol vapour phase HDO reaction over Pt/SiO_2 catalyst at 573 K. In contrast, Bykova et al., [226] employed fundamental mass balances to describe the kinetics of guaiacol HDO reaction over $Ni–Cu/SiO_2–ZrO_2–La_2O_3$ at 553 K to 633 K under 17 MPa. Despite the long history of successful modelling of different oxygenated compounds HDO reaction kinetics, these models may not be adequate in describing the kinetics of real bio-oil HDO reaction because they fail to consider interactions with other compounds. Moreover, the interaction between the studied model compounds and surface of the catalysts may change when surrounded by other model compounds. Besides, the relative adsorption of non-model compounds may alter the rate of adsorption of model compounds onto the catalyst surface and lead to different reaction rates. Based on the identified shortcomings of models developed for specific model compounds, lumped expressions were developed to describe bio-oil HDO reaction kinetic. HDO reaction kinetics of pine bio-oil over $Pt/Al_2O_3/SiO_2$, $CoMoS_2/Al_2O_3$ and $NiMoS_2/Al_2O_3$ catalysts in a packed bed was modelled on the basis of equation 2.8 by Sheu et al.[227]

$$-\frac{dw_{oxy}}{dZ} = k\, w^m_{oxy} P^n \qquad (2.8)$$

where w_{oxy} is the ratio of oxygen mass in the product to the oxygen mass in bio-oil, Z is the axial position in the reactor, k is the rate constant, P is the total hydrogen pressure, m is the order of reaction for oxygen, and n is the order of reaction for the system total pressure. However, the assumption of general first order dependence on w_{oxy} was perceived as rough by other researchers. The model also received heavy criticism for using mass related concentration and axial position of the reactor since this non-fundamental form makes it specific to the system used. These assumptions therefore raised concern on possibility of correlating the result with other systems.[125, 130] Su Ping et al., [228] used similar approach as Sheu et al., [227] to describe the kinetics of bio-oil HDO reaction over $CoMoS_2/Al_2O_3$ at temperatures between 633 K and 663

K. However, Su Ping et al.,[228] assumed dependence on pressure was low and therefore omitted the term for pressure in the expression used to model the kinetic of bio-oil HDO reaction. Zhang et al.,[229] also successfully demonstrated the fit of a four lumped species kinetic model containing five rate constants to bio-oil HDO reaction experimental data. However, these models are all flawed because they do not consider every possible reactions that occurred during bio-oil HDO reaction. Of course given the complexity of bio-oil this is extremely difficult to achieve. LHHW models which have been successfully used to model the kinetics of specific model compounds remains the most promising approach. The kinetics of aqueous phase hydrogenation of levoglucosan was described in the work of Bindwal et al.,[221] through single site LHHW kinetic model assuming surface reaction as the rate determining step and competitive adsorption of dissociatively chemisorbed H_2 and levoglucosan. Interestingly, the same assumptions were used in the work of Jain et al.,[225] to successfully describe the kinetics of aqueous phase hydrogenation of other model substrates of bio-oil such as xylenols and maltol via single site LHHW kinetic model. While in the work of Chen et al.,[223] the kinetics of hydrogenation reactions of lactic acid, propanoic acid and their mixtures were described using dual site LHHW kinetic models assuming surface reaction as the rate determining step and non-competitive adsorption between dissociatively chemisorbed H_2 and the acids. Despite the success in past studies on kinetic modelling of specific model compound hydrogenation reactions, more studies on mixtures reflective of the functional groups present in bio-oils are required. Besides, mixture studies are normally used in the industry to describe the kinetics of conventional hydrotreating processes (i.e. HDS and hydrocracking).[130]

2.8. Chapter Summary

It has become increasingly important to explore alternative renewable and sustainable energy sources because future global energy demand is increasing, capacity of fossil reserves are on a rapid decline and awareness of the negative implication fossil fuels consumption has on the environment is quickly growing. Bio-oils produced from plant biomass through fast pyrolysis are the only renewable and sustainable liquid hydrocarbon fuels that can be used directly in existing infrastructures. However, when compared to convention fuel such as crude oil, bio-oil contain significant amount of oxygen and water content. Consequently, bio-oils have undesirable properties such as high acidity, high viscosity, low energy density etc. that must be removed before they can function effectively as fuel and valuable chemical feedstock to other processes. The preferred technology for upgrading bio-oil properties is hydrodeoxygenation (HDO). But HDO remains far from industrial application because of the following challenges: i) Rapid deactivation of catalyst, ii) Source of hydrogen to meet the high pressure requirement, and iii) Lack of models to accurately describe HDO reaction kinetics.

The complexity of bio-oil has compelled HDO studies at research scale to specific model compounds, especially lignin derived phenolics such as guaiacols, cresols and anisole. These studies proved useful in understanding mechanism of HDO reaction in some of the functional groups present in bio-oil. Additionally, the desired features for HDO catalysts were established from these studies. However, given the vast number of compounds present in bio-oils, less investigated compounds such as vanillin, eugenol, syringol etc. must be used as representative model of bio-oil to expand the knowledge base on HDO reaction of the actual bio-oil. To date catalysts that have been used to study bio-oil and representative model compounds HDO reaction include sulfided transition metal (TMS), noble metals, base metals, transition metal phosphides (TMPs), transition metal nitrides (TMNs), transition metal carbides (TMCs),

bifunctional and amorphous catalyst. Nonetheless, these catalysts suffered from one or more defects that must be improved before they can be applied on industrial scale. Hence, catalyst design continues to be an area of strong research interest in the development of HDO process. The deposition of carbon on the surface of catalysts (i.e. coking) has been confirmed as the primary source of deactivation. Different HDO studies have shown that catalyst acidity and operating conditions are strongly responsible for coking. However, excellent activity cannot be achieved without sufficient acid sites on the catalyst. Hence, a mandatory requirement in the design of catalyst for HDO is to maintain balanced acidic level. The evolution of noble metals as catalyst for HDO is particularly promising because it eliminates high temperature operation, and consequently reduce the problem of coking. In addition, meeting the high pressure requirement for HDO looks more feasible with options of hydrogen donating solvent as reaction medium and aqueous phase reforming to supply fresh hydrogen. The kinetics of specific model compounds of bio-oil HDO reaction were successfully described by Langmuir – Hinshelwood – Hougen – Watson (LHHW) models. Furthermore, lumped expressions have been used to model the kinetics of bio-oil HDO reaction in the past. However, developed models are flawed because of the underlying assumptions. These assumptions make developed models either compound or system specific. LLHW models that have been successfully used to describe the kinetics of specific model compound HDO reaction are the most promising. Nonetheless, their application must be extended to complex system mimicking real bio-oil.

Chapter 3

Materials and Methods.

3.1. Introduction

The specific objective of the present chapter is to describe the experimental procedures and analytical methods used in the research studies conducted. Information on purity and suppliers of the materials which include catalysts, supports, and chemicals used in the various experiments performed are presented in Section 3.2. While Section 3.3 provides detail information on the rig used to conduct the experiments as well as the procedures employed. The final section summarises the analytical methods employed and highlights the working principles of the various tools used.

3.2. Materials

The percentage purity and supplier of the gases, supports and chemicals used in the experiments conducted are presented in Table 3.1. It is worth mentioning that chemicals and gases were used as received from the suppliers. However, commercial catalysts which include 5 wt % and 10 wt % Pd/C (supplier: Alfar Aesar), 5 wt % Pt/C (supplier: Sigma-Aldrich), 5 wt % Pd/Al$_2$O$_3$ (supplier: Johnson-Matthey), 2 wt % Pd/Al$_2$O$_3$ (supplier: Johnson-Matthey), 5 wt % Rh/Al$_2$O$_3$ (supplier: Johnson-Matthey), and 5 wt % Pt/SiO$_2$ (supplier: Johnson-Matthey) were crushed and sieved to particle size ≤ 90 μm before use in experiments. Likewise, the synthesised bimetallic PdRh/Al$_2$O$_3$ catalyst particles were crushed and sieved to particle size ≤ 90 μm before using them.

Table 3.1. List of Suppliers and Purity for Gases, Chemicals and Commercial Supports Powder.

Items	Supplier	Purity (%)
Gases		
Hydrogen(H_2)	BOC,UK	99.9
Nitrogen(N_2)	BOC,UK	99.9
Chemicals		
Ethyl Acetate (solvent)	Fischer Scientific,UK	99.9
Toluene (solvent)	Fischer Scientific,UK	99.9
2-Propanol (solvent)	Sigma-Aldrich,UK	99.9
Tetrahydrofuran (solvent)	Sigma-Aldrich,UK	99.9
Water (solvent)	Fischer Scientific,UK	99.9
Cyclohexane (solvent)	Fischer Scientific,UK	99.9
Methanol (solvent)	Fischer Scientific,UK	99.9
$PdCl_2$ solution (5 wt % in 10 wt % HCl)	Alfa Aesar,UK	99.9
Vanillin (GC standard/reactant)	Sigma-Aldrich,UK	99.0
Acetic Acid (GC standard)	Sigma-Aldrich,UK	99.0
Guaiacol (GC standard)	Sigma-Aldrich,UK	99.0
Vanillyl Alcohol (GC standard)	Sigma-Aldrich,UK	99.0
Creosol (GC standard)	Sigma-Aldrich,UK	99.0
Supports		
Activated Carbon (C)	Sigma-Aldrich,UK	n/a
Silica (SiO_2)	Alfa Aesar, UK	n/a
Alumina ($Y-Al_2O_3$)	Alfa Aesar, UK	n/a

3.3. Experimental Set-Up

A schematic of the rig used to perform all the experiments reported in this thesis is presented in Figure 3.1. It shows that the rig contained a 100 ml batch autoclave reactor made of stainless steel, an electric heating jacket, a mechanical stirrer, and ports for liquid product sampling and venting of gases. According to the operating manual provided by the manufacturer of the autoclave reactor, Parr, the maximum permissible temperature and pressure for safe operation

of the reactor is 648 K and 10 MPa. In addition, the reactor was accompanied by a Parr 4848 controller to control the reaction temperature and speed of agitation. The specification of the temperature control loop is presented in Table 3.2. The temperature control loop was applied to heat and maintain the reaction temperature, while at the end of reaction the reactor was cooled rapidly through an ice bath. Direct measurement of the actual temperature in the reactor was aided by a Type J thermocouple with uncertainty of ±2 K. While the pressure within the reactor was monitored through a pressure gauge with uncertainty of ±0.1 MPa.
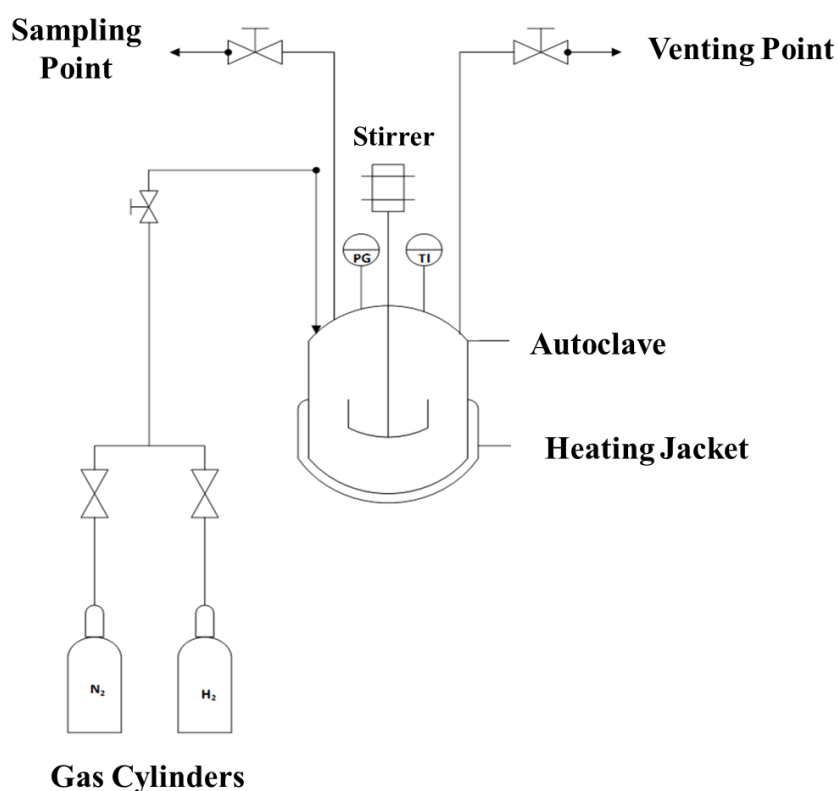
Fig. 3.1. Schematic of the rig used to conduct vanillin (VL) hydrodeoxygenation (HDO) experiments.

Table 3.2. Heating Loop Specification.

Parameters	Heating Loop	Units
Proportional Band	285	K
Integral Time	375	sec
Derivative	93	K/sec
Cycle Time	20	sec

3.3.1. <u>Standard Procedure</u>

The step by step procedure employed to set up the experiments reported in this work include:

1. Filling of the autoclave with pre-determined amount of solvent, catalyst and vanillin;

2. Sealing of the autoclave and flushing with nitrogen gas three times to create an inert atmosphere for the impending reaction;

3. Heating of the autoclave content gently under slow stirring rate of 150 rpm until the desired reaction temperature was achieved;

4. Addition of hydrogen gas to pressurise the autoclave content to the target value;

5. Ramping of the stirring rate from 150 rpm to the desired value of 1000 rpm.

It is worth mentioning that the point at which hydrogen gas was added to the autoclave represented the beginning of each experiment, and sample collected at this point denotes the initial concentration of vanillin. The end of each reaction was marked by the point at which the stirrer was stopped and the electric heating jacket was removed from the autoclave. At the end of each reaction, an ice bath was used to rapidly cool down the autoclave. The desired agitation speed of 1000 rpm used in the experiments eliminate external mass transfer resistances. This was established by conducting the experiments under different speed of agitation. As expected, findings from the literature[75, 160,221] was used to develop the standard procedure employed in this work.

3.3.2. <u>Preparation of Bimetallic PdRh/Al$_2$O$_3$ Catalyst</u>

This section summarises the step by step procedure followed to ensure successful impregnation of Pd metals into a commercial 5 wt % Rh/Al$_2$O$_3$ catalyst. A technique commonly reported in the literature for synthesising heterogeneous catalysts known as incipient wetness impregnation method was used to prepare the bimetallic PdRh/Al$_2$O$_3$ catalyst.[26, 74,230,231] In

order to prepare the metal precursor solution, 10.0 g of PdCl$_2$ solution was dissolved in 30ml of the impregnating solvent which is methanol. Subsequently 10.0 g of the commercial catalyst was added to the impregnating Pd metal solution under vigorous stirring using a magnetic stirrer to ensure the formation of a homogeneous mixture. The mixture was left under stirring for another 4 h and then dried overnight under atmospheric condition in the fume cupboard. In order to completely drive off volatile components, prior to calcination the resultant solid was further dried for a duration of 2 h in an oven set at 358 K. Finally, the solid was crushed and calcined at 773 K for 4 h to ensure deposition of the metals on the catalyst surface and remove any contaminant left. The calcination was conducted under static air in a quartz tube with the heating rate set at 5 K/min.

3.3.3. Experimental Procedure for Blank Investigation

In order to discern the role of support and non-catalytic effect in vanillin hydrodeoxygenation reaction, blank experiments were performed under no catalyst, activated carbon (C) support, alumina (Al$_2$O$_3$) support, and silica (SiO$_2$) support. These experiments were conducted at temperature of 338 K, hydrogen gas partial pressure of 2.0 MPa, agitation speed of 1000 rpm, feed vanillin concentration of 263 mM, 3.4 kg/m^3 support loading (mass of support in kg per unit volume of solvent in m^3), and batch time of 1 h with ethyl acetate as the solvent. The step by step process described in Section 3.3.1 was used to set up each of the experiments. It is worth mentioning that the feed concentration of vanillin selected for the blank experiment was driven by the desired operating condition.

3.3.4. Experimental Procedure for Catalyst Screening

In order to establish the hydrogen consumption during vanillin HDO reaction over the different catalysts, it was deemed necessary to conduct preliminary studies at 318 K, starting

hydrogen gas partial pressure of 5.6 MPa, starting vanillin concentration of 263 mM, agitation speed of 1000 rpm, and batch time of 0.5 h with ethyl acetate as the solvent. The catalysts considered in this screening investigation include commercial 5 wt % Pd/C catalyst, commercial 5 wt % Pt/C catalyst, commercial 5 wt % Pt/SiO$_2$ catalyst, commercial 5 wt % Pd/Al$_2$O$_3$ catalyst, commercial 5 wt % Rh/Al$_2$O$_3$ catalyst, and the prepared bimetallic 6.5 wt % PdRh/Al$_2$O$_3$ catalyst. These are noble metal catalysts renowned for excellent hydrogenating properties even at mild condition. From past studies on vanillin HDO reaction over palladium based catalyst in the literature[74, 76], a reaction time of 0.5 h is considered sufficient and therefore used in the preliminary studies. Likewise, to ensure the same amount of metals are involved in all the reactions, the loading of catalyst (i.e. mass of catalyst in kg per unit volume of solvent in m^3) used to conduct the experiments was 7.0 kg/m^3 for monometallic catalyst and 5.0 kg/m^3 for bimetallic catalyst. The loading of catalyst selected was driven by the feed concentration of vanillin. In the literature[71, 115,130], it has been documented that compounds such as vanillin with more than one oxygen atoms in their structure are prone to polymerisation especially at high temperatures. As a result, mild temperatures are used in the present work. Below a reaction temperature of 338 K, the kinetics of vanillin HDO reaction over Ru/C catalyst was successfully investigated by Bindwal et al.[160] Hence, HDO performance under the different catalysts was assessed in the present work at temperature of 338 K, hydrogen gas partial pressure of 2.0 MPa, agitation speed of 1000 rpm, feed vanillin concentration of 263 mM and batch time of 1 h using the standard experimental procedure described in Section 3.3.1. Finally, the stability of each of the catalyst was examined through reusability test. During the reusability test, catalysts were recovered from the reactor effluent through filtration and then dried at room condition overnight. Each catalyst was used three times at temperature of 338 K, hydrogen gas

partial pressure of 2.0 MPa, agitation speed of 1000 rpm, feed vanillin concentration of 263 mM and batch time of 1 h.

3.3.5. Experimental Procedure for Solvent Screening

From the review of past HDO studies in the literature [64, 70] on vanillin (VL) HDO reaction, it was established in Section 2.5.2 of Chapter 2 that conversion, and product distribution from VL HDO reaction are affected by the reaction solvent. As a result, VL HDO reaction over the prepared bimetallic PdRh/Al$_2$O$_3$ catalyst was conducted in six different solvents at 318 K temperature, 5.6 MPa hydrogen gas partial pressure, 263 mM feed vanillin concentration, 1000 rpm agitation speed, 5.0 kg/m^3 catalyst loading, and 0.5 h batch time. The solvents include water, cyclohexane, toluene, 2-propanol, ethylacetate, and tetrahydrofuran. By conducting VL HDO reaction in these solvents, it is possible to compare performance of the synthesised catalyst under the various classes of solvents. According to the literature [232], there are three classes of solvents, these includes:

- Polar protic solvents: These solvents have high polarity and hydrogen bond donor capability ($\alpha > 0.7$) e.g. water and 2-propanol;

- Aprotic polar solvents: These solvents have high polarity but low hydrogen bond donor capability ($\alpha \approx 0.0$) e.g. ethyl acetate and tetrahydrofuran;

- Aprotic apolar solvents: These solvents have no hydrogen bond donor capability, have extremely low dielectric constant (ε), and dipole moment (μ). Toluene and cyclohexane are typical examples of these solvent class.

The rationale behind the selection of more than one solvent from each class is to facilitate comparison within class.

3.3.6. Experimental Procedure for Process Parameter Investigation

To evaluate parametric interactions and determine the best combination of processing parameters that maximises catalytic performance, Taguchi method of experimental design was employed. This method of experimental design has been used in many engineering and manufacturing applications.[233] The processing parameters considered include temperature, hydrogen gas partial pressure, agitation speed and catalyst loading. Table 3.3 shows the levels for each of the processing parameters (i.e. control factors). To ensure liquid-phase only reaction, mild temperature and pressure are considered in this investigation. A commercial 10 wt % Pd/C catalyst was used to conduct this study, hence the consideration of low catalyst loadings in Table 3.3. The term catalyst loading used here refers to the weight of catalyst in kg per unit volume of the reaction solvent in m^3. It is worth mentioning that the solvent used is ethylacetate.

Table 3.3. Selected control factors and their values per level.

Control Factors	Control Factor Levels		
	Level 1	Level 2	Level 3
Reaction Temperature (K)	318	328	338
H_2 gas Partial Pressure (MPa)	1.0	2.0	3.0
Catalyst Loading (kg/m^3)	0.5	0.3	0.1
Agitation Speed (rpm)	500	700	900

The levels for agitation speed presented in Table 3.3 mirrored the range considered in the work of Bindwal et al[160] to eliminate mass transfer limitation. Based on the number of factors and levels shown in Table 3.3, using a factorial experimental design, 27 (i.e. 3^4) experiments will ensure the parameter space is completed. However, from Taguchi design of experiment it was established that 9 runs are required to determine the best combination of control factors

that maximises performance. Table 3.4 represents the standard L$_9$ orthogonal array of experiments designed through the Taguchi method. These experiments were conducted in duplicates using all three levels of each control factor. Catalytic performance which include conversion, degree of deoxygenation and ratio of deoxygenation to hydrogenation at different levels were analysed using the signal to noise (S/N) ratio. The S/N ratio at each level of the control factors was determined using "higher-the-better' function presented in equation 3.7. Other relevant formulae used are represented by equations 3.1 to 3.6.

Table 3.4. Designed Orthogonal Array of Experimental Conditions to Optimise Vanillin Hydrodeoxygenation Performance.

Run	T(K)	P$_H$(MPa)	ω(kg/m^3)	Agitation Speed (RPM)
1	318	1	0.5	500
2	318	2	0.3	700
3	318	3	0.1	900
4	328	1	0.3	900
5	328	2	0.1	500
6	328	3	0.5	700
7	338	1	0.1	700
8	338	2	0.5	900
9	338	3	0.3	500

Note: T is reaction temperature, P$_H$ is H$_2$ gas partial pressure, and ω is the weight of catalyst per unit volume of solvent.

$$X_{VL} \ (\%) \ = \frac{C_{VL0} - C_{VL}}{C_{VL0}} \times 100 \qquad (3.1)$$

$$S_{VA} \ (\%) \ = \frac{C_{VA}}{\sum C_i} \times 100 \qquad (3.2)$$

$$S_{CR} \ (\%) \ = \frac{C_{CR}}{\sum C_i} \times 100 \qquad (3.3)$$

$$DOD \ (\%) \ = \frac{C_{CR}}{C_{VL0}} \times 100 \qquad (3.4)$$

$$HYD \ (\%) \ = \frac{C_{VA}}{C_{VL0}} \times 100 \qquad (3.5)$$

$$DOD/HYD(\%) \ = \frac{C_{CR}}{C_{VA}} \times 100 \qquad (3.6)$$

$$S/N = -10 \log \left(\frac{1}{n} \sum_{i=1}^{n} \frac{1}{y_i^2} \right) \hspace{2cm} (3.7)$$

Herein C_{VL0} represents the starting concentration of vanillin, C_{VL} denotes the final concentration of vanillin, C_{VA} denotes the concentration of vanillyl alcohol formed, and C_{CR} represents the concentration of creosol formed. X_{VL} represents conversion, S_{VA} represents selectivity toward vanillyl alcohol, S_{CR} represents selectivity toward creosol, DOD represents degree of deoxygenation, HYD represents degree of hydrogenation, DOD/HYD represents relative rate of deoxygenation to hydrogenation, i is the number of replicate, and n is the number of trial experiments performed under each of the conditions in Table 3.4.

3.3.7. Experimental Procedure for Transport Limitation Verification

In order to model the kinetics of vanillin hydrodeoxygenation reaction it is necessary to collect the experimental data in the reaction-controlled regime. As a result, agitation speed and particle size test were conducted to rule out external and internal transport limitation. The prepared bimetallic 6.5 wt % $PdRh/Al_2O_3$ catalyst and commercial 10 wt % Pd/C catalyst were used to conduct the agitation test. Under the prepared bimetallic $PdRh/Al_2O_3$ catalyst, the test was carried out at 318 K temperature, 2.0 MPa hydrogen gas partial pressure, 3.4 kg/m^3 catalyst loading, 50 mins batch time, and 263 mM feed concentration of vanillin by varying the agitation speed from 100 rpm to 1300 rpm. In the case of commercial 10 wt % Pd/C catalyst, the test was conducted at 338 K temperature, 1.0 MPa hydrogen gas partial pressure, 0.27 kg/m^3 catalyst loading, 30 mins batch time, and 65 mM feed concentration of vanillin by varying the agitation speed from 300 rpm to 1100 rpm. The agitation test under the prepared bimetallic catalyst was conducted at a slightly lower temperature to reduce the likelihood of deactivation due to change in the catalyst support. In order to eliminate internal transport limitation, vanillin hydrodeoxygenation reactions were carried out using samples from different fractions of

commercial 2 wt % Pd/Al_2O_3 particles. Sieving technique was used to separate the Pd/Al_2O_3 particles into different size fractions; the size fractions include: particles >250 μm, particles within the range of 180 – 250 μm, particles within the range of 90 – 180 μm, and particles < 90 μm. Agitation speed was fixed at 1000 rpm during each of the experiments performed to investigate the effect of particle size on the reaction. In addition, liquid samples were collected in equally spaced time interval of 5 mins during the agitation speed and particle size experiments. To ensure less than 0.05 MPa loss in pressure during sampling, the volume of liquid collected per sample was fixed at 0.0005 dm^3 and fresh H_2 gas was added at the end of each sample collection. The standard procedure described in Section 3.3.1 was used to set up all the experiments. It is worth mentioning that the commercial 10 wt % Pd/C catalyst and synthesised bimetallic $PdRh/Al_2O_3$ catalyst were not available in different size fractions. As a result, the commercial 2 wt % Pd/Al_2O_3 catalyst available in different size fractions was used to probe the effect of particle size on the reaction.

3.3.8. Procedure used to investigate the Kinetics of Vanillin Hydrodeoxygenation Reaction over Monometallic and Bimetallic Palladium Based Catalysts.

The entries in Table 3.5 represent the conditions employed to investigate the kinetics of vanillin (VL) hydrodeoxygenation reaction over commercial 10 wt % Pd/C catalyst with ethyl acetate as the reaction solvent. Entries 1 – 6 in Table 3.5 was used to probe the effect of changes in catalyst loading (ω) on the initial rate of VL disappearance (r_0) at 318 K and 328 K. It is worth mentioning that probing the effect of changes in ω on r_0 at two different reaction temperatures is necessary to establish whether or not mass and heat transfer resistances exist in the system. Furthermore, the reaction conditions displayed in Table 3.5 are identical to those used in the work of Bindwal et al[160] on VL HDO reaction over Ru/C catalyst. The effect of changes in hydrogen gas partial pressure (P_H) on r_0 was probed by varying P_H over the range of 1 – 3 MPa

while keeping all other parameters at constant values (Table 3.5, entries 7 – 12). Subsequently, the initial concentration of VL (C_{VL0}) was varied between 35 mM and 65 mM with all other parameters kept at constant values to establish the influence of C_{VL0} on r_0 (Table 3.5, entries 13 – 20). The effect of temperature on r_0 was examined over the temperature range of 318 K – 338 K with all other variables kept constant (Table 3.5, entries 13, 17, and 21). Finally, the effect of adding products from the reaction to feed solution was tested at 328 K, 1000 rpm, 1.0 MPa, and 0.1 kg/m^3. Composition of the feed solution used to investigate the product effects include 55 mM vanillin and 10 mM vanillyl alcohol, 55 mM vanillin and 55 mM vanillyl alcohol, 55 mM vanillin and 10 mM creosol, 55 mM vanillin and 55 mM creosol.

Table 3.5. Overview of experimental conditions for VL HDO reaction kinetics over commercial 10 wt % Pd/C catalyst with ethyl acetate as solvent.

Entry	C_{VL0} (mM)	P_H (MPa)	T(K)	ω (kg/m^3)	t (mins)
1	65.0	1.0	318	0.1	40
2	65.0	1.0	318	0.2	40
3	65.0	1.0	318	0.3	40
4	65.0	1.0	328	0.1	40
5	65.0	1.0	328	0.2	40
6	65.0	1.0	328	0.3	40
7	65.0	1.0	318	0.3	40
8	65.0	2.0	318	0.3	40
9	65.0	3.0	318	0.3	40
10	65.0	1.0	328	0.3	40
11	65.0	2.0	328	0.3	40
12	65.0	3.0	328	0.3	40
13	35.0	1.0	318	0.1	40
14	45.0	1.0	318	0.1	40
15	55.0	1.0	318	0.1	40
16	65.0	1.0	318	0.1	40
17	35.0	1.0	338	0.1	40
18	45.0	1.0	338	0.1	40
19	55.0	1.0	338	0.1	40
20	65.0	1.0	338	0.1	40
21	35.0	1.0	328	0.1	40

C_{VL0} represent starting concentration of vanillin, P_H represent hydrogen gas partial pressure, T represent reaction temperature, ω represent catalyst loading, and t represent reaction time.

The kinetics of VL HDO reaction over commercial 5 wt % Pd/Al_2O_3 catalyst was probed using entries in Table 3.6 with ethyl acetate as the reaction solvent. Entries 1 – 8 in Table 3.6 depicts the conditions used to examine the effect of catalyst loading (ω) on initial rate of VL disappearance (r_0) at two different temperatures by varying ω between 2.0 and 5.0 kg/m^3 while all other parameters were kept at constant values. It is worth mentioning that the reaction time and concentrations used to investigate VL HDO reaction kinetics over Pd/Al_2O_3 catalyst is identical to those applied in Hao et al[76] work. The influence of hydrogen gas partial pressure (P_H) on initial rate of VL disappearance (r_0) was examined by varying P_H between 1.0 and 4.0 MPa while all other variables were kept at constant values (Table 3.6, entries 9 – 12). Likewise, the effect of starting vanillin concentration (C_{VL0}) on r_0 was investigated by varying C_{VL0} between 98 mM and 512 mM while all other variables were kept at constant values (Table 3.6, entries 13 – 16). Finally, the effect of temperature on initial rate of VL disappearance (r_0) was investigated in a temperature range of 308 – 328 K with all other variables kept constant (Table 3.6, entries 15, 17 – 18). Due to the high concentrations considered during VL HDO reaction over Pd/Al_2O_3 catalyst, the catalyst loading range was scaled up from the 0.1 – 0.3 kg/m^3 under Pd/C catalyst to 2.0 – 5.0 kg/m^3. The susceptibility of alumina support to deactivation at high temperature and polymerisation tendencies of vanillin was the rationale behind the temperature range of 308 – 328 K used to investigate the kinetics of VL HDO reaction over Pd/Al_2O_3 catalyst.

Table 3.6. Overview of experimental conditions for VL HDO reaction kinetics over commercial 5 wt % Pd/Al_2O_3 catalyst with ethyl acetate as solvent.

Entry	C_{VL0} (mM)	P_H (MPa)	T(K)	ω (kg/m^3)	t (mins)
1	263.0	2.0	308	2.0	60
2	263.0	2.0	308	3.0	60
3	263.0	2.0	308	4.0	60
4	263.0	2.0	308	5.0	60
5	263.0	2.0	318	2.0	60
6	263.0	2.0	318	3.0	60
7	263.0	2.0	318	4.0	60
8	263.0	2.0	318	5.0	60
9	263.0	1.0	308	5.0	60
10	263.0	2.0	308	5.0	60
11	263.0	3.0	308	5.0	60
12	263.0	4.0	308	5.0	60
13	98.0	2.0	318	5.0	60
14	189.0	2.0	318	5.0	60
15	350.0	2.0	318	5.0	60
16	512.0	2.0	318	5.0	60
17	350.0	2.0	308	5.0	60
18	350.0	2.0	328	5.0	60

C_{VL0} represent starting concentration of vanillin, P_H represent hydrogen gas partial pressure, T represent reaction temperature, ω represent catalyst loading, and t represent reaction time.

The kinetics of vanillin (VL) HDO reaction over the prepared bimetallic catalyst was examined using the entries in Table 3.7 with ethyl acetate as the solvent. Entries 1 – 8 in Table 3.7 depicts the conditions used to investigate the effect of catalyst loading (ω) on initial rate of VL disappearance (r_0) at 318 K and 328 K by varying ω between 2.0 and 5.0 kg/m^3 while all other parameters were kept at constant values. In a similar manner, the influence of hydrogen gas partial pressure (P_H) on r_0 was examined at 318 K by varying P_H between 1 and 4 MPa while all other variables were maintained at constant values (Table 3.7, entries 9 – 12). The effect of changes in starting concentration of vanillin (C_{VL0}) on r_0 was investigated at 318 K by altering C_{VL0} between 263 mM and 526 mM while all other parameters were maintained at constant values (Table 3.7, entries 13 – 16). Finally, the influence of reaction temperature (T) on r_0 was probed in a temperature range of 308 – 328 K with other variables kept at constant values.

Table 3.7. Overview of experimental conditions for VL HDO reaction kinetics over prepared 6.5 wt % PdRh/Al$_2$O$_3$ catalyst with ethyl acetate as solvent.

Entry	C_{VL0} (mM)	P_H (MPa)	T(K)	ω (kg/m^3)	t (mins)
1	263.0	3.0	318	2.0	50
2	263.0	3.0	318	3.0	50
3	263.0	3.0	318	4.0	50
4	263.0	3.0	318	5.0	50
5	263.0	3.0	328	2.0	50
6	263.0	3.0	328	3.0	50
7	263.0	3.0	328	4.0	50
8	263.0	3.0	328	5.0	50
9	263.0	1.0	318	5.0	50
10	263.0	2.0	318	5.0	50
11	263.0	3.0	318	5.0	50
12	263.0	4.0	318	5.0	50
13	263.0	2.0	318	5.0	50
14	351.0	2.0	318	5.0	50
15	438.0	2.0	318	5.0	50
16	526.0	2.0	318	5.0	50
17	263.0	2.0	308	5.0	50
18	263.0	2.0	328	5.0	50

C_{VL0} represent starting concentration of vanillin, P_H represent hydrogen gas partial pressure, T represent reaction temperature, ω represent catalyst loading, and t represent reaction time.

3.3.9. Procedure used to investigate the Kinetics of Vanillin Hydrodeoxygenation Reaction in Different Solvents.

As follow-up to the solvent screening experiments, the kinetics of vanillin (VL) hydrodeoxygenation (HDO) over the prepared bimetallic PdRh/Al$_2$O$_3$ catalyst in 2-propanol, toluene, and tetrahydrofuran was investigated under mild conditions. Possible deactivation of the PdRh/Al$_2$O$_3$ catalyst in large presence of water led to the decision to use 2-propanol as the representative polar protic solvent. Likewise, tetrahydrofuran was preferred to ethyl acetate as the representative aprotic polar solvent because the later was used extensively as the base solvent. Toluene was preferred to cyclohexane as the representative aprotic apolar solvent

because it was available in the laboratory in significant amount. Based on the literature[180, 181], the rate of VL HDO reaction has strong tendency to increase dramatically following a change in the reaction solvent. As a result, it was deemed necessary to investigate the kinetics of VL HDO reaction over PdRh/Al$_2$O$_3$ catalyst in the selected solvents over a temperature range of 298 K – 318 K. The kinetics of VL HDO reaction over PdRh/Al$_2$O$_3$ catalyst using 2-propanol as solvent was probed using the entries in Table 3.8. Entries 1 – 4 in Table 3.8 represent the conditions used to probe the effect of hydrogen gas partial pressure (P_H) on the initial rate of VL disappearance (r_0) at 318 K by varying P_H between 1.0 MPa and 4.0 MPa while all other variables were kept at constant values. The influence of starting concentration of vanillin (C_{VL0}) on r_0 was investigated at 318 K by altering C_{VL0} between 248 mM and 531 mM while all other parameters were maintained at constant values (Table 3.8, entries 5 – 8). In a similar manner, the effect of temperature (T) on r_0 was examined in the range of 298 K – 318 K with other parameters kept at constant values (Table 3.8, entries 6, 9 – 10).

Table 3.8. Overview of experimental conditions for VL HDO reaction kinetics over prepared 6.5 wt % PdRh/Al$_2$O$_3$ catalyst with 2-propanol as the solvent.

Entry	C_{VL0} (mM)	P_H (MPa)	T(K)	ω (kg/m^3)	t (mins)
1	598.0	1.0	318	5.0	60
2	598.0	2.0	318	5.0	60
3	598.0	3.0	318	5.0	60
4	598.0	4.0	318	5.0	60
5	248.0	2.0	318	5.0	60
6	351.0	2.0	318	5.0	60
7	427.0	2.0	318	5.0	60
8	531.0	2.0	318	5.0	60
9	351.0	2.0	298	5.0	60
10	351.0	2.0	308	5.0	60

C_{VL0} represent starting concentration of vanillin, P_H represent hydrogen gas partial pressure, T represent reaction temperature, ω represent catalyst loading, and t represent reaction time.

The kinetics of VL HDO reaction over PdRh/Al$_2$O$_3$ catalyst using toluene as solvent was examined under the conditions in Table 3.9. Entries 1 – 4 in Table 3.9 depicts the conditions used to investigate the effect of hydrogen gas partial pressure (P_H) on the initial rate of VL

disappearance (r_0) at 318 K by varying P_H between 1.0 MPa and 4.0 MPa with all other variables maintained at constant values.

Table 3.9. Overview of experimental conditions for VL HDO reaction kinetics over prepared 6.5 wt % PdRh/Al$_2$O$_3$ catalyst with toluene as the solvent.

Entry	C_{VL0} (mM)	P_H (MPa)	T(K)	ω (kg/m^3)	t (mins)
1	526.0	1.0	318	5.0	100
2	526.0	2.0	318	5.0	100
3	526.0	3.0	318	5.0	100
4	526.0	4.0	318	5.0	100
5	243.0	2.0	318	5.0	100
6	272.0	2.0	318	5.0	100
7	369.0	2.0	318	5.0	100
8	384.0	2.0	318	5.0	100
9	272.0	2.0	298	5.0	100
10	272.0	2.0	308	5.0	100

C_{VL0} represent starting concentration of vanillin, P_H represent hydrogen gas partial pressure, T represent reaction temperature, ω represent catalyst loading, and t represent reaction time.

The influence of starting concentration of vanillin (C_{VL0}) on initial rate of VL disappearance (r_0) was probed at 318 K by altering C_{VL0} between 243 mM and 384 mM, while all the other parameters were kept at constant values (Table 3.9, entries 5 – 8). Entries 6, 9 – 10 in Table 3.9 represent the conditions used to probe the effect of changes in reaction temperature (T) on (r_0) over the range of 298 K – 318 K with all other variables maintained at constant values. The kinetics of VL HDO reaction over PdRh/Al$_2$O$_3$ catalyst using tetrahydrofuran as solvent was examined under the conditions in Table 3.10. Entries 1 – 4 in Table 3.10 depicts the conditions used to probe the effect of hydrogen gas partial pressure (P_H) on r_0 at 318 K by varying P_H between 1.0 MPa and 4.0 MPa while all other parameters were maintained at constant values. The effect of changes in C_{VL0} on r_0 was examined at 318 K by varying C_{VL0} between 69 mM and 335 mM with the other variables kept at constant values (Table 3.10, entries 5 – 8). Entries 7, 9 – 10 in Table 3.10 represent the conditions used to probe the effect of changes in reaction

temperature (T) on (r_0) over the range of 298 K – 318 K with all other variables maintained at constant values.

Table 3.10. Overview of experimental conditions for VL HDO reaction kinetics over prepared 6.5 wt % PdRh/Al$_2$O$_3$ catalyst with tetrahydrofuran as the solvent.

Entry	C_{VL0} (mM)	P_H (MPa)	T(K)	ω (kg/m^3)	t (mins)
1	175.0	1.0	318	5.0	100
2	175.0	2.0	318	5.0	100
3	175.0	3.0	318	5.0	100
4	175.0	4.0	318	5.0	100
5	69.0	2.0	318	5.0	100
6	147.0	2.0	318	5.0	100
7	250.0	2.0	318	5.0	100
8	335.0	2.0	318	5.0	100
9	250.0	2.0	298	5.0	100
10	250.0	2.0	308	5.0	100

C_{VL0} represent starting concentration of vanillin, P_H represent hydrogen gas partial pressure, T represent reaction temperature, ω represent catalyst loading, and t represent reaction time. Reaction Solvent: Ethyl Acetate.

It is worth mentioning that differences in VL solubility and amount of VL consumed in the heating phase are responsible for the changes in range of VL starting concentration during the kinetic investigation of VL HDO reaction under the various solvents.

3.4. <u>Procedure used to investigate the Kinetics of Vanillin Hydrodeoxygenation Reaction in Binary Environments.</u>

At the discretion of this work author, a preliminary investigation was deemed necessary to evaluate the effect of other model compounds presence on vanillin (VL) conversion during hydrodeoxygenation (HDO) reaction of VL over the prepared bimetallic PdRh/Al$_2$O$_3$ catalyst in a binary environment. The readily available alternative model compounds of bio-oil in the laboratory at the time of this investigation include furfural, acetaldehyde, guaiacol, and acetic acid. As a result, these compounds were considered as possible secondary compounds in the

investigation of VL HDO reaction in binary environments. The composition of the binary mixtures used in the preliminary investigation are presented in Table 3.11.

Table 3.11. Composition of feed used to investigate inhibitory effect of common bio-oil model compounds on VL HDO reaction over prepared $PdRh/Al_2O_3$ catalyst with ethyl acetate as solvent.

S/N	Feed Composition				
	C_{VL}(mM)	C_{AA}(mM)	C_{GUA}(mM)	C_{FUR}(mM)	C_{ACET}(mM)
1	263	0	0	211	0
2	263	0	0	0	1004
3	263	1166	0	0	0
4	263	0	683	0	0

C_{VL} represent concentration of vanillin, C_{AA} represent concentration of acetic acid, C_{GUA} represent concentration of guaiacol, C_{FUR} represent concentration of furfural, and C_{ACET} represent concentration of acetaldehyde.

The composition of the mixtures in Table 3.11 were selected to reflect the ratios of the secondary compounds concentration to VL concentration in real bio-oil environment. This was achieved by multiplying a fixed VL concentration of 263 mM with established scale factor in the literature[234] relating concentration of VL to the concentration of the various secondary compounds in real bio-oil environment. A fixed VL concentration of 263 mM was arbitrarily selected because it was used frequently in previous investigation on VL HDO reaction over $PdRh/Al_2O_3$ catalyst with ethyl acetate as the solvent. The preliminary investigation was conducted at 318 K, 2.0 MPa, and 5.0 kg/m^3 using the feed compositions in Table 3.11 and ethyl acetate as the solvent. Subsequently, comprehensive investigation into the kinetics of VL HDO reaction over $PdRh/Al_2O_3$ catalyst in binary environments were conducted using the conditions in Table 3.12 and Table 3.13. Table 3.12 depicts the conditions used to investigate the kinetics of VL HDO reaction over $PdRh/Al_2O_3$ catalyst in the presence of acetic acid with ethyl acetate as the solvent. It is important to emphasise that the ratio in which VL exist to acetic acid (AA) in Table 3.12 represent their actual proportion in typical bio-oil. The effect of

hydrogen gas partial pressure (P_H) on initial rate of VL disappearance (r_0) was examined using entries 1 – 4 in Table 3.12 by varying P_H between 1.0 and 4.0 MPa while all other parameters were kept at constant values.

Table 3.12. Overview of experimental conditions for VL HDO reaction kinetics over prepared 6.5 wt % PdRh/Al$_2$O$_3$ catalyst in the presence of acetic acid with ethyl acetate as solvent.

Entry	C_{VL0} (mM)	C_{AA0}	P_H (MPa)	T(K)	ω (kg/m^3)	t (mins)
1	263.0	1166.0	1.0	318	5.0	60
2	263.0	1166.0	2.0	318	5.0	60
3	263.0	1166.0	3.0	318	5.0	60
4	263.0	1166.0	4.0	318	5.0	60
5	351.0	1559.0	2.0	318	5.0	60
6	438.0	1944.0	2.0	318	5.0	60
7	526.0	2331.0	2.0	318	5.0	60
8	263.0	1166.0	2.0	308	5.0	60
9	263.0	1166.0	2.0	328	5.0	60

C_{VL0} represent starting concentration of vanillin, C_{AA0} represent starting concentration of acetic acid, P_H represent hydrogen gas partial pressure, T represent reaction temperature, ω represent catalyst loading, and t represent reaction time.

The influence of starting VL concentration (C_{VL0}) on r_0 was investigated at 318 K by varying C_{VL0} and C_{AA0} according to entries 2, 5 – 7 in Table 3.12 with all other parameters maintained at constant values. Likewise, the effect of reaction temperature (T) on initial rate of VL disappearance (r_0) was probed in the range 308 K – 328 K using the conditions in entries 2, 8 – 9 of Table 3.12. Table 3.13 represent the conditions used to probe the kinetics of VL HDO reaction over PdRh/Al$_2$O$_3$ catalyst in the presence of guaiacol with ethyl acetate as the solvent. Entries 1 – 4 in Table 3.13 depicts the conditions used to investigate the effect of changes in hydrogen gas partial pressure (P_H) on r_0 at 318 K by varying P_H between 1.0 MPa and 4.0 MPa while all other variables were kept at constant values. In the same manner, the influence of starting VL concentration (C_{VL0}) on r_0 was probed at 318 K by varying C_{VL0} and C_{GUA0} according to entries 2, 5 – 6 in Table 3.13 with all other variables maintained at constant values. Finally, the influence of T on r_0 was examined in the range 308 K – 328 K using the conditions in entries

2, 7 – 8 of Table 3.13. It is worth mentioning that the range of temperatures and concentrations of VL used in the vanillin – acetic acid and vanillin – guaiacol environments are based on those used in previous investigation on vanillin-only environment.

Table 3.13. Overview of experimental conditions for VL HDO reaction kinetics over prepared 6.5 wt % PdRh/Al$_2$O$_3$ catalyst in the presence of guaiacol with ethyl acetate as solvent.

Entry	C$_{VL0}$ (mM)	C$_{GUA0}$	P$_H$ (MPa)	T(K)	ω (kg/m^3)	t (mins)
1	263.0	683.0	1.0	318	5.0	60
2	263.0	683.0	2.0	318	5.0	60
3	263.0	683.0	3.0	318	5.0	60
4	263.0	683.0	4.0	318	5.0	60
5	351.0	912.0	2.0	318	5.0	60
6	438.0	1139.0	2.0	318	5.0	60
7	263.0	683.0	2.0	308	5.0	60
8	263.0	683.0	2.0	328	5.0	60

C$_{VL0}$ represent starting concentration of vanillin, C$_{GUA0}$ represent starting concentration of guaiacol, P$_H$ represent hydrogen gas partial pressure, T represent reaction temperature, ω represent catalyst loading, and t represent reaction time.

3.5. Nitrogen Gas Adsorption

The procedure widely reported in the literature for determining the textural properties of solid catalysts such as specific surface area, specific pore volume, and average pore size is gas adsorption experiments.[235] Presently, nitrogen gas is generally considered the most suitable adsorbate for these experiments because it does not react with the catalyst surface, is available in high purity, and the molecular size is well defined in the literature.[236] Hence, in conformity with ASTM C1274, nitrogen gas adsorption experiments were performed at liquid nitrogen temperature of 77 K using Micromeritics Analytical Instrument ASAP 2010 to determine the textural properties of all the catalysts used in this work. In order to remove physisorbed species from the surface of the adsorbents i.e. catalysts, it was deemed necessary to degas catalyst samples at the conditions presented in Table 3.14. These conditions were obtained from the literature. However, in practice through thermogravimetric analysis the decomposition

temperature of the catalyst samples can be establish and use to determine the appropriate temperature to degas each of the catalyst sample. The general rule of thumb is that the degassing process takes place at half the decomposition temperature. In the present work, on-going maintenance work did not permit determination of the catalyst samples decomposition temperature. This limitation compelled the author of this work to use the literature values in Table 3.14 to degas the catalyst samples. Upon completing the degassing process, liquid nitrogen was used to cool down the samples to 77 K. In order to measure complete adsorption isotherm, the pressure (P) above each sample was gradually increased until it closely approached the saturation pressure (P_0) of 101.3 kPa. During the process of increasing P, the adsorbent samples remove some of the nitrogen gas. The quantity of adsorbed gas and the corresponding equilibrated pressure were recorded every 20 s to enable plots of adsorbed gas quantity against the equilibrium relative pressure (P/P_0). From these plots the specific surface area of each catalysts was determined by applying the widely accepted Brunauer, Emmet, and Teller (BET) method in the appropriate range of P/P_0 to satisfy the required linearity condition for BET validity.

Table 3.14. Degassing Conditions.

Catalyst	T(K)	t(h)
Pd/C	623	12
Pt/C	373	4
Pd/Al$_2$O$_3$	523	4
Rh/Al$_2$O$_3$	523	4
PdRh/Al$_2$O$_3$	523	4
Pt/SiO$_2$	393	2

The BET equation which relates the measured amount of gas adsorbed at standard temperature and pressure (STP) to P/P_0 is presented in equation 3.5. It shows that when the underlying assumptions of BET method are satisfied, the plot of measured amount of gas

adsorbed $\frac{P}{V(P_0-P)}$ against the equilibrium relative pressure $\frac{P}{P_0}$ gives a straight line. The slope of

this line denoted as "s" is represented by equation 3.6, while the intercept denoted as "i" is

represented by equation 3.7. Hence, solving equations 3.6 and 3.7 produces equations 3.8 and

3.9 which represents the monolayer capacity "V_m" and the BET constant "C".

$$\frac{P}{V(P_0-P)} = \frac{1}{V_m C} + \frac{(C-1)P}{V_m C P_0} \qquad (3.5)$$

$$s = \frac{(C-1)}{V_m C} \qquad (3.6)$$

$$i = \frac{1}{V_m C} \qquad (3.7)$$

$$V_m = \frac{1}{s+i} \qquad (3.8)$$

$$C = \frac{s}{i} + 1 \qquad (3.9)$$

The specific surface area of each catalysts was then calculated from the estimated V_m using

equation 3.6.

$$S_{BET} = \frac{V_m n_a a_m}{m_V} \qquad (3.10)$$

Herein n_a is the Avogadro's number (6.022×10^{23} molecules/mol), a_m is the cross-sectional

area occupied by each adsorbate molecule at 77 K (0.162 nm^2), and m_V is the volume of one

mole of an ideal gas at STP (0.0224 m^3/mol). The BET plots and calculations are presented in

appendix A3.1. In order to determine the total specific pore volume (V) and average pore size

(d_{AVG}) for each of the catalysts, the measured amount of adsorbed gas at the maximum

equilibrium relative pressure (V_{gas}) was converted to the volume of liquid nitrogen (V_{liq})

through equation 3.11. It is worth mentioning that this method is based on the assumption that

pores of the catalysts were filled with liquid nitrogen. Under the assumption that existing pores

in each of the catalysts are cylindrical, d_{AVG} was estimated from V through equation 3.12.

Herein V_N is the molar volume of liquid nitrogen (34.6 cm^3/mol).

$$V = V_{liq} = \frac{V_{gas} \times V_N}{m_V} \qquad (3.11)$$

$$d_{AVG} = \frac{4V}{S_{BET}} \qquad (3.12)$$

3.5.1. Mercury Intrusion Porosimetry

Autopore[TM] IV 9500 Micromeritics mercury porosimeter was employed to determine other important properties such as porosity, characteristic length, and apparent density of the catalysts used to investigate the kinetics of vanillin hydrodeoxygenation reaction. The operation of this equipment is based on the basic principle that mercury is a non-wetting liquid and therefore requires external pressure to penetrate the pores of porous materials such as Pd/C, Pd/Al$_2$O$_3$, and PdRh/Al$_2$O$_3$ catalysts through capillary action.[237] The Washburn equation presented in equation 3.13 relates the required external pressure (P) to the pore size (D$_P$), contact angle between mercury and the surface (θ), and surface tension of mercury (Y).[238] Clearly, on the basis of this equation an inverse relationship exists between P and D$_P$. Hence, the low and high pressure chambers of the equipment were used during each of the analysis conducted.

$$P = \frac{4\gamma\cos\theta}{D_p} \qquad (3.13)$$

In a standard analysis, the weight of empty penetrometer was determined and used to calibrate the equipment. Subsequently, the weight of penetrometer containing the sample was measured and then placed in the low pressure chamber. The low pressure chamber operates over the range of 0 to 345 kPa, here filling of the penetrometer with mercury occurs. Prior to starting the high pressure analysis, the combined weight of the penetrometer, sample and mercury was measured and recorded. In the high pressure chamber, changes in volume of mercury was continuously recorded as applied pressure increases from 0.1 MPa to 228 MPa to generate the intrusion curve. Finally, as the applied pressure decreases from 228 MPa to 0.1 MPa changes in volume of mercury was constantly recorded to establish the extrusion curve. It is worth

mentioning that the Washburn equation derivation was based on the assumption that porous materials contain cylindrical shaped pores with circular cross-section.[237] Hence, equation 3.14 represents the characteristic length of the catalyst particles. The porosity of the catalysts was estimated from equation 3.15, while equation 3.16 was used to determine the apparent density of the catalysts.

$$L = \frac{4V}{\pi D_p{}^2} \qquad (3.14)$$

$$P_{pc} = \frac{100 \times V_{tot}}{V_b} \qquad (3.15)$$

$$\rho_s = \frac{W_s}{V_s} \qquad (3.16)$$

where L is the characteristic length of the catalyst pore, V is the cylindrical pore volume, D_P is the pore diameter, P_{PC} is the porosity of the catalyst in percentage, V_{tot} is the total intrusion volume, V_b is the bulk volume of the sample, ρ_s is the apparent catalyst density, W_s is the weight of the sample, and V_s is the skeletal volume of the sample.

3.5.2. Scanning Electron Microscopy (SEM)-Energy Dispersive X-Ray (EDX) Analysis

The differences in surface morphology and texture of fresh and spent catalysts were investigated through HITACHI TM3030Plus Tabletop Scanning Electron Microscope (SEM) equipped with Energy Dispersive X-ray (EDX) analyzer. Figure 3.2 shows the workstation and components of the SEM-EDX analyzer. All the images were captured under the EDX mode using 15 kV accelerating voltage and working distance of 7 mm to 10 mm. The selected accelerating voltage ensures images with the best resolution were captured.

Fig. 3.2. HITACHI TM3030Plus Tabletop Scanning Electron Microscope Main Unit Front View. Components: 1- AIR mode indicator, 2- EVACUATION mode indicator, 3- Specimen Stage, 4- EVAC/AIR Switch, and 5 - X & Y axes control knobs.

The step by step procedure used to operate the equipment involves: i) pressing the EVAC/AIR switch labelled 4 to safely open the specimen stage denoted as 3 for placement of the sample holder which contain the sample material; ii) Use of X&Y axes control knobs labelled 5 to adjust the position of the sample material vertically and horizontally to enhance the focus of electron beam on the material; iii) pressing the EVAC/AIR switch to evacuate the specimen stage and commence the actual measurement; iv) selection of EDX as the source as oppose to secondary or back scattered electron to ensure the X-ray signals originate from further down into the sample surface and allow elemental composition determination; v) selection of 800X as the magnification. To determine the size of catalyst particles displayed on the captured SEM micrographs, a software imaging tool known as "image J" was employed. The software assumes all particles are circular in nature and therefore utilises the expression for area of a

circle in determining the size of particles on display in each of the SEM micrographs. It is worth mentioning that the particles counted from the single SEM images of the commercial catalysts were above 500.

3.5.3. Powdered X-Ray Diffraction (XRD) Analysis

A commonly reported method in the literature for identifying the phases present in solid materials, and estimate the average metal particle size is X-Ray Diffraction (XRD) analysis.[1, 221,239–241] XRD analysis relies on the fact that when a beam of X-ray photons are incident on a solid material such as a catalyst they undergo diffraction from the different planes of atoms within the material to produce distinct diffraction pattern. This diffraction pattern provides a fingerprint of the crystalline phases present in the material.[242] A Bruker AXS GmbH (D8 Advanced XRD, Karlsruhe, Germany) with a Braun detector and Cu K_α radiation was used to record the intensity, shape, position and width of the diffraction lines for each of the catalysts examined in the present work. The data generator was operated over the range of 5° to 100° using step size of 0.04°, count time of 22.35 s, constant wavelength of 1.54 Å, and scan rate of 1°/min. The diffraction patterns obtained were compared to literature to ensure accurate conclusion on the phases present in the various catalysts. In order to estimate the average metal particle size from the recorded XRD data, Scherrer's formula presented in equation 3.17 was employed by the analytical software package known as DIFFRAC.EVA which accompanied the XRD measuring equipment.

$$L = \frac{k\lambda}{\beta cos\theta} \qquad (3.17)$$

Herein L represents the average metal particle size, k denotes the designated shape factor for the particles, λ represent the known wavelength of X-ray source which is 1.54 Å, β stands for

full width at half maxima (FWHM) of the most intense diffraction peak, and θ is the Bragg angle.

3.5.4. Gas Chromatography (GC) Analysis

To identify the products formed from the reactions conducted, liquid samples collected were sent to the Department of Chemistry for comprehensive analysis via a Shimadzu gas chromatography unit coupled to a mass spectrometer (GC-MS). Consequently, multipoint calibration curves for vanillin and the identified products which include vanillyl alcohol, creosol, and guaiacol were developed using an automated Trace gas chromatography unit equipped with flame ionization detector (GC-FID) shown in Figure 3.3.
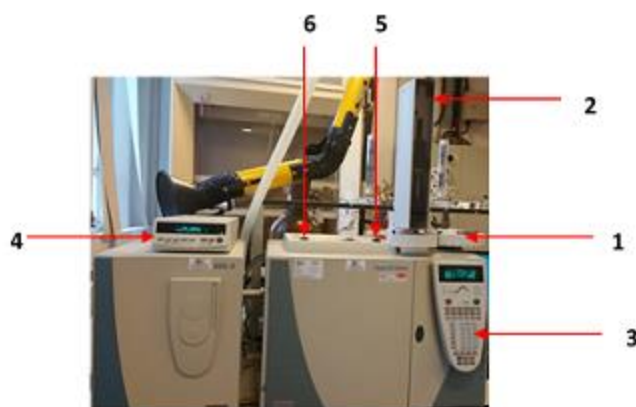
Fig. 3.3. Thermo Trace GC Ultra equipped with a 90 tray and autosampler unit used to analyse liquid samples from reactions. Components: 1-trays, 2-syringe compartment, 3-control panel to manually configure the GC, 4-control panel for adjusting autosampler setting, 5-injector side, and 6-detector side.

On the basis of recommendation from leading experts on GC analysis in the Department of Chemistry, a mild polar capillary column that goes by the commercial name Zebron Zb-Wax-Phenomenex was deemed suitable for the GC-FID analysis conducted in-house. The ZB-Wax column utilised has a specification of 250 μm internal diameter, 0.25 μm film thickness, 30 m column length, and temperature limits of 313 to 523/533 K. As a result the temperature program

applied to analyse the samples include a ramp of 10 K/min from an initial oven temperature of 313 K to a final temperature of 523 K, followed by isothermal operation at 523 K for additional 5 mins. The settings for other important parameters include a constant split ratio of 1:50, injector temperature of 513 K, and detector temperature of 523 K. This GC method was not developed by the author of this work. The method was previously applied in the work of Huang et al[71] on homogeneous catalytic hydrogenation of vanillin. During standard operation of the GC-FID, the 10 µl syringe in the syringe compartment was cleaned at least 5 times to prevent contamination. Subsequently, the syringe was used to withdraw liquid sample of 0.5 µl from the vial situated in a specified position on the tray for injection into the GC. The variability between injections using coefficient of variation was measured to be in the range of 0.05% to 3.62%. In general, GC analysis is based on the theory that components within any sample interact differently with the column. As a result of the expected variation in the strength of interaction of the components with the column, these components exit the column for detection by the FID at different retention times. The retention times of the components established from injecting standard samples and their respective boiling points are presented in Table 3.15.

Table 3.15. Retention Time and Boiling Point of Compounds.

Compound	Boiling Point (K)	Retention Time (min)
Vanillin	558	18.68 ± 0.01
Vanillyl Alcohol	566	20.59 ± 0.02
Creosol	494	12.71 ± 0.02
Guaiacol	478	11.65 ± 0.01

To determine the quantity of vanillin and products in the liquid samples analysed, peaks at the expected retention times for the components were integrated using the software tools which accompanied the GC-FID. Subsequently, the areas were converted to concentrations via the developed multipoint calibration curves presented in appendix A3.2.

3.5.5. CO Pulse Chemisorption Measurement

Due to unavailability of equipment, CO pulse chemisorption using a Quantachrome ChemBet Pulsar TPR/TPD equipped with a thermal conductivity detector (TCD) was used to determine the metal dispersion, metal particle size, and metallic surface area of Pd/C and PdRh/Al$_2$O$_3$ catalysts. The measurements were performed by Dr. Helen Daly at the University of Manchester. In a standard experiment, 40 mg of the catalyst was loaded into a quartz U-tube reactor and reduced at 573 K for 1 h under 5% H$_2$/Ar gases mixture. Subsequently, the reactor was purged using Helium gas and cooled down to 193 K. Finally, the CO chemisorption measurement was performed using 1% CO/He gases mixture at 193 K. In order to estimate the metal particle size, metallic surface area, and metal dispersion from the CO chemisorption data, catalyst particles were assumed to be hemispherical and a stoichiometric factor of 2 was considered appropriate for the calculations.

3.5.6. X-Ray Fluorescence (XRF) Method

One of the most widely used analytical method for determining the elemental composition of catalysts is the X-Ray Fluorescence (XRF) [243, 244]. The XRF method is preferred to alternatives such as inductively coupled plasma mass spectrometry because it is independent of the chemical bonding of the elements present in the unknown sample. Moreover, it requires less complicated sample preparation technique, consume less time, and the best method for elemental analysis[244]. The basic principle behind the XRF method is that the unknown sample is bombarded with X-ray beams which in turn ejects electrons out of the innermost atomic shells (i.e. K and L) of elements to create vacancies.[243] Electrons from the outer atomic shells with higher energies then drop to occupy the vacancies in the innermost atomic shells. As electron drops from the higher energy atomic shell into the vacancies, excess energies are emitted as X-ray fluorescence

radiation. The emitted X-ray fluorescence radiation has characteristic wavelength for each of the element present in the sample. In the present work, elemental analysis of the prepared bimetallic $PdRh/Al_2O_3$ catalyst was carried out by Dr. Laura Driscoll at the Department of Chemistry using a wavelength Dispersive X-Ray Fluorescence Spectrometer (WD-XRF) S8 Bruker with a rhodium tube operated at 4 kW. 300 mg of powdered catalyst sample was used to conduct the measurement and the oxide program on the machine was used to analyse the result.

Chapter 4

Effect of Catalyst, Solvent and Processing Condition on Vanillin Upgrading via Hydrodeoxygenation Reaction.

4.1. Introduction

Research studies on the upgrading of model compounds through hydrodeoxygenation (HDO) reaction in the literature were reported to be carried out at temperatures of 373 K – 673 K, hydrogen gas pressures of 0.04 MPa – 13.8 MPa under different catalysts and solvents.[125, 130,213] The differences in processing conditions (i.e. temperature, hydrogen gas partial pressure, catalyst loading, and agitation speed), solvents and catalysts make comparison of studies in the literature difficult. In this chapter, the effect of changes in catalyst, solvent, and processing condition on HDO reaction were studied systematically using vanillin, a prominent component of real bio-oil. The results in this chapter represent a more complete and systematic evaluation of the parameters affecting vanillin HDO compared to those previously reported in the literature. The textural properties, surface morphology, and composition of the catalysts (i.e. Pd/C, Pt/C, Pt/SiO$_2$, Pd/Al$_2$O$_3$, Rh/Al$_2$O$_3$, and PdRh/Al$_2$O$_3$) used in the investigation are presented in Section 4.2. In Section 4.3, the result of blank experiments performed to examine non-catalytic and catalyst support effect on vanillin HDO reaction is presented. While Section 4.4 sheds light on the effect of changes in active element of the catalyst on HDO reaction of vanillin. In Section 4.5, the effect of solvent on HDO reaction of vanillin is presented. Finally, the effects of processing conditions on vanillin HDO reaction are presented in Section 4.6. Indicators commonly used to assess HDO performance include conversion, product selectivity, degree of deoxygenation, hydrogen consumption, and catalyst stability.[129, 135,149,172] As a result,

these indicators were used in this chapter to evaluate vanillin HDO performance under the different catalysts, solvents, and processing conditions.

4.2. Catalyst Characterisation

4.2.1. Nitrogen (N$_2$) Physisorption Isotherms

The N$_2$ adsorption-desorption isotherms obtained for each of the catalyst are presented in Figures 4.1a to 4.1c.
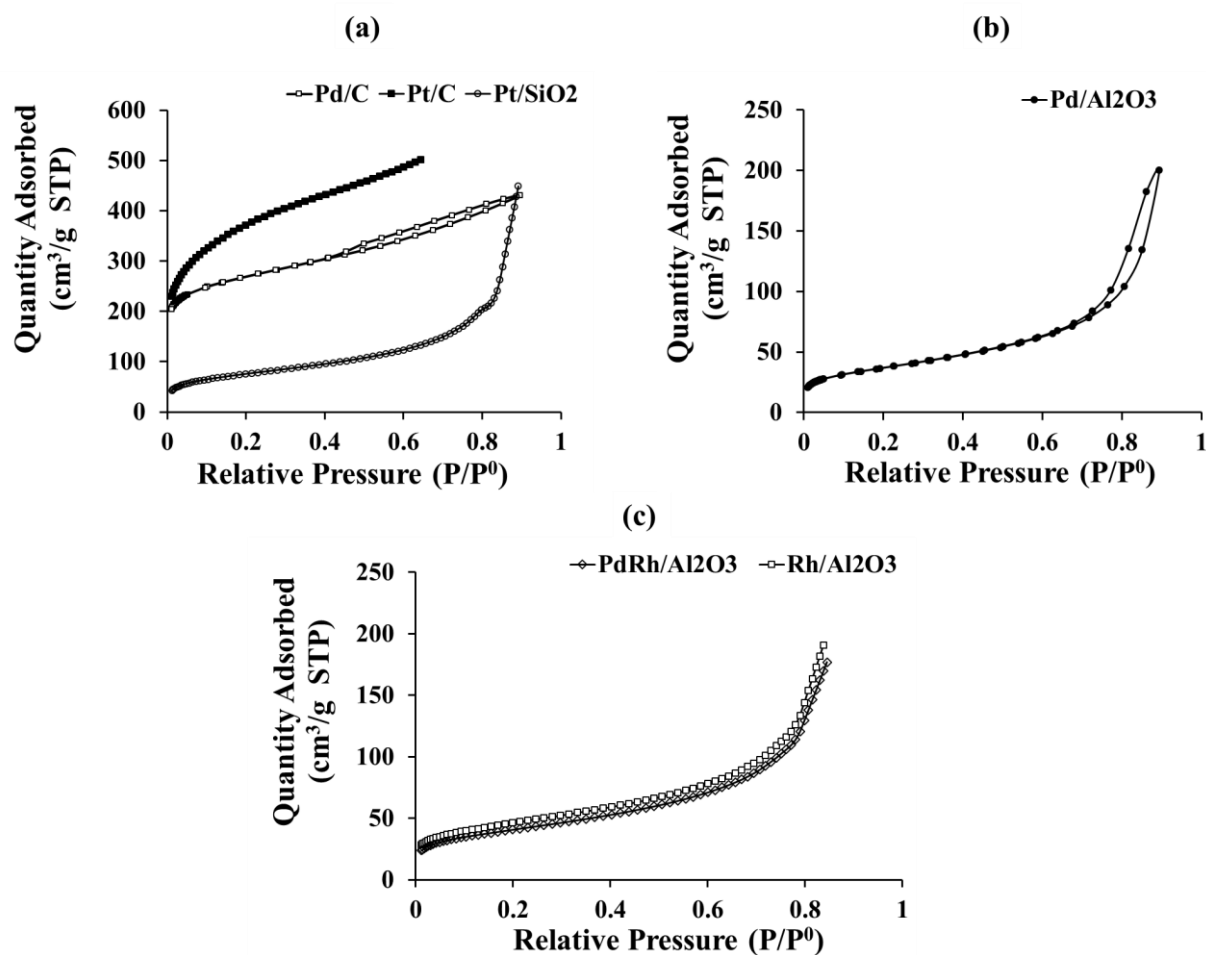
Fig. 4.1. N$_2$ adsorption-desorption isotherms of (a) 5 wt % Pd/C, 5 wt % Pt/C, and 5 wt % Pt/ SiO$_2$ catalysts, (b) 5 wt % Pd/Al$_2$O$_3$ catalyst , and (c) 6.5 wt % PdRh/Al$_2$O$_3$, and 5 wt % Rh/Al$_2$O$_3$ catalysts.

Figure 4.1 shows significantly higher levels of adsorption for activated carbon supported catalysts (i.e. Pd/C and Pt/C) at low relative pressures (P/P^0) compared to alumina and silica

supported catalysts. This suggest activated carbon supported catalysts have lower average pore sizes than those supported on either alumina or silica. The adsorption-desorption isotherm for Pd/C catalyst in Figure 4.1a is concave relative to P/P^0 axis and the adsorbed amount approaches a limiting value of 431 cm^3/g as P/P^0 tends to 1, these characteristics are in conformity with the expected features of Type I isotherm normally displayed by catalysts supported on activated carbon. It is well documented that micropores filling are responsible for the initial steep part which resulted into the concave shape while multilayer adsorption on small external area accounts for the low slope of the plateau.[245,246] On this basis it can be concluded that micropores are present in the Pd/C catalyst. Furthermore, the H4 hysteresis loop displayed in the adsorption-desorption isotherm of Pd/C catalyst in Figure 4.1a confirms the presence of mesopores.[235] Notably, the adsorption-desorption isotherm of Pt/C catalyst in Figure 4.1a displayed expected features of Type I curve and thus reinforces the claim in literature about catalysts supported on activated carbon.[245,246] In contrast, the adsorption-desorption isotherms of silica and alumina supported catalysts in Figures 4.1a , 4.1b, and 4.1c are less concave in shape relative to the P/P^0 axis when compared to the isotherms of the activated carbon supported catalysts. This suggests alumina and silica supported catalysts (i.e. Pd/Al_2O_3, Rh/Al_2O_3, $PdRh/Al_2O_3$, and Pt/SiO_2) contained less micropores. Infact, the adsorption-desorption isotherm of Pd/Al_2O_3 catalyst in Figure 4.1b displayed characteristic hysteresis loop usually attributed to Type IV isotherms and exhibits a plateau with reduced limiting adsorption value of 200 cm^3/g at high P/P^0. As oppose to the H4 type hysteresis loop found in Pd/C catalyst adsorption-desorption isotherm in Figure 4.1a, the adsorption-desorption isotherm of Pd/Al_2O_3 catalyst in Figure 4.1b contain H2 type hysteresis loop. This shows that Pd/Al_2O_3 catalyst contained complex, interconnected pore structure with narrow pore openings, while the Pd/C catalyst contained narrow slit-like pores that are usually associated to micropores.[247, 248] The

observed difference in pore structure of these two Pd-based monometallic catalysts highlight the effect of change in support on a catalytic system. It is worth mentioning that the observed hysteresis loops in both Pd/C and Pd/Al$_2$O$_3$ catalysts is a testament to the sequence of multilayer adsorption followed by capillary condensation within the mesopores of these catalysts.[235] The Brunauer – Emmett – Teller (BET) method was used to determine the specific surface area of the catalysts from their isotherm data. In conformity with the standard procedure for computing the specific surface area via BET method, isotherm data within the relative pressure range of 0.05 to 0.30 were used for the less porous catalysts which include Pd/Al$_2$O$_3$, Rh/Al$_2$O$_3$, PdRh/Al$_2$O$_3$, and Pt/SiO$_2$.[246] However, for the highly porous catalysts such as Pd/C and Pt/C, isotherm data within relative pressures below 0.04 were deemed appropriate to comply with Rouquerol et al.,[249] recommendation for materials containing appreciable amount of micropores. The BET plots obtained for the catalysts are presented in Figure A3.1 of appendix A3.1. Table 4.1 summarises the specific surface areas (S$_{BET}$), BET constant (C), total specific pore volumes (V), and average pore sizes (d$_{AVG}$) of the catalysts.

Table 4.1. Textural Properties of Catalysts from N$_2$ Adsorption-Desorption Isotherms.[250]

Catalyst	S$_{BET}$ (m^2/g)	S* (m^2/g)	BET Constant (C)	V (cm^3/g)	V* (cm^3/g)	d$_{AVG}$ (nm)
5 wt.% Pd/C	989	1050	734	0.659	0.610	2.7
5 wt.% Pt/C	1241	1023	351	0.768	0.790	2.5
5 wt.% Pd/Al$_2$O$_3$	131	110	166	0.306	N/A	9.3
5 wt.% Rh/Al$_2$O$_3$	164	100	265	0.292	0.40	7.1
6.5 wt.% PdRh/Al$_2$O$_3$	145	N/A	150	0.271	N/A	7.5
5 wt.% Pt/SiO$_2$	266	400	182	0.687	N/A	10.3

[S$_{BET}$: BET measured specific surface area, S*: strem manufacturer specific surface area, V: total specific pore volume calculated from nitrogen physisorption data, V*: strem manufacturer pore volume, d$_{AVG}$: measured pore volume from the nitrogen physisorption data, N/A: not available].

Table 4.1 shows that C values obtained from BET analysis of the catalysts nitrogen adsorption-desorption isotherm ranges between 150 and 734. From the literature, C values below 20 indicates invalid BET method and strong interaction between the adsorbate N_2 gas and the adsorbent surface.[249,251] Hence, the BET method applied to estimate the surface areas of the catalysts is valid since values obtained for the BET constants are significantly greater than 20. According to the literature C values above 200 indicates significant porosity.[249,251] Indeed, the C values obtained for the activated carbon supported catalysts were significantly greater than 200 and thus reaffirms the claim of significant porosity in Pt/C and Pd/C catalysts. In contrast, C values for the less porous catalysts such as Pt/SiO_2, Pd/Al_2O_3, and $PdRh/Al_2O_3$ lies within the typical range of 100 to 200. Most importantly, the values presented in Table 4.1 are in conformity with those reported in the literature.[74,252–254] In addition, Table 4.1 shows that estimated values from the catalysts physisorption data reasonably agrees with those reported in strem manufacturer's manual on properties of commercial heterogeneous catalysts. Interestingly, Table 4.1 shows that the average pore size of all the catalysts ranges between 2.5 nm to 10.3 nm. Based on IUPAC classification of pores, all the catalysts are mesoporous materials.[255] In summary, the trend in average pore sizes of the catalysts follows the order: $Pt/SiO_2 > Pd/Al_2O_3 > PdRh/Al_2O_3 > Rh/Al_2O_3 > Pd/C > Pt/C$. Whereas in terms of total specific pore volume, the trend is $Pt/C > Pt/SiO_2 > Pd/C > Pd/Al_2O_3 > Rh/Al_2O_3 > PdRh/Al_2O_3$. The trend in specific surface area of the catalysts follows the order: $Pt/C > Pd/C > Pt/SiO_2 > Rh/Al_2O_3 > PdRh/Al_2O_3 > Pd/Al_2O_3$. As expected the highly porous activated carbon supported catalysts have the smallest average pore size and largest specific surface area. Negligible differences exist in the average pore size of the two activated carbon supported catalysts. However, the total specific pore volume of Pt/C catalyst is 17% bigger than the total specific pore volume of Pd/C catalyst. This suggest the former catalyst contain more pores. As

a result, the specific surface area of Pt/C catalyst is 26% bigger than the specific surface area of Pd/C catalyst. This analysis highlights modification which takes place in the pore structure of a catalytic system following change in the catalyst active element. Similar effect can be observed between Pd/Al$_2$O$_3$ and Rh/Al$_2$O$_3$ catalysts, on average the pore size of Rh/Al$_2$O$_3$ is 24% smaller than the pore size of Pd/Al$_2$O$_3$ catalyst. Consequently, the specific surface area of Rh/Al$_2$O$_3$ catalyst is 25% bigger than the specific surface area of Pd/Al$_2$O$_3$ catalyst. Notably, the average pore size of the prepared bimetallic PdRh/Al$_2$O$_3$ catalyst is approximately the same as that of the precursor Rh/Al$_2$O$_3$ catalyst. However, the total specific pore volume of the in-house prepared bimetallic PdRh/Al$_2$O$_3$ catalyst is approximately 7% lower than that of Rh/Al$_2$O$_3$ catalyst. This suggest slight reduction in the number of alumina pores post impregnation of Pd into the Rh/Al$_2$O$_3$ catalyst. As a result, the specific surface area of the prepared bimetallic catalyst is approximately 12% lower than the specific surface area of the precursor Rh/Al$_2$O$_3$ catalyst. Plausible reasons for the decrease in the number of alumina pores include high Pd loading and deposition of Pd nanoparticles into pores of the alumina support. However, the insignificant change in average pore size confirmed negligible difference between the pore size distribution (PSD) of the unmodified Rh/Al$_2$O$_3$ and Pd-modified Rh/Al$_2$O$_3$ catalyst. Hence, integrity of the alumina support was maintained despite the observed changes in specific pore volume and surface area.

4.2.2. Scanning Electron Microscopy (SEM)-Energy Dispersive X-Ray (EDX) Analysis

The surface morphology of all the catalysts was examined using Scanning Electron Microscopy (SEM)-Energy Dispersive X-ray (EDX) spectroscopy analysis. In addition, this analysis was used to determine the size range of particles present in each of the catalyst. The SEM image and elemental mapping of the commercial 5 wt % Rh/Al$_2$O$_3$ catalyst used to prepare a bimetallic PdRh/Al$_2$O$_3$ catalyst are presented in Figure 4.2. While Figure 4.3 represent the

SEM image and elemental mapping of the synthesised bimetallic PdRh/Al$_2$O$_3$ catalyst. The SEM images and elemental mappings of all the other catalysts considered in this work are presented in Figures A4.1 to A4.4 in appendix A4.1.
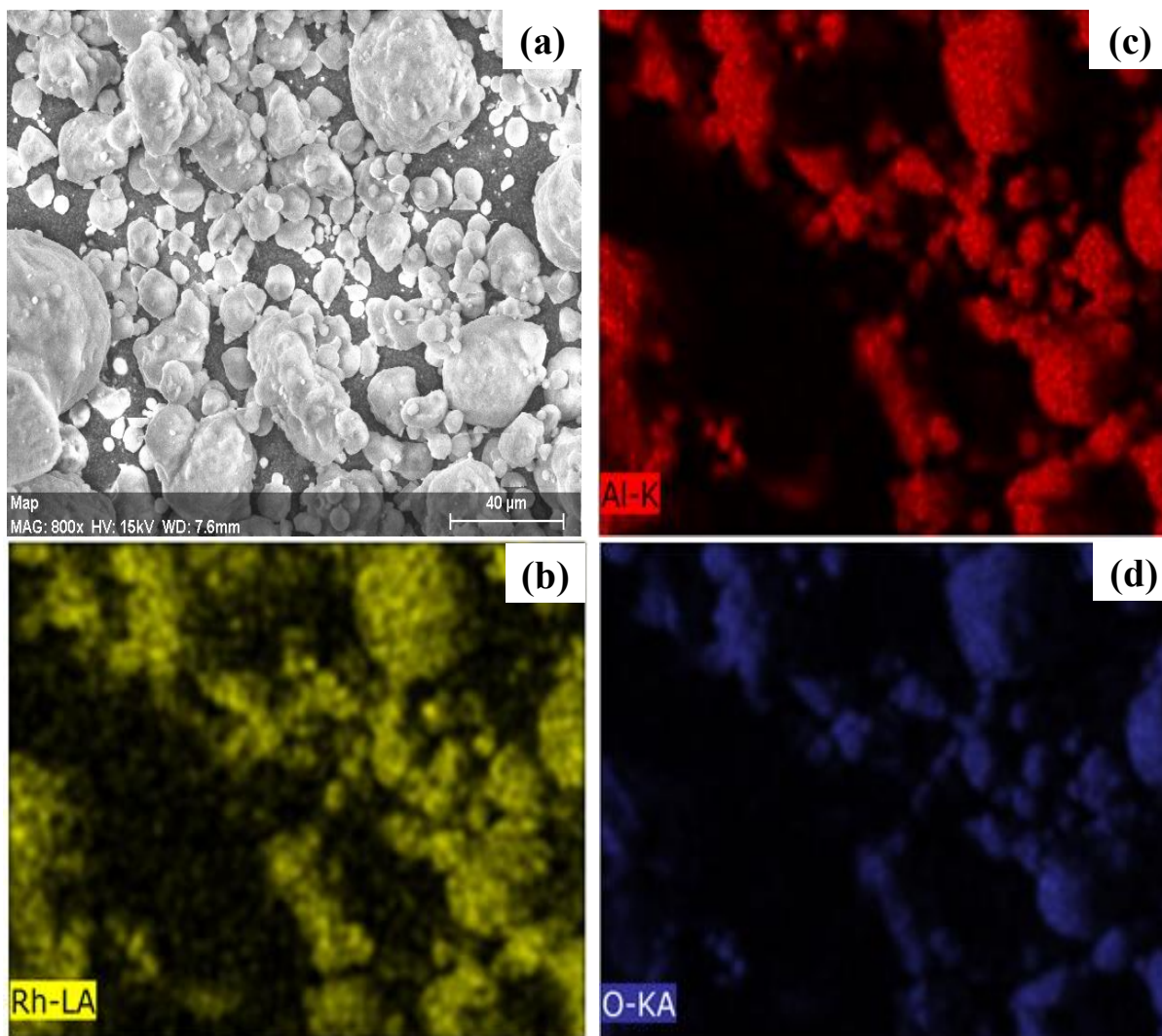
Fig. 4.2. SEM image and elemental mapping of Fresh 5 wt % Rh/Al$_2$O$_3$ catalyst [(a) SEM micrograph, (b) Rh mapping, (c) Al mapping, and (d) O mapping].

Figures 4.2b, 4.2c, and 4.2d indicates uniform spread of Rh, Al, and O in the commercial 5 wt % Rh/Al$_2$O$_3$ catalyst. While the SEM micrograph in Figure 4.2a shows the commercial 5 wt % Rh/Al$_2$O$_3$ catalyst is made up of granular particles.
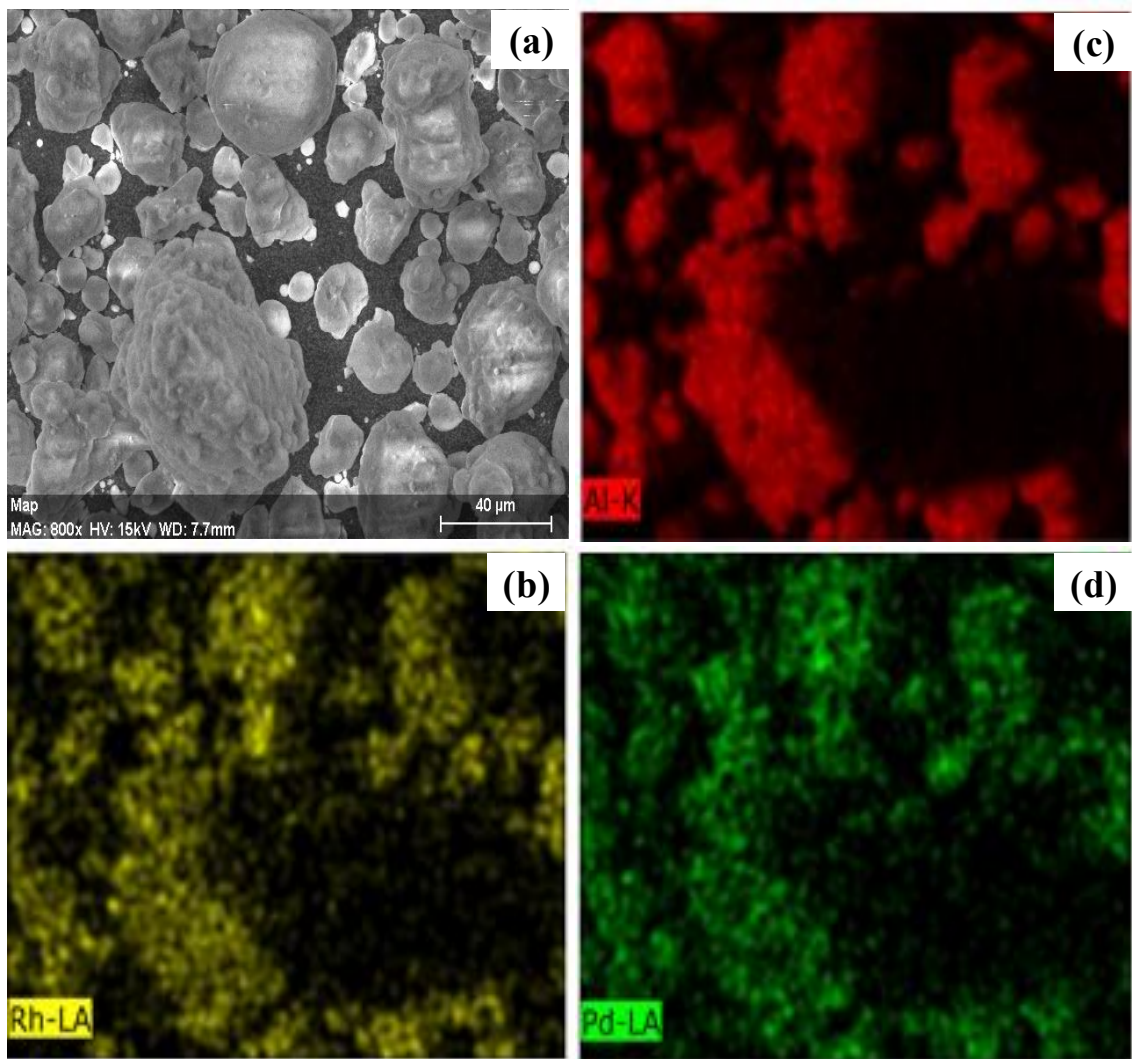
Fig. 4.3. SEM image and elemental mapping of Fresh bimetallic 6.5 wt % PdRh/Al$_2$O$_3$ catalyst [(a) SEM micrograph, (b) Rh mapping, (c) Al mapping, and (d) Pd mapping].

In comparison to the SEM micrograph of the precursor catalyst in Figure 4.2a, Figure 4.3a shows agglomeration of particles post-impregnation of Pd into the commercial 5 wt % Rh/Al$_2$O$_3$ catalyst. Figures 4.3b, 4.3c, and 4.3d indicates Rh, Al and Pd spread uniformly in the synthesised bimetallic PdRh/Al$_2$O$_3$ catalyst. The EDX images obtained for the commercial 5 wt % Rh/Al$_2$O$_3$ catalyst and synthesised PdRh/Al$_2$O$_3$ catalyst are presented in Figure 4.4. As expected Figure 4.4a shows Rh, Al and O peaks for the precursor commercial catalyst, while Figure 4.4b shows Pd, Rh, Al, and O peaks. This indicates successful doping of the commercial

5 wt % Rh/Al$_2$O$_3$ catalyst with Pd particles. However, to ascertain the percentage weight of Rh

and Pd in the prepared bimetallic catalyst, X-ray Fluorescence (XRF) analysis was conducted.
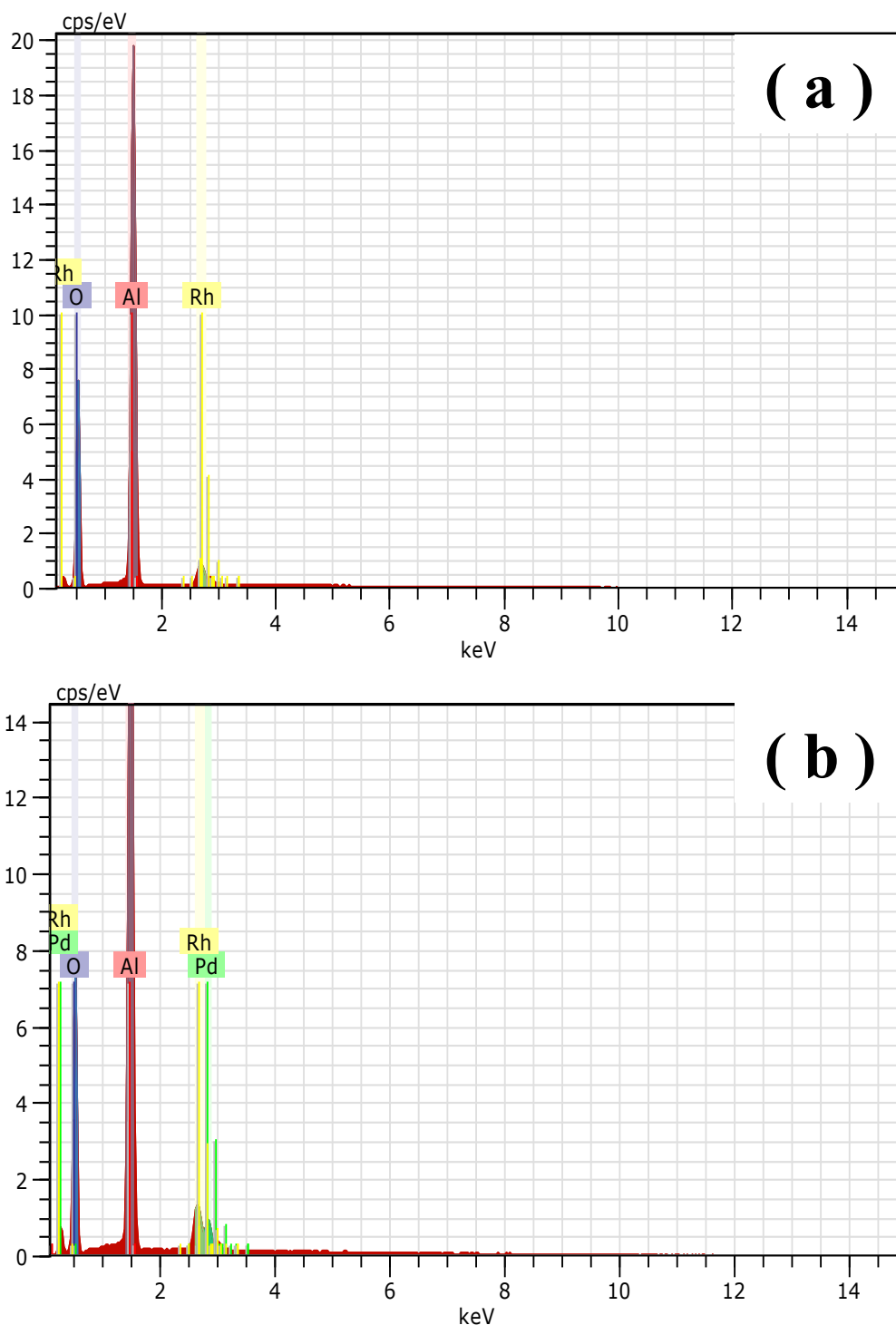
Fig. 4.4. EDX image of (a) commercial 5 wt % Rh/Al$_2$O$_3$ catalyst, and (b) prepared bimetallic PdRh/Al$_2$O$_3$ catalyst.

The result of XRF analysis shows the prepared bimetallic catalyst has a composition of 3.8 wt % Rh and 2.7 wt % Pd. A common feature of the SEM micrographs in Figures 4.2a, 4.3a, and A4.1a is that they all contained granular particles. Nonetheless, the size of the granular particles on display in Figures 4.2a, 4.3a and A4.1a differs remarkably. This is supported by the corresponding size distribution of the particles in Figures 4.5a, and 4.5b.
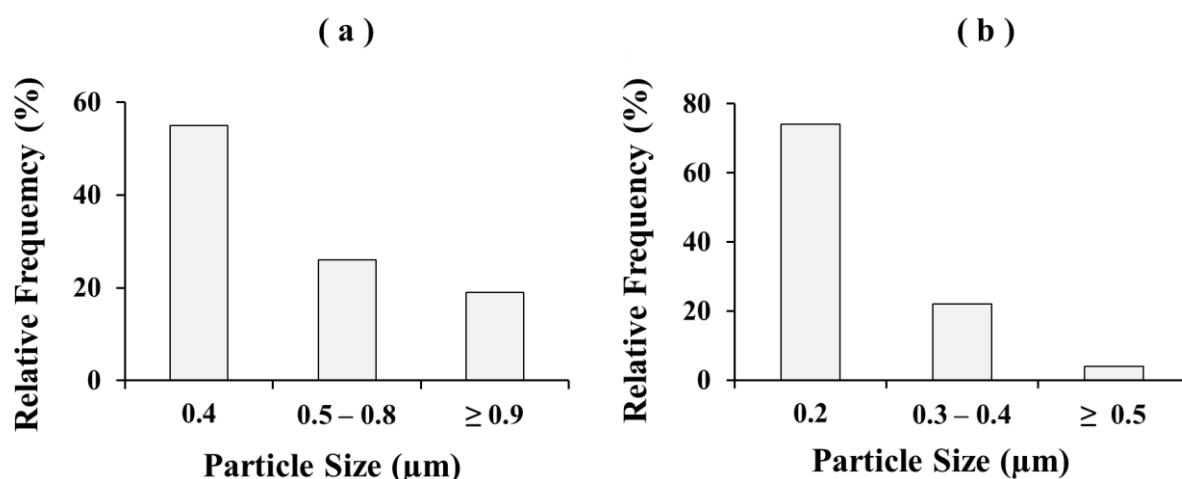
Fig. 4.5. Particle size distribution of fresh (a) commercial 5 wt % Rh/Al$_2$O$_3$ catalyst, particles counted = 1200, and (b) prepared bimetallic PdRh/Al$_2$O$_3$ catalyst, particles counted = 125.

According to Figure 4.5a, majority of the Rh/Al$_2$O$_3$ catalyst particles used as precursor in preparing the bimetallic PdRh/Al$_2$O$_3$ catalyst are 0.4 μm – 0.8 μm in size. In contrast, Figure 4.5b shows that majority of the synthesised bimetallic PdRh/Al$_2$O$_3$ particles are 0.2 μm in size. The observed difference in size of the prepared PdRh/Al$_2$O$_3$ particles and unmodified Rh/Al$_2$O$_3$ particles can be attributed to the impregnation and calcination processes. Figure 4.6a shows that majority of the Pd/Al$_2$O$_3$ particles are within the range of 0.6 μm to 1.2 μm in size. As a result, bigger lumps can be seen in Figure A4.1a compared to Figures 4.2a and 4.3a. Interestingly, the SEM micrograph of the remaining commercial catalysts in Figures A4.2 to A4.4 in appendix A4.1 are remarkably different in appearance from those in Figures 4.2a, 4.3a,

and A4.1. This observed variation highlights the morphological differences between alumina support and the other alternative supports (i.e. activated carbon and silica). Notably, the SEM micrograph of Pd/C catalyst in Figure A4.2a differs in appearance from that of the Pt/C catalyst in Figure A4.3a. This may be as a result of differences in the original type of activated carbon support used by the suppliers of these catalysts. Figure 4.6c shows that majority of the Pt/C particles are less than 0.6 µm, while from Figure 4.6b it can be concluded that most of the Pd/C particles are 0.6 µm to 1.2 µm in size.
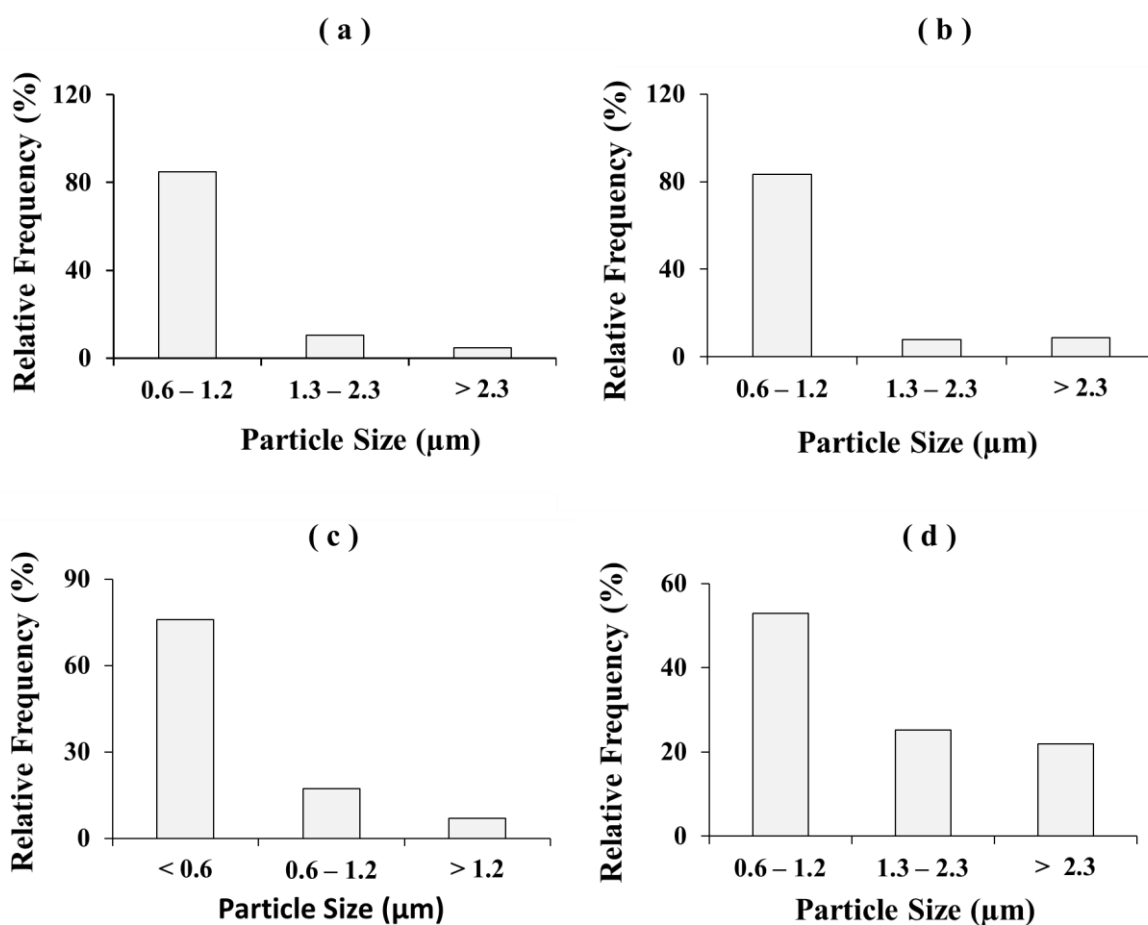
Fig. 4.6. Particle size distribution of fresh (a) commercial 5 wt % Pd/Al_2O_3 catalyst, particles counted = 4690, (b) commercial 5 wt % Pd/C catalyst, particles counted = 2997, (c) commercial 5 wt % Pt/C catalyst, particles counted = 978, and (d) commercial 5 wt % Pt/SiO_2 catalyst, particles counted = 1915.

The SEM micrograph of Pt/SiO$_2$ catalyst in Figure A4.4a are distinctly different from that of Pt/C catalyst in Figure A4.3a. This obviously reflects the morphological differences between silica and activated carbon support. In contrast to Pt/C catalyst, Figure 4.6d shows that close to 80% of Pt/SiO$_2$ catalyst are 0.6 μm – 2.3 μm in size.

4.2.3. X-Ray Diffraction (XRD) Pattern Analysis

X-ray diffraction patterns were acquired to determine the phases present in each of the catalyst and their respective average crystallite sizes using Scherrer's formula. The diffraction patterns obtained for the fresh catalysts are presented in Figure 4.7.
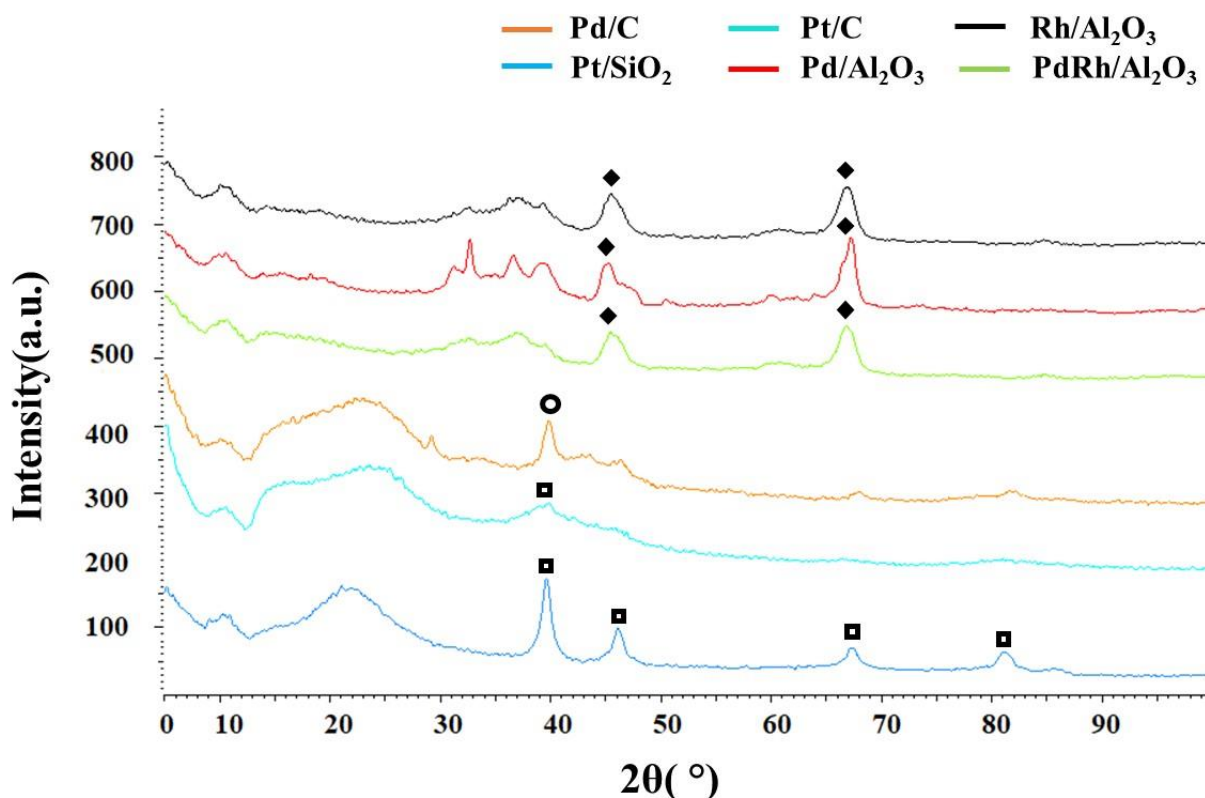
Fig. 4.7. XRD patterns of fresh commercial monometallic catalysts and synthesised bimetallic PdRh/Al$_2$O$_3$ catalyst.

At first glance, Figure 4.7 shows that the XRD pattern of the synthesised bimetallic PdRh/Al$_2$O$_3$ catalyst resembles that of the unmodified commercial Rh/Al$_2$O$_3$ catalyst. Likewise, distinct diffraction peaks at 2θ = 46°, and 67° can be seen in the XRD pattern of

Rh/Al$_2$O$_3$, PdRh/Al$_2$O$_3$, and Pd/Al$_2$O$_3$ catalyst. According to He et al.,[256] these peaks can be ascribed to cubic ɣ-Al$_2$O$_3$ phase present in the support material of Rh/Al$_2$O$_3$, PdRh/Al$_2$O$_3$, and Pd/Al$_2$O$_3$ catalyst. On this basis, it seems addition of the Pd metals did not damage the original structure of the alumina support material present in the unmodified Rh/Al$_2$O$_3$. Interestingly, this claim is consistent with findings from the pore size analysis in Section 4.2.1. However, in comparison to the unmodified Rh/Al$_2$O$_3$ catalyst XRD pattern, the intensity of the characteristic peaks of ɣ-Al$_2$O$_3$ phase reduced slightly in the XRD pattern of the prepared bimetallic PdRh/Al$_2$O$_3$ catalyst. The strong resemblance between XRD patterns of the unmodified Rh/Al$_2$O$_3$ and the prepared bimetallic PdRh/Al$_2$O$_3$ catalyst can be attributed to the following: i) Absence of metallic rhodium peaks, and ii) overlap of positional peaks of metallic Pd with the expected positional peaks for ɣ-Al$_2$O$_3$ phase. Notably, the expected positional peaks of metallic rhodium at $2\theta = 41.0°$, $47.8°$, and $84.4°$ corresponding to reflections of the (111), (200), and (311) planes respectively, were absent in the XRD pattern of the Rh/Al$_2$O$_3$ catalyst in Figure 4.7.[74] Likewise, characteristic diffraction line of metallic Pd at $2\theta = 40.0°$ depicting face centered cubic structure coincided with one of the prominent peak position for ɣ-Al$_2$O$_3$ phase.[173,231] Hence, the difficulty in using XRD analysis to discern the unmodified Rh/Al$_2$O$_3$ catalyst from the synthesised PdRh/Al$_2$O$_3$ catalyst. However, XRF analysis already confirmed the composition of the synthesised catalyst to be 2.7 wt % Pd and 3.8 wt % Rh. Table 4.2 shows the average crystallite size of all the six catalysts. The average crystallite size for most of the catalysts are within the permissible range of 1 nm to 10 nm for economic use of noble metals.[257] Pt/SiO$_2$ catalyst is the only exception with an average crystallite size just outside the specified range. The metal crystallite size for two of the catalysts which include Pd/C and the prepared bimetallic PdRh/Al$_2$O$_3$ were also estimated from CO chemisorption data for comparison purpose. It was found that the CO chemisorption approach yielded a lower value of 3.6 nm for

the Pd/C catalyst and higher value of 8.2 nm for PdRh/Al$_2$O$_3$ catalyst. Ideally, this should have been repeated for all the catalysts considered. However, unavailability of equipment necessitate consideration of only the prepared bimetallic 6.5 wt % PdRh/Al$_2$O$_3$ catalyst and commercial 5 wt % Pd/C catalyst. The dispersion of metals on these two catalysts are 28.1% for Pd/C catalyst and 12.1% for the prepared bimetallic PdRh/Al$_2$O$_3$ catalyst. Interestingly, the average crystallite size of the in-house prepared bimetallic PdRh/Al$_2$O$_3$ catalyst was found to be 11% higher than that of the precursor commercial Rh/Al$_2$O$_3$ catalyst. However, compared to the average crystallite size of the commercial Pd/Al$_2$O$_3$ catalyst, the average crystallite size of the synthesised bimetallic catalyst is 22% smaller.

Table 4.2. Summary of Fresh Catalysts Average Crystallite Size from XRD Analysis

Catalyst	Crystallite Size (nm)
5 wt.% Pd/C	10.0 ± 0.10
5 wt.% Pt/C	6.69 ± 0.08
5 wt.% Pd/Al$_2$O$_3$	8.14 ± 0.02
5 wt.% Rh/Al$_2$O$_3$	5.74 ± 0.06
6.5 wt.% PdRh/Al$_2$O$_3$	6.37 ± 0.07
5 wt.% Pt/SiO$_2$	10.2 ± 0.08

The XRD pattern of Pd/C catalyst in Figure 4.7 shows distinct diffraction line corresponding to reflection of (111) family planes which are normally associated to metallic Pd at $2\theta = 40.0°$. However, the intensity of other expected peaks associated to Pd at $2\theta = 47.0°$, $68.0°$, and $82.0°$ corresponding to reflection of the (200), (220), and (311) family planes are not strong.[74,253] This can be attributed to the low Pd loading and the well documented difficulty in using XRD to detect crystalline Pd phases.[239] The expected positional peak of activated carbon support at $2\theta = 25.0°$ corresponding to reflection of the (002) family planes appeared to have drifted slightly to the right (i.e. $2\theta = 29.0°$).[74] While other characteristic diffraction lines for activated carbon support at $2\theta = 44.0°$, and $80.0°$ corresponding to reflection of (100) and (110) family planes

respectively were absent in the XRD patterns of both Pd/C and Pt/C in Figure 4.7.[74] In contrast, four prominent distinct diffraction peaks can be seen in the XRD pattern of Pt/SiO_2 at $2\theta =$ 40.0°, 46.0°, 67.0°, and 81.0°. These peaks can be ascribed to reflection of the (111), (200), (220), and (331) family planes, and thus confirmed the presence of face centered cubic Pt phase in Pt/SiO_2 catalyst.[258,259] In addition, the XRD pattern of Pt/SiO_2 catalyst shows a very broad diffraction peak around $2\theta = 23°$, this can be attributed to the amorphous silica (SiO_2) support. According to the information presented in Table 4.2, the average crystallite size of Pt/SiO_2 catalyst is remarkably bigger than that of Pt/C but roughly the same with that of Pd/C catalyst.

4.3. Blank Experiments

To establish a benchmark for catalytic activity, the extent of vanillin HDO reaction during the heating phase was evaluated. In addition, vanillin HDO reactions were conducted in the presence of supports only without metal to understand the role of support in the reaction. Section 3.3.3 in Chapter 3 provide details on the procedure employed to conduct these experiments. The result obtained from both the non-catalytic and support-only experiments are presented in Table 4.3.

Table 4.3. Result of Blank Experiments.

Experiments	C_{VL0} (mM)	C_{VL} (mM)	C_{VA} (mM)	C_{CR} (mM)	X (%)
No Catalyst	255.07	254.62	0.04	0.01	0.18 ± 0.01
Activated Carbon (C)	254.12	244.63	0.57	0.38	3.73 ± 0.04
Alumina (Al_2O_3)	258.58	255.95	0.24	0.03	1.02 ± 0.02
Silica (SiO_2)	257.38	255.42	0.17	0.03	0.76 ± 0.03

Reaction Condition: T = 338 K, P_H = 2.0 MPa, Agitation Speed = 1000 rpm, support loading = 3.4 kg/m³, batch time = 1h, and solvent is ethyl acetate. Note: C_{VL0} is the feed vanillin concentration, C_{VL} is the final concentration of vanillin, C_{VA} is the concentration of vanillyl alcohol formed, C_{CR} is the concentration of creosol formed, and X is conversion in percentage.

From the data presented in Table 4.3, it can be seen that the standard deviations in conversion calculated from triplicate experiments carried out to investigate non-catalytic and support-only effect are significantly smaller than 1%. This indicates the results presented are reproducible and reliable. In addition, Table 4.3 shows that less than 0.2% of the starting vanillin was converted after 1 h during the non-catalytic reaction. This shows that vanillin is stable under the reaction condition examined. Likewise, Table 4.3 shows that in the presence of supports without metal, less than 4% of the starting vanillin was converted after 1 h. Hence, it can be concluded that insignificant conversion occurred in non-catalytic and support-only reaction environments. This conclusion is consistent with findings from the work of He et al [63]. However, the presence of vanillyl alcohol and creosol in mixtures from the non-catalytic and support-only reactions in small quantities suggest little hydrogenation and deoxygenation took place. This indicates possible differences in the amount of vanillin adsorbed onto the supports cannot solely be responsible for the observed variation in conversion achieved under the various supports (see Table 4.3). The highest conversion was achieved under activated carbon (AC) support. Interestingly, it has been reported in the literature that hydrocarbon/carbon system can readily be used in place of molecular hydrogen and metal catalysts to facilitate hydrogenation of compounds containing C=O bond.[260–262] This possibly explains the superior performance witnessed under AC support since ethyl acetate which is the reaction solvent is also a hydrocarbon. Moreover, AC support with specific surface area up to 2000 m^2/g offers larger area for hydrogen adsorption compared to the alternative supports with specific surface areas up to 600 m^2/g.[242]

4.4. **Effect of Catalyst**

The specific objective of this section was to systematically investigate the effect of changes in active element of the catalyst on vanillin HDO reaction using noble metals which include

palladium (Pd), platinum (Pt), and rhodium (Rh). In addition, performance of the prepared bimetallic PdRh/Al$_2$O$_3$ catalyst was compared to the commercial monometallic catalysts. As previously mentioned in Section 2.5 of Chapter 2, evaluation of catalyst performance in HDO reaction normally requires comparison of the hydrogen consumption, conversion, selectivity toward the deoxygenated product, and stability. Hence, these criteria were used to analyse vanillin HDO performance under the various catalysts. The experimental procedure employed to investigate the performance of the various catalysts in vanillin HDO reaction was described in Section 3.3.4 of Chapter 3.

4.4.1. <u>Effect of Catalyst on Conversion and Product Selectivity</u>

The conversion and product selectivity from vanillin (VL) HDO reactions under the different catalysts are presented in Figure 4.8. Notably, the standard deviations in the results displayed in Figure 4.8 are less than 2%. This indicates results obtained from the experiments performed to probe the effect of catalyst are reproducible and reliable. It was established in Section 4.3 that approximately 4% is the maximum conversion achievable from vanillin HDO reaction in the presence of catalytic support without the metals. Conversely, under the same condition, Figure 4.8 shows that 21% was the lowest conversion achieved in the presence of catalytic supports with metals. This represent a minimum gain of 17% in conversion and illustrates the important role of metal catalyst in vanillin HDO reaction. Additionally, the data presented in Figure 4.8 clearly shows that product selectivity from the reactions varied remarkably with the type of metal catalyst used. For instance, 21% conversion and 15% selectivity toward creosol was achieved from the reaction when catalysed by Rh/Al$_2$O$_3$ particles. In contrast, 99% conversion and 4% selectivity toward creosol was achieved from the same reaction using Pd/Al$_2$O$_3$ catalyst under the same condition.
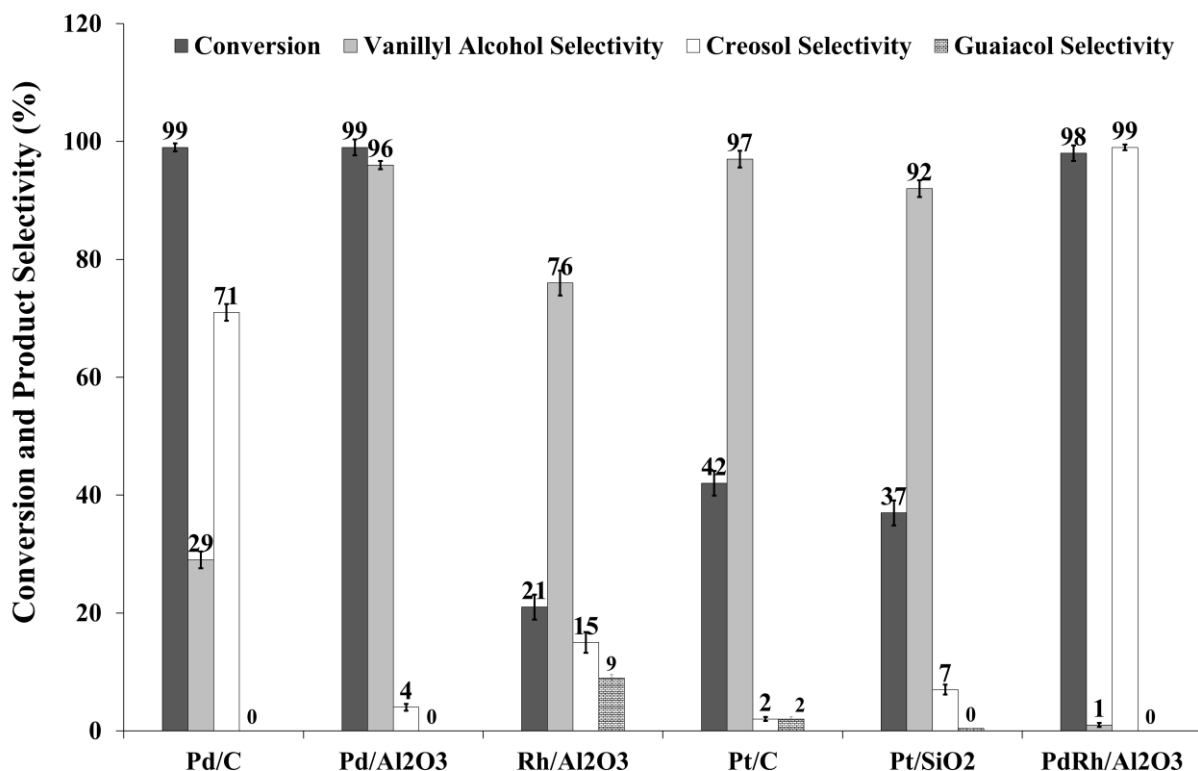
Fig. 4.8. Effect of changes in catalyst on conversion and product selectivity from vanillin HDO reaction using ethyl acetate at 1000 rpm, $C_{VL0} = 263$ mM, T = 338 K, P = 2.0 MPa, $\omega = 7.0$ kg/m^3 (monometallic catalyst) and 5.0 kg/m^3 (bimetallic catalyst), and t = 1 h.

The observed discrepancy in HDO performance under Rh/Al$_2$O$_3$ catalyst and Pd/Al$_2$O$_3$ catalyst can be ascribed to either difference in catalytic activity of the metals or metal dispersion. Remarkably, this result complement findings in the work of Santos et al.,[74] that Pd is more catalytically active than Rh in vanillin HDO reaction. Nonetheless, superior selectivity toward creosol was achieved in the presence of Rh/Al$_2$O$_3$ catalyst in the present work. As mentioned in Section 4.2, the specific surface area of Rh/Al$_2$O$_3$ is 25% greater than the specific surface area of Pd/Al$_2$O$_3$. This means that available area for hydrogen adsorption is significantly greater on Rh/Al$_2$O$_3$ and possibly explain the superior selectivity toward creosol in the presence of Rh/Al$_2$O$_3$ as oppose to Pd/Al$_2$O$_3$ catalyst. To buttress this argument, it can be seen in Figure 4.8 that conversion remained at 99% while selectivity toward creosol increased to 71% when the reaction was catalysed by Pd/C particles with specific surface area 7.5 times greater than

that of Pd/Al$_2$O$_3$ particles with specific surface area of 131 m^2/g. Interestingly, it has been reported in the work of Liu et al., [263] that Pd/C catalyst is more active than Pd/Al$_2$O$_3$ in hydrogenation reaction. The superior activity of Pd/C catalyst for hydrogenation can be linked to the AC support which promotes hydrogen transfer in the presence of a hydrocarbon solvent such as ethyl acetate.[260–262] This reinforces the conclusion in Section 4.3 on support-only investigation. Despite the effectiveness of activated carbon as hydrogen transfer agent, Figure 4.8 shows that 42% conversion and 2% selectivity toward creosol was achieved when vanillin HDO reaction was catalysed by Pt/C particles. This represent a decline of 57% in conversion and 69% in selectivity toward creosol when compared to the performance under Pd/C catalyst. The decrease in performance on changing from Pd/C catalyst to Pt/C catalyst can be attributed to the difference in catalytic activity of the two metals. Infact, in the work of Deepa and Dhepa[264] on hydrogenation of guaiacol, Pd demonstrated superior catalytic activity over Pt. The trend in catalytic activity of the metals considered can be summarised as follows: Pd > Pt > Rh. However, in terms of selectivity toward creosol the product of interest, the trend follows the order: Pd > Rh > Pt. The trend in selectivity toward creosol reported here is in conformity with findings from the work of Santos et al.[74] This stimulated preparation of a bimetallic catalyst comprising Pd and Rh. Although, activated carbon supported catalysts performed better than metals on other types of supports. The result of vanillin HDO reactions conducted under supports-only presented in Section 4.3 suggest the influence of support on vanillin HDO reaction is insignificant. Consequently, in this work a bimetallic of PdRh on alumina support was prepared. In comparison to the mono-metal catalysts, combining Pd and Rh positively affected selectivity toward creosol from vanillin HDO reaction. As shown in Figure 4.8, selectivity toward creosol from the reaction catalysed by PdRh/Al$_2$O$_3$ particles is 99%. While for the most promising mono-metal catalyst which is Pd/C, selectivity toward creosol of 71%

was achieved. Hence, doping the commercial Rh/Al$_2$O$_3$ catalyst with Pd improved selectivity toward creosol from the reaction by at least 28% while maintaining conversion in the high region of 98%. By further comparing the performance under the commercial Rh/Al$_2$O$_3$ catalyst to that achieved under the synthesised bimetallic PdRh/Al$_2$O$_3$ catalyst, it is clear that the presence of Pd dopant significantly enhanced conversion and selectivity toward creosol. This indicates that the hydrogenation capacity of the precursor Rh/Al$_2$O$_3$ catalyst improved remarkably following addition of the Pd. The improvement in hydrogenation capacity of the precursor commercial Rh/Al$_2$O$_3$ catalyst suggest adsorptive and catalytic properties of Rh were successfully tuned by the Pd dopant. A plausible reason for the enhanced properties is a shift in d-band electron density of the Rh metal. According to the literature[208], in systems dominated by ligand effect, the modifying metal is not present on the surface layer. Likewise, historically subsurface transition-metal alloys demonstrated enhanced HDO activity and selectivity toward deoxygenated product.[265, 266] The improvement in activity and selectivity have always been attributed to the adsorbates binding less strongly to the metal alloy than the pure metal. In addition, it is well-documented that the electron density of Pd metal increases when alloyed with a more electropositive metal.[267, 268] Consequently, Pd alloyed to a more electropositive metal such as Rh favours C=O bond hydrogenation. The present work could have benefited from further characterisation via X-ray Photoelectron Spectroscopy (XPS). However, XPS analysis was not carried out because the equipment was not available. As previously mentioned in Section 2.6.3 of Chapter 2, bimetallic catalysts usually contain a hydrogenating metal and an oxophilic metal. According to the literature[208], the strength of Rh–O bond is 377 kJ/mol and Pd–O bond is 234 kJ/mol. This means that during VL HDO reaction over PdRh/Al$_2$O$_3$ catalyst, vanillin probably adsorbed strongly onto Rh sites. While hydrogen dissociation occurred on Pd sites, Figure 4.9 depicts the proposed mechanism for VL HDO reaction over

PdRh/Al$_2$O$_3$catalyst.   In the present work, the overall trend in performance of the catalysts based on conversion can be summarised as follows: Pd/C = Pd/Al$_2$O$_3$ > PdRh/Al$_2$O$_3$>> Pt/C > Pt/SiO$_2$ > Rh/Al$_2$O$_3$.   While in terms of selectivity toward creosol it follows the order: PdRh/Al$_2$O$_3$ > Pd/C >> Rh/Al$_2$O$_3$ >> Pt/SiO$_2$ > Pd/Al$_2$O$_3$ > Pt/C.
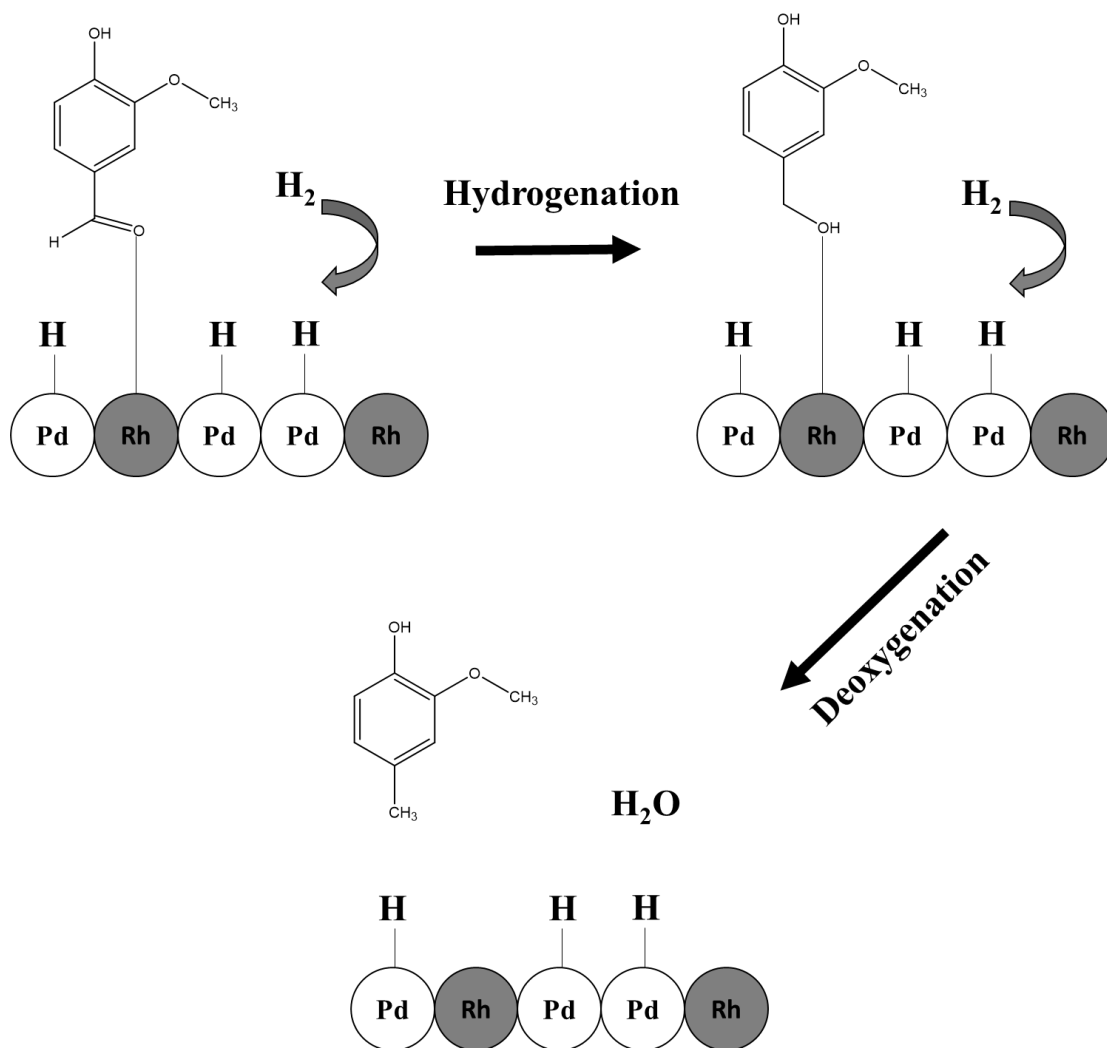
Fig. 4.9   Proposed mechanism for VL HDO reaction over bimetallic PdRh/Al$_2$O$_3$ catalyst.

4.4.2.   Effect of Catalyst on Hydrogen Consumption

In order to compare the hydrogen requirement for vanillin (VL) HDO reaction over different catalysts, the procedure described in Section 3.3.4 of Chapter 3 was used to perform VL HDO

experiments with ethyl acetate as the reaction solvent.   Figure 4.10 represent the percentage

change in starting hydrogen gas pressure of 5.6 MPa as the reaction proceeded over the various

catalysts.
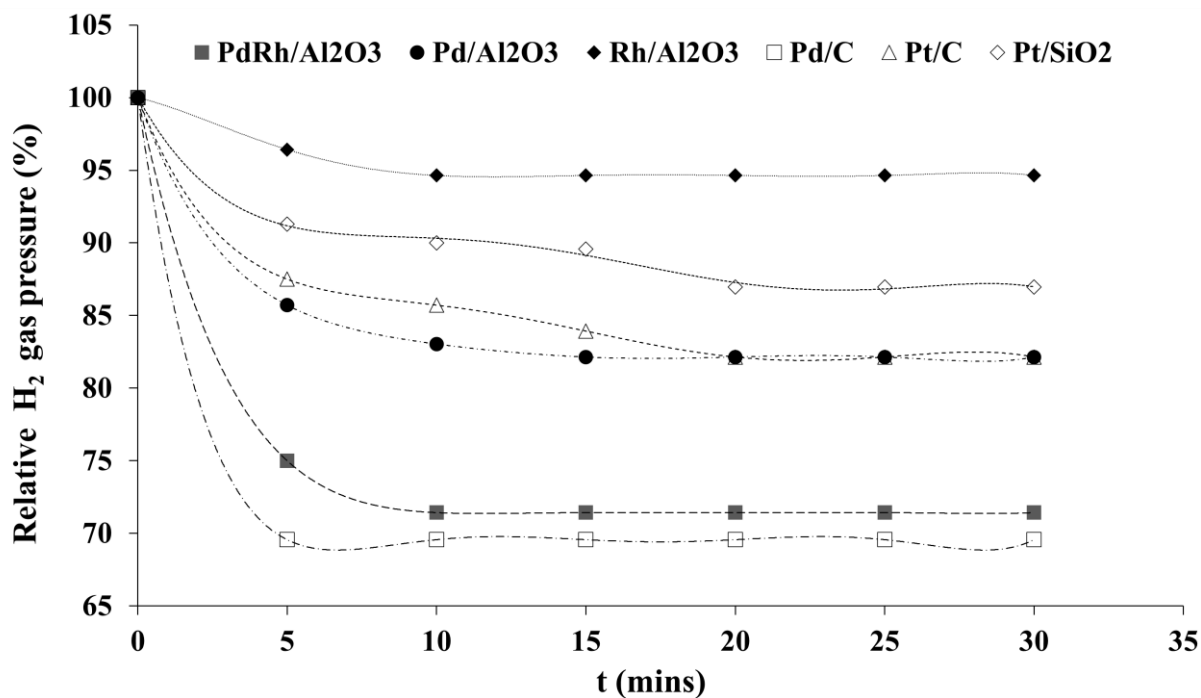
Fig. 4.10.   Temporal change in H_2 gas pressure for vanillin HDO reaction under the different
catalysts using ethyl acetate at 1000 rpm, T = 318 K, P_0 = 5.6 MPa, C_{VL0} = 263 mM, ω = 7.0
kg/m^3 (monometallic catalyst) and 5.0 kg/m^3 (bimetallic catalyst), and t = 0.5 h. Lines are drawn
to guide the eye while the shapes represent actual data points.

As expected, Figure 4.10 shows remarkable differences in the overall percentage decrease in

the starting hydrogen gas pressure for the same reaction over different catalysts. The highest

percentage decrease in the starting hydrogen gas pressure of 30.4% was achieved using Pd/C

catalyst. This was followed by a 28.6% decrease under the prepared bimetallic PdRh/Al_2O_3

catalyst, then 17.9% under both Pd/Al_2O_3 catalyst and Pt/C catalyst, followed by 13.0% under

Pt/SiO_2 catalyst and finally 5.4% under Rh/Al_2O_3 catalyst. These percentages were converted

to moles of hydrogen consumed, the values found include 48 mmol of H_2 under Pd/C catalyst,

46 mmol of H_2 under PdRh/Al_2O_3 catalyst, 34 mmol of H_2 under Pd/Al_2O_3 or Pt/C catalyst, 29

mmol of H_2 under Pt/SiO$_2$ catalyst, and 20 mmol of H_2 under Rh/Al$_2$O$_3$ catalyst. Interestingly, the highest amount of hydrogen was consumed under Pd/C catalyst in which the highest conversion was achieved. Likewise, the least amount of hydrogen was consumed under Rh/Al$_2$O$_3$ catalyst in which the least amount of vanillin was converted. From the stoichiometry of VL HDO reaction, 2 mmol of H_2 is required to completely convert 1 mmol of vanillin to 1 mmol of creosol. This translate to a stoichiometric ratio of 0.5 for vanillin converted and creosol formed per mole of hydrogen consumed. Table 4.4 summarises the ratio of vanillin converted to hydrogen consumed (n_{VL}/n_H), and the ratio of creosol formed to hydrogen consumed (n_{CR}/n_H) under the different catalysts.

Table 4.4. Vanillin converted, hydrogen consumed, and creosol formed during VL HDO reaction under the different catalyst.

Catalyst Type	n_{VL} (mmol)	n_H (mmol)	n_{CR} (mmol)	n_{VL}/n_H (mmol per mmol)	n_{CR}/n_H (mmol per mmol)
Pd/C	14.121	48.177	12.717	0.293	0.264
Pd/Al$_2$O$_3$	14.377	34.091	0.950	0.422	0.028
Rh/Al$_2$O$_3$	4.630	20.303	0.090	0.228	0.004
PdRh/Al$_2$O$_3$	14.253	46.150	12.533	0.309	0.272
Pt/C	12.806	34.091	0.131	0.376	0.004
Pt/SiO$_2$	9.483	28.569	0.465	0.332	0.016

Reaction Condition: Agitation Speed = 1000 rpm, T = 318 K, P_0 = 5.6 MPa, ω = 7.0 kg/m^3 (monometallic catalyst) and 5.0 kg/m^3 (bimetallic catalyst), Feed concentration = 263 mM, solvent is ethyl acetate, and t = 0.5 h. Note: n_{VL} represent amount of vanillin converted in millimoles, n_H represent amount of hydrogen consumed in millimoles, and n_{CR} represent amount of creosol formed in millimoles.

Table 4.4 shows that n_{VL}/n_H ranges from 0.228 under Rh/Al$_2$O$_3$ catalyst to 0.422 under Pd/Al$_2$O$_3$ catalyst. Likewise, n_{CR}/n_H changes from 0.004 under Rh/Al$_2$O$_3$ catalyst or Pt/C catalyst to 0.272 under PdRh/Al$_2$O$_3$ catalyst. These values are smaller than the theoretical value

of 0.5 for n_{VL}/n_H and n_{CR}/n_H. Hence, the amount of hydrogen consumed to convert VL to creosol under the various catalysts was higher than the stoichiometric amount. The hierarchy of the catalysts in terms of n_{VL}/n_H follows the order: $Pd/Al_2O_3 > Pt/C > Pt/SiO_2 > PdRh/Al_2O_3 > Pd/C > Rh/Al_2O_3$, while the trend in terms of n_{CR}/n_H is $PdRh/Al_2O_3 > Pd/C >> Pd/Al_2O_3 > Pt/SiO_2 >> Pt/C = Rh/Al_2O_3$. On the basis of these trends, the most attractive and efficient candidate among the catalysts tested appears to be the prepared bimetallic $PdRh/Al_2O_3$ catalyst. The other promising alternatives such as Pd/Al_2O_3 catalyst and Pt/C catalyst with values of n_{VL}/n_H very close to 0.5 have n_{CR}/n_H values significantly smaller than 0.5, hence they are not as efficient as the prepared bimetallic $PdRh/Al_2O_3$ catalyst.

4.4.3. Stability and Reusability Test

As previously mentioned in Section 2.7.1 of Chapter 2, one of the most challenging problems hindering continuous upgrading of bio-oil and its model compound via hydrodeoxygenation (HDO) is catalyst deactivation.[117, 125,130] The prime objective of this section is to examine the stability and reusability of the different catalysts. To achieve this objective, the procedure described in Section 3.3.4 of Chapter 3 was employed. Table 4.5 summarises the conversion and distribution of products per cycle under each of the catalyst. It shows negligible changes in conversion over the three cycles for reactions conducted using metal catalysts on activated carbon support. Since conversion can be interpreted as a measure of catalyst activity, it can be concluded that negligible changes occurred in activity of metal catalysts on activated carbon support over the three cycles. In contrast over the three cycles using Pd/Al_2O_3 catalyst, conversion diminished marginally by 2%. Nonetheless, activity of this catalyst remained relatively unaltered because distribution of the reaction products between cycles were not significantly different (See Table 4.5).

Table 4.5. Summary of Stability and Reusability Test.

Catalysts	Conversion (%)			Vanillyl Alcohol Selectivity (%)			Creosol Selectivity (%)		
	1	2	3	1	2	3	1	2	3
Pd/C	98.5	99.5	99.9	28.6	27.7	24.3	71.4	72.2	75.6
Pd/Al$_2$O$_3$	99.0	97.9	97.1	95.6	96.0	93.0	4.3	3.9	7.0
Rh/Al$_2$O$_3$	21.1	34.8	43.6	76.1	86.5	76.3	15.3	9.5	19.6
PdRh/Al$_2$O$_3$	97.8	98.9	99.9	0.8	14.3	17.0	99.2	85.3	82.7
Pt/C	41.9	39.4	45.0	96.6	83.5	92.9	1.9	15.6	6.3
Pt/SiO$_2$	36.6	59.5	46.0	92.4	96.7	98.2	7.2	3.3	1.7

Reaction Condition: Agitation Speed = 1000 rpm, T = 338 K, P = 2.0 MPa, ω = 7.0 kg/m^3 (monometallic catalyst) and 5.0 kg/m^3 (bimetallic catalyst), Feed concentration = 263 mM, solvent is ethyl acetate, and t = 1 h.

Interestingly, conversion from the reaction increased by 22% over three cycles when catalysed by Rh/Al$_2$O$_3$ particles. Likewise, conversion increased by 23% between cycle 1 and 2 and then decreased by 14% between cycle 2 and 3 when the reaction was catalysed by Pt/SiO$_2$ particles. The observed unexpected trends in conversion per cycle under Rh/Al$_2$O$_3$ catalyst and Pt/SiO$_2$ catalyst can be attributed to the oxidation state of the metals in these catalysts. It appears both Rh and Pt were initially present in oxide forms and then gradually reduces to metallic state in the hydrogen reaction environment. As shown in Table 4.5, from the second cycle to the third cycle, conversion increased by 9% under Rh/Al$_2$O3 catalyst. Conversely, in the presence of Pt/SiO$_2$ catalyst, conversion decreased by 14% from the second cycle to the third cycle. The opposing trend in conversion from second to third cycle under Rh/Al$_2$O$_3$ and Pt/SiO$_2$ catalysts indicates the activation time for these catalysts are different. On the basis of the observed trends between the second and third cycle, it appears Pt/SiO$_2$ catalyst requires shorter activation time

compared to Rh/Al_2O_3 catalyst. The remarkable difference in specific surface areas of these catalysts is a plausible reason for the observed discrepancies in activation time. As shown earlier in Table 4.1 of Section 4.2, the specific surface area of Pt/SiO_2 is 266 m^2/g while that of Rh/Al_2O_3 is 164 m^2/g. Hence, the active area available on Pt/SiO_2 catalyst for hydrogen adsorption is approximately 1.5 times the active area provided by Rh/Al_2O_3 catalyst for similar function. This analysis complement claim in Section 4.4.2 that the hydrogen requirement for VL HDO reaction is relatively higher in the presence of Pt/SiO_2 catalyst compared to Rh/Al_2O_3 catalyst. Of course, independent measurements of both catalyst reduction temperatures via temperature-programmed reduction (TPR) could also be used to justify the observed discrepancies in activation time of these two catalysts. However, limitation on availability of this equipment prevented further investigation via TPR. The trend in conversion after three consecutive cycles follows the order: $Pd/C = PdRh/Al_2O_3 > Pd/Al_2O_3 \gg Pt/SiO_2 > Pt/C > Rh/Al_2O_3$. While in terms of selectivity toward creosol the trend is $PdRh/Al_2O_3 > Pd/C \gg Rh/Al_2O_3 \gg Pd/Al_2O_3 > Pt/C > Pt/SiO_2$. This shows that Pd/C catalyst continued to demonstrate superior performance over the other monometallic candidates. However, the prepared bimetallic $PdRh/Al_2O_3$ catalyst continued to outperform the commercial Pd/C catalyst in terms of selectivity toward creosol after three consecutive runs. In general, deactivation was not significant in most of the catalysts as established trends after the first and third cycle mirrored each other. This can be attributed to the mild temperature used in the investigation, since mechanisms such as coking and sintering often responsible for deactivation are known to be significant at elevated reaction temperatures.[115,126,130] Nonetheless, noticeable change can be seen in selectivity toward creosol between the first and third cycle under the prepared bimetallic $PdRh/Al_2O_3$ catalyst. This could be attributed to leaching of active metals from the support material or reduction in strength of the active sites after successive reactions. In order

to establish changes in surface morphology of each catalyst post reaction, Scanning Electron Microscopy (SEM) was employed. Figure 4.11(a) to (b) represents the surface morphology and particle size distribution of fresh Rh/Al_2O_3 catalyst, while Figure 4.11(c) to (d) represents the surface morphology and particle size distribution of spent Rh/Al_2O_3 catalyst.
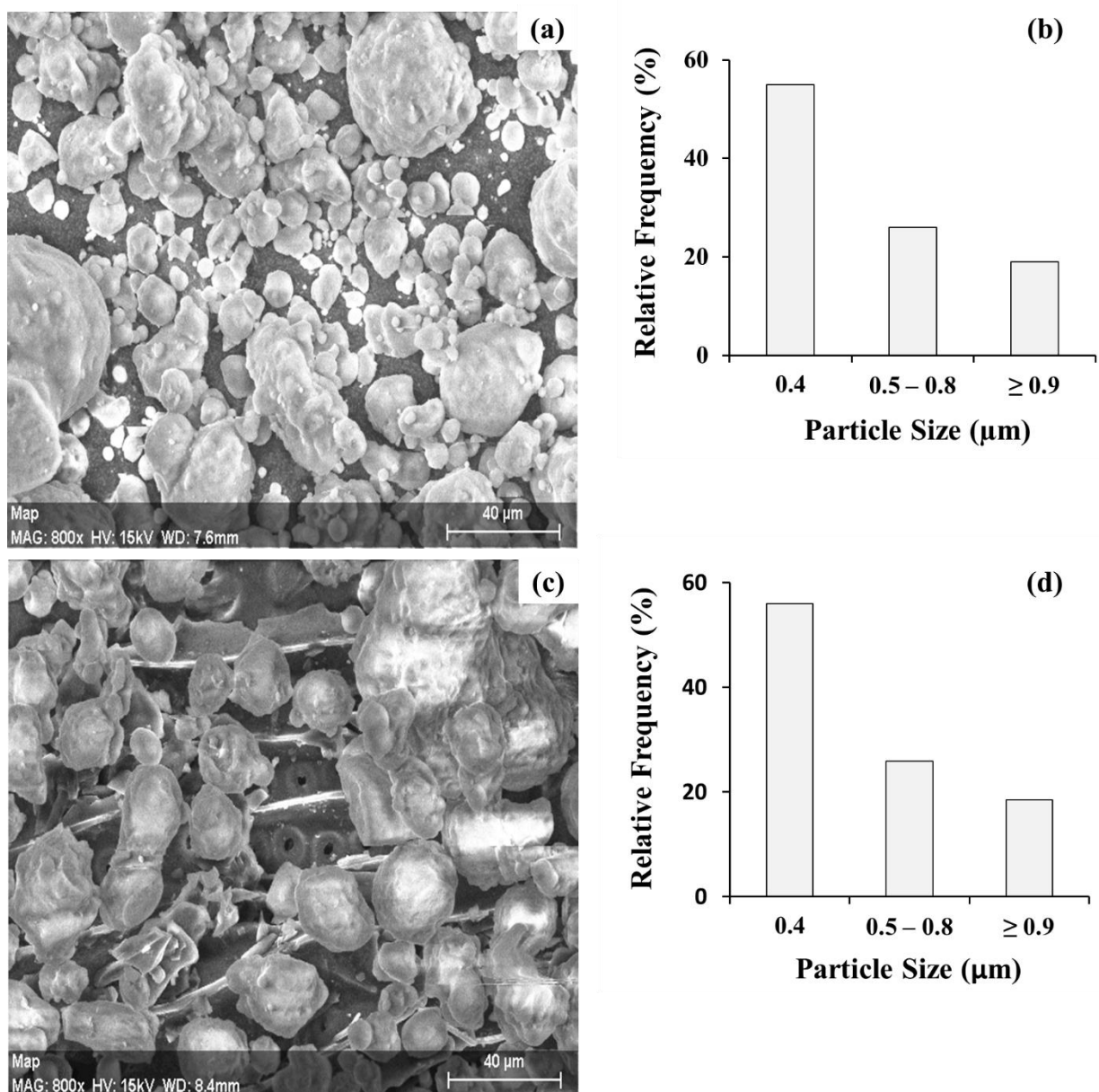
Fig. 4.11. SEM images and size distribution of (a to b) Fresh Rh/Al_2O_3 particles, count: 1200 and (c to d) Spent Rh/Al_2O_3 particles, count: 1549.

The SEM micrograph of fresh Rh/Al$_2$O$_3$ catalyst in Figure 4.11a differs from that of the spent Rh/Al$_2$O$_3$ catalyst in Figure 4.11c in appearance, with the latter showing slightly increased agglomeration. Nonetheless, the size distribution of Rh/Al$_2$O$_3$ particles was relatively unchanged in Figure 4.11b and 4.11d. Likewise, the surface morphology of fresh and spent samples of the prepared bimetallic catalyst in Figures 4.12a and 4.12c are different from each other. However, in this case the change was caused by physical attrition of PdRh/Al$_2$O$_3$ particles within the size range of 0.3 μm to 0.5 μm to smaller particles.
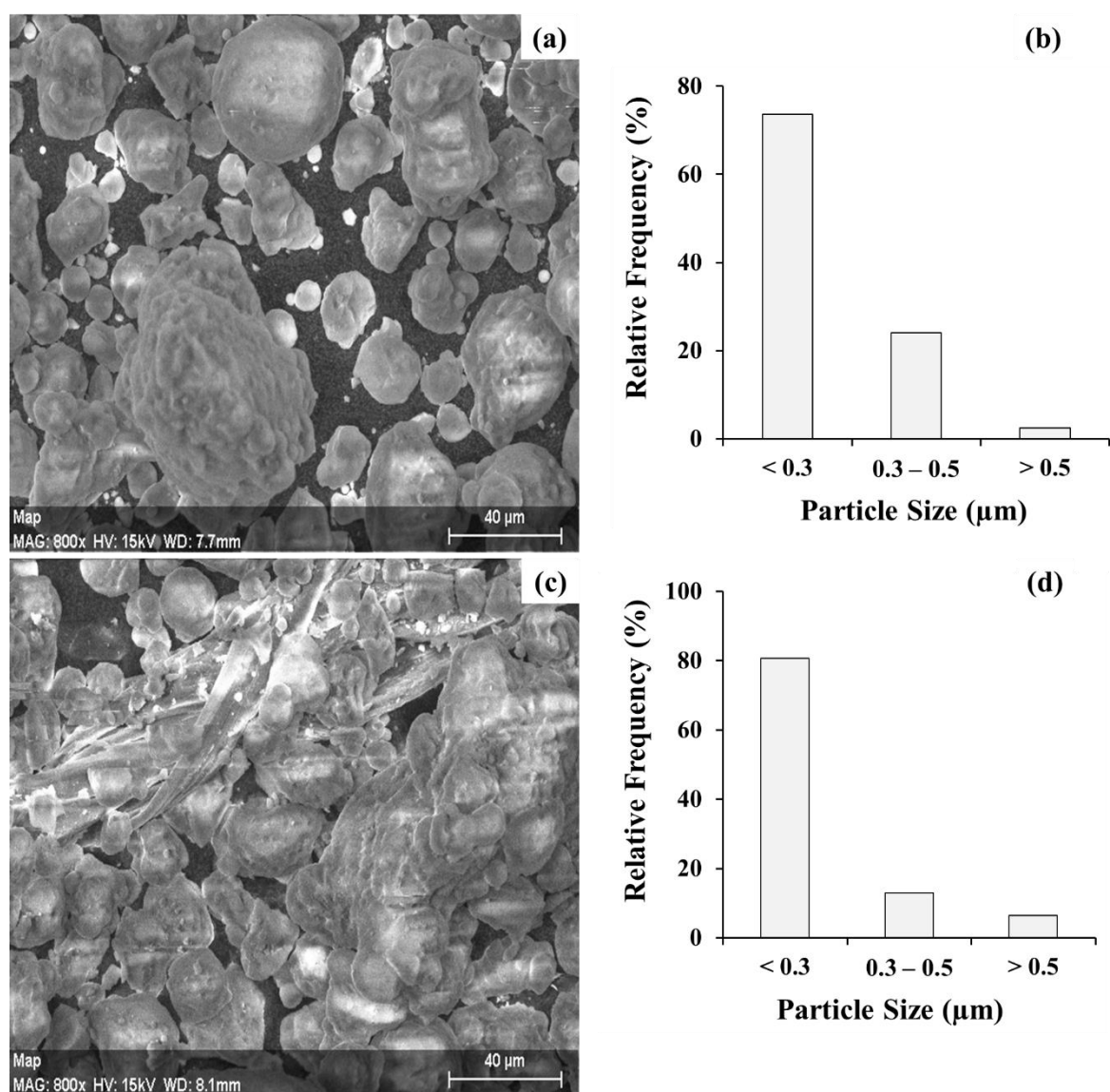
Fig. 4.12. SEM images and size distribution of (a to b) Fresh PdRh/Al$_2$O$_3$ particles, count: 125 and (c to d) Spent PdRh/Al$_2$O$_3$ particles, count: 31.

In support of the claim of physical attrition in $PdRh/Al_2O_3$ particles, Figure 4.12a shows that the proportion of fresh $PdRh/Al_2O_3$ particles within the size range of 0.3 μm to 0.5 μm was 24% while Figure 4.12c shows that post reaction the fraction of spent $PdRh/Al_2O_3$ particles within the same size range of 0.3 μm to 0.5 μm dropped to 13%. As a result of the 11% decrease in fraction of $PdRh/Al_2O_3$ particles within the size range of 0.3 μm to 0.5 μm, the proportion of $PdRh/Al_2O_3$ particles smaller than 0.3 μm increased by 7% while those greater than 0.5 μm increased by 4%. Of course, the marginal increase in proportion of $PdRh/Al_2O_3$ particles greater than 0.5 μm can be attributed to agglomeration of some of the $PdRh/Al_2O_3$ particles smaller than 0.3 μm. The SEM images and particle size distribution of fresh and spent Pd/Al_2O_3 catalyst are presented in Figure 4.13.
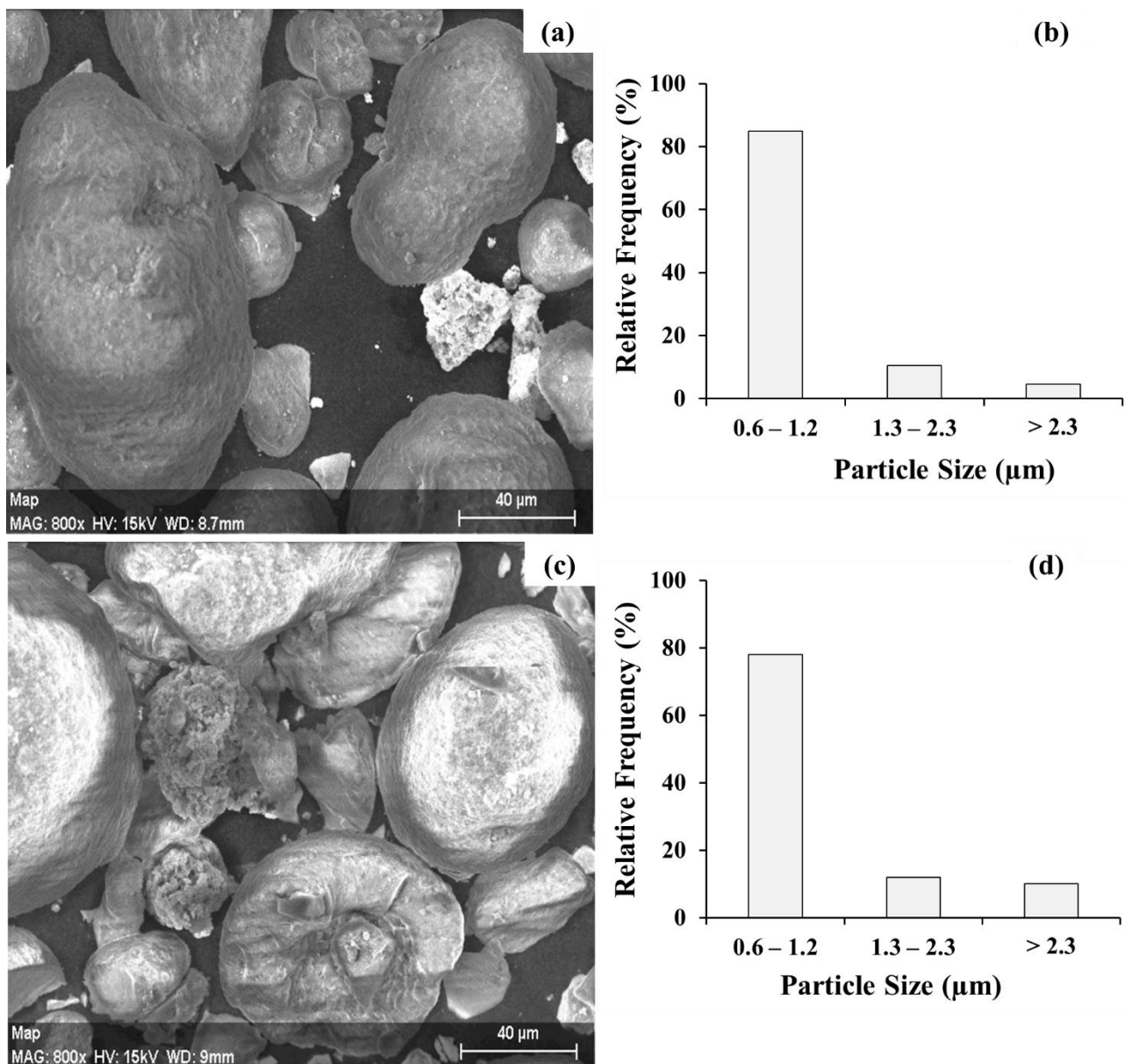
Fig. 4.13. SEM images and size distribution of (a to b) Fresh Pd/Al$_2$O$_3$ particles, count: 4690 and (c to d) Spent Pd/Al$_2$O$_3$ particles, count: 5295.

Notably, fraction of Pd/Al$_2$O$_3$ particles greater than 2.3 µm doubled after the reaction while those in the range of 0.6 µm to 1.2 µm decreased by 7 % (see Figures 4.13b and 4.13d). This possibly explain the observed differences in appearance of the SEM micrographs of the fresh and spent Pd/Al$_2$O$_3$ catalysts in Figures 4.13a and 4.13c. Unlike Pd/Al$_2$O$_3$ particles, the SEM

micrographs of fresh and spent Pd/C particles in Figures 4.14a and 4.14c are identical in appearance.
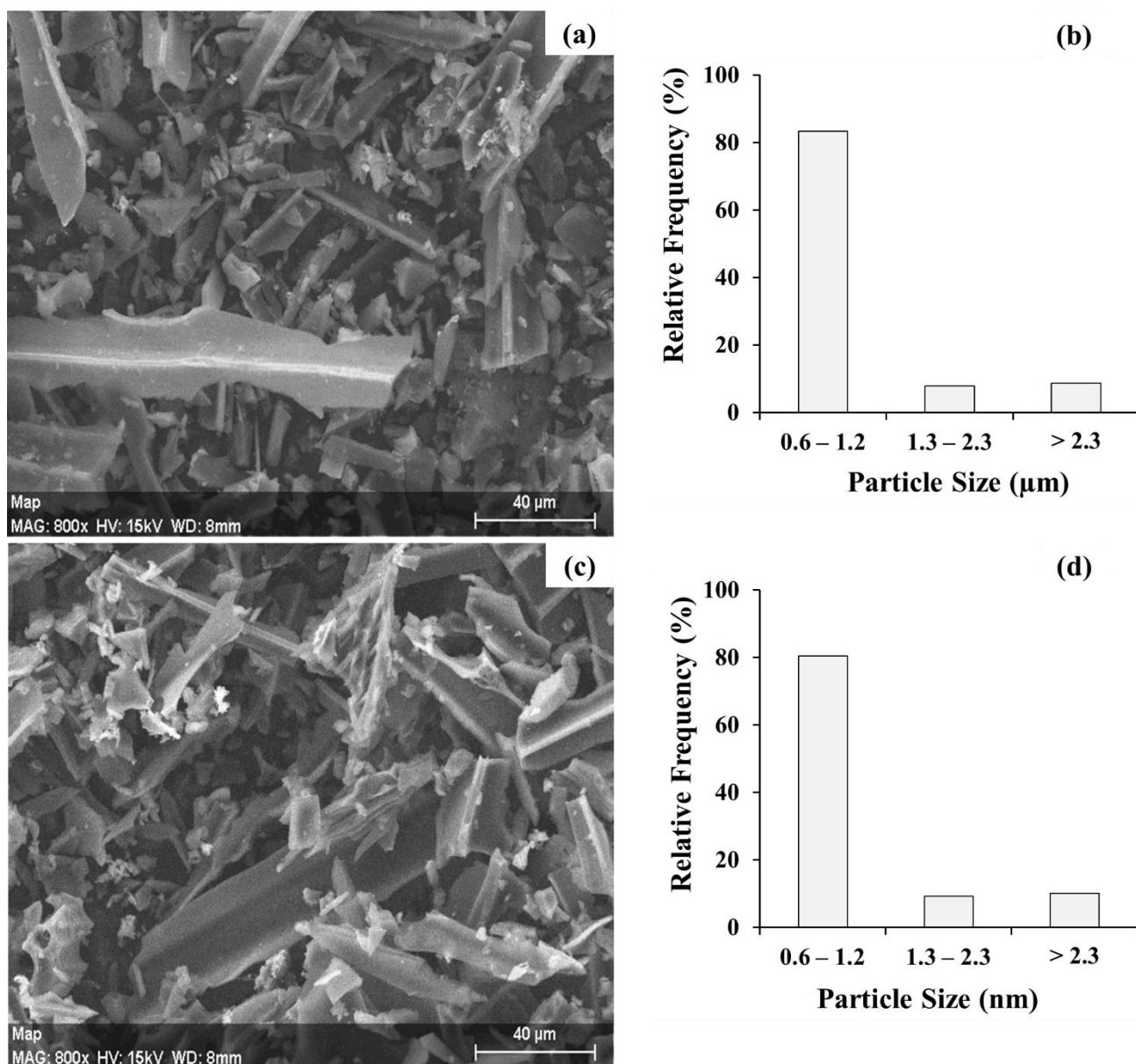
Fig. 4.14. SEM images and distribution of (a to b) Fresh Pd/C particles, count: 2997 and (c to d) Spent Pd/C particles, count: 3748.

The proportion of Pd/C particles bigger than 1.3 μm increased marginally post reaction at the expense of those within the range of 0.6 μm to 1.2 μm (see Figures 4.14b and 4.14d). Figure 4.15 shows the SEM micrographs and size distribution of fresh and spent Pt/C particles. Similar to Pd/C particles, there was no remarkable difference between the SEM micrograph of fresh

and spent Pt/C particles in Figures 4.15a and 4.15c respectively. However, the fraction of Pt/C particles smaller than 0.6 μm increases at the expense of Pt/C particles within the size range of 0.6 μm to 1.2 μm post-reaction. This indicates slight reduction in the size of Pt/C particles post-reaction possibly as a result of contact with the rotating stirrer used during the reaction to ensure uniform mixing within the reactor.
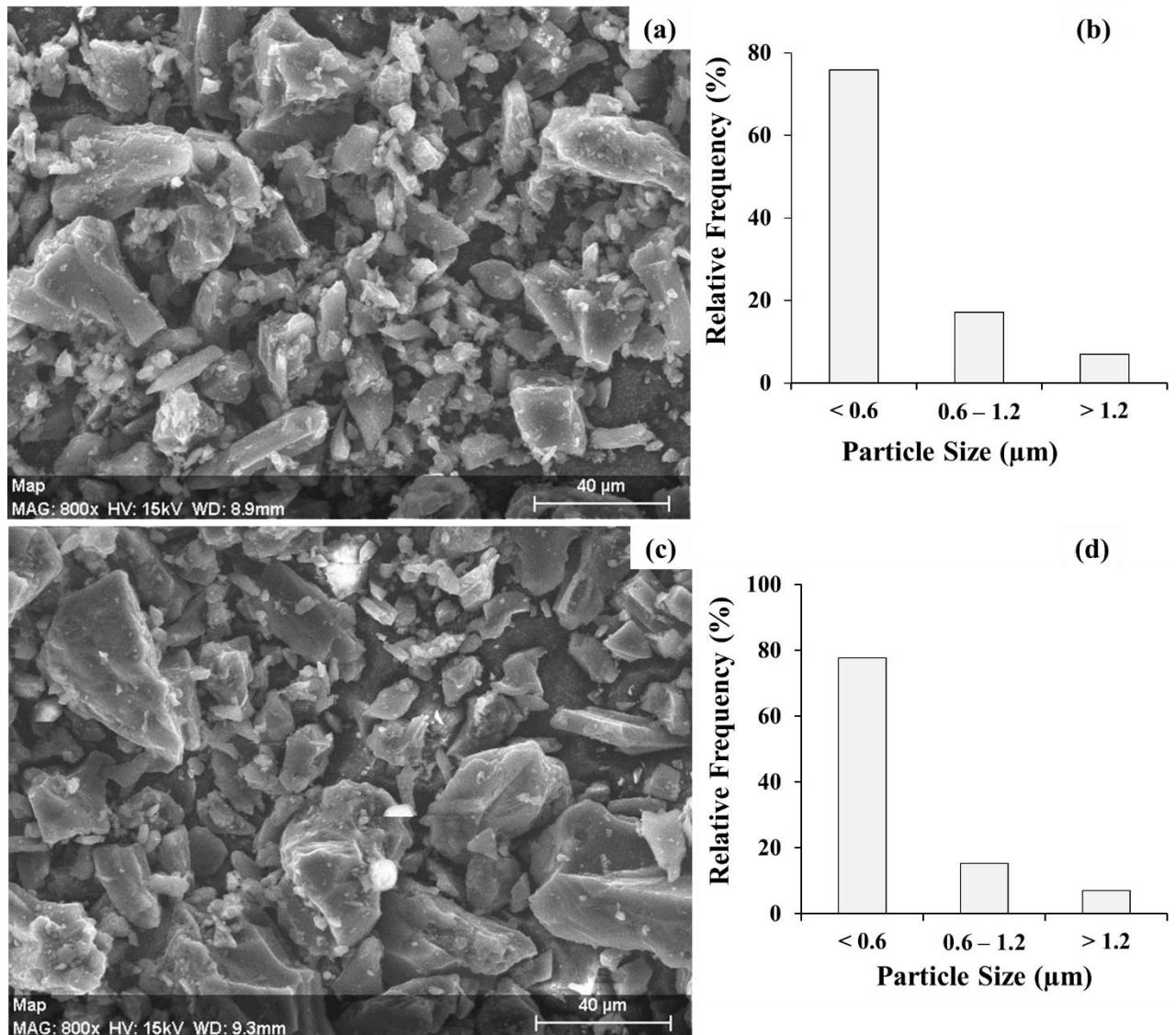
Fig. 4.15. SEM images and size distribution of (a to b) Fresh Pt/C particles, count: 978 and (c to d) Spent Pt/C particles, count: 1069.

The SEM images and size distribution of fresh and spent Pt/SiO_2 particles are presented in Figure 4.16. As expected, the SEM micrograph of fresh Pt/SiO_2 particles in Figure 4.16a is

remarkably different from that of spent Pt/SiO_2 particles in Figure 4.16c. This is consistent with the observed decline in activity of Pt/SiO_2 catalyst between the second and third cycle. Further examination of Pt/SiO_2 particles size distribution pre-reaction in Figure 4.16b and post-reaction in Figure 4.16d indicates significant drop in size of Pt/SiO_2 particles greater than 1.3 μm. This led to a proportional increase in Pt/SiO_2 particles within the size range of 0.6 μm to 1.2 μm and agglomeration of the particles into a fine big lump (see Figure 4.16c).
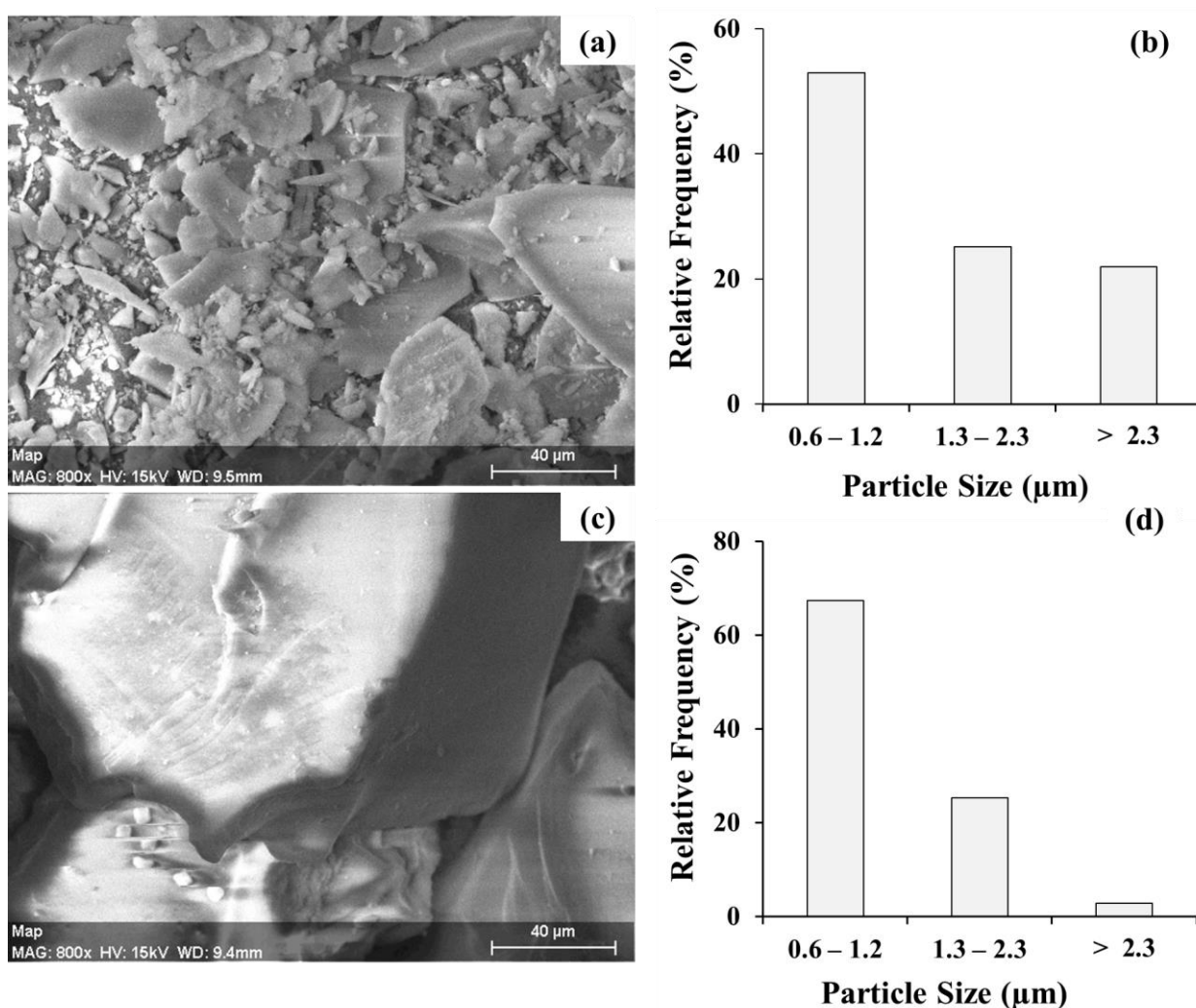
Fig. 4.16. SEM images and distribution of (a to b) Fresh Pt/SiO_2 particles, count: 1915 and (c to d) Spent Pt/SiO_2 particles, count: 2251.

Figure 4.17 shows that the number of peaks on the XRD pattern of the spent catalysts are the same as those on the fresh catalysts for all six catalysts. The absence of new peaks on the spent

catalysts XRD pattern suggest new phases were not formed as a result of vanillin HDO reaction. This agrees with findings from the SEM analysis which showed little or no differences. However, notable changes occurred in the average crystallite sizes of most of the catalysts before and after reaction (see Table 4.6). The only exceptions are Rh/Al_2O_3 catalyst and the synthesised $PdRh/Al_2O_3$ catalyst which showed negligible changes.

Table 4.6. Average Crystallite Sizes of Catalysts before and After Reaction.

Catalysts	Before (nm)	After (nm)
5 wt % Pd/C	10.0 ± 0.10	8.32 ± 0.06
5 wt % Pt/C	6.69 ± 0.08	16.1 ± 0.10
5 wt % Pd/Al$_2$O$_3$	8.14 ± 0.02	7.74 ± 0.03
5 wt % Rh/Al$_2$O$_3$	5.74 ± 0.06	5.78 ± 0.04
6.5 wt % PdRh/Al$_2$O$_3$	6.37 ± 0.07	6.11 ± 0.03
5 wt % Pt/SiO$_2$	10.2 ± 0.08	11.4 ± 0.05
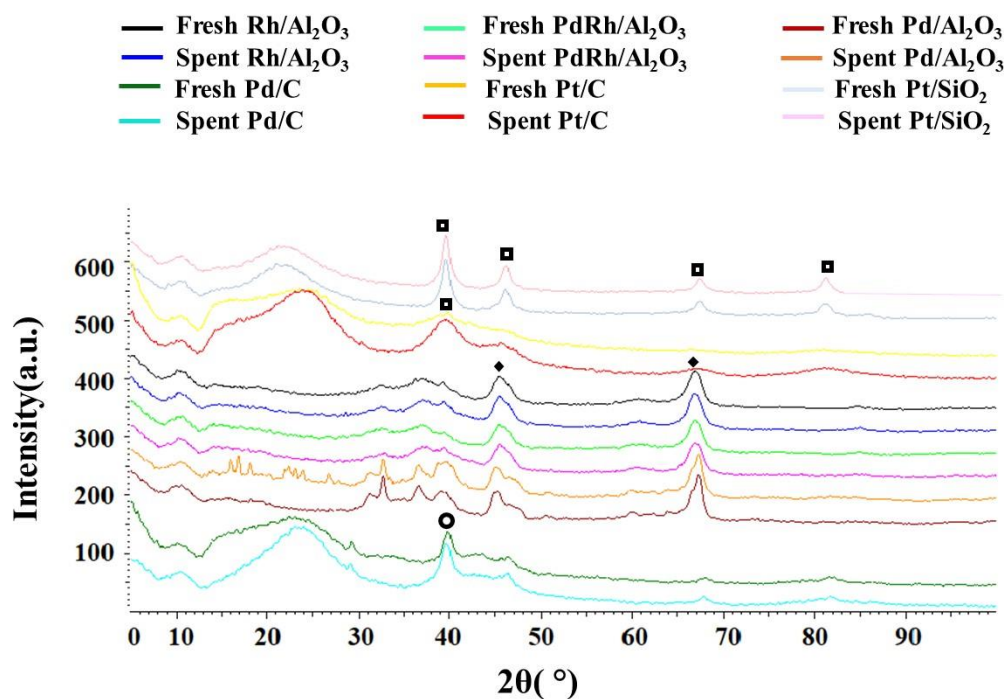
Fig. 4.17. XRD patterns of fresh and spent catalysts.

4.5. Effect of Solvent

In this section, the effect of changes in reaction media on vanillin HDO reaction was probed using six different solvents. As explained in Section 3.3.5 of Chapter 3, the solvents considered in this investigation represent the various classes of solvents available. Likewise, the experimental condition and procedure used to conduct the investigation has been described in Section 3.3.5 of Chapter 3. Conversion, selectivity toward creosol and hydrogen consumption were used to assess performance under the different solvents. As a reminder the solvents considered include: water and 2-propanol (polar protic solvents), ethyl acetate and tetrahydrofuran (aprotic polar solvents), and cyclohexane and toluene (aprotic apolar solvents). The solvatochromic properties of these solvents together with the estimated initial turn over frequencies of the prepared bimetallic $PdRh/Al_2O_3$ catalyst under each solvent are displayed in Table 4.7.

Table 4.7. Solvatochromic Parameters for Different Solvents and Estimated Initial Turn over Frequencies (TOF).[269, 270]

Solvent	ε	μ	π^*	$E_T (30)$	Z	α	β	TOF (1/min)
Water	78.5	1.85	1.09	63.1	94.6	1.17	0.47	1.3
2-Propanol	20.1	1.68	0.48	50.7	78.3	0.76	0.95	31.7
Ethylacetate	6.0	1.88	0.55	38.1	64.0	0.00	0.45	25.9
Tetrahydrofuran	7.6	1.63	0.58	37.4	58.8	0.00	0.55	19.3
Toluene	2.4	0.39	0.54	33.9	N/A	0.00	0.11	11.0
Cyclohexane	2.0	0.00	0.00	30.9	60.1	0.00	0.00	13.7

Reaction Condition: Agitation Speed = 1000 rpm, T = 318 K, P_0 = 5.6 MPa, ω = 5.0 kg/m^3 (bimetallic $PdRh/Al_2O_3$ catalyst), Feed concentration = 263 mM, and t = 0.5 h.

Using the method described in Wan.et.al., [232] the estimated initial turn over frequencies (TOF) of the prepared bimetallic $PdRh/Al_2O_3$ catalyst in Table 4.7 varies from 1.3 per min under water

to 31.7 per min under 2-propanol. This shows that the average number of reactions which occurred on active sites of the prepared bimetallic PdRh/Al$_2$O$_3$ catalyst changed remarkably with the type of solvent used in the reaction. In general, Table 4.7 shows that the prepared bimetallic catalyst is most active in polar protic solvents followed by aprotic polar solvents and then aprotic apolar solvents. The only exception to this rule is water in which the catalyst appears to be the least active. According to the literature[115, 271], metal catalysts on alumina support are prone to deactivation in aqueous environment due to changes in the alumina support composition to a new compound called boehmite. Hence, changes in the alumina support possibly explains the significantly reduced activity of the bimetallic PdRh/Al$_2$O$_3$ catalyst in a water reaction environment. Interestingly, Table 4.7 shows an inverse relationship between the measured initial TOF and the dielectric constant for solvents within the same class. Likewise, for solvents within the same class, the measured initial TOF is higher in solvent with lower hydrogen bond acceptor.

4.5.1. Effect of Solvent on Conversion and Product Selectivity

The distribution of products and conversion under the different solvents are presented in Figure 4.18. It shows that changes in the reaction solvent altered both conversion and product distribution. Thus, agrees with findings from past studies on low temperature hydrogenation reactions.[189,232,272] Most importantly the observed differences in conversion emphasises changes in activity of the catalyst and reinforces the reported variations in the initial TOF of the catalyst under different reaction solvent. Notably, even between solvents within the same class remarkable differences can be observed in conversion and product distribution. For instance, water and 2-propanol are both polar protic solvents. Yet 100% conversion and selectivity toward creosol was achieved under 0.5 h using 2-propanol. While over the same

duration, less than 80% conversion and 50% selectivity toward creosol was achieved with water as the reaction solvent.
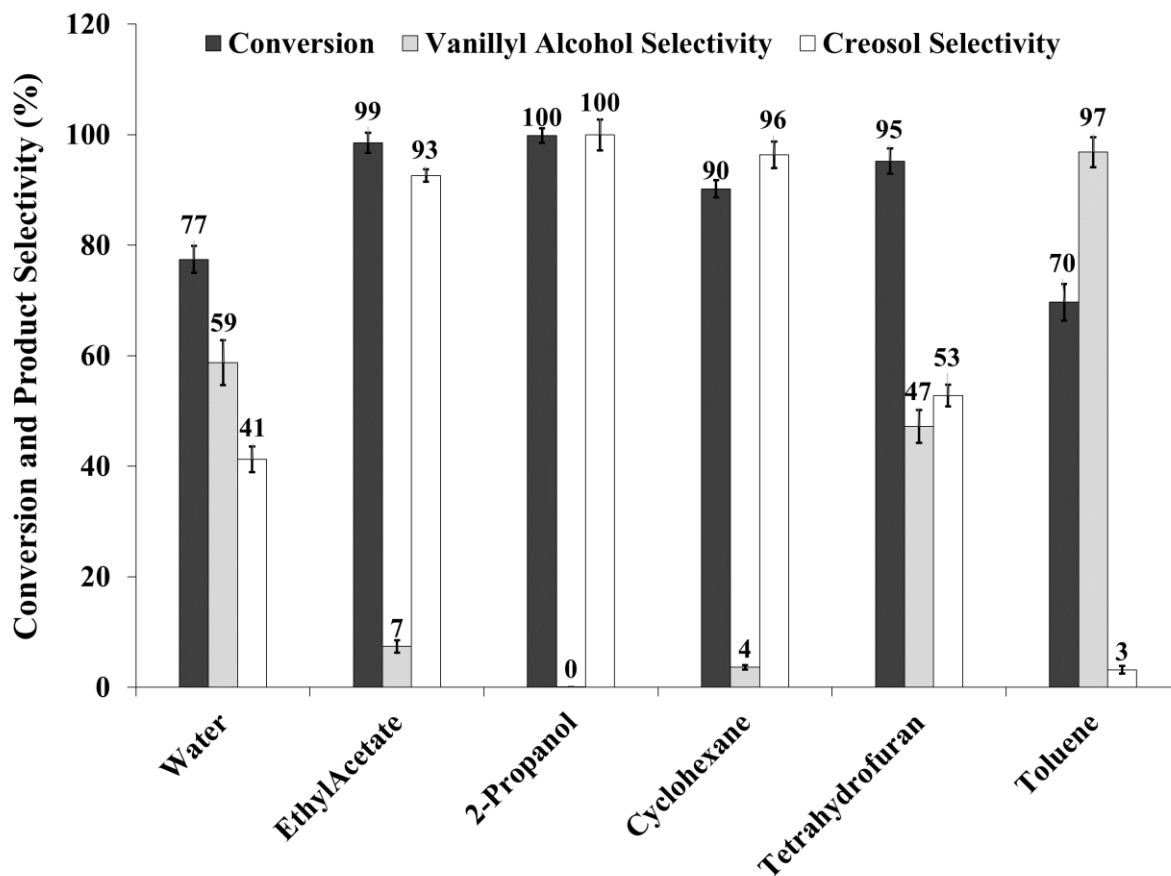
Fig. 4.18. Influence of solvent on conversion and product distribution from vanillin HDO reaction. Reaction Condition: Agitation Speed = 1000 rpm, T = 318 K, P_0 = 5.6 MPa, ω = 5.0 kg/m^3 (bimetallic PdRh/Al$_2$O$_3$ catalyst), C_{VL0} = 263 mM, and t = 0.5 h.

The trend in performance under the various solvents based on conversion follows the order: 2-Propanol > Ethyl Acetate > Tetrahydrofuran > Cyclohexane > Water > Toluene. While in terms of selectivity toward the product of interest creosol, the increasing order of solvent effectiveness is 2-Propanol > Cyclohexane > Ethyl Acetate >> Tetrahydrofuran > Water >> Toluene. It is worth mentioning that the standard deviations calculated from triplicate experiments displayed in Figure 4.18 are less than 5%, thus validates the reproducibility of the results discussed in this section. According to the literature[182], catalytic reactions performed

under mass transfer limitations are severely influenced by solubility of the reagents in the reaction solvents. Table 4.8 summarises the solubility of hydrogen gas in each of the solvents, it shows that the trend in hydrogen solubility follows the order: 2-propanol >> Cyclohexane > Ethyl Acetate > Toluene > Tetrahydrofuran >> Water. This differs from the trend in catalytic performance and thus means changes in solubility of hydrogen gas cannot be used to explain the observed variation in conversion and product distribution from vanillin (VL) HDO reaction in different solvents. Likewise, the volume of solvent used in the experiments ensured VL completely dissolves in each of the solvents. Consequently, it can be concluded that the reactions were performed under conditions in which mass transfer resistances are negligible.

Table 4.8. Solubility of Hydrogen in the different Solvents at 298 K and 0.1 MPa H_2 gas pressure.[273]

Solvent	H_2 Solubility (mol/mol)
Water	1.4×10^{-5}
2-Propanol	2.4×10^{-3}
Ethyl Acetate	3.5×10^{-4}
Tetrahydrofuran	2.7×10^{-4}
Toluene	3.2×10^{-4}
Cyclohexane	3.8×10^{-4}

As expected, high selectivity toward creosol was achieved in most of the solvents which favoured conversion of vanillin. However, conversion and selectivity toward creosol from reactions conducted using cyclohexane and tetrahydrofuran as solvents displayed an unexpected trend. In the presence of cyclohexane, 90% conversion and 96% selectivity toward creosol was achieved. Under tetrahydrofuran, 95% conversion was achieved yet selectivity toward creosol was just above 50%. This unusual scenario can tentatively be attributed to adsorption of the intermediate species in the solvents. Vanillyl alcohol, which is the intermediate species from the reaction, is a polar substance, and in the literature it is well documented that non-polar solvent favours the adsorption of polar substances.[274] Consequently,

it can be argued that the adsorption of vanillyl alcohol is more favourable in cyclohexane than tetrahydrofuran. This possibly explains the high selectivity toward creosol under cyclohexane compared to tetrahydrofuran. Interestingly, the trend in activity of the catalyst under the various solvents differ slightly from that reported in the work of Sulman et al.[75] These discrepancies can be attributed to differences in operating condition, catalyst active element and support.[275]

4.5.2. Effect of Solvent on Hydrogen Consumption

The effect of changes in solvent on the amount of hydrogen consumed during VL HDO reaction is discussed in this section. Figure 4.19 depicts the relative change in starting pressure of hydrogen gas pressure of 5.6 MPa over time during VL HDO reaction in different solvents. In conformity with the literature[232], Figure 4.19 shows that the relative change in starting hydrogen gas pressure over time varies with the type of solvent. The highest percentage decrease of 35.7% in the starting hydrogen gas pressure occurred when 2-propanol was used as the reaction solvent. This was followed by ethylacetate (28.6%), tetrahydrofuran (25.0%), toluene (16.1%), cyclohexane (14.6%), and water (5.4%). These percentages were subsequently used to determine the moles of hydrogen consumed during VL HDO reaction under the different solvents. The estimated amount of hydrogen consumed under the different solvents include 54 mmol under 2-propanol, 20 mmol under water, 46 mmol under ethyl acetate, 42 mmol under tetrahydrofuran, 32 mmol under toluene, and 30 mmol under cyclohexane. Hence, the highest amount of hydrogen was consumed during VL HDO reaction under 2-propanol and the least amount of hydrogen was consumed when water was the reaction solvent. This analysis justifies the high initial TOF of the prepared bimetallic catalyst under 2-propanol and low initial TOF under water. To establish the most efficient reaction solvent, the ratio of vanillin converted to moles of hydrogen consumed (n_{VL}/n_H), and ratio of creosol formed

to hydrogen consumed (n_{CR}/n_H) during VL HDO reaction in the different solvents were calculated and presented in Table 4.9.
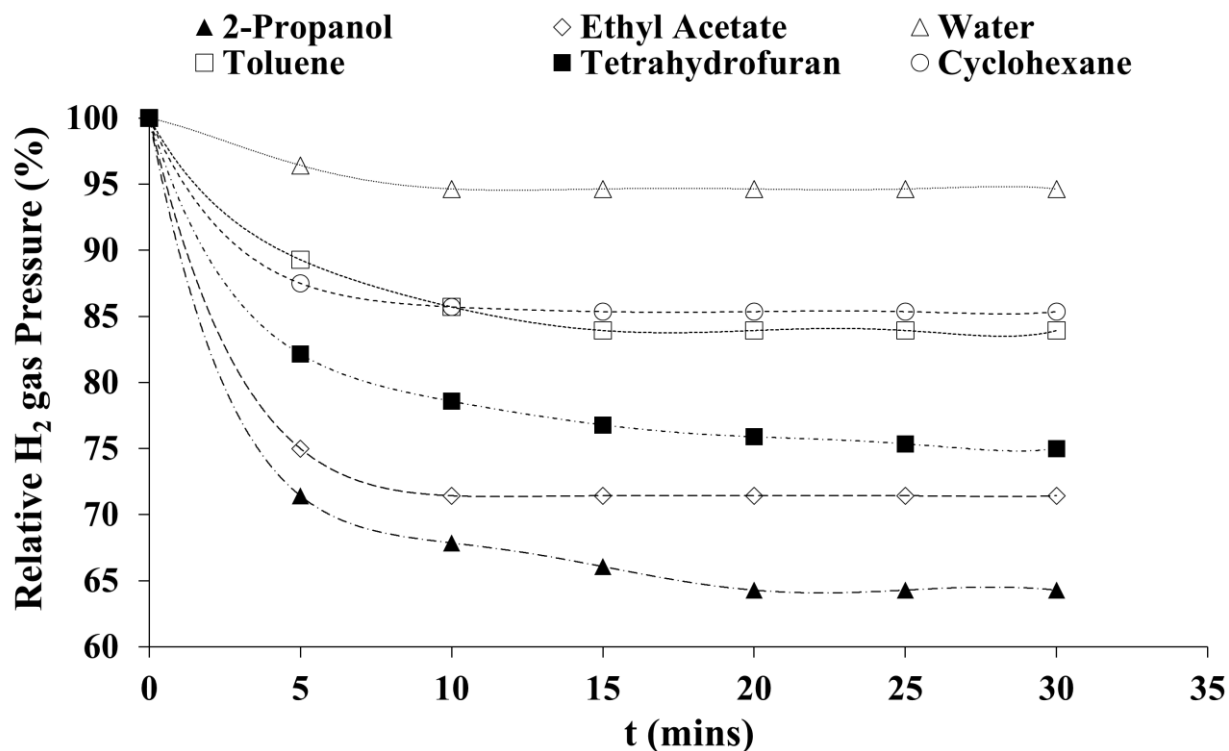
Fig. 4.19. Temporal change in hydrogen gas pressure during vanillin HDO reaction under different solvents. Reaction Condition: Agitation Speed = 1000 rpm, T = 318 K, P_0 = 5.6 MPa, ω = 5.0 kg/m^3 (bimetallic PdRh/Al$_2$O$_3$ catalyst), C_{VL0} = 263 mM, and t = 0.5 h.

Table 4.9 shows that the values of n_{VL}/n_H changed from 0.267 in 2-propanol to 0.549 in water. Likewise, n_{CR}/n_H values changed from 0.01 in toluene to 0.316 in water. This result indicates that n_{VL}/n_H is less than the stoichiometric value of 0.5 under all the solvents except water, while n_{CR}/n_H is less than the theoretical value of 0.5 under the various solvents including water. The hierarchy of the solvents in terms of n_{VL}/n_H follows the order water > cyclohexane > tetrahydrofuran > toluene > ethyl acetate > 2-propanol, while in terms of n_{CR}/n_H the trend in performance is water > ethyl acetate > 2-propanol > tetrahydrofuran > cyclohexane > toluene. On the basis of these trends, it is clear that water commonly reported as the solvent in past studies on vanillin (VL) and other model compounds of bio-oil HDO is the most efficient

medium for the reaction. According to the literature[172], the intermediate compound called vanillyl alcohol (VA) formed during VL HDO reaction is more soluble in aqueous environment than organic environment. The ease at which VA dissolves in water therefore possibly explains the superior efficiency of water over the other solvents as medium for the reaction. However, it has been established in Section 4.5 that activity of the synthesised bimetallic catalyst is remarkably lower in aqueous environment compared to other reaction media. Table 4.9 shows that the lowest value of n_{VL}/n_H was achieved using 2-propanol, while the lowest value of n_{CR}/n_H was achieved using toluene. This suggest higher moles of hydrogen was consumed to convert one mole of VL under 2-propanol compared to toluene. Interestingly, Table 4.9 shows that the value of n_{CR}/n_H under 2-propanol is approximately 21 times more than that achieved under toluene. This indicates remarkably high amount of hydrogen was consumed to convert VL into creosol (CR) under toluene compared to 2-propanol. Hence, among the solvents tested for VL HDO reaction in this work, toluene is the least efficient medium for the reaction.

Table 4.9. Vanillin converted, hydrogen consumed, and creosol formed during VL HDO reaction under different solvents.

Solvent	n_{VL} (mmol)	n_H (mmol)	n_{CR} (mmol)	n_{VL}/n_H (mmol per mmol)	n_{CR}/n_H (mmol per mmol)
2-Propanol	14.465	54.150	11.296	0.267	0.209
Ethyl Acetate	14.320	46.149	12.533	0.309	0.272
Tetrahydrofuran	13.742	42.093	6.756	0.326	0.161
Toluene	10.126	32.063	0.330	0.316	0.010
Cyclohexane	13.019	30.373	1.726	0.429	0.057
Water	11.138	20.302	6.424	0.549	0.316

Reaction Condition: Agitation Speed = 1000 rpm, T = 318 K, P_0 = 5.6 MPa, ω = 5.0 kg/m^3 (bimetallic PdRh/Al$_2$O$_3$ catalyst), C_{VL0} = 263 mM, and t = 0.5 h. Note: n_{VL} represent amount of vanillin converted in millimoles, n_H represent amount of hydrogen consumed in millimoles, and n_{CR} represent amount of creosol formed in millimoles.

4.6. Effect of Processing Condition

As explained in Section 3.3.6 of Chapter 3, the effect of changes in processing conditions on vanillin (VL) HDO reaction was investigated under the conditions listed in Table 3.4. These conditions were established using a standard L_9 orthogonal array as recommended by the Taguchi design. The reasons for applying Taguchi design has been covered in Section 3.3.6 of Chapter 3. However, as a reminder they include reduced number of experiments and consideration of parameter interactions.[276] The processing parameters considered in this study include temperature, pressure, catalyst loading, and agitation speed. Table 3.3 in Section 3.3.6 of Chapter 3 summarises the three levels for each of the processing parameters. In the case of reaction temperature, it was varied from 318 K (Level 1) to 338 K (Level 3). The hydrogen gas partial pressure was varied from 1.0 MPa (Level 1) to 3.0 MPa (Level 3), while catalyst loading was altered from 0.5 kg/m^3 (Level 1) to 0.1 kg/m^3 (Level 3). Finally, the speed of agitation was changed from 500 rpm (Level 1) to 900 rpm (Level 3). Justification for the ranges considered in this study has been provided in Section 3.3.6 of Chapter 3. Figure 4.20 shows the conversion and product distribution under each of the nine conditions in Table 3.4 of Chapter 3. The standard deviation in the data presented in Figure 4.20 are less than 5%, this indicates the results from the experiments conducted are reliable and reproducible.
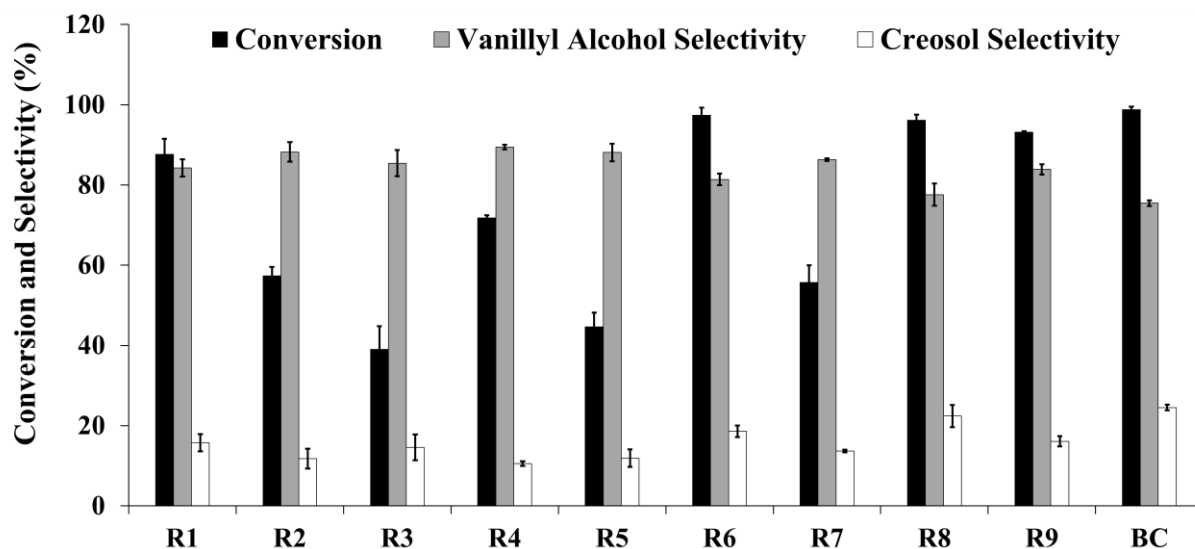
Fig. 4.20. Effect of changes in processing conditions on conversion and the distribution of products from vanillin HDO reaction. [Solvent: Ethyl acetate, Type of Catalyst: 10 wt % Pd/C, Reaction time: 1 h, Feed vanillin concentration: 65.0 mM]. Note: BC represent performance under the best condition derived via signal to noise ratio analysis. The values of T, P, and ω are specified in Table 3.4 of Chapter 3.

As expected changes in the reaction conditions caused significant variation in conversion and the distribution of products from vanillin HDO reaction (see Figure 4.20). For instance, 39% conversion and 15% selectivity toward creosol was achieved from vanillin HDO reaction conducted under R3 (see Table 3.4 in Chapter 3 for specific information on R3 condition). In contrast, 96% conversion and 22% selectivity toward creosol was achieved from the same reaction when conducted under R8 (see Table 3.4 in Chapter 3 for specific information on R8 condition). To isolate the effect of changes in the processing parameters on conversion, degree of deoxygenation (DOD), and relative rate of deoxygenation to hydrogenation (DOD/HYD), the S/N ratio discussed in Section 3.3.6 of Chapter 3 is employed here. Since the objective is to maximise the performance parameters (i.e. conversion, DOD, and DOD/HYD), the best level for each process parameter correspond to the level with highest S/N ratio.

4.6.1. Effect of Changes in Reaction Temperature

The effect of changes in reaction temperature on conversion, degree of deoxygenation, and the ratio of deoxygenation to hydrogenation are presented in Figure 4.21.
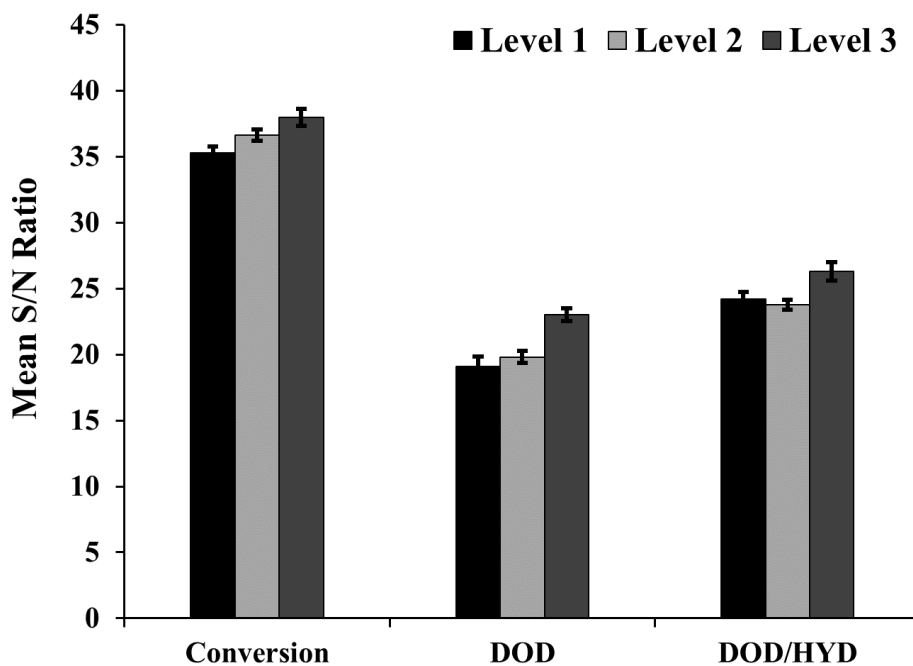
Fig. 4.21. Effect of changes in reaction temperature on conversion, degree of deoxygenation and the ratio of deoxygenation to hydrogenation from vanillin HDO reaction. Note: Level 1 is 318 K, Level 2 is 328 K, and Level 3 is 338 K. S/N represent signal to noise.

Notably, the degree of deoxygenation (DOD) and conversion from vanillin HDO reaction increases as reaction temperature increased from level 1 (318 K) to level 3 (338 K). This is in conformity with the well-known Arrhenius behaviour of reaction rates increasing with temperature and consistent with findings from the work of Mahfud et al.[70] Hence, it can be concluded that within the range of temperatures considered, 338 K maximises the conversion of vanillin to the deoxygenated product creosol.

4.6.2. Effect of Changes in Reaction Pressure

Figure 4.22 shows the effect of changes in the reaction pressure from level 1 (1.0 MPa) to level 3 (3.0 MPa) on conversion, degree of deoxygenation, and the ratio of deoxygenation to hydrogenation.
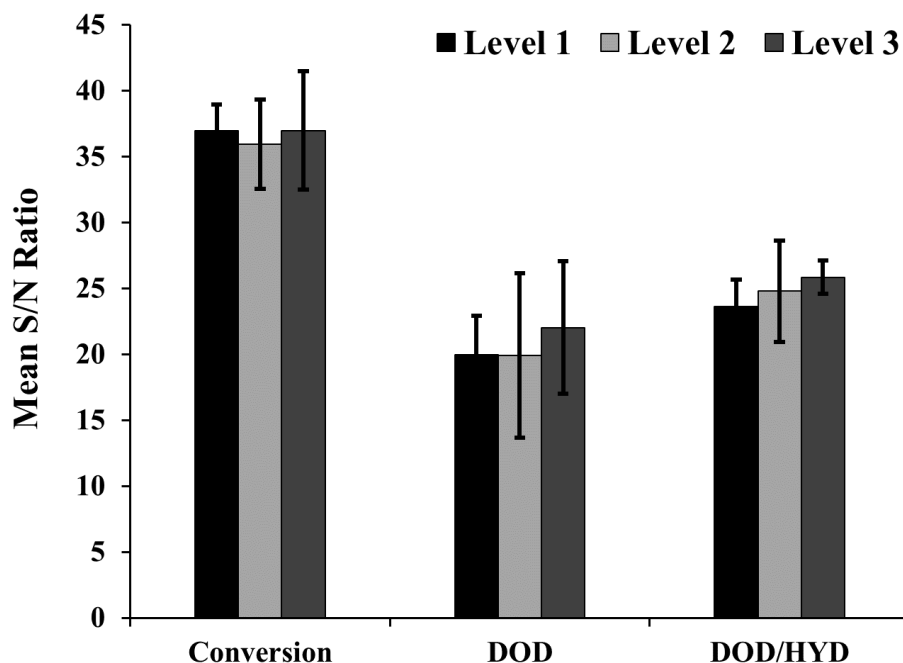
Fig. 4.22. Influence of reaction pressure on conversion, degree of deoxygenation and the ratio of deoxygenation to hydrogenation from vanillin HDO reaction. Note: Level 1 is 1.0 MPa, Level 2 is 2.0 MPa, and Level 3 is 3.0 MPa. S/N represent signal to noise ratio.

It can be seen in Figure 4.22 that changes in reaction pressure did not significantly alter the amount of vanillin converted. Nonetheless, the ratio of deoxygenation to hydrogenation (DOD to HYD) was affected as pressure increased from 1.0 to 3.0MPa. Likewise, remarkable change can be seen in the degree of deoxygenation (DOD) as the reaction pressure increased from 2.0 to 3.0 MPa. The improvement in DOD as reaction pressure increases can be attributed to higher availability of hydrogen around the catalyst. Interestingly, in the work of He et al., [63] and Bindwal et al., [69] it was also reported that increase in hydrogen gas pressure accelerates the

deoxygenation of vanillin to creosol. Hence, the observed dependence of DOD on hydrogen gas pressure in this study is in agreement with the literature. On the basis of the data presented in Figure 4.22, it can be concluded that within the range examined, 3.0MPa is the hydrogen gas partial pressure that maximises the DOD of vanillin to creosol.

4.6.3. Effect of Changes in Agitation Speed

The effect of changes in agitation speed from level 1 (500 rpm) to level 3 (900 rpm) on conversion, degree of deoxygenation (DOD), and the ratio of deoxygenation to hydrogenation (DOD/HYD) are presented in Figure 4.23. It can be seen that negligible changes occurred in all three parameters as the agitation speed was increased from 500 to 900 rpm.
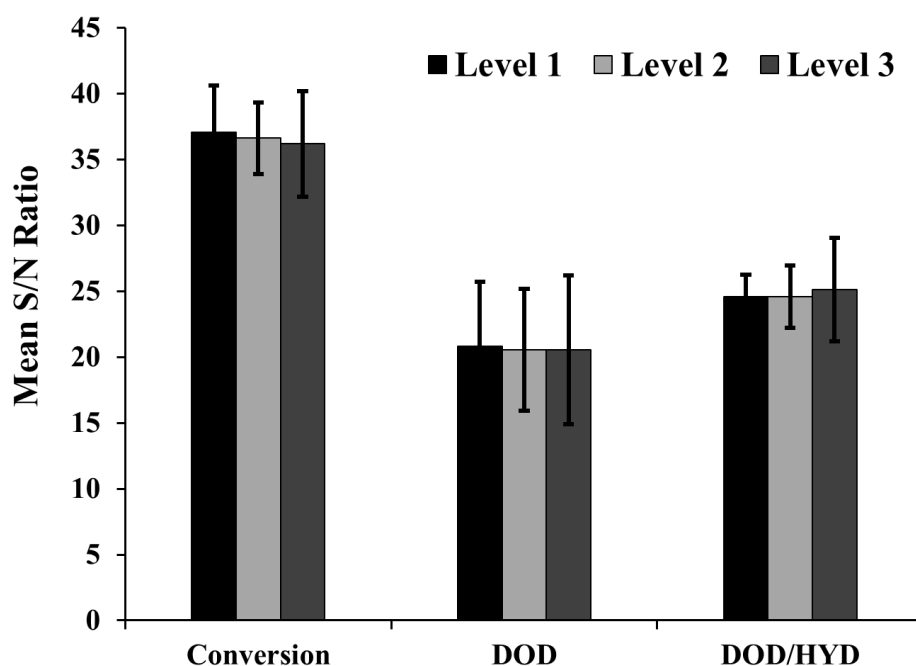
Fig. 4.23. Influence of agitation speed on conversion, degree of deoxygenation and the ratio of deoxygenation to hydrogenation from vanillin HDO reaction. Note: Level 1 is 500 rpm, Level 2 is 700 rpm, and Level 3 is 900 rpm. S/N represent signal to noise ratio.

This result confirms the absence of external mass transfer limitation within the reaction system.[277] Hence, the lowest agitation speed of 500 rpm is considered the optimum speed because higher agitation speed will increase spending on energy.

4.6.4. Effect of Changes in Catalyst Loading

Figure 4.24 depicts the impact of changes in catalyst loading from level 1 (0.5 kg/m^3) to level 3 (0.1 kg/m^3) on conversion, degree of deoxygenation (DOD), and the ratio of deoxygenation to hydrogenation (DOD/HYD). It is worth mentioning here that catalyst loading in the context of this discussion refers to weight of the catalyst in kg per unit volume of solvent in m^3. Notably, conversion and the degree of deoxygenation decreases as catalyst loading decreases from 0.5 to 0.1 kg/m^3. Likewise, DOD/HYD decreases significantly as catalyst loading reduces from 0.5 to 0.3 kg/m^3. This trend suggests active sites on the catalyst available for adsorption of the reactants decreases as catalyst loading reduces. As a result, conversion and the DOD of vanillin to creosol reduces as the catalyst loading decreases. This analysis reaffirms the discussion in Section 4.6.3 that the reaction is not mass transfer limited. Within the range investigated, it can be concluded that 0.5 kg/m^3 is the catalyst loading that maximises conversion and the DOD of vanillin to creosol.
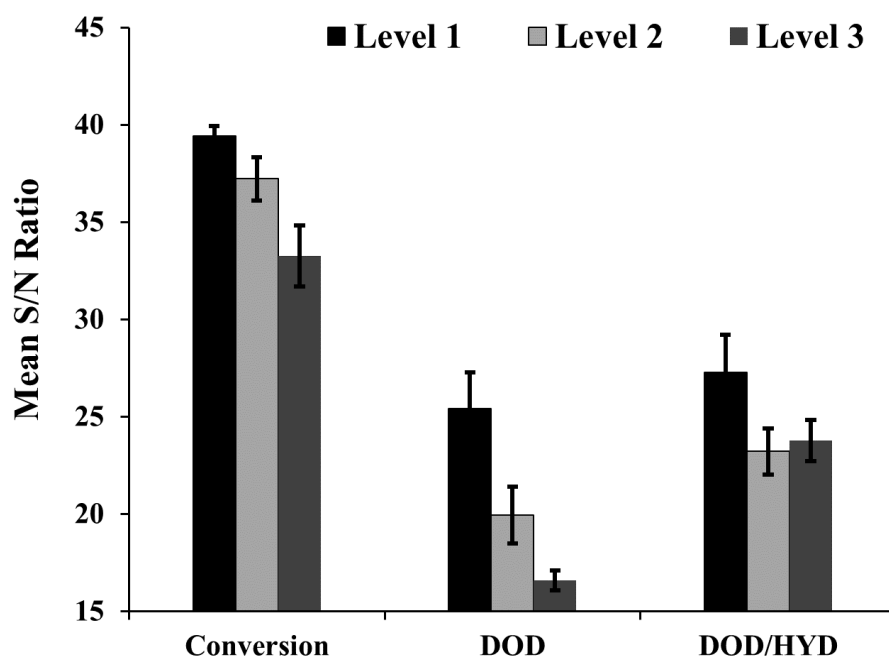
Fig. 4.24. Effect of changes in catalyst loading on conversion, degree of deoxygenation and the ratio of deoxygenation to hydrogenation from vanillin HDO reaction. Note: Level 1 is 0.5 kg/m^3, Level 2 is 0.3 kg/m^3, and Level 3 is 0.1 kg/m^3. S/N is the signal to noise ratio.

In summary, the best condition (BC) derived includes: reaction temperature 338 K, hydrogen gas partial pressure 3.0 MPa, catalyst loading 0.5 kg/m^3, and agitation speed 500 rpm. Vanillin HDO reaction was conducted at the derived BC for validation. The conversion, and product selectivity achieved under the derived BC are displayed in Figure 4.20 to enable direct comparison with other experimental conditions (i.e. R1 – R9) examined. Clearly, from Figure 4.20 the derived BC is valid because under this condition the highest conversion (98.8%) and selectivity toward creosol (24.5%) was achieved.

4.6.5. Analysis of Variance (ANOVA)

The significance of the various processing parameters was tested using analysis of variance (ANOVA). For this purpose, the degree of deoxygenation (DOD) achieved at each of the conditions examined was used to calculate the corresponding S/N ratio. The S/N ratios were determined using the "larger is better approximation" defined in equation 3.7 of Chapter 3. Table A4.1 in appendix A4.1 summarises the DOD, S/N ratios and computed square of differences between the individual and mean S/N ratios. Using the information in Table A4.1, the sum of squares deviation, mean variance and percentage contribution (P) for each of the parameters was determined. The results are presented in Table 4.10, sample calculations of sum of squares deviation, mean variance and percentage contribution are reported in appendix A4.1.

Table 4.10. Result of Analysis of Variance (ANOVA) Test

Parameter	DOF	Sum of Squares	Mean variance	P (% cont.)	Rank
Temperature(K)	2	26.4	13.2	17.1	2
Pressure(MPa)	2	8.7	4.3	5.6	3
Catalyst loading (kg/m^3)	2	119.6	59.8	77.2	1
Agitator Speed (RPM)	2	0.2	0.1	0.1	4
Error	1	0	0	0	
Total	9	154.8	77.4	100.0	

Note: DOF represents the degree of freedom, and P represents percentage contribution.

Table 4.10 shows that changes in the degree of deoxygenation (DOD) can be explained completely by variation in the processing parameters selected. However, changes in the various parameters have different significance on the DOD. On the basis of percentage contribution displayed in Table 4.10, catalyst loading with contribution greater than 77 percent has the most significant effect. This is followed by reaction temperature, hydrogen gas partial pressure and then agitation speed. Remarkably, less than one percent of the changes in DOD can be explained by variation in the speed of agitation. In conclusion the ANOVA analysis performed shows that the effect of processing parameters on vanillin HDO reaction studied in this work was conducted in the reaction-controlled regime.

4.7. Conclusions

In this chapter, the effect of changes in active element of the catalyst, support material, solvent, and processing condition on hydrodeoxygenation (HDO) reaction was probed using vanillin, a typical compound present in bio-oil. It was established that contribution from non-catalytic and support-only reactions toward vanillin HDO reaction are insignificant. In contrast, the reaction was strongly affected by changes in active element of the catalyst. Following further analysis, the observed variation in vanillin HDO performance under different active elements was correlated to differences in hydrogen requirement and other physicochemical properties such as metal dispersion and specific surface area. The highest conversion of 99% was achieved using Pd-based catalysts, this was followed by Pt-based and then Rh-based catalyst. Notably, the prepared bimetallic PdRh/Al_2O_3 catalyst emerged as the most efficient and attractive catalyst for the reaction producing the highest amount of creosol per mole of hydrogen consumed. Reusability experiments conducted confirmed Pd/C as the most stable

and superior catalyst among the monometallic catalysts considered. However, the prepared bimetallic PdRh/Al$_2$O$_3$ catalyst demonstrated excellent stability over long-term and continue to outperform the commercial mono-metal Pd/C catalyst in terms of selectivity toward creosol. Additionally, it was established that conversion and product distribution from vanillin HDO reaction varied significantly with the reaction solvent. These variations were later related to changes in the hydrogen requirement for vanillin hydrodeoxygenation reaction over the prepared bimetallic PdRh/Al$_2$O$_3$ catalyst in different reaction media. Interestingly, water commonly reported as solvent in the literature on hydrodeoxygenation reaction emerged as the most efficient medium for the reaction. While toluene was found to be the least efficient medium for the reaction producing the lowest amount of creosol per mole of hydrogen consumed. Finally, the work completed in this chapter shows that vanillin hydrodeoxygenation reaction is sensitive to changes in the processing parameters. Within the operational range considered, the condition which maximises conversion and selectivity toward creosol was 338 K reaction temperature, 3.0 MPa hydrogen gas partial pressure, 0.5 kg/m^3 catalyst loading, and 500 rpm agitation speed. Among these processing parameters, catalyst loading was found to be the most influential parameter on the degree of deoxygenation of vanillin to creosol. In contrast, agitation speed was established to be the least influential parameter on degree of deoxygenation of vanillin to creosol.

Chapter 5

Kinetics of Vanillin Hydrodeoxygenation Reaction in Ethyl Acetate Using Monometallic and Bimetallic Palladium Based Catalysts.

5.1. Introduction

Noble metals which include palladium (Pd), platinum (Pt), ruthenium (Ru), and rhodium (Rh) continue to be the leading candidates among the various type of catalysts tested for hydrodeoxygenation (HDO) reaction of bio-oil and model compounds.[32, 44–47,131,278] These metals are the most promising candidate because they are active at low temperatures, and thus permit operation at mild temperatures. Additionally, operation at mild temperatures reduces occurrence of thermal reactions which often result in coke formation and catalyst deactivation.[70, 200,279] Due to the listed benefits, the kinetics of vanillin HDO reaction over noble metals such as Ru, Pt, and Pd have been reported previously in limited number of publications.[70–72, 74, 75,160,280] Sulman and co-worker[75] successfully investigate the kinetics of vanillin HDO reaction over Pt/C catalyst. However, the lumped approach utilised in their work to model the reaction made it impossible to deduce information on kinetic parameters such as the adsorption and reaction rate constants. Likewise, recent investigation on kinetics of vanillin HDO reaction over Pd/C catalyst by Santos et al.,[74] failed to provide information on activation energy which represent the barrier to the reaction and adsorption coefficients which represent the strength of adsorptions onto the catalyst surface. To date the most comprehensive and successful modelling work on kinetics of vanillin HDO reaction was carried out by Bindwal et al.,[160] using Ru/C catalyst in an aqueous environment. Nonetheless, it has been shown in past studies and in Section 4.4 of Chapter 4 that Pd is the most active metal for vanillin HDO reaction. Hence, the present chapter investigate the reaction kinetics of vanillin HDO over Pd-

based catalysts. Remarkably, the kinetics of vanillin HDO reaction over bimetallic catalysts which are known to exhibit excellent stability and selectivity toward the deoxygenated product creosol has not been reported in the literature. As a result, the present chapter compare the kinetics of vanillin HDO reaction over commercial mono-metal Pd-based catalysts (i.e. Pd/C and Pd/Al$_2$O$_3$) and synthesised bimetallic PdRh/Al$_2$O$_3$ catalyst. In conformity with most studies on reaction kinetics, established techniques such as Weisz and Prater criterion, agitation, and particle size test were used in Section 5.2 to examine the role of transport limitations. While the concentration – time profiles observed during vanillin HDO reaction under the different catalysts are presented in Section 5.3. The sensitivity of vanillin HDO reaction to changes in catalyst loading (ω) was investigated and reported in Section 5.4. Likewise the effect of changes in hydrogen gas partial pressure (P_H) on initial rate of vanillin HDO reaction (r_0) is presented in Section 5.5. The effect of changes in starting concentration of vanillin on the initial rate of reaction (r_0) is examined and reported in Section 5.6. While the effect of temperature on r_0 and product distribution are presented in Section 5.7. The impact of reaction products (i.e. vanillyl alcohol and creosol) on conversion is discussed in Section 5.8. The mechanism for vanillin HDO reaction, the statistical test carried out to examine the fit of different Langmuir – Hinshelwood – Hougen – Watson (LHHW) kinetic models to the experimental data and estimated values of the kinetic parameters are presented in Section 5.9.

5.2. <u>Transport Limitation Considerations</u>

Hydrodeoxygenation (HDO) reaction of vanillin is a typical example of three-phase reaction involving hydrogen gas (G), solution of vanillin and the products (L), and solid catalyst (S). Consequently, different physical and chemical steps must take place for the reaction to occur.[190] These steps include:

1. External diffusion of vanillin and hydrogen gas through the boundary layer surrounding the catalyst particles;

2. Intraparticle diffusion of vanillin and hydrogen gas through pores of the catalyst particles to the active sites;

3. Adsorption of vanillin and hydrogen gas onto the catalyst active sites;

4. Surface reaction between adsorbed vanillin and hydrogen to form intermediates;

5. Desorption of the products (i.e. creosol and vanillyl alcohol) from active sites of the catalyst;

6. Intraparticle diffusion of the products and unreacted vanillin through the catalyst pores;

7. External diffusion of products and unreacted vanillin across the boundary surrounding the catalyst.

As a result of the series of steps involved, different rate controlling regimes are possible, these include[277]:

   I.   Film diffusion control regime (steps 1 and 7);

  II.   Pore diffusion control regime (steps 2 and 6);

 III.   Intrinsic reaction kinetics control regime (steps 3 to 5).

However, the scope of the present work necessitates conditions which ensures data collection within the intrinsic reaction kinetics control regime. In this regime, transport resistances are negligible. As a result, the overall rate of reaction will be independent of transport resistances in this regime. The collection of data in the intrinsic kinetics control regime permits the development of model that accurately describes reaction kinetics of vanillin HDO.

5.2.1. External Transport Limitations Consideration

The prerequisite for uniform temperature and concentration throughout the reactor (i.e. negligible external transport limitation) is perfect mixing[223]. Hence, the minimum agitation speeds necessary for complete suspension of the various catalysts were estimated using the Zwietering correlation and the reactor dimensions in appendix A5.1.[281] The values obtained can be seen in Table 5.1. As expected the predicted minimum agitation speed varied with the catalyst type from 101 rpm to 206 rpm. Most importantly these values provides a benchmark for subsequent agitation test to rule out external transport limitation.

Table 5.1. Minimum Agitation Speed Calculated from Zwietering Correlation.[281]

Catalyst	Catalyst Density (g/ml)	Characteristic Length(μm)	Minimum Agitation Speed (rpm)
Pd/C	3.863	145.9	206
Pd/Al$_2$O$_3$	3.432	26.33	113
PdRh/Al$_2$O$_3$	4.909	13.82	101

The effect of changes in agitation speed on initial rate of vanillin HDO reaction was examined experimentally using the procedure described in Section 3.3.7 of Chapter 3. Differential analysis method described in the literature was used to estimate the initial reaction rate from the polynomial fitted to the conversion – time data.[223, 282,283] Figure A5.2 shows how the method was applied to the data to determine the initial reaction rate. The changes in estimated initial reaction rates following variation in the agitation speed are presented in Figure 5.1a. Notably, the initial reaction rate increases from $(6.57 \pm 0.32) \times 10^{-4}$ kmol/kg$_{cat}$min to $(22.9 \pm 0.24) \times 10^{-4}$ kmol/kg$_{cat}$min as agitation speed increases from 100 rpm to 500 rpm. Similarly, the initial reaction rate increases from $(22.9 \pm 0.24) \times 10^{-4}$ kmol/kg$_{cat}$min to $(25.3 \pm 0.48) \times 10^{-4}$ kmol/kg$_{cat}$min as agitation speed increases from 500 rpm to 900 rpm. However, further increase in

the agitation speed from 900 rpm to 1300 rpm caused insignificant change in the initial reaction rate. On this basis, it seems the use of agitation speed above 900 rpm eliminates external transport limitation in the reactor. To validate this conclusion, a commercial 10 wt % Pd/C catalyst was used to repeat the test at higher temperature of 338 K following the procedure described in Section 3.3.7 of Chapter 3. Figure 5.1b summarises observed changes in conversion as agitation speed increases from 300 rpm to 1100 rpm.
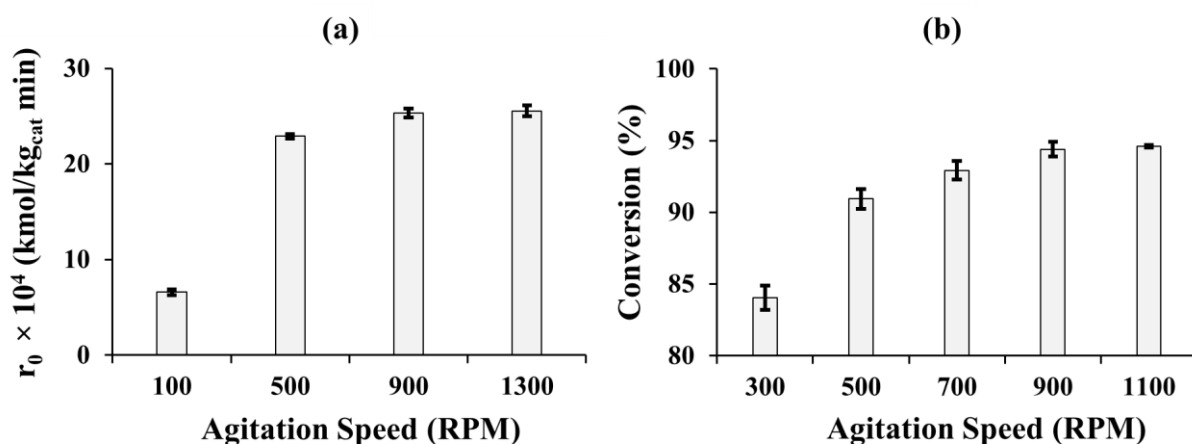
Fig. 5.1. (a) Effect of changes in agitation speed on initial reaction rate of VL at T = 318 K, P_H = 2.0 MPa, ω = 3.4 kg/m³, C_{VL0} = 263.0 mM, and t = 50 mins using the prepared bimetallic 6.5 wt % PdRh/Al₂O₃ catalyst, and (b) Effect of changes in agitation speed on VL conversion at T = 338 K, P_H = 1.0 MPa, ω = 0.27 kg/m³, C_{VL0} = 65.0 mM, and t = 30 mins using commercial 10 wt % Pd/C catalyst. Reaction solvent is ethyl acetate.

In agreement with findings from the initial test, it can be seen that conversion increases from (84.1 ± 0.86) % to (90.9 ± 0.69) % as agitation speed increases from 300 rpm to 500 rpm. Likewise, further increase in the agitation speed from 500 rpm to 700 rpm improves conversion from (90.9 ± 0.69) % to (92.9 ± 0.64) %. Interestingly, the improvement in conversion diminishes as the speed of agitation increases. In fact, conversion remains unchanged following increase in the agitation speed from 900 rpm to 1100 rpm. This result validates earlier conclusion that using an agitation speed above 900 rpm eliminates external transport limitation in the reactor. Furthermore, this result is in line with agitation speed often reported in the

literature as sufficient to eliminate external transport limitation in similarly scaled laboratory reactors.[282,284] Hence, subsequent results reported in this chapter were obtained from experiments carried out using agitation speed of 1000 rpm.

5.2.2. Internal Transport Limitations Consideration

As previously mentioned in Section 5.2, the reaction rate can be affected severely by internal transport limitations, such as pore diffusion. Consequently, it is necessary to eliminate internal transport limitations in the reaction system. To fulfil this objective, reactions were carried out based on the procedure described in Section 3.3.7 of Chapter 3 using samples of 2 wt % Pd/Al$_2$O$_3$ catalyst sieved into different particle sizes. This approach has been used in numerous studies on kinetics to probe the significance of internal transport limitations.[190,277,285] Figure 5.2 depicts the influence of particle size on initial reaction rates of vanillin HDO. It clearly shows that the initial reaction rate increases from $(2.84 \pm 0.07) \times 10^{-4}$ kmol/kg$_{cat}$min to $(3.38 \pm 0.06) \times 10^{-4}$ kmol/kg$_{cat}$min as the particle size decreases from fraction > 250 μm to 180 μm – 250 μm fraction. Likewise, as the particle size decreases from 180 μm – 250 μm fraction to 90 μm – 180 μm fraction, the initial reaction rate increases from $(3.38 \pm 0.06) \times 10^{-4}$ kmol/kg$_{cat}$min to $(3.57 \pm 0.05) \times 10^{-4}$ kmol/kg$_{cat}$min. Nonetheless, the initial reaction rate seems less sensitive to the change in particle size from 180 μm – 250 μm fraction to 90 μm – 180 μm fraction. In fact, it can be seen in Figure 5.2 that further decrease in the particle size caused negligible change in the initial reaction rate. From this analysis, it seems the use of catalyst particles smaller than 250 μm eliminates internal transport limitation. As a result of this finding, particles smaller than 250 μm were used in subsequent investigations in this chapter.
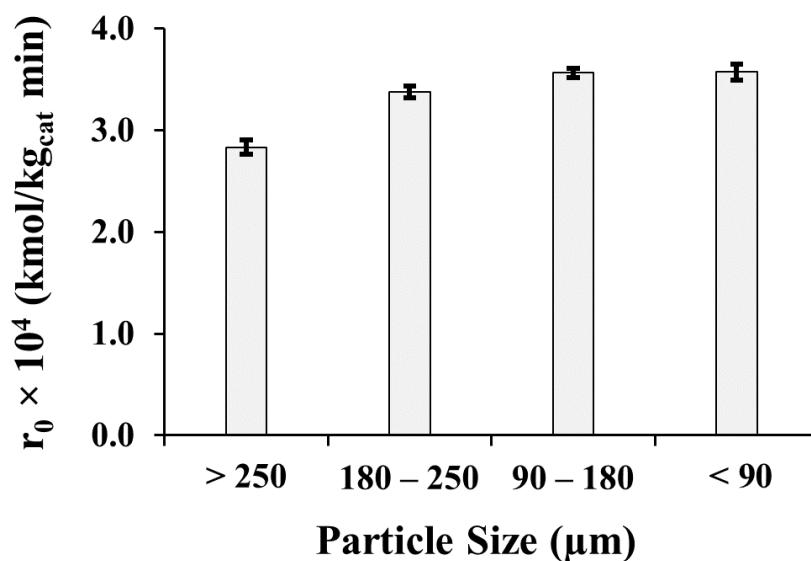
Fig. 5.2. Influence of particle size on initial reaction rate of VL at 1000 rpm, T = 318 K, P_H = 2.0 MPa, ω = 3.4 kg/m³, C_{VL0} = 263.0 mM, and t = 50 mins using commercial 2 wt % Pd/Al₂O₃ catalyst. Reaction solvent is ethyl acetate.

To reaffirm the absence of internal transport limitation, the role of pore diffusion from the three catalysts on the reaction were characterised via Weisz and Prater criterion using a dimensionless parameter called observable modulus. The observable modulus which represent the ratio of reaction rate to transport rate was estimated using equation 5.1.

$$\eta\phi^2 \; = \frac{r_0\omega L^2}{C_i D_{ei}} \; , \quad \text{where i} = \text{VL, H}_2 \tag{5.1}$$

Herein, r_0 represents the initial reaction rate, η the effectiveness factor, ϕ the Thiele Modulus, ω the catalyst loading and L the characteristic length of the catalyst particle. Liquid-phase effective diffusivities (D_{ei}) of the reactants were estimated from Wilke – Chang equation[284], while correlation suggested by Pintar et al[287] was used to calculate the concentration of hydrogen C_{H2} (kmol/m³). The results are presented in Table 5.2, it shows that for each of the catalyst, the estimated observable moduli for both vanillin and hydrogen were significantly less than 1. This indicates faster internal transport rate compared to the reaction rate, therefore, the reactions were not limited by internal transport. According to Chen et al.,[223,282] when the ratio

of hydrogen observable moduli to the model compound observable moduli is much greater than 1, hydrogen is the limiting reactant within the system. Notably, under each of the catalysts, the computed observable moduli for hydrogen gas were at least three times bigger than that of vanillin. Hence, it can be concluded that hydrogen gas is the limiting reactant in the system. Additionally, since the computed observable modulus for both vanillin and hydrogen gas were significantly less than 0.3, it indicates the order of reaction with respect to hydrogen gas partial pressure and vanillin concentration will be less than or equal to 2.[284]

Table 5.2. Results of Weisz – Prater Analysis at 318 K

Parameters	Catalyst Type		
	Pd/C	Pd/Al$_2$O$_3$	PdRh/Al$_2$O$_3$
	Values	Values	Values
ω (kg/m^3)	0.27	4.6	4.6
C_{VL0} (mM)	65.0	74.6	263
C_{H2} (mM)	1.18	2.36	2.70
r × 10^3(kmol/ (kg$_{catalyst}$ min))	8.53	2.09	1.56
L (μm)	146	26.3	13.8
$D_{e, VL}$ × 10^9 (m^2/s)	2.01	2.01	2.01
$D_{e, H2}$ × 10^8 (m^2/s)	1.77	1.77	1.77
$\eta\phi_{vl}^2$	6.26 ×10^{-3}	7.40 ×10^{-4}	4.40 ×10^{-5}
$\eta\phi_{H}^2$	3.90 ×10^{-2}	2.65 ×10^{-3}	4.80 ×10^{-4}

5.3. Proposed Reaction Scheme

In the course of investigating the kinetics of vanillin HDO reaction under the various catalysts, typical concentration – time profiles observed are presented in Figures 5.3a to 5.3c. In conformity with the literature[74, 75,280], Figure 5.3 shows that over monometallic and bimetallic Pd-based catalysts, the products formed from the reaction include vanillyl alcohol and creosol

because the concentration of these compounds increases over time as the vanillin concentration decreases. However, in recent work by Shit et al.,[73] on vanillin hydrodeoxygenation over a bimetallic Cu_3Pd nanoalloy anchored on N-rich porous organic polymer at 413 K, guaiacol, p-cresol and cyclohexanol were reported as products from undesirable side reactions such as decarbonylation, deeper hydrogenation and hydrogenolysis. Hence, at temperatures higher than the maximum temperature of 338 K considered in this work, undesirable products such as those mentioned in the work of Shit et al., [73] may appear.
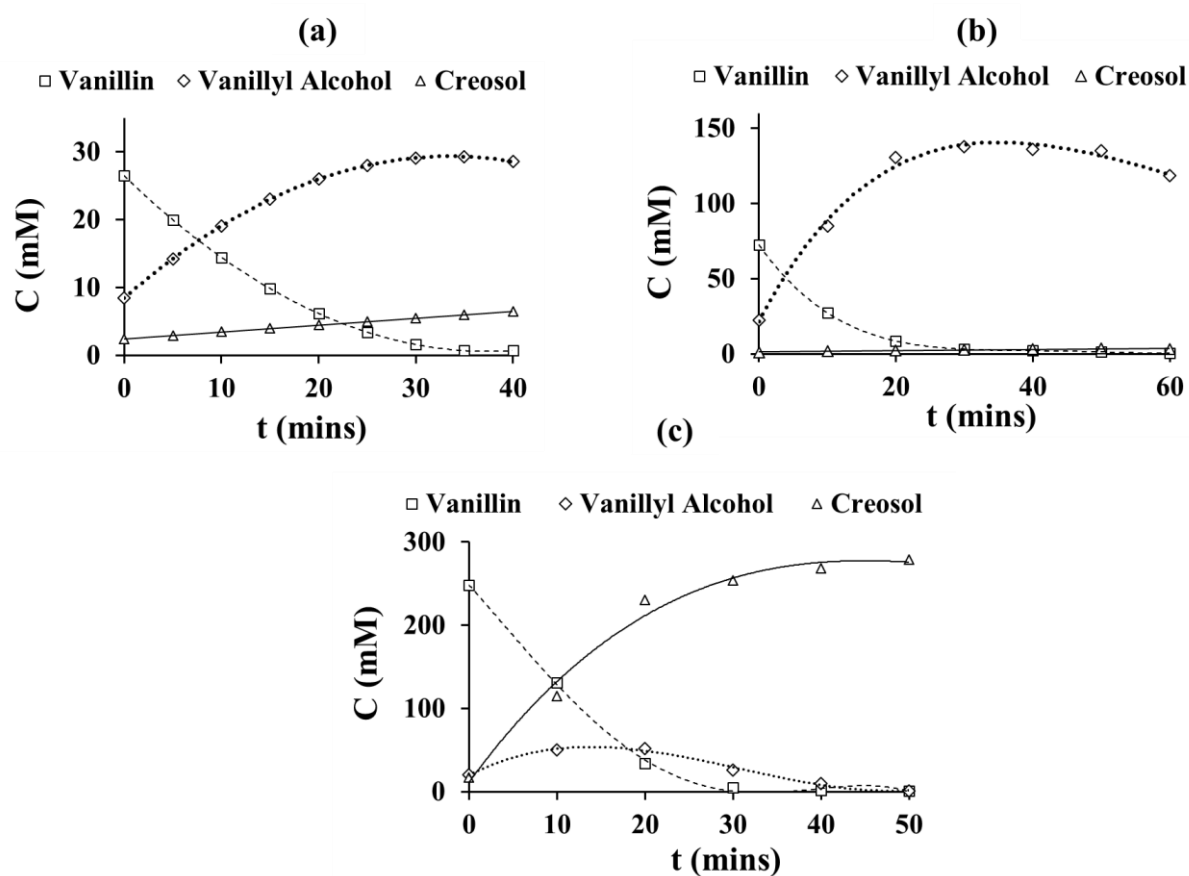
Fig. 5.3. Typical concentration against time profile during vanillin HDO reaction over (a) commercial 10 wt % Pd/C catalyst , (b) commercial 5 wt % Pd/Al$_2$O$_3$ catalyst, and (c) synthesised 6.5 wt % PdRh/Al$_2$O$_3$ catalyst. Reaction solvent is ethyl acetate. Lines represent best polynomial fit to the data.

Interestingly, Figure 5.3 shows that creosol formation was less prominent in the presence of monometallic Pd-based catalysts compared to the prepared bimetallic PdRh/Al$_2$O$_3$ catalyst.

This observation is in line with the previous claim in Section 4.4 of Chapter 4. The sequence in which the products appeared indicates the reaction proceeded via hydrogenation of vanillin to vanillyl alcohol followed by hydrogenolysis of the vanillyl alcohol to creosol. Notably the same sequence was reported in the work of Bindwal et al., [160] and Santos et al., [74] on vanillin hydrodeoxygenation reaction over noble metals supported on activated carbon. Moreover, the concentration – time profile observed under the prepared bimetallic PdRh/Al$_2$O$_3$ catalyst represented by Figure 5.3c further validates the proposed sequence displayed in Scheme 1 because it shows significant decline in concentration of the intermediate product vanillyl alcohol from a maximum of 52.2 mM at t = 20 mins to 1.4 mM at t = 50 mins.

Scheme 1. Reaction Steps for Vanillin HDO over Monometallic and Bimetallic Pd-based Catalysts

Vanillin   Vanillyl Alcohol   Creosol
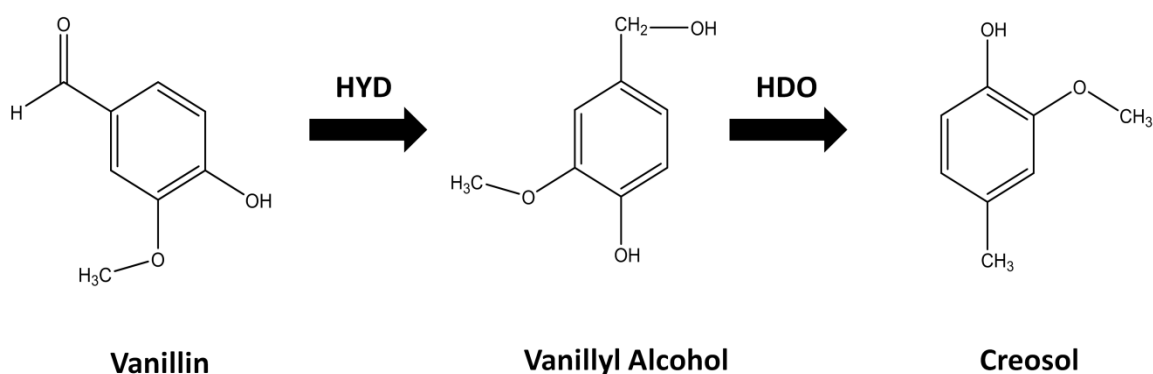
5.4. Effect of Catalyst Loading

The influence of catalyst loading (ω) on initial rates of vanillin (VL) disappearance (r_0) during VL hydrodeoxygenation over commercial 10 wt % Pd/C, commercial 5 wt % Pd/Al$_2$O$_3$, and the prepared 6.5 wt % PdRh/Al$_2$O$_3$ catalysts was experimentally examined through the procedure described in Section 3.3.8 of Chapter 3. Figure 5.4A summarises observed changes in r_0 as ω increases per catalyst at different reaction temperatures.
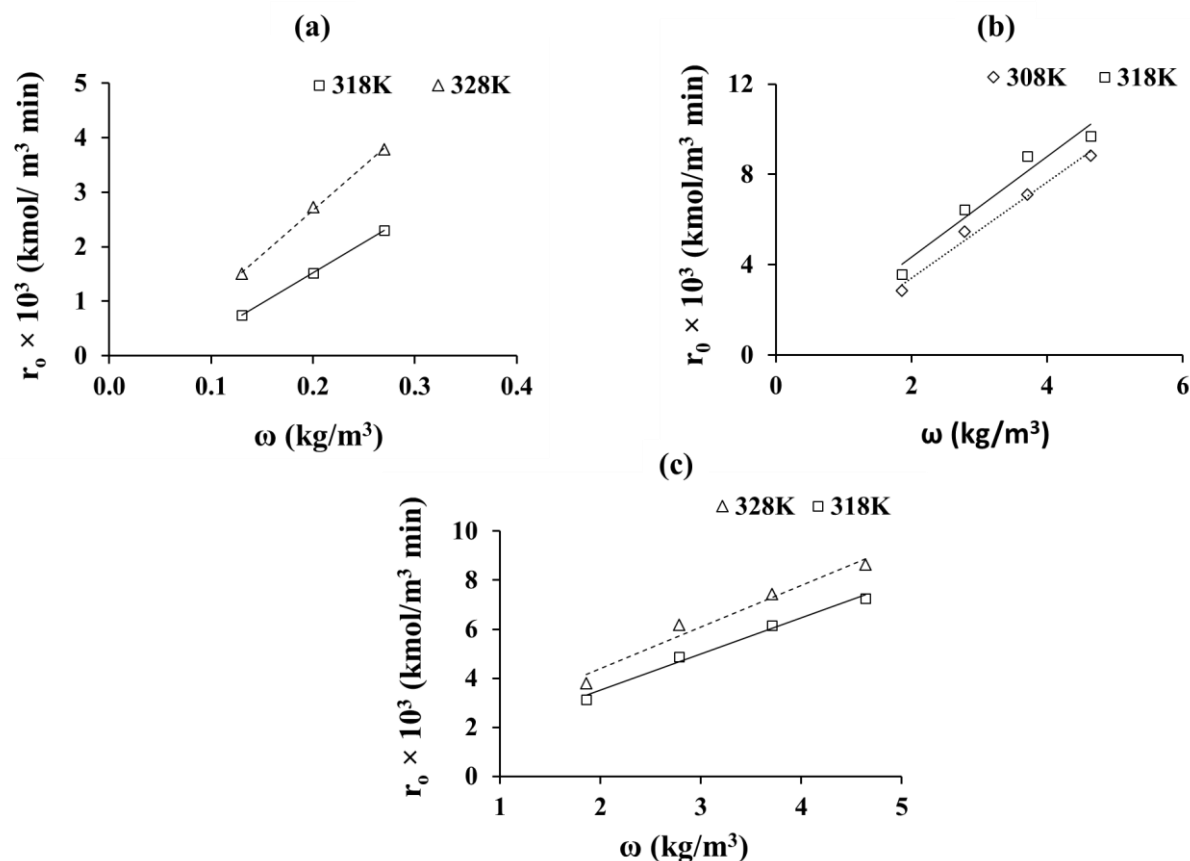
Fig. 5.4A. Effect of catalyst loading on vanillin HDO reaction over (a) commercial 10 wt % Pd/C catalyst at 1000 rpm, T = 318 K and 328 K, P_H = 1.0 MPa,, and C_{VL0} = 65.0 mM, (b) commercial 5 wt % Pd/Al$_2$O$_3$catalyst, at 1000 rpm, T = 308 K and 318 K, P_H = 2.0 MPa,, and C_{VL0} = 263.0 mM, and (c) prepared 6.5 wt % PdRh/Al$_2$O$_3$ catalyst at 1000 rpm, T = 318 K and 328 K, P_H = 3.0 MPa,, and C_{VL0} = 263.0 mM. Reaction Solvent is ethyl acetate. Lines represent best linear fit to the data.

At the different temperatures considered, Figure 5.4A shows that r_0 increases as ω increases. This is not surprising since reaction rates are expected to change in proportion with the number of active sites in a kinetically controlled regime.[284] Hence, the results presented in Figure 5.4A reaffirms the claim in Section 5.2 that transport limitations are negligible in the reaction system. The most definitive test for transport limitation check in laboratory scale reactor is the Madon Boudart test.[284] According to this test, for reactions conducted under internal transport limitation, slope of the ln – ln plot of the catalyst activity against surface metal concentration will be 0.5, while for reactions conducted under external transport limitation their slope will be

zero. Figure 5.4B represents the Madon Boudart test for vanillin HDO reaction under the different catalysts. It shows linear correlation between ln – ln activity of the catalysts and the surface metal concentrations at two different temperatures. Most importantly the slope of lines displayed in Figure 5.4B are greater than 0.5. This result suggest mass and heat transport resistances are absent within the range of conditions considered in this work.
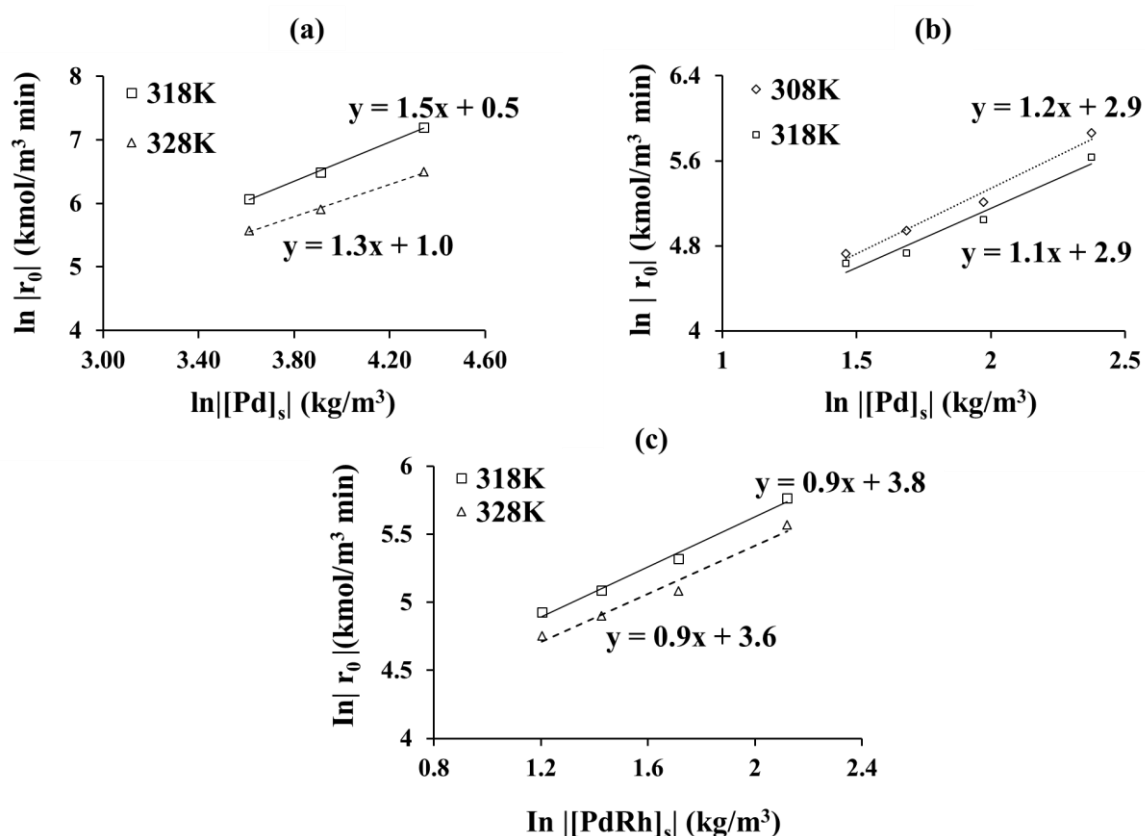
Fig. 5.4B. Madon Boudart test for vanillin HDO reaction over (a) commercial 10 wt % Pd/C catalyst, (b) commercial 5 wt % Pd/Al$_2$O$_3$ catalyst, and (c) prepared bimetallic 6.5 wt % PdRh/Al$_2$O$_3$ catalyst.

The maximum initial turnover frequency (TOF) estimated using procedure described in appendix A5.2 was 12.0 per min for the Pd/C catalyst, 0.8 per min for the Pd/Al$_2$O$_3$ catalyst, and 27.9 per min for the prepared bimetallic PdRh/Al$_2$O$_3$ catalyst. This result is expected because it confirms superior activity of the prepared bimetallic PdRh/Al$_2$O$_3$ catalyst over the

mono-metal catalysts. Notably, the estimated maximum initial TOF values for the mono-metals are lower than the value of 15.6 per min reported in the work of Zhang et al., [282] which utilised Ru/C catalyst with 13% metal dispersion. The remarkable difference between the metal dispersion of the mono-metals used in this work and that of the Ru/C catalyst in the literature possibly explains the observed discrepancies in the maximum initial TOF values. In addition, the prepared bimetallic PdRh/Al$_2$O$_3$ catalyst demonstrated superior activity over Ru/C since the maximum initial TOF value for the former is higher than the value reported in the literature for Ru/C catalyst.[282]

5.5. Effect of Hydrogen Gas Pressure

The procedure described in Section 3.3.8 of Chapter 3 was used to examine the influence of hydrogen gas partial pressures (P_H) on initial rates of vanillin (VL) disappearance (r_0) during VL HDO reaction over commercial 10 wt % Pd/C catalyst, commercial 5 wt % Pd/Al$_2$O$_3$ catalyst, and the prepared bimetallic 6.5 wt % PdRh/Al$_2$O$_3$. Figure 5.5A depicts observed variation in r_0 as P_H increases under the different catalysts. As shown in Figure 5.5Aa which represent reactions under Pd/C catalyst, the value of r_0 increases from 0.72×10^{-2} kmol/kg$_{cat}$min to 1.00×10^{-2} kmol/kg$_{cat}$min as P_H increases from 1.0 MPa to 3.0 MPa. In addition, Figure 5.5Aa shows that r_0 increases from 0.86×10^{-2} kmol/kg$_{cat}$min to 1.28×10^{-2} kmol/kg$_{cat}$min following changes in P_H from 1.0 MPa to 3.0 MPa at elevated temperature of 328 K. Interestingly, the same trend is repeated in Figures 5.5Ab and 5.5Ac representing reactions in the presence of Pd/Al$_2$O$_3$ and PdRh/Al$_2$O$_3$ catalyst respectively. This result suggest increase in H$_2$ gas partial pressure generally enhances the initial rate of vanillin disappearance. Likewise, this conclusion complements claim in Section 5.2.2 that H$_2$ gas is the limiting reactant in the system. In addition, this conclusion is in line with claim in the literature that elevated operating

pressure enhances the rate of HDO reaction due to higher hydrogen availability in vicinity of the catalyst.[130]
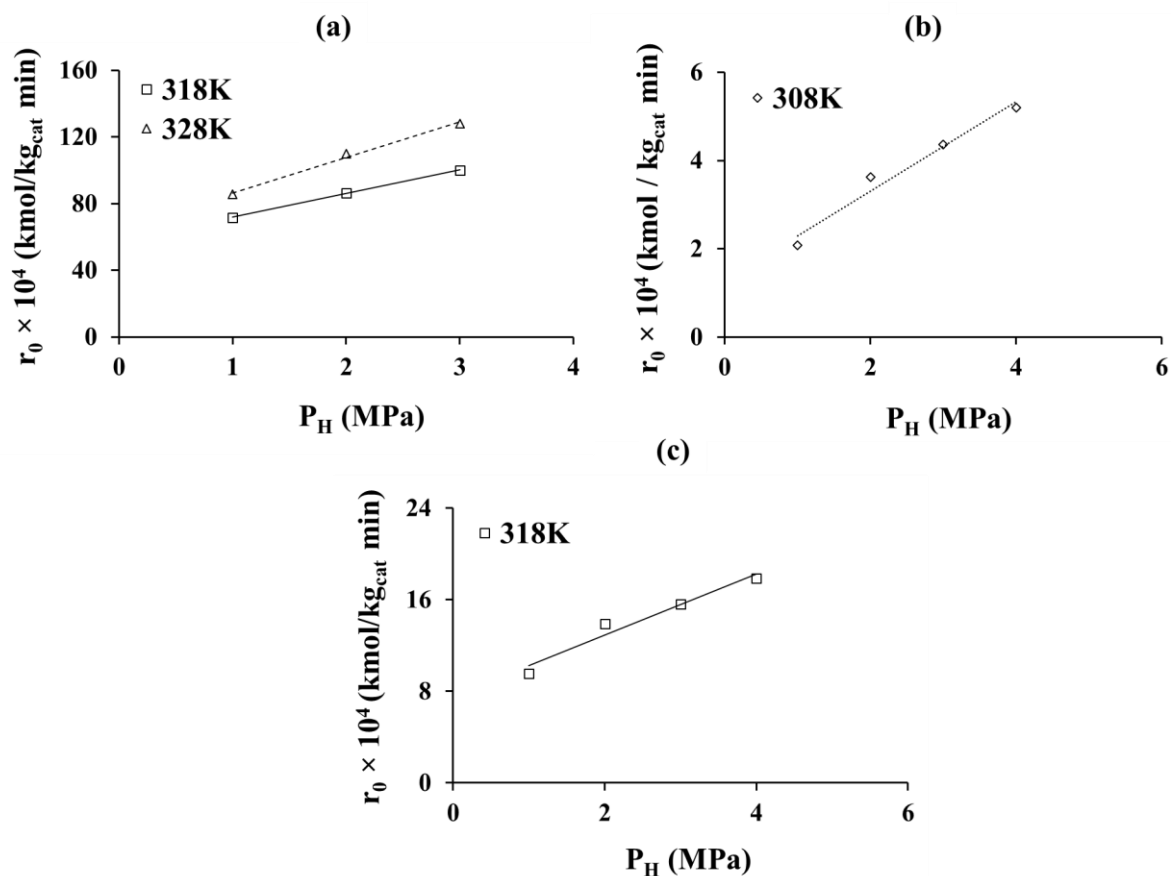
Fig. 5.5A. Influence of H_2 gas partial pressure (P_H) on initial rates of VL disappearance (r_0) at (a) commercial 10 wt % Pd/C catalyst at 1000 rpm, T = 318 K and 328 K, C_{VL0} = 65.0 mM, and ω = 0.3 kg/m³, (b) commercial 5 wt % Pd/Al₂O₃ catalyst at 1000 rpm, T = 308 K, C_{VL0} = 263.0 mM, , and ω = 5.0 kg/m³ and (c) prepared 6.5 wt % PdRh/Al₂O₃ catalyst at 1000 rpm, T = 318 K, C_{VL0} = 263.0 mM, and ω = 5.0 kg/m³. Reaction solvent is ethyl acetate. Lines represent best linear fit to the data.

In order to determine the order of reaction with respect to hydrogen gas partial pressure (P_H), the natural logarithm of the initial reaction rate (r_0) against the natural logarithm of P_H was plotted (see Figure 5.5B). The orders of reaction with respect to P_H found from the slope of ln (r_0) versus ln (P_H) in Figure 5.5B were all fractional numbers. These includes 0.3 to 0.4 under Pd/C catalyst, 0.7 under Pd/Al₂O₃catalyst, and 0.4 under PdRh/Al₂O₃ catalyst. As a result, it

can be concluded that vanillin HDO reaction exhibits nonfirst-order kinetics with respect to P_H.

Again, this conclusion is in conformity with the initial claim in Section 5.2.2 that the order of reaction with respect to P_H will be ≤ 2. Interestingly, a nonfirst-order dependence on hydrogen gas pressure has been reported previously in the work of Wan et al.,[232] on hydrogenation of 2-butanone in water using Ru/C catalyst. It is clear from the order of reactions found at two different temperatures with Pd/C as the catalyst, changes in temperature had insignificant effect on dependence of the initial reaction rate (r_0) on hydrogen gas partial pressure (P_H). As a result, the author of this work decided to investigate the effect of P_H on r_0 under Pd/Al$_2$O$_3$ catalyst and PdRh/Al$_2$O$_3$ catalyst at different single temperatures.
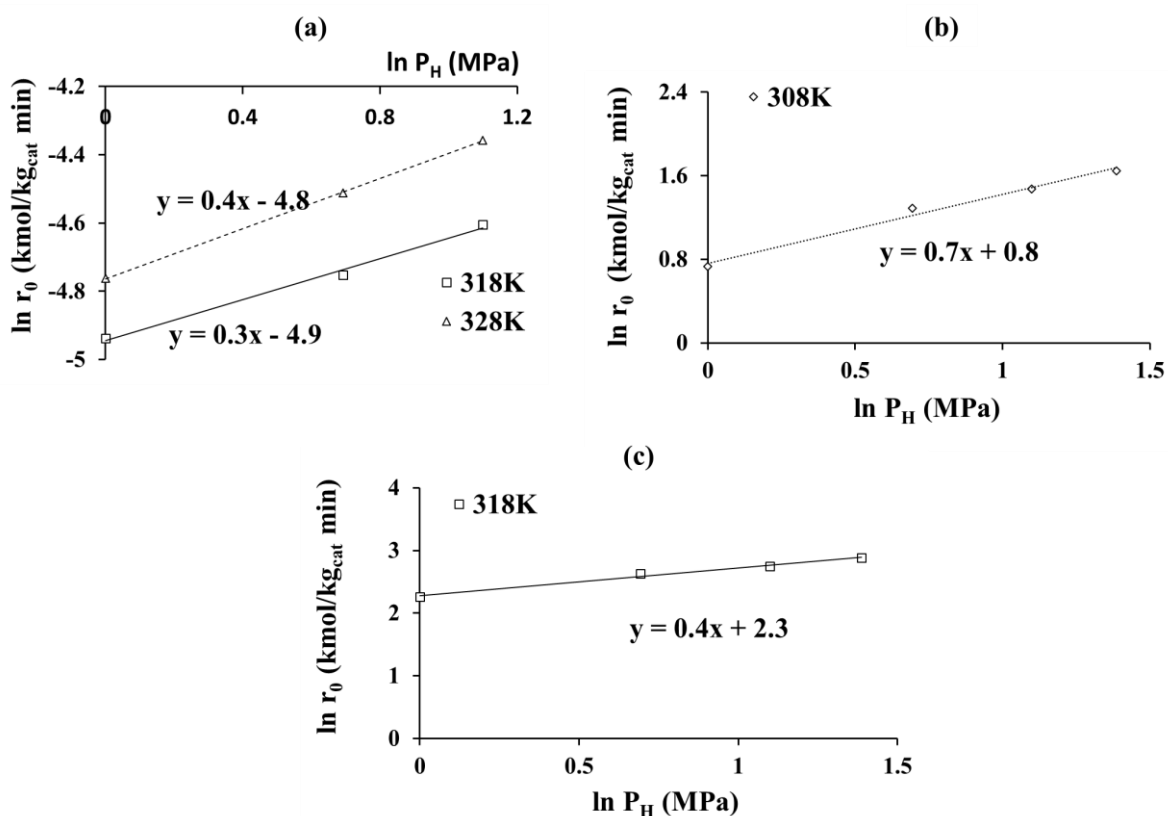
Fig. 5.5B. ln – ln plot of catalyst activity (r_0) against P_H under (a) commercial 10 wt % Pd/C ,(b) commercial 5 wt % Pd/Al$_2$O$_3$ catalyst, and (c) prepared 6.5 wt % PdRh/Al$_2$O$_3$ catalyst.

In order to tentatively establish the region of limitation in the system, the conventional approach involving plot of (C_H/r_0) against $1/\omega$ reported in the literature was employed.[288] The

plot is presented in Figure 5.6, it has an intercept of 0.03 min which represent the resistance against gas absorption through the liquid film at the gas – liquid interface.

$y = 1.51x + 0.03$
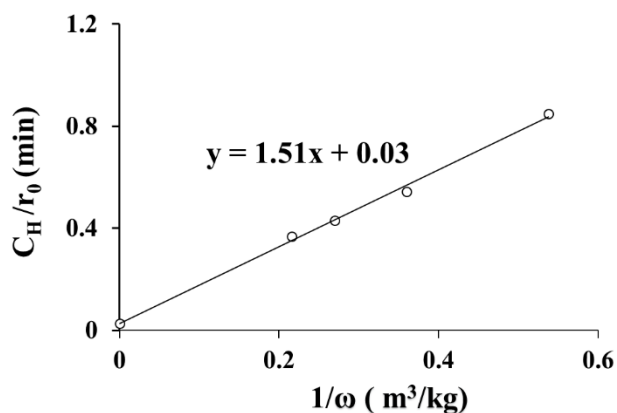
Fig. 5.6. Effect of catalyst loading on controlling resistance in a batch reactor using prepared bimetallic 6.5 wt % $PdRh/Al_2O_3$ catalyst at 1000 rpm, T = 318 K, P_H = 3.0 MPa,, and C_{VL0} = 263.0 mM. Reaction solvent is ethyl acetate. Line represent best linear fit to the data and shape represent actual data point.

In comparison to the total resistance of 0.43 min, it can therefore be concluded that the resistance against gas absorption was not significant. As a result, resistance against surface reaction between vanillin and hydrogen appears to be the most likely region of limitation in the system because external and internal diffusional resistances have been ruled out previously in Sections 5.2.1 and 5.2.2. Nonetheless, it is worth mentioning that the present analysis only provides an insight into resistances within the system. Besides, the method was originally developed under the assumption of first-order kinetics with respect to the limiting reactant, which of course is not the case here.

5.6. Effect of Initial Vanillin Concentration

The effect of changes in starting concentration of vanillin (C_{VL0}) on the initial rate of vanillin disappearance (r_0) during vanillin (VL) HDO reaction over the different catalysts was experimentally studied using the procedure described in Section 3.3.8 of Chapter 3. Figure 5.7Aa shows the observed changes in r_0 as C_{VL0} increases from 35 mM to 65 mM at different

reaction temperatures using Pd/C catalyst. While Figure 5.7Ab represent changes in r_0 as C_{VL0}

increases from 98 mM to 512 mM at 318 K using Pd/Al$_2$O$_3$ catalyst. Figure 5.7Ac depicts

observed changes in r_0 as C_{VL0} increases from 263 mM to 526 mM at 318 K using the prepared

bimetallic PdRh/Al$_2$O$_3$ catalyst.
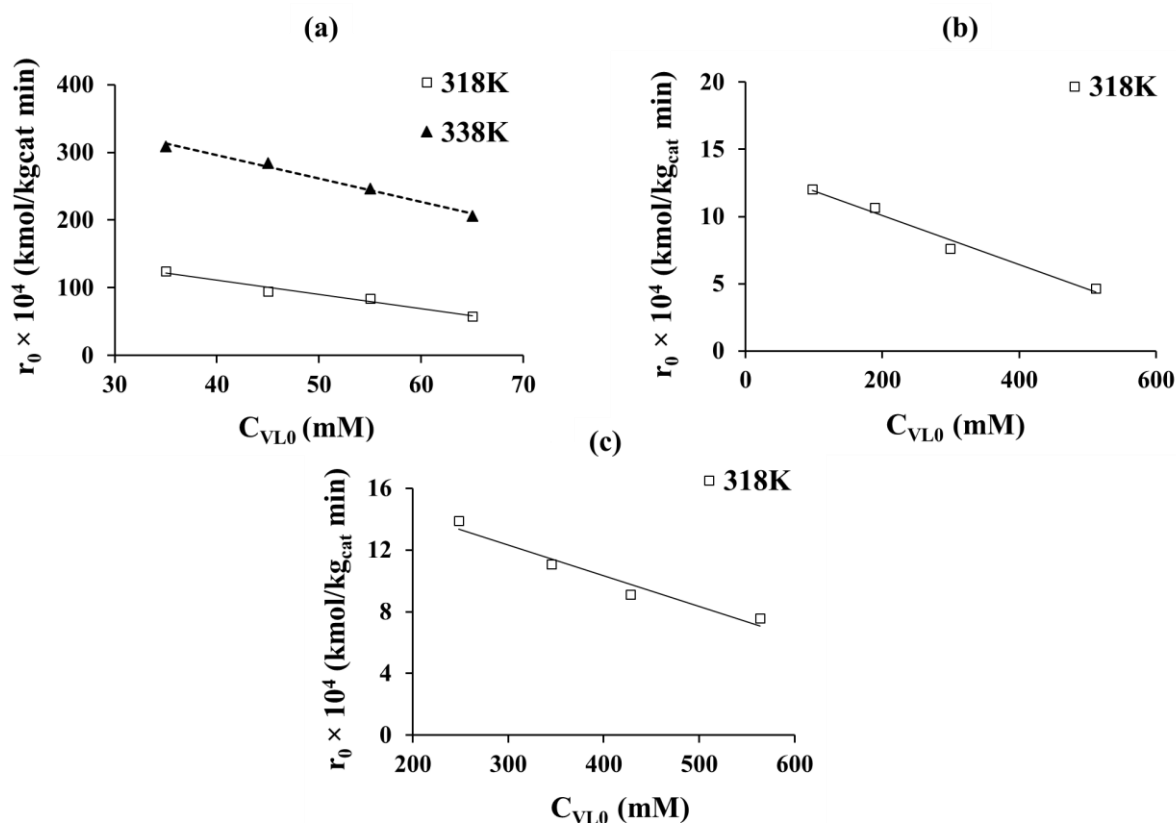
Fig.5.7A. Effect of changes in the starting concentration of vanillin on initial rate of vanillin disappearance (a) commercial 10 wt % Pd/C catalyst at 1000 rpm, T = 318 K and 338 K , P$_H$ = 1.0 MPa, and ω = 0.1 kg/m^3 (b) commercial 5 wt % Pd/Al$_2$O$_3$ catalyst at 1000 rpm, T = 318 K, P$_H$ = 2.0 MPa, and ω = 5.0 kg/m^3, and (c) prepared 6.5 wt % PdRh/Al$_2$O$_3$ catalyst at 1000 rpm, T = 318 K, P$_H$ = 2.0 MPa, and ω = 5.0 kg/m^3. Reaction solvent is ethyl acetate. Lines represent best linear fit to the data.

It can be seen that under each of the catalysts, r_0 decreases as C_{VL0} increases. For instance,

Figure 5.7Aa shows that the value of r_0 decreases from 3.04×10^{-2} kmol/kg$_{cat}$min to 2.16×10^{-2}

kmol/kg$_{cat}$min as C_{VL0} increases from 35 mM to 65 mM at 338 K using Pd/C catalyst. Likewise,

Figure 5.7Ac indicates that r_0 decreases from 13.9×10^{-4} kmol/kg$_{cat}$min to 7.6×10^{-4}

kmol/kg$_{cat}$min as C_{VL0} increases from 263 mM to 526 mM using the synthesised PdRh/Al$_2$O$_3$ catalyst. In the case of Pd/Al$_2$O$_3$ catalyst, Figure 5.7Ab shows that r$_0$ decreases from 12.0 ×10^{-4} kmol/kg$_{cat}$min to 4.7 × 10^{-4} kmol/kg$_{cat}$min as C_{VL0} increases from 98 mM to 512 mM. Hence, it can be concluded that activity of the three catalysts decreases as C_{VL0} increases. This conclusion contradicts the expected trend of reaction rate increasing with starting reactant concentration. Nonetheless, similar trend of decreasing reaction rate as initial concentration of the reactant increases has been reported previously in the work of Maccarrone et al., [285] and Wan et al., [232] on hydrogenation of 1-heptyne and 2-butanone respectively. Hence, the observed phenomenon is unusual but possible in heterogeneous catalysed reaction. A plausible explanation for this unusual but interesting phenomenon is that the number of active sites available for adsorption of hydrogen gas which is the limiting reactant reduces as C_{VL0} goes up. On the basis of the observed trend in activity of the catalyst as C_{VL0} increases, it can be concluded that vanillin HDO reaction exhibits nonfirst-order dependence on vanillin concentration. It can be observed from the slopes of the plots of ln (r$_0$) against ln (C_{VL0}) in Figures 5.7Ba, 5.7Bb, and 5.7Bc that the orders of reaction with respect to vanillin concentration ranges from −1.2 to −0.6. This result reaffirms the conclusion in Section 5.2.2 that the order of reaction with respect to vanillin concentration will be ≤ 2 since the estimated observable moduli based on vanillin were significantly smaller than 0.3. More importantly, the nonfirst-order dependence of the reaction on starting concentration of vanillin suggests the development of model describing vanillin HDO reaction kinetics requires consideration of processes such as adsorption, surface reaction, and desorption which occurred on the catalyst surface. Hence, reaction kinetics of vanillin HDO would be better described using Langmuir – Hinshelwood (L – H) type of rate expression.
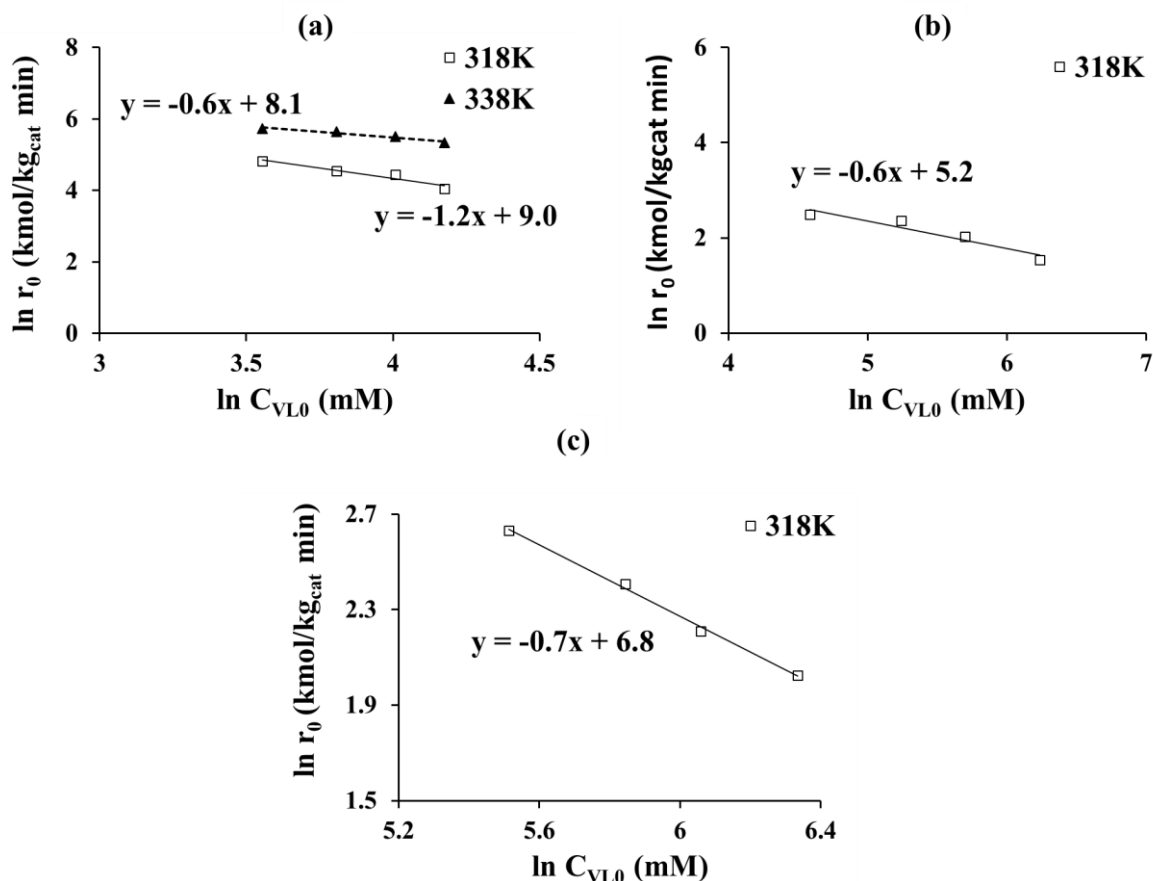
Fig.5.7B. ln – ln plot of catalyst activity against starting concentration of vanillin using (a) commercial 10 wt % Pd/C catalyst, (b) commercial 5 wt % Pd/Al$_2$O$_3$catalyst, and (c) synthesised 6.5 wt % PdRh/Al$_2$O$_3$ catalyst.

5.7. Effect of Temperature

The procedure described in Section 3.3.8 of Chapter 3 was used to examine the influence of reaction temperature on vanillin HDO. In conformity with the theory that reaction rates generally increases with temperature, the plot of initial rate of vanillin disappearance (r_0) against reaction temperature for each of the catalyst presented in Figures 5.8Aa, 5.8Ab, and 5.8Ac shows that increase in the reaction temperature enhances r_0.
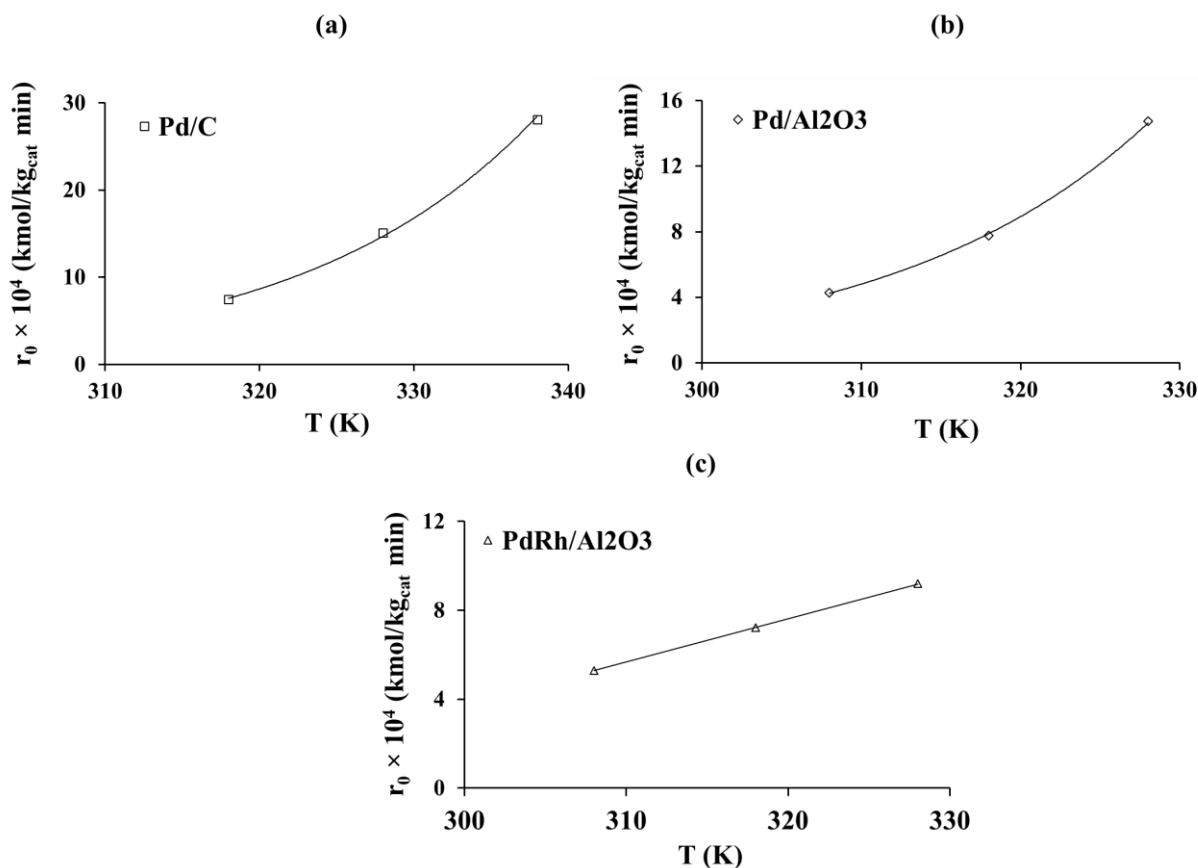
Fig.5.8A. Effect of changes in reaction temperature on initial rate of vanillin disappearance. (a) commercial 10 wt % Pd/C catalyst at 1000 rpm, P_H = 1.0 MPa, C_{VL0} = 35.0 mM, and ω = 0.1 kg/m^3, (b) commercial 5 wt % Pd/Al$_2$O$_3$ catalyst at 1000 rpm, P_H = 2.0 MPa, C_{VL0} = 350.0 mM, and ω = 5.0 kg/m^3, and (c) prepared 6.5 wt % PdRh/Al$_2$O$_3$ catalyst at 1000 rpm, P_H = 2.0 MPa, C_{VL0} = 263.0 mM, and ω = 5.0 kg/m^3. Lines represent best polynomial fit to the data.

As expected from Arrhenius equation, Figures 5.8Aa and 5.8Ab shows that in the presence of mono-metal catalysts, r_0 increases exponentially with the reaction temperature. Conversely, Figure 5.8Ac shows that under the prepared bimetallic PdRh/Al$_2$O$_3$ catalyst, r_0 increases linearly with the reaction temperature. Hence, a 10 K change in the reaction temperature resulted into an average change of 90% in r_0 for reactions carried out with the monometallic Pd-based catalysts and 32% for those catalysed by the prepared bimetallic PdRh/Al$_2$O$_3$ particles. From slope of the plots of natural logarithm of initial rate of vanillin disappearance (r_0) versus reciprocal of the absolute temperature for the reactions in Figures 5.8Ba, 5.8Bb and 5.8Bc, the

estimated experimental activation energy (E_A) for vanillin HDO reaction was 59.2 kJ/mol using Pd/C catalyst, 51.9 kJ/mol using Pd/Al$_2$O$_3$ catalyst, and 23.2 kJ/mol using the prepared PdRh/Al$_2$O$_3$ catalyst. When compared to typical values of 12 to 21 kJ/mol reported as activation energy for reactions conducted under transport limitation, the estimated experimental activation energy values reaffirms the absence of transport limitation and collection of the experimental data in the kinetically controlled regime. [70, 289–291]
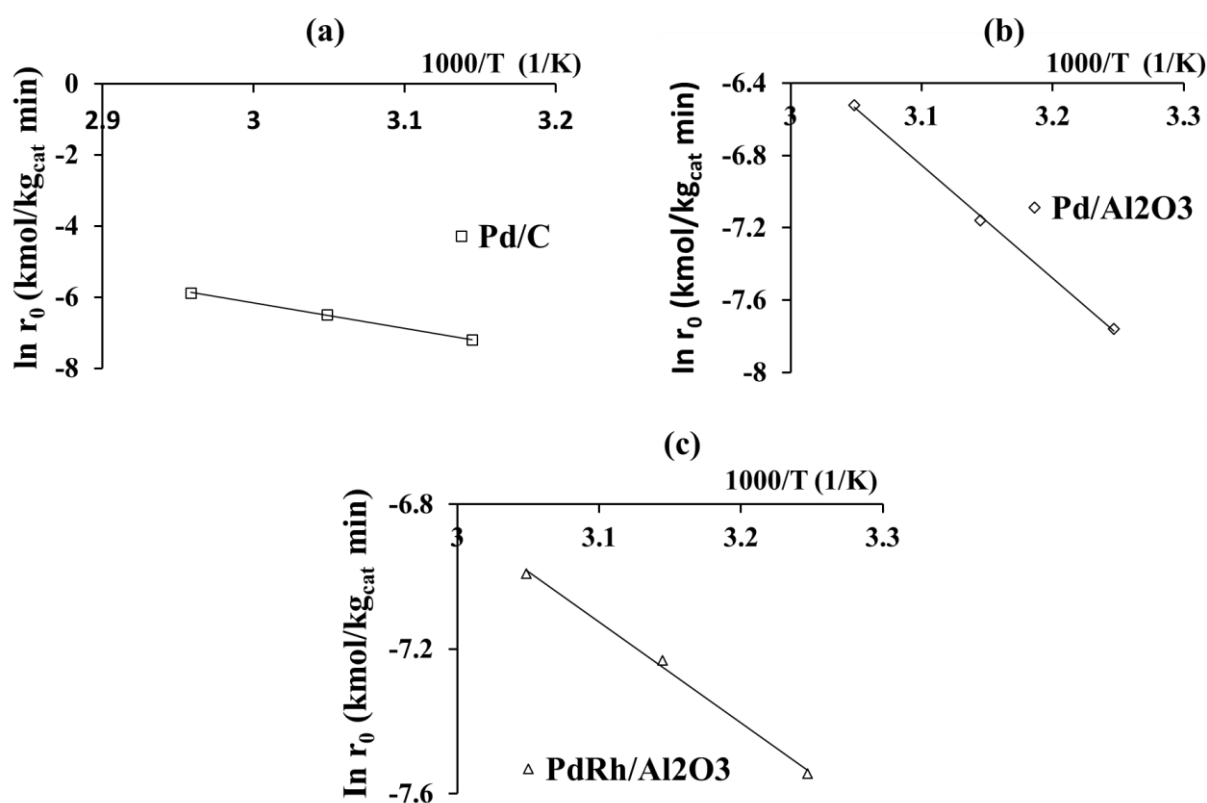
Fig.5.8B. ln – ln plot of catalyst activity against reaction temperature for vanillin HDO reaction over (a) commercial 10 wt % Pd/C catalyst, (b) commercial 5 wt % Pd/Al$_2$O$_3$ catalyst, and (c) synthesised 6.5 wt % PdRh/Al$_2$O$_3$ catalyst.

In agreement with the claim in Section 5.4, the experimental activation energy estimated for the reaction under the prepared bimetallic PdRh/Al$_2$O$_3$ catalyst was remarkably lower than those measured using the mono-metal catalysts. The ligand effect between Pd and Rh metals on the

alumina support possibly encouraged an alternative reaction path with significantly reduced

activation energy. Figures 5.9A and 5.9B summarises changes in selectivity toward vanillyl

alcohol and creosol as the reaction progresses at different temperatures under each of the

catalysts.

Fig.5.9A. Vanillyl alcohol selectivity as function of the reaction time and temperature. (a)
commercial 10 wt % Pd/C catalyst at 1000 rpm, T = 318 K and 338 K, P_H = 1.0 MPa, C_{VL0} =
35.0 mM, and ω = 0.1 kg/m^3 (b) commercial 5 wt % Pd/Al$_2$O$_3$ catalyst at 1000 rpm, T = 308
K and 328 K, P_H = 2.0 MPa, C_{VL0} = 350.0 mM, and ω = 5.0 kg/m^3, and (c) prepared 6.5 wt %
PdRh/Al$_2$O$_3$ catalyst at 1000 rpm, T = 308 K and 328 K, P_H = 2.0 MPa, C_{VL0} = 263.0 mM, and
ω = 5.0 kg/m^3. Reaction solvent is ethyl acetate. Lines represent best polynomial fit to the
data.

Fig.5.9B. Creosol selectivity as function of the reaction time and temperature. (a) commercial 10 wt % Pd/C catalyst at 1000 rpm, T = 318 K and 338 K, P_H = 1.0 MPa, C_{VL0} = 35.0 mM, and ω = 0.1 kg/m³   (b) commercial 5 wt % Pd/Al$_2$O$_3$ catalyst at 1000 rpm, T = 308 K and 328 K, P_H = 2.0 MPa, C_{VL0} = 350.0 mM, and ω = 5.0 kg/m³, and (c) prepared 6.5 wt % PdRh/Al$_2$O$_3$ catalyst at 1000 rpm, T = 308 K and 328 K, P_H = 2.0 MPa, C_{VL0} = 263.0 mM, and ω = 5.0 kg/m³. Reaction solvent is ethyl acetate. Lines represent best polynomial fit to the data.

As shown in Figure 5.9Aa which represent the change in selectivity toward vanillyl alcohol over time for reactions carried out using Pd/C catalyst, the selectivity toward vanillyl alcohol marginally increased from t = 0 mins to t = 10 mins and remained relatively unchanged from t = 10 mins to t = 40 mins at T = 318 K. Conversely, the selectivity toward vanillyl alcohol diminished from t = 10 mins to t = 40 mins at T = 338 K. In the case of vanillin HDO reaction under Pd/Al$_2$O$_3$ catalyst, Figure 5.9Ab shows that selectivity toward vanillyl alcohol from t = 0 mins to t = 40 mins at T = 308 K marginally increased. While at higher reaction temperature

of 318 K, the selectivity toward vanillyl alcohol marginally increased from t = 0 mins to t = 20 mins and then decreased from t = 20 mins to t = 40 mins. Under the prepared bimetallic PdRh/Al$_2$O$_3$ catalyst in Figure 5.9Ac, it can be seen that the selectivity toward vanillyl alcohol increased from t = 0 mins to t = 10 mins and then diminished from t = 10 mins to t = 50 mins at T = 308 K and T = 328 K. As expected for consecutive reactions, Figures 5.9Ba to 5.9Bc which represent the selectivity toward creosol are mirror images of Figures 5.9Aa to 5.9Ac. Notably, Figure 5.9Ba shows that under the commercial Pd/C catalyst, selectivity toward the deoxygenated product creosol remained relatively constant after t = 10 mins at T = 318 K. While at T = 338 K, the selectivity toward creosol increased with time from t = 10 mins to t = 40 mins. Likewise, Figure 5.9Bc which represent the selectivity toward creosol from VL HDO reactions under the prepared bimetallic PdRh/Al$_2$O$_3$ catalyst, it can be seen that selectivity toward creosol increased from t = 10 mins to t = 50 mins at T = 308 K and T = 328 K. On the basis of this analysis, increase in the reaction temperature favoured selectivity toward creosol from VL HDO reactions conducted using either the commercial Pd/C catalyst or the prepared bimetallic PdRh/Al$_2$O$_3$ catalyst. Interestingly, Mahfud et al., [176] reported the same change in distribution of products following alteration in the reaction temperature for vanillin HDO. However, Figure 5.9Bb shows marginal decrease in the selectivity toward creosol as the reaction temperature increases over the range of 308 K to 328 K. Hence, it seems hydrogenation of vanillin to vanillyl alcohol was more favourable than hydrogenolysis of vanillyl alcohol to creosol when the reaction was catalysed by Pd/Al$_2$O$_3$ particles.

5.8. Effect of Reaction Products

The procedure described in Section 3.3.8 of Chapter 3 was used to examine the effect of vanillyl alcohol and creosol on vanillin conversion. Figures 5.10a and 5.10b depicts the effect of vanillyl alcohol and creosol on conversion respectively.
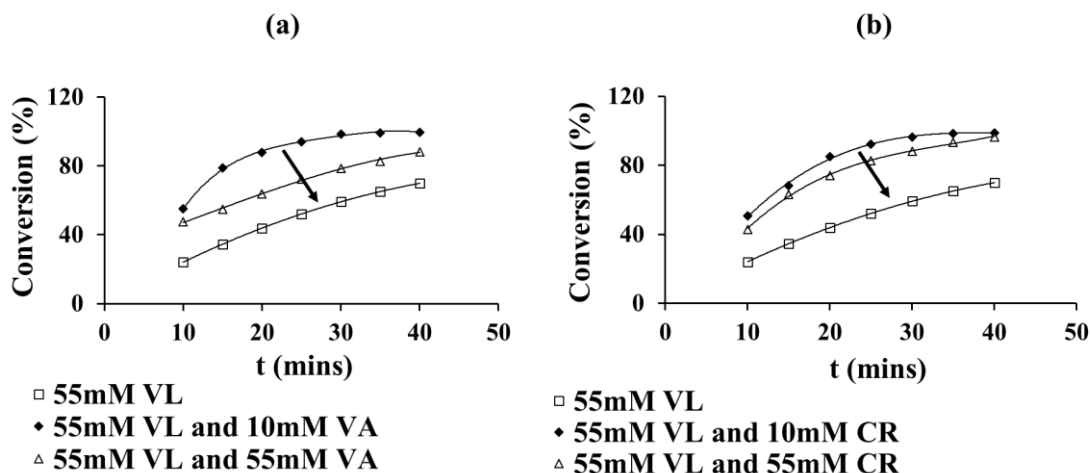
Fig.5.10. (a) Effect of vanillyl alcohol on conversion, and (b) Effect of creosol on conversion at 1000 rpm, T = 328 K, P_H = 1.0 MPa, and ω = 0.1 kg/m^3. Reaction solvent is ethyl acetate, and catalyst type is commercial 10 wt % Pd/C catalyst. Lines represent best polynomial fit to the data. Note: VL represent vanillin, VA represent vanillyl alcohol, and CR represent creosol.

As shown in Figure 5.10a, 76% conversion was achieved after 40 mins when the starting reaction mixture contained no vanillyl alcohol. However, with starting reaction mixtures containing 10 mM and 55 mM vanillyl alcohol, conversion after 40 mins reaction under the same condition increased to 99.6% and 88.2% respectively. This indicates that the presence of vanillyl alcohol in the starting reaction mixture improves the rate at which vanillin changes. Nonetheless, Figure 5.10a shows that the promoting effect from vanillyl alcohol reduces as the concentration of vanillyl alcohol in the starting reaction mixture increases from 10 mM to 55 mM. Interestingly, Figure 5.10b shows similar effect with conversions of 98.8% and 96.5% achieved after 40 mins when the starting reaction mixture contained 10 mM and 55 mM creosol respectively. However, increase in the concentration of creosol in the starting reaction mixture from 10 mM to 55 mM had less effect on rate at which vanillin changes. A plausible reason for the observed differences in effect of the products on conversion is their interaction with hydrogen. The promoting effect of vanillyl alcohol diminishes with increase in concentration probably as a result of increased competition between vanillyl alcohol and vanillin for the

hydrogen available in the system. While in contrast, increase in concentration of creosol had negligible impact on vanillin conversion because creosol do not undergo further hydrogenation under the condition examined. This analysis reaffirms the proposed mechanism for vanillin HDO reaction in Section 5.3 (scheme 1), with vanillyl alcohol as the intermediate product and creosol as the final product. To the best knowledge of this work author, the impact of the reaction products on conversion from vanillin HDO reaction is missing in the literature.

5.9. Model Development for Vanillin HDO Reaction Kinetics

The reusability and stability of Pd/C, Pd/Al$_2$O$_3$, and PdRh/Al$_2$O$_3$ catalyst have been thoroughly examined and reported in Section 4.4.3 of Chapter 4. It was found that conversion remained relatively unchanged throughout three consecutive cycles under each of these catalysts. This suggest contributions from deactivation toward the estimated reaction rates are negligible. Besides, since the reaction rates were calculated from conversion – time data, and the conversion achieved was relatively unchanged after three cycles, it follows that a deactivation term is not required in the model which describes the kinetics of vanillin HDO reaction at the conditions examined. As previously mentioned in Section 2.7.2. of Chapter 2, dual site Langmuir – Hinshelwood – Hougen – Watson (LHHW) approach have been utilised in the literature to successfully model HDO reaction kinetics of compounds such as levoglucosan, lactic acid, propanoic acid, 2-butanone etc.[221, 223,232,282] This approach offers a unique opportunity to consider all processes (i.e. adsorption, desorption, and surface reaction) which occur on the surface of the catalyst. Besides, a rate equation derived via this method can be extrapolated to concentrations outside the experimental range with caution.[242] Interestingly, simplified version of the LHHW approach has been used in the past to successfully model the kinetics of aqueous phase HDO reaction of vanillin over Ru/C catalyst.[160] Notably, the

alternative approach of describing the reaction system by ordinary differential equations (ODEs) from mass balances on the reactants and products cannot offer the above-mentioned benefits provided by LHHW approach. Moreover, the ODE approach often relies on assumption of first order dependence on both the reactants and the products. On the basis of data presented so far, it will be misleading and technically wrong to assume first order dependence for the reactants. Hence, in this study LHHW approach was used to model the kinetics of vanillin HDO reaction over the different catalysts.

5.9.1 Mechanism of Vanillin HDO Reaction and Validation of Rate Expressions

It is widely reported in the literature that hydrogen adsorption onto the surface of metals take place dissociatively.[223, 284] As a result, it was assumed that hydrogen adsorption onto the surface of the catalysts occurred dissociatively. The elementary steps used to derive rate expression for competitive adsorption of dissociatively chemisorbed hydrogen (H_2) and vanillin (VL) are represented by equations 5.2 to 5.4. While the sequence of elementary steps used to derive the rate expression for noncompetitive adsorption of dissociatively chemisorbed H_2 and VL are represented by equations 5.5 to 5.7. Additional information on derivation of these rate expressions is provided in appendix A5.3, while Table 5.3 summarises the two plausible rate expressions for modelling HDO reaction of vanillin.

Competitive Adsorption of Dissociatively Chemisorbed H_2 and VL (Model I)
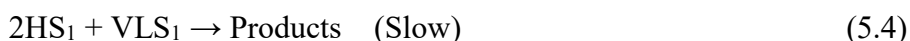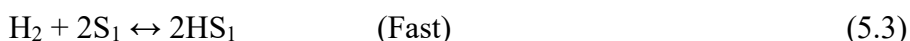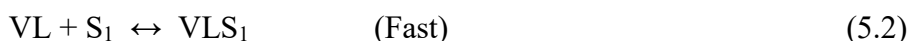
$VL + S_1 \leftrightarrow VLS_1$ \qquad (Fast) \hfill (5.2)

$H_2 + 2S_1 \leftrightarrow 2HS_1$ \qquad (Fast) \hfill (5.3)

$2HS_1 + VLS_1 \rightarrow$ Products \quad (Slow) \hfill (5.4)

NonCompetitive Adsorption of Dissociatively Chemisorbed H_2 and VL (Model II)

$VL + S_1 \leftrightarrow VLS_1$ \qquad (Fast) \hfill (5.5)

$H_2 + 2S_2 \leftrightarrow 2HS_2$ \qquad (Fast) \hfill (5.6)

$$2HS_2 + VLS_1 \rightarrow \text{Products} \quad \text{(Slow)} \qquad\qquad (5.7)$$
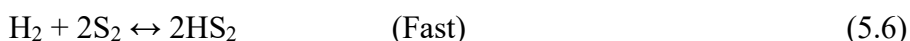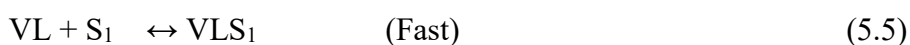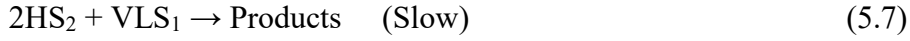
Table 5.3. Rate Expressions for Plausible Kinetic Models

Model	Rate Expression	Model Description
I	$r = \dfrac{k_s K_H K_{VL} C_H C_{VL}}{\left(1 + \sqrt{K_H C_H} + K_{VL} C_{VL}\right)^3}$	Competitive adsorption of dissociative H_2 and VL
II	$r = \dfrac{k_s K_H K_{VL} C_H C_{VL}}{\left(1 + \sqrt{K_H C_H}\right)^2 (1 + K_{VL} C_{VL})}$	NonCompetitive adsorption of dissociative H_2 and VL

In both models I and II presented in Table 5.3, the surface reaction step was assumed to be the rate-determining step (RDS). Hence, other plausible rate expressions derived from assuming adsorption processes as the rate-determining steps for competitive and noncompetitive dissociative chemisorbed H_2 and VL presented in appendix A5.3 were evaluated and found to be unsuitable models for describing the kinetics of VL HDO reaction. The linearised formats of models I and II are represented by equations 5.8 and 5.9 respectively,

where b represents $\dfrac{1 + (K_H C_H)^{\frac{1}{2}}}{(K_s K_H K_{VL} C_H)^{\frac{1}{3}}}$, m represents $\dfrac{K_{VL}}{(K_s K_H K_{VL} C_H)^{\frac{1}{3}}}$, m* represents $\dfrac{K_{VL}\left(1 + \sqrt{K_H C_H}\right)^2}{K_s K_H K_{VL} C_H}$

, and b* represents $\dfrac{\left(1 + \sqrt{K_H C_H}\right)^2}{K_s K_H K_{VL} C_H}$.

$$\left(\frac{C_{VL}}{r}\right)^{\frac{1}{3}} = mC_{VL} + b \qquad (5.8)$$

$$\frac{C_{VL}}{r} = m^* C_{VL} + b^* \qquad (5.9)$$

At constant concentration of dissolved hydrogen gas (C_H), the plot of $(C_{VL0}/r_0)^{1/3}$ vs C_{VL0} should be linear for model I, while for model II the plot of (C_{VL0}/r_0) vs C_{VL0} should be linear. Figure 5.11A represent the fit of model I to the experimental data from VL HDO reaction under the different catalysts. Indeed, the plots of $(C_{VL0}/r_0)^{1/3}$ vs C_{VL0} in Figures 5.11Aa to 5.11Ac are linear with R^2 values in the range of 0.995 to 1.000.
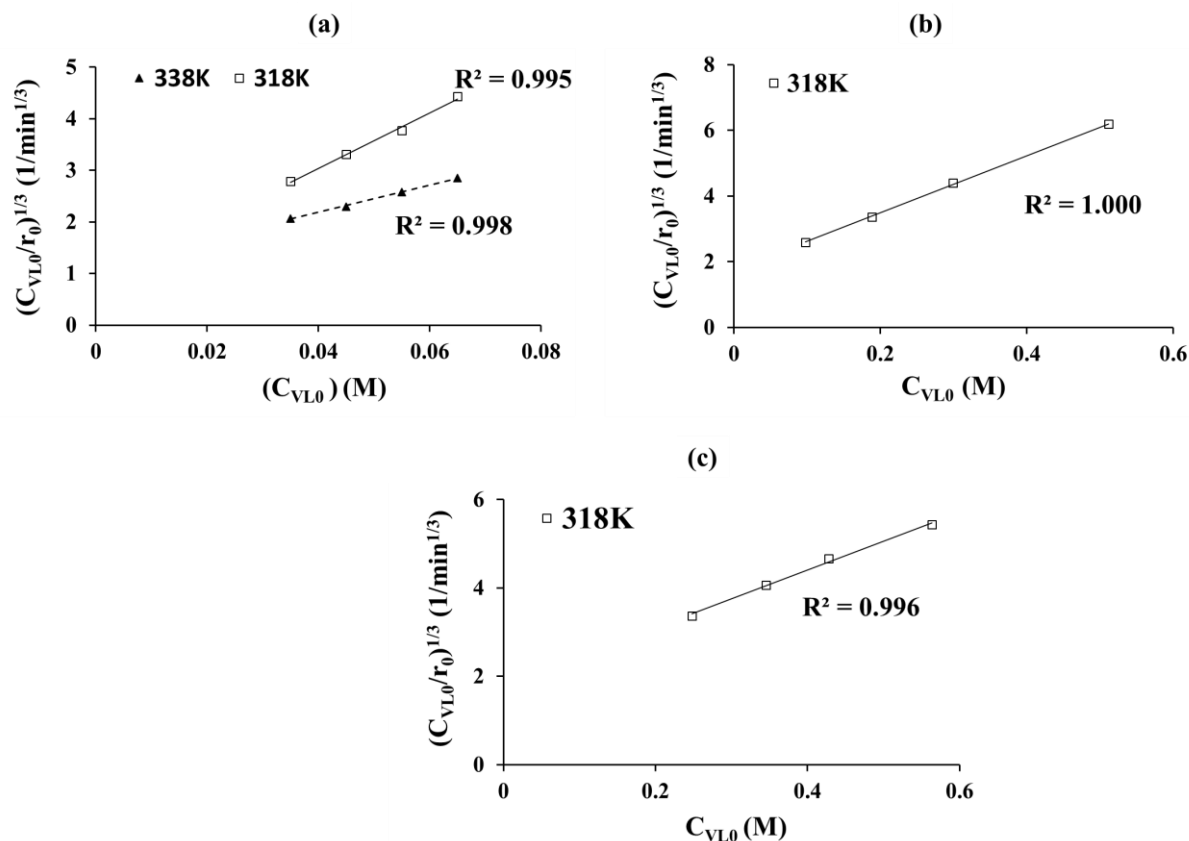
Fig. 5.11A. Fit of linearised version of model I to experimental data. (a) commercial 10 wt % Pd/C catalyst at 1000 rpm, T = 318 K and 338 K, P_H = 1.0 MPa, and ω = 0.1 kg/m^3 (b) commercial 5 wt % Pd/Al$_2$O$_3$ catalyst, at 1000 rpm, T = 318 K, P_H = 2.0 MPa, and ω = 5.0 kg/m^3 and (c) prepared bimetallic 6.5 wt % PdRh/Al$_2$O$_3$ catalyst at 1000 rpm, T = 318 K, P_H = 2.0 MPa, and ω = 5.0 kg/m^3.

The R^2 values which is better known as coefficient of determination, represent the proportion of variation in the dependent variable that can be predicted completely from the independent variable. In theory R^2 values are between 0 and 1, with a value of 1 indicating the dependent variable can be predicted without error from the independent variable. While R^2 value of 0 means the dependent variable cannot be predicted from the independent variable. Hence, with R^2 values between 0.995 and 1.000, the dependent variable $(C_{VL0}/r_0)^{1/3}$ can be predicted reliably from C_{VL0}. Figure 5.11B depicts the fit of model II to the experimental data from VL HDO

reaction under the different catalysts. It shows the plots of (C_{VL0}/r_0) vs C_{VL0} are indeed linear as expected, with R^2 values between 0.961 and 0.992.
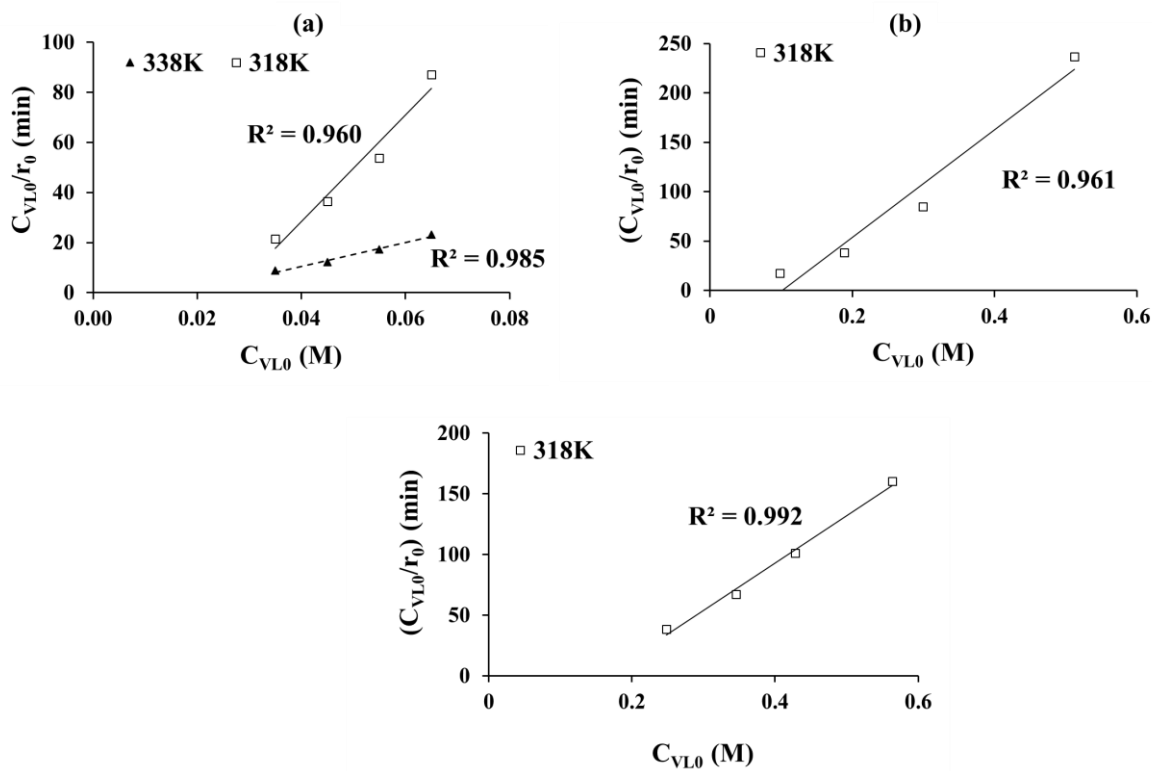
Fig. 5.11B. Fit of linearised version of model II to experimental data. (a) commercial 10 wt % Pd/C catalyst at 1000 rpm, T = 318 K and 338 K, P_H = 1.0 MPa, and ω = 0.1 kg/m³ (b) commercial 5 wt % Pd/Al$_2$O$_3$ catalyst, at 1000 rpm, T = 318 K, P_H = 2.0 MPa, and ω = 5.0 kg/m³ and (c) prepared bimetallic 6.5 wt % PdRh/Al$_2$O$_3$ catalyst at 1000 rpm, T = 318 K, P_H = 2.0 MPa, and ω = 5.0 kg/m³.

On the basis of the R^2 values displayed in Figures 5.11A and 5.11B, it is clear that model I predicts the experimental data better than model II. For this reason, model II was rejected in favour of model I. This conclusion complements the initial claim in Section 5.6 that competition for active sites on the catalyst surface increases as the starting concentration of vanillin increases. Interestingly, model I has been reported as the best fit in other studies on kinetics of bio-oil model compounds hydrogenation reaction. For instance, model I was used in the work of Jain et al[225] to successfully model the kinetics of aqueous-phase hydrogenation reactions of alcohols over a Ru/C catalyst. Likewise, this same model was successfully used in

the work of Bindwal et al[221] to model the kinetics of aqueous-phase hydrogenation reaction of levoglucosan over a Ru/C catalyst.

5.9.2 **Model Parameter Estimation**

In order to determine values of kinetic parameters such as surface reaction rate constant (K_S), adsorption constants (K_H and K_{VL}), heat of adsorption (ΔH_H and ΔH_{VL}), and intrinsic activation energy (E_A), a nonlinear generalized reduced gradient (GRG) solver in Microsoft Excel was used to minimize the objective function defined as residual sum of squares (RSS) in equation 5.10. Herein, r^{Exp} and r^{Mod} represents the experimental reaction rates and rates computed from model I rate expression in Table 5.3 respectively.

$$RSS = \sum\left(r^{Exp} - r^{Mod}\right)^2 \qquad (5.10)$$

For vanillin HDO reaction over Pd/C catalyst, the estimated values for model I parameters are presented in Table 5.4. While Table 5.5 and Table 5.6 summarises values of model I parameters for VL HDO reaction over Pd/Al$_2$O$_3$ catalyst and PdRh/Al$_2$O$_3$ catalyst respectively. In conformity with chemical reaction kinetics theory, Table 5.4 shows that at 95% confidence level K_S increased from 12.29 kmol/kg$_{cat}$min to 38.06 kmol/kg$_{cat}$min as the temperature for VL HDO reaction increased from 318 K to 338 K. Likewise, for VL HDO reaction over Pd/Al$_2$O$_3$ catalyst, Table 5.5 indicates that at 95% confidence level K_S increased from 17.65 kmol/kg$_{cat}$min at 308 K to 81.17 kmol/kg$_{cat}$min at 328 K. In the case of VL HDO reaction over PdRh/Al$_2$O$_3$ catalyst, Table 5.6 shows that at 95% confidence level K_S increased from 49.08 kmol/kg$_{cat}$min at 308 K to 87.06 kmol/kg$_{cat}$min at 328 K. Thus, the reported increase in the rate of VL HDO reactions over each of the catalyst as temperature increases in Section 5.7 can be attributed to increase in the rate constants. Based on the observed trends in the reaction rate constants relative to temperature, it can be concluded that VL HDO reaction obeys the Arrhenius expression. As a result, the intrinsic activation energies for VL HDO reaction over

the different catalysts were determined from the Arrhenius expression and presented in Table 5.7. As expected, Table 5.7 shows that at 95% confidence level the intrinsic activation energy for VL HDO reaction varies with the type of catalyst from 50.60 kJ/mol under Pd/C catalyst and 64.08 kJ/mol under Pd/Al$_2$O$_3$ catalyst to 24.10 kJ/mol under PdRh/Al$_2$O$_3$ catalyst.

Table 5.4. Estimated Values of Model Parameters for VL HDO Reaction over Pd/C Catalyst.

Temperature	Model Parameters	95% confidence level
318 K	K_S (kmol/kg$_{cat}$ min)	$12.29 \pm 4.93 \times 10^{-2}$
	K_H (m^3/kmol)	$10.25 \pm 6.40 \times 10^{-2}$
	K_{VL} (m^3/kmol)	$14.41 \pm 1.48 \times 10^{-2}$
328 K	K_S (kmol/kg$_{cat}$ min)	$25.02 \pm 9.41 \times 10^{-1}$
	K_H (m^3/kmol)	$8.80 \pm 3.99 \times 10^{-1}$
	K_{VL} (m^3/kmol)	$11.21 \pm 3.45 \times 10^{-2}$
338 K	K_S (kmol/kg$_{cat}$ min)	$38.06 \pm 1.45 \times 10^{-2}$
	K_H (m^3/kmol)	$5.35 \pm 4.93 \times 10^{-3}$
	K_{VL} (m^3/kmol)	$6.95 \pm 9.85 \times 10^{-2}$

Table 5.5. Estimated Values of Model Parameters for VL HDO Reaction over Pd/Al$_2$O$_3$ Catalyst.

Temperature	Model Parameters	95% confidence level
308 K	K_S (kmol/kg$_{cat}$ min)	$17.65 \pm 1.31 \times 10^{-1}$
	K_H (m^3/kmol)	$0.06 \pm 4.67 \times 10^{-4}$
	K_{VL} (m^3/kmol)	$1.40 \pm 3.27 \times 10^{-2}$
318 K	K_S (kmol/kgcat min)	$39.15 \pm 4.63 \times 10^{-1}$
	K_H (m^3/kmol)	$0.05 \pm 3.27 \times 10^{-4}$
	K_{VL} (m^3/kmol)	$1.23 \pm 9.35 \times 10^{-3}$
328 K	K_S (kmol/kg$_{cat}$ min)	$81.17 \pm 1.96 \times 10^{-1}$
	K_H (m^3/kmol)	$0.04 \pm 1.87 \times 10^{-4}$
	K_{VL} (m^3/kmol)	$1.08 \pm 4.67 \times 10^{-3}$

Table 5.6. Estimated Values of Model Parameters for VL HDO Reaction over PdRh/Al$_2$O$_3$ Catalyst.

Temperature	Model Parameters	95% confidence level
308 K	K_S (kmol/kg$_{cat}$min)	$49.08 \pm 13.37 \times 10^{-1}$
	K_H (m^3/kmol)	$4.80 \times 10^{-2} \pm 2.80 \times 10^{-3}$
	K_{VL} (m^3/kmol)	$2.21 \pm 1.40 \times 10^{-2}$
318 K	K_S (kmol/kg$_{cat}$min)	$68.03 \pm 8.83 \times 10^{-1}$
	K_H (m^3/kmol)	$4.30 \times 10^{-2} \pm 1.87 \times 10^{-3}$
	K_{VL} (m^3/kmol)	$1.99 \pm 8.41 \times 10^{-2}$
328 K	K_S (kmol/kg$_{cat}$min)	$87.06 \pm 15.33 \times 10^{-1}$
	K_H (m^3/kmol)	$3.96 \times 10^{-2} \pm 1.40 \times 10^{-3}$
	K_{VL} (m^3/kmol)	$1.61 \pm 2.34 \times 10^{-2}$

Table 5.7. Estimated Values of Kinetic Constants for VL HDO Reaction over Different Catalysts.

Kinetic Constants	95% Confidence Level		
	Pd/C Catalyst	Pd/Al$_2$O$_3$ Catalyst	PdRh/Al$_2$O$_3$ Catalyst
E_A (kJ/mol)	$50.60 \pm 9.26 \times 10^{-1}$	$64.08 \pm 2.36 \times 10^{-1}$	$24.10 \pm 20.34 \times 10^{-1}$
ΔH_H (kJ/mol)	$-28.56 \pm 6.42 \times 10^{-2}$	$-10.36 \pm 5.03 \times 10^{-4}$	$-7.77 \pm 3.14 \times 10^{-3}$
ΔH_{VL} (kJ/mol)	$-32.52 \pm 9.96 \times 10^{-2}$	$-10.90 \pm 3.30 \times 10^{-2}$	$-13.37 \pm 2.73 \times 10^{-2}$
ΔS_H (kJ/mol k)	$-71.03 \pm 5.91 \times 10^{-2}$	$-78.47 \pm 21.12 \times 10^{-1}$	$-51.46 \pm 3.41 \times 10^{-1}$
ΔS_{VL} (kJ/mol k)	$-79.58 \pm 1.77 \times 10^{-1}$	$-32.65 \pm 12.10 \times 10^{-1}$	$-36.26 \pm 6.59 \times 10^{-1}$

In comparison to a value of 41.2 kJ/mol reported in the work of Bindwal et al[160] as the activation energy for VL HDO reaction over monometallic Ru/C catalyst, the intrinsic activation energies for the reaction over monometallic Pd/C and Pd/Al$_2$O$_3$ catalyst in Table 5.7 are higher but still within the same order of magnitude. To examine and compare the effect of 10 K change in the reaction temperature on the rate of VL HDO reaction over the different

catalysts, equation 5.11 derived from combining linearised Arrhenius expressions at different temperatures was employed. By substituting the estimated activation energies in Table 5.7 into equation 5.11, a 10 K change in the reaction temperature is expected to cause approximately 80% change in the rate of reaction using Pd/C catalyst, 109% under Pd/Al_2O_3 catalyst, and 32% under $PdRh/Al_2O_3$ catalyst. These predictions are consistent with the reported changes of 90% under monometallic catalysts and 32% under the bimetallic catalyst in Section 5.7. The little discrepancies between the actual and predicted effect of change in temperature on rate of VL HDO reaction can be attributed to uncertainties in the rate constants used to determine the intrinsic activation energies.

$$\ln \left(\frac{K_{S2}}{K_{S1}}\right) = -\frac{E_A}{R}\left[\frac{1}{T_2} - \frac{1}{T_1}\right] \qquad (5.11)$$

Herein, K_{S1} represent rate constant at temperature 1 (T_1), K_{S2} represent rate constant at temperature 2 (T_2), E_A represent the activation energy, and R represent the universal gas constant. From the result presented in Table 5.4, Table 5.5 and Table 5.6, the adsorption constant for the reactants (i.e. VL and H_2) decreases as the temperature at which the reaction occurs increases. This behaviour suggest increase in the reaction temperature favours desorption of VL and H_2 from the monometallic and bimetallic catalyst surfaces. A plausible reason for the observed behaviour is that increase in temperature increases oscillation of the reactants at the catalyst surface and this consequently lowers the possibility of strong adsorption. In addition, the inverse relationship between the adsorption constant and reaction temperature reaffirms claim in the literature[160] that VL HDO reaction is an exothermic process. As a result of the exothermic nature of VL HDO reaction, the classical Van't Hoff isochore in equation 5.12 was used to estimate the changes in enthalpy and entropy of the reactants.

$$\ln K_{ads} = \left(\frac{-\Delta H_{ads}}{RT}\right) + \left(\frac{\Delta S}{R}\right) \qquad\qquad (5.12)$$

Herein, K_{ads} is the adsorption equilibrium constant, ΔH_{ads} is the enthalpy change due to adsorption, ΔS is the change in entropy of the system, R is the universal gas constant, and T is the reaction temperature. The values of change in entropies and enthalpies determined are shown in Table 5.7. In conformity with thermodynamics[292], the estimated change in enthalpies and entropies reported in Table 5.7 are all negative. Hence, model I is thermodynamically consistent and values of the kinetic parameters reported in this work are reasonable. On the basis of the enthalpies of adsorption in Table 5.7, it can be concluded that the strength of adsorption of vanillin onto each of the catalyst surface was marginally stronger than that of hydrogen. Nonetheless, it seems both reactants adsorbed weakly onto the surface of all the catalysts since significantly high values of enthalpy change represent strong interaction. The extent to which rates predicted from model I matches the experimental rates was examined using parity plots in Figures 5.12a to 5.12c. Clearly with R^2 values greater than or equal to 0.99, the predicted reaction rates strongly agree with the experimental reaction rates.
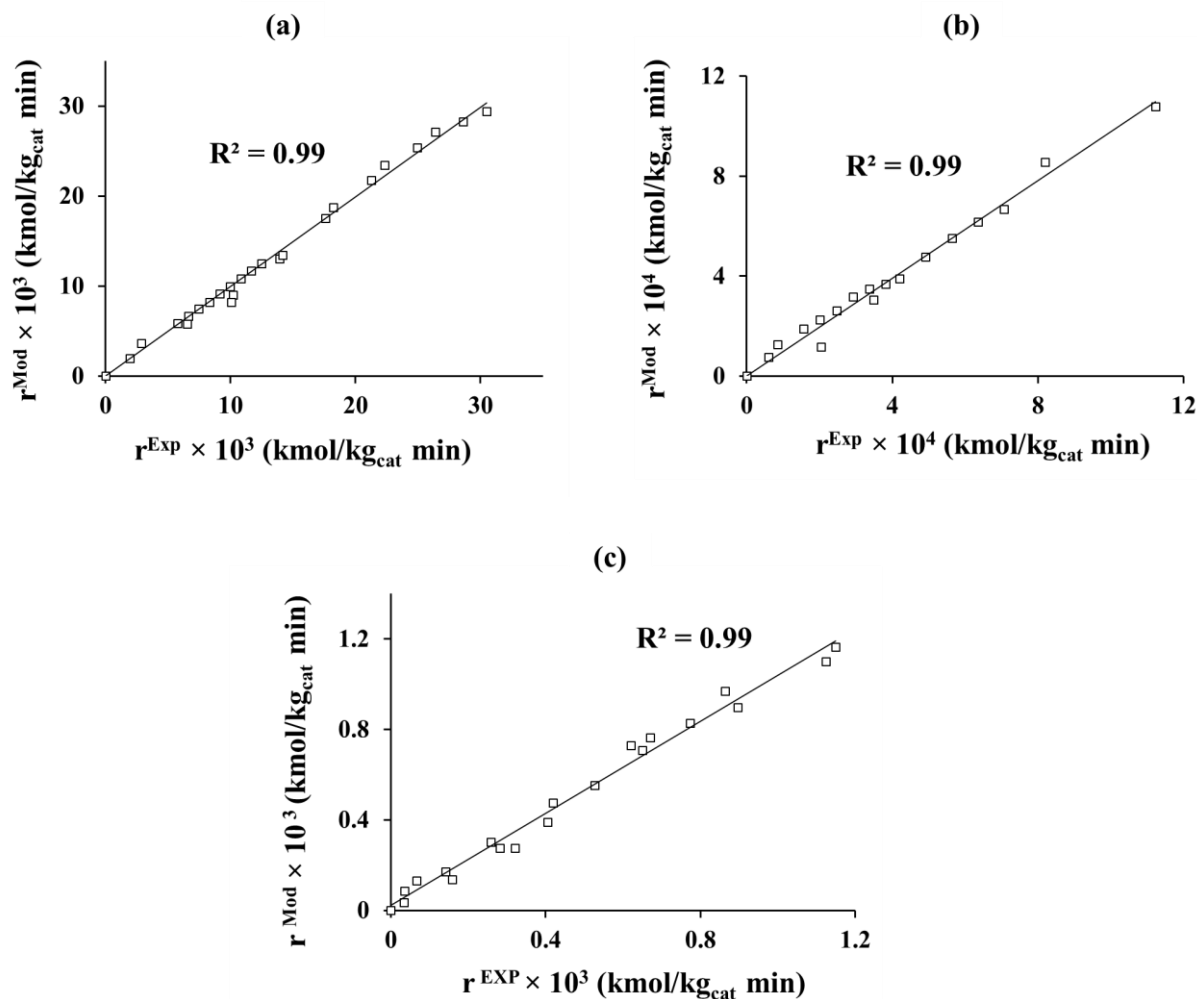
Fig. 5.12. Parity Plot of model I to compare predicted reaction rates and experimental reaction rates under different catalyst. (a) commercial 10 wt % Pd/C catalyst, (b) commercial 5 wt % Pd/Al$_2$O$_3$ catalyst, and (c) prepared bimetallic 6.5 wt % PdRh/Al$_2$O$_3$ catalyst. Lines represent the best fit to data.

The average absolute percentage error in predicting the rate of VL HDO reaction over the different catalysts was estimated using equation 5.13. In the case of VL HDO reaction over Pd/C catalyst, the average absolute percentage error estimated was 4.35%. While for VL HDO reaction over Pd/Al$_2$O$_3$ catalyst and PdRh/Al$_2$O$_3$ catalyst, the average absolute percentage error found was 12.53% and 20.84% respectively. Noteworthy, the method used here to estimate the average percentage error amplifies little deviation at low reaction rates because reaction rates are weighed equally. When the errors were measured relative to the average rate over all the

data points, the average absolute percentage errors found improved to 3.34% for Pd/C catalyst, 7.15% for Pd/Al$_2$O$_3$ catalyst, and 10.43% for PdRh/Al$_2$O$_3$ catalyst. In the literature[223], average percentage errors less than 30% has been cited as acceptable in kinetic modelling. As a result, the average percentage errors reported in the present work are within the acceptable range.

$$\text{Error}(\%) = \frac{\Sigma_n\left(\frac{\left|r^{Mod} - r^{Exp}\right|}{r^{Exp}}\right)}{n} \times 100 \qquad (5.13)$$

 Figures 5.13a to 5.13c illustrate the fit of vanillin concentration predicted from model I to the experimental concentration of vanillin at different reaction temperatures. At all the temperatures considered, Figures 5.13a to 5.13c shows that VL concentrations predicted from model I matches the experimental VL concentrations. Hence, it can be concluded that model I reliably describes the kinetics of vanillin HDO reaction in a batch system operated at mild conditions.
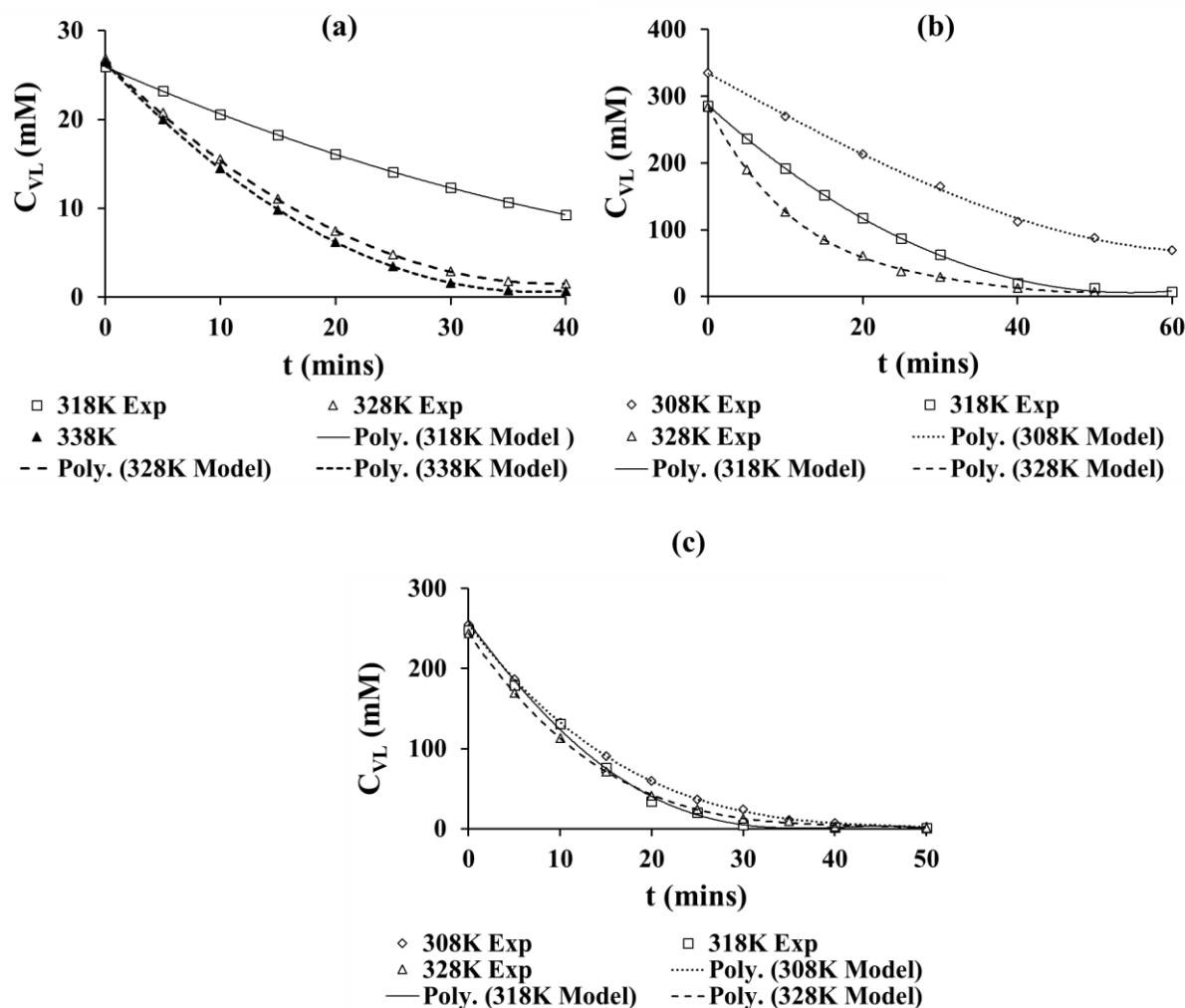
Fig.5.13. Comparison of the changes in predicted and experimental concentrations of vanillin over time during HDO reaction over (a) commercial 10 wt % Pd/C catalyst at 318 K, 328 K, and 338 K, (b) commercial 5 wt % Pd/Al₂O₃ catalyst at 308 K, 318 K, and 328 K, and (c) prepared bimetallic 6.5 wt % PdRh/Al₂O₃ catalyst at 308 K, 318 K, and 328 K. Lines represent fit of proposed kinetic model to the experimental data which are represented by the shapes.

Figure 5.14 shows the changes in fractional coverage of hydrogen gas, vanillin and unoccupied sites on each of the catalysts with the reaction time. From Figure 5.14, it is clear that the coverage of hydrogen gas was remarkably smaller in Pd/Al₂O₃ catalyst and PdRh/Al₂O₃ catalyst compared to Pd/C catalyst. This observation can be attributed to the significant difference in the area available for adsorption of hydrogen on the alumina supported catalysts compared to Pd/C catalyst. However, as expected the trend in fractional coverage of the vanillin

mirrored that of the vacant sites under the different catalysts. The fixed external supply of hydrogen gas applied during the experiments to maintain constant reaction pressure ensured the amount of dissolved hydrogen gas in the reaction solvent was fixed. As a result, negligible changes occurred in fractional coverage of dissolved hydrogen gas over time under all the catalysts.
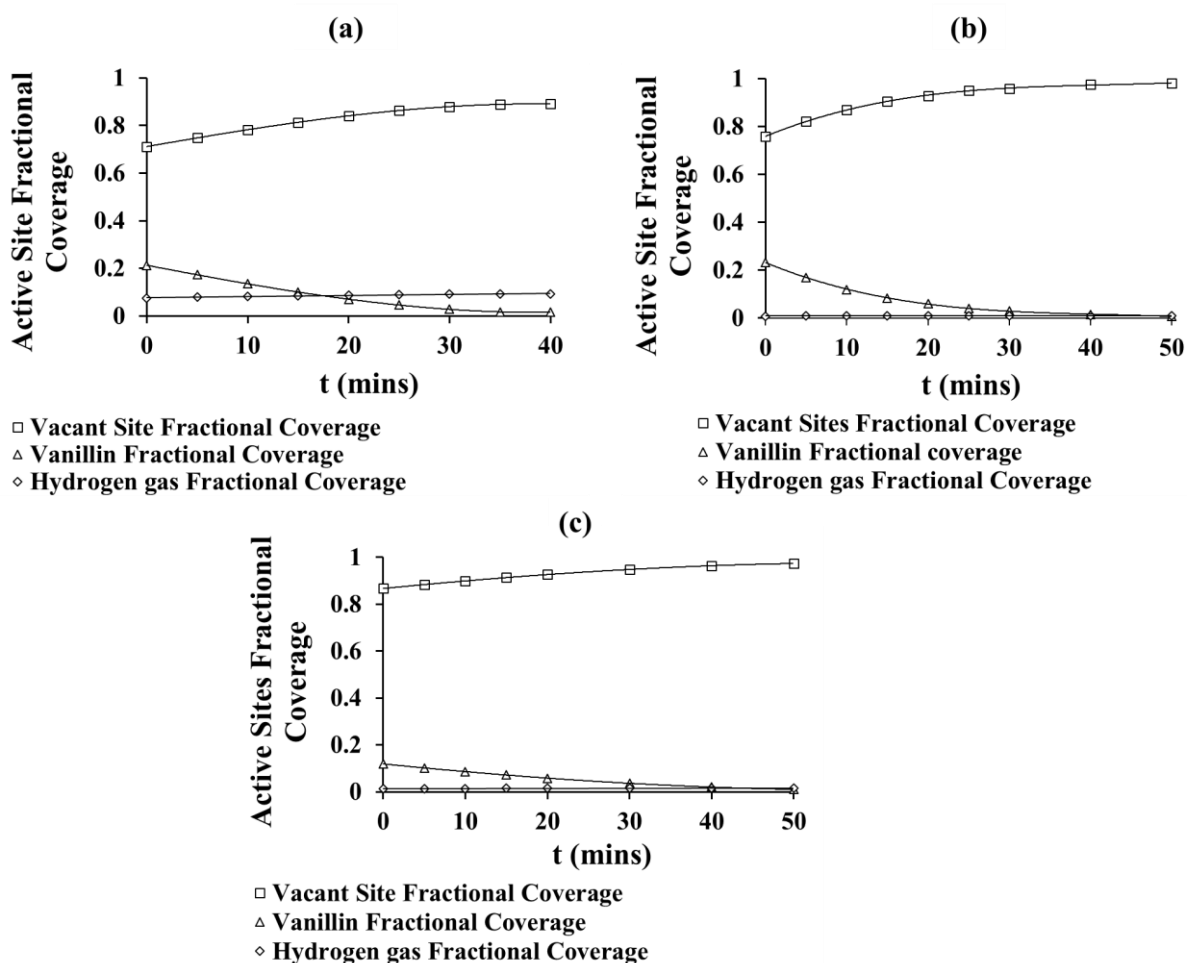
Fig. 5.14. Changes in Fractional Coverage of vanillin, hydrogen gas, and vacant sites on (a) commercial 10 wt % Pd/C catalyst, (b) commercial 5 wt % Pd/Al$_2$O$_3$ catalyst, (c) prepared bimetallic 6.5 wt % PdRh/Al$_2$O$_3$ catalyst over time at 328 K. Lines represent best polynomial fit to the data.

5.10 Conclusions

In summary, this chapter examines the kinetics of vanillin hydrodeoxygenation (HDO) reaction over commercial monometallic Pd-based catalysts (i.e. Pd/C and Pd/Al$_2$O$_3$) and a synthesised bimetallic PdRh/Al$_2$O$_3$ catalyst in a batch reactor operated at mild conditions using ethylacetate as the reaction solvent. Transport limitations in the system were ruled out through Weisz − Prater criterion, agitation, and particle size test. Interestingly, the investigation showed that vanillin HDO reaction occurred in two steps which include hydrogenation of vanillin to vanillyl alcohol followed by hydrogenolysis of vanillyl alcohol to the desired deoxygenated product creosol. Under the different catalysts, nonfirst-order reaction kinetics with respect to vanillin concentration and hydrogen gas partial pressure was found. The order of reaction with respect to vanillin concentration lies in the range of −1.2 to −0.6, while relative to hydrogen gas partial pressure the interval is 0.3 to 0.7. As expected for reactions conducted under intrinsic kinetic controlled conditions, estimated values of slope from plots of natural logarithm of activity against surface metal concentrations were greater than 0.5 under the different catalysts. In addition, from this study it was established that increase in the reaction temperature favours production of creosol from vanillin HDO provided Pd/C or PdRh/Al$_2$O$_3$ particles are used to catalyse the reaction. Conversely, selectivity toward creosol from the reaction diminished marginally as temperature increases under Pd/Al$_2$O$_3$ catalyst. Interestingly, higher conversions were achieved when the starting feed mixture contained either vanillyl alcohol or creosol which are products from the reaction. Langmuir – Hinshelwood – Hougen − Watson (LHHW) method was successfully used to derive plausible rate expressions to model the reaction. However, rate expression obtained under the assumption of competitive dissociative hydrogen adsorption (model I) emerged as the best fit to the experimental data with R^2 values greater than or equal to 99.5%. For vanillin HDO reactions catalysed by Pd/C catalyst, at 95 % confidence level the

estimated values from the model include intrinsic activation energy of 50.6 kJ/mol, −28.9 kJ/mol for the adsorption enthalpy of H_2 gas, and −32.5 kJ/mol for the adsorption enthalpy of vanillin. Likewise, for vanillin HDO reactions under Pd/Al_2O_3 catalyst, the values predicted at 95% confidence level from the model include intrinsic activation energy of 64.1 kJ/mol, −10.9 kJ/mol for the adsorption enthalpy of vanillin, and −10.4 kJ/mol for the H_2 gas adsorption enthalpy. In contrast, for reactions catalysed by the prepared bimetallic $PdRh/Al_2O_3$ catalyst values predicted at 95% confidence level for the kinetic parameters from the model include intrinsic activation energy of 24.1 kJ/mol, −13.4 kJ/mol enthalpy of adsorption for vanillin, and −7.8 kJ/mol enthalpy of adsorption for H_2 gas. Hence, it can be concluded that the energy barrier for vanillin HDO reaction reduces significantly in the presence of bimetallic $PdRh/Al_2O_3$ catalyst.

Chapter 6

Kinetics of Vanillin Hydrodeoxygenation Reaction in Different Solvents and Binary Environments.

6.1. Introduction

The dramatic effect of solvents on kinetics of low temperature hydrogenation reactions are well documented in the literature on heterogeneous catalysis.[293–300] In the work of Bertero et al., [301] on liquid-phase hydrogenation of acetophenone over Ni/SiO$_2$ catalyst in different solvents, it was reported that the measured initial hydrogenation rate varied remarkably from 2.75×10^{-5} mol/min.g in methanol to 1.09×10^{-3} mol/min.g in 2-propanol. Likewise, in the work of Mukherjee et al., [293] the measured initial turn over frequencies of Pt/SiO$_2$ catalyst during hydrogenation of citral in different solvents changed from 0.11/s in n-amyl acetate to 0.62/s in p-Dioxane. However, the mechanism responsible for the reported changes in activity of various catalysts under different solvents remains unclear. The effect of solvent on hydrogenation reactions has mostly been rationalised through correlation to properties such as solvent polarity or dielectric constant.[183–186] Nonetheless, more work is required to quantitatively characterise and understand the effect of solvent on hydrogenation reactions. Especially hydrogenation reactions involving the use of   supported noble metal catalysts.[284] Vanillin (VL) hydrodeoxygenation (HDO) reaction is a typical example of hydrogenation reactions in which supported noble metal catalysts are often utilised. Interestingly, Section 4.5.1 of Chapter 4 showed that selectivity toward the deoxygenated product creosol from VL HDO reaction varied significantly from 100% in 2-propanol to 3% in toluene. In addition, it was found in Section 4.5.2 of Chapter 4 that the amount of hydrogen consumed during the reaction varied appreciably

from 54 mmol in 2-propanol to 20 mmol in water. Likewise, during vanillin hydrogenation over bimetallic Cu_3Pd_1 nanoalloy anchored on N-rich porous organic polymer catalyst in different solvents remarkable changes in selectivity toward creosol and conversion was reported in the work of Shit et al.[73] With conversions ranging from 9.6% using water/oil mixture to 99.3% using 2-propanol, while the selectivity toward creosol changed from 72.7% in 2-propanol/water mixture to 98.3% in water. Despite the well documented changes in conversion and selectivity toward the deoxygenated product from VL HDO reaction under different solvents, information on kinetics of this reaction in different solvents is missing in the literature. As a result, the first section of this chapter investigate the impact of changes in solvent on intrinsic kinetic parameters of VL HDO reaction such as activation energy, adsorption constant, and rate constant. The solvents selected for this purpose include 2-propanol, to represent polar protic solvents; tetrahydrofuran, to represent aprotic polar solvents; and toluene, to represent aprotic apolar solvents. Furthermore, past studies on kinetics of VL HDO reaction were conducted in pure environment containing only the solvent and vanillin. However, real bio-oil contain over 400 different compounds, and how these compounds affects the kinetics of VL HDO reaction has not been reported anywhere.[32, 46, 47] Considering that only a finite number of active sites are available on the catalyst surface, the presence of other compounds in the vicinity for VL HDO reaction will most certainly increase the energy barrier for the reaction due to the increased competition for vacant active sites. Consequently, the second section of this chapter test the validity of this hypothesis by investigating the kinetics of VL HDO reaction in vanillin – acetic acid and vanillin – guaiacol environments. It was established previously in Section 5.2.1 and 5.2.2 of Chapter 5 that agitation speed above 900 rpm and catalyst particles smaller than 250 μm are needed to eliminate transport limitation. Likewise it has been documented in the literature that diffusion through the film and pores occurs more rapidly compared to surface

reactions when heterogeneous reactions are carried out at low temperatures.[190] Hence, to fulfil the objectives of this chapter, the experiments were conducted using catalyst particles smaller than 250 μm, 1000 rpm agitation speed and reaction temperatures less than 338 K.

6.2. Solvent Effect on Kinetics of Vanillin HDO Reaction

This section examines the effect of changes in solvent on kinetics of vanillin HDO reaction over the prepared bimetallic $PdRh/Al_2O_3$ catalyst experimentally through the procedure described in Section 3.3.9 of Chapter 3. The solvents employed in this investigation are 2-propanol, toluene, and tetrahydrofuran. This investigation is a follow-up to the solvent screening experiment reported in Section 4.5 of Chapter 4. The rationale behind the representative solvents considered in the present investigation has been covered in Section 3.3.9 of Chapter 3. Likewise, details about the experimental conditions and procedures employed have been discussed in Section 3.3.9 of Chapter 3. Figures 6.1a to 6.1c represent typical concentration – time profiles observed during vanillin HDO reaction over the synthesised bimetallic $PdRh/Al_2O_3$ catalyst with 2-propanol, tetrahydrofuran, and toluene as the reaction solvents. In conformity with findings reported in Section 4.5.1 of Chapter 4, products from vanillin HDO reaction under the different solvents include vanillyl alcohol and creosol. Interestingly, they have been reported previously in the literature as the main products from vanillin HDO reaction over Pt/C catalyst in the presence of 2-propanol and tetrahydrofuran.[116] However, unwanted products such as ethyl vanillyl ether, pentanol, 1, 4-butanediol, and pentanol were also reported in the literature.[75] The absence of these undesirable products in the present work can be attributed to the mild reaction temperature and the ligand effect between Pd and Rh metals discussed in Section 4.4.1 of Chapter 4.
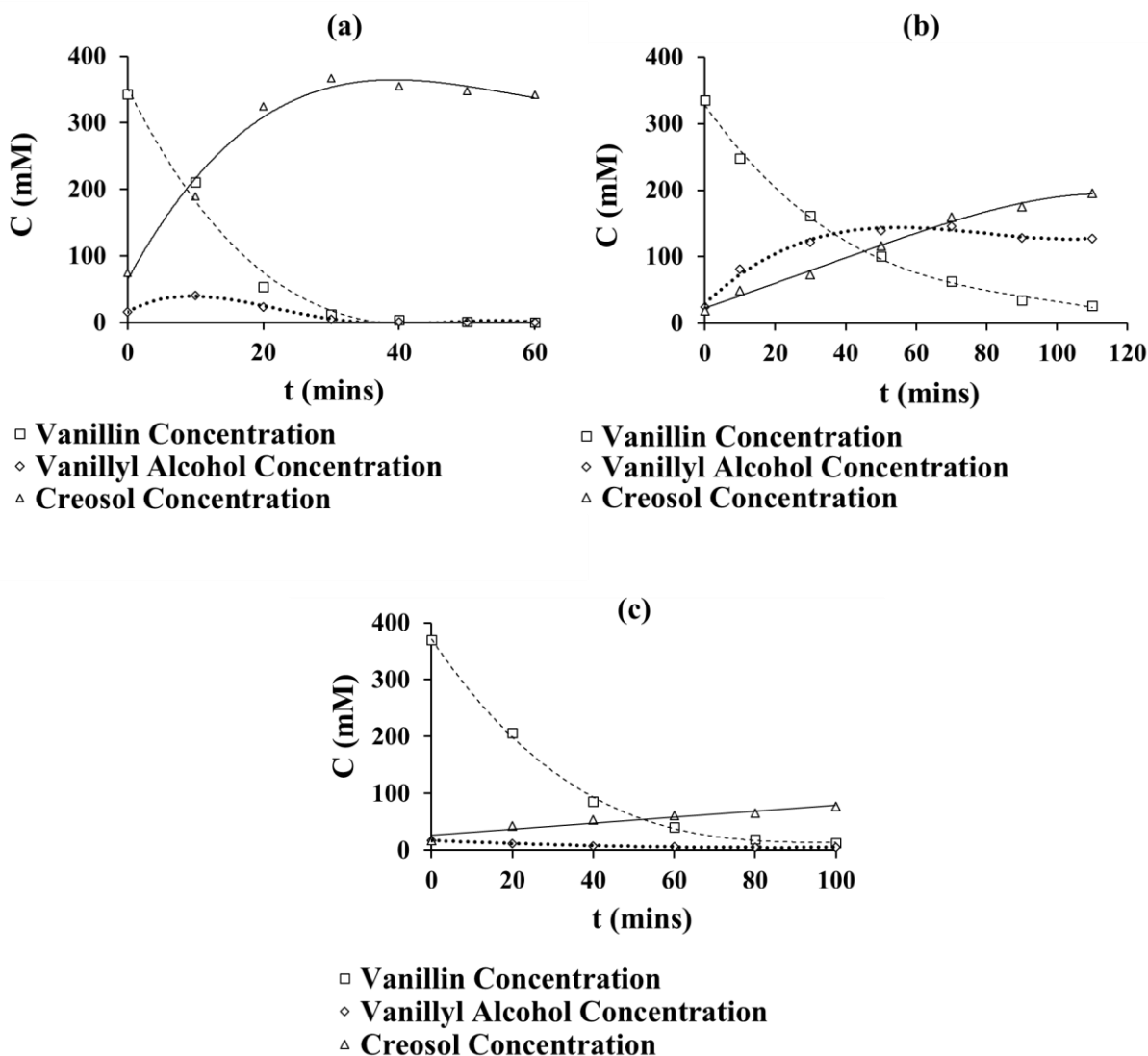
Fig. 6.1. Typical concentration against time profile during vanillin HDO reaction over prepared bimetallic 6.5 wt % PdRh/Al$_2$O$_3$ catalyst under different solvents. (a) 2-propanol, (b) Tetrahydrofuran, and (c) Toluene. Lines represent best polynomial fit to the data and the shapes represent actual data points.

6.2.1. Effect of H$_2$ gas Partial Pressure on Vanillin HDO Reaction

It was established earlier in Section 4.5.2 of Chapter 4 that the amount of hydrogen consumed during vanillin HDO reaction changes appreciably with the type of solvent. As a reminder, the initial turn over frequency of the prepared bimetallic PdRh/Al$_2$O$_3$ catalyst varied remarkably from 1.3 per min in water to 31.7 per min in 2-propanol. To shed more light on the observed

changes, the present section examines the dependence of initial rate of VL disappearance (r_0) on hydrogen gas partial pressure (P_H). Section 3.3.9 of Chapter 3 provides details on the experimental conditions and procedure used to investigate the effect of changes in P_H on r_0. Figure 6.2A summarises the observed variation in r_0 as P_H increases from 1.0 MPa to 4.0 MPa under the various solvents.
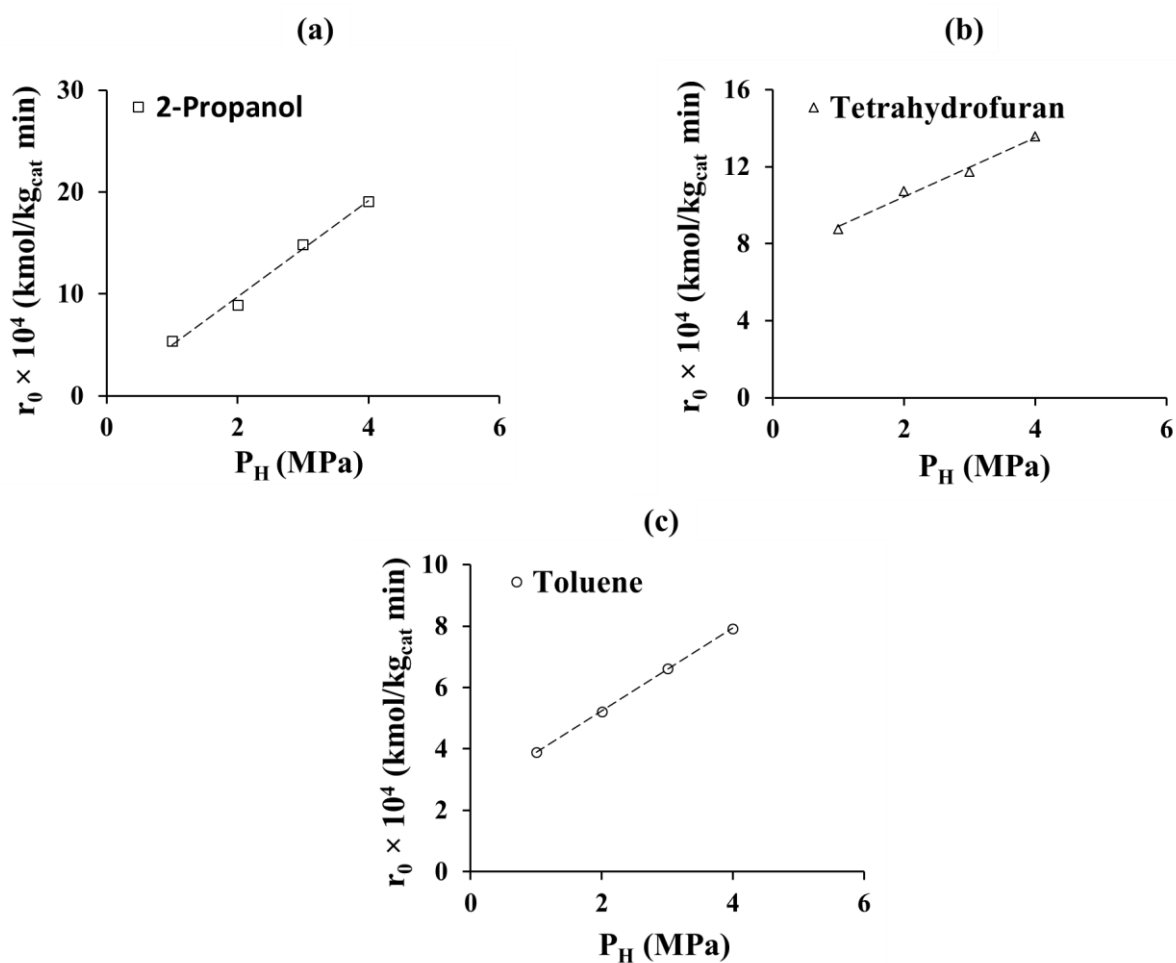
Fig. 6.2A. Influence of H_2 gas partial pressure (P_H) on initial rates of VL disappearance during VL HDO reaction over 6.5 wt % PdRh/Al$_2$O$_3$ catalyst using (a) 2-Propanol at 1000 rpm, T = 318 K, C_{VL0} = 598.0 mM, and ω = 5.0 kg/m^3, (b) Tetrahydrofuran at 1000 rpm, T = 318 K, C_{VL0} = 175.0 mM, and ω = 5.0 kg/m^3, and (c) Toluene at 1000 rpm, T = 318 K , C_{VL0} = 526.0 mM, and ω = 5.0 kg/m^3. Lines represent best linear fit to the data and shapes represent actual data point.

In the case of VL HDO reactions in 2-propanol, Figure 6.2Aa shows that r_0 increases from

0.05×10^{-2} kmol/kg$_{cat}$min to 0.19×10^{-2} kmol/kg$_{cat}$min as P_H increases from 1.0 MPa to 4.0

MPa. Likewise, following 3.0 MPa increase in P_H, Figures 6.2Ab and 6.2Ac shows that r_0

increases from 0.09×10^{-2} kmol/kg$_{cat}$min to 0.14×10^{-2} kmol/kg$_{cat}$min with tetrahydrofuran as

the reaction solvent and 0.04×10^{-2} kmol/kg$_{cat}$min to 0.08×10^{-2} kmol/kg$_{cat}$min under toluene.

Hence, it can be concluded that under each of the solvents examined increase in P_H enhances

the initial rate of VL disappearance. Interestingly, this conclusion is consistent with the finding

in Section 5.5 of Chapter 5 that increase in P_H improves r_0 during VL HDO reaction in the

presence of ethyl acetate. This indicates that high hydrogen gas partial pressure generally

ensures high rate of VL disappearance during the reaction under any class of solvent. Notably,

this conclusion is in agreement with the claim in literature that VL HDO reaction is highly

sensitive to changes in P_H, with the catalyst activity increasing with P_H.[173] To establish the

order of reaction with respect to P_H under the various solvents examined, the natural logarithm

of r_0 against natural logarithm of P_H were plotted. Figure 6.2B summarises the ln-ln plots of

the catalyst activity against hydrogen gas partial pressure for VL HDO reaction under the

different solvents. It shows linear relationship between ln r_0 and ln P_H under each of the

solvents, the slope of the lines displayed in Figure 6.2B represent the order of reaction with

respect to P_H. Hence, the order of reaction with respect to P_H found is 0.9 when the reaction

solvent is 2-propanol, 0.3 under tetrahydrofuran, and 0.5 under toluene. This analysis suggest

vanillin HDO reaction exhibits nonfirst-order kinetics with respect to P_H under aprotic polar

and aprotic apolar solvents, while in contrast it shows an approximate first-order kinetics

relative to P_H in polar protic solvents. Interestingly, Bindwal et al.,[160] reported first-order

kinetics with respect to P_H during vanillin HDO reaction over Ru/C in water which is a well-

known polar protic solvent. Hence, the dependence of vanillin HDO reaction rate on P_H changes

remarkably with the solvent class. This conclusion provides further insight to the claim in Section 4.5 of Chapter 4 that the amount of hydrogen consumed during vanillin HDO reaction changes remarkably with the type of solvent.
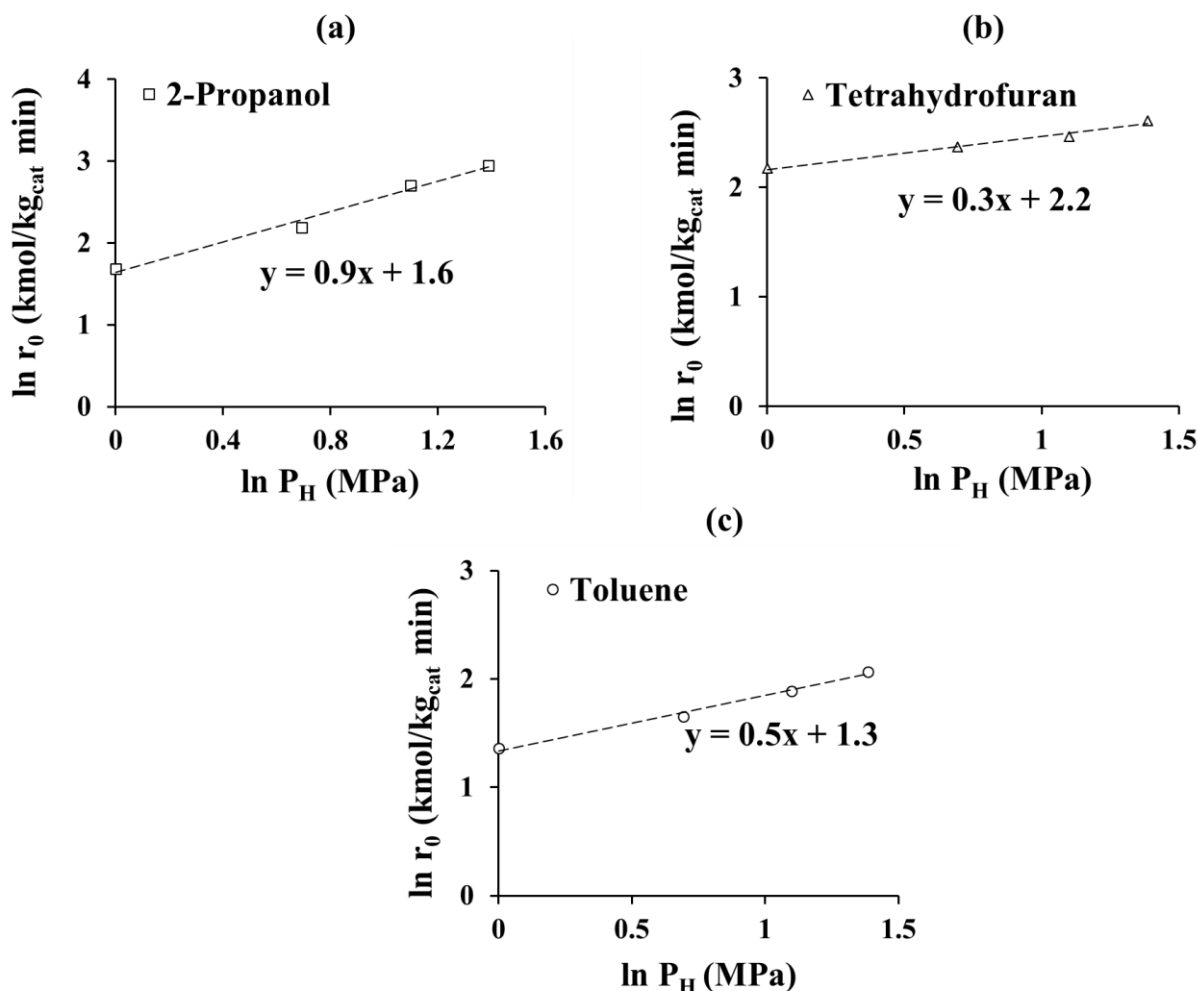
Fig. 6.2B. ln – ln plot of r_0 against P_H for VL HDO reaction over 6.5 wt % PdRh/Al$_2$O$_3$ catalyst using (a) 2-propanol, (b) Tetrahydrofuran, and (c) Toluene. Lines represent best linear fit to the data and shapes represent actual data point.

6.2.2. Effect of Initial Vanillin Concentration

The experimental conditions and procedure described in Section 3.3.9 of Chapter 3 was used to examine the effect of changes in starting concentration of vanillin (C_{VL0}) on initial rate of vanillin (VL) disappearance (r_0) during VL HDO under 2-propanol, tetrahydrofuran, and

toluene. Figures 6.3Aa, 6.3Ab, and 6.3Ac summarises observed changes in r_0 as C_{VL0} increases during VL HDO reaction under each of the solvents.
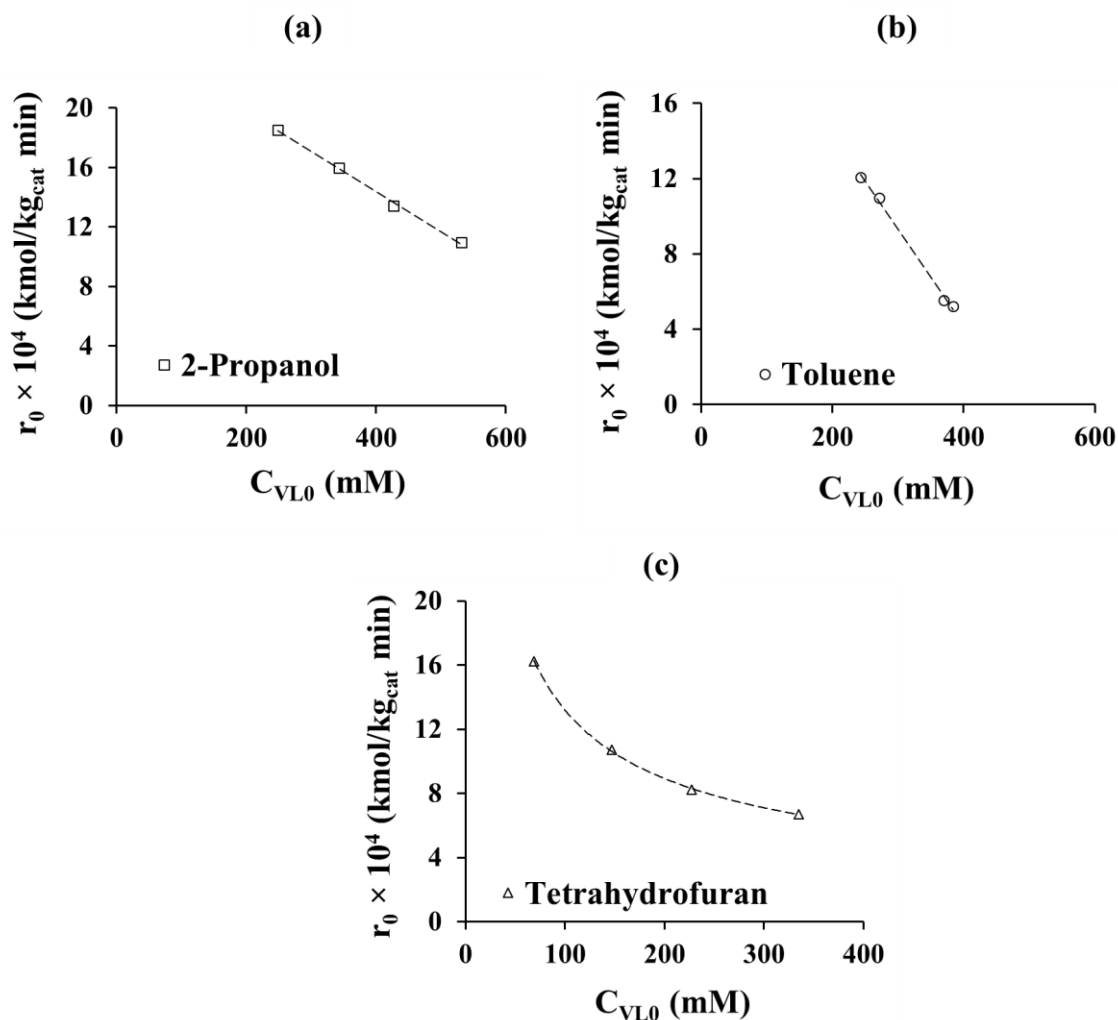
Fig. 6.3A. Effect of initial VL concentration (C_{VL0}) on initial rate of VL disappearance over 6.5 wt % PdRh/Al$_2$O$_3$ catalyst using (a) 2-Propanol at 1000 rpm, T = 318 K, P_H = 2.0 MPa, and ω = 5.0 kg/m^3, (b) Toluene at 1000 rpm, T = 318 K, P_H = 2.0 MPa, and ω = 5.0 kg/m^3, and (c) Tetrahydrofuran at 1000 rpm, T = 318 K, P_H = 2.0 MPa, and ω = 5.0 kg/m^3. Lines represent best fit to the data and shapes represent actual data point.

With 2-propanol as the reaction solvent, Figure 6.3Aa shows that r_0 decreases from 18.5 $\times$ 10^{-4} kmol/kg$_{cat}$min to 10.9 $\times$ 10^{-4} kmol/kg$_{cat}$min as C_{VL0} increases from 248 mM to 531 mM. Under tetrahydrofuran, it can be seen in Figure 6.3Ac that r_0 decreases from 16.2 $\times$ 10^{-4} kmol/kg$_{cat}$min to 6.7 $\times$ 10^{-4} kmol/kg$_{cat}$min as C_{VL0} increases from 69 mM to 335 mM. Likewise

with toluene as the reaction solvent, Figure 6.3Ab shows that as C_{VL0} increases from 243 mM to 384 mM, r_0 decreases from 12.1×10^{-4} kmol/kg$_{cat}$min to 5.2×10^{-4} kmol/kg$_{cat}$min. On the basis of the trends observed, it can be concluded that activity of the prepared bimetallic PdRh/Al$_2$O$_3$ catalyst diminished as C_{VL0} increases under the various solvents considered. This reaffirms the conclusion in Section 5.6 of Chapter 5 that available sites on the catalyst for hydrogen adsorption or product formation reduces as the concentration of vanillin increases. The natural logarithm of r_0 against C_{VL0} were plotted to determine the order of reaction relative to VL concentration under each of the solvents. Figure 6.3B summarises the ln – ln plot of r_0 against C_{VL0} for VL HDO reaction under different solvents.
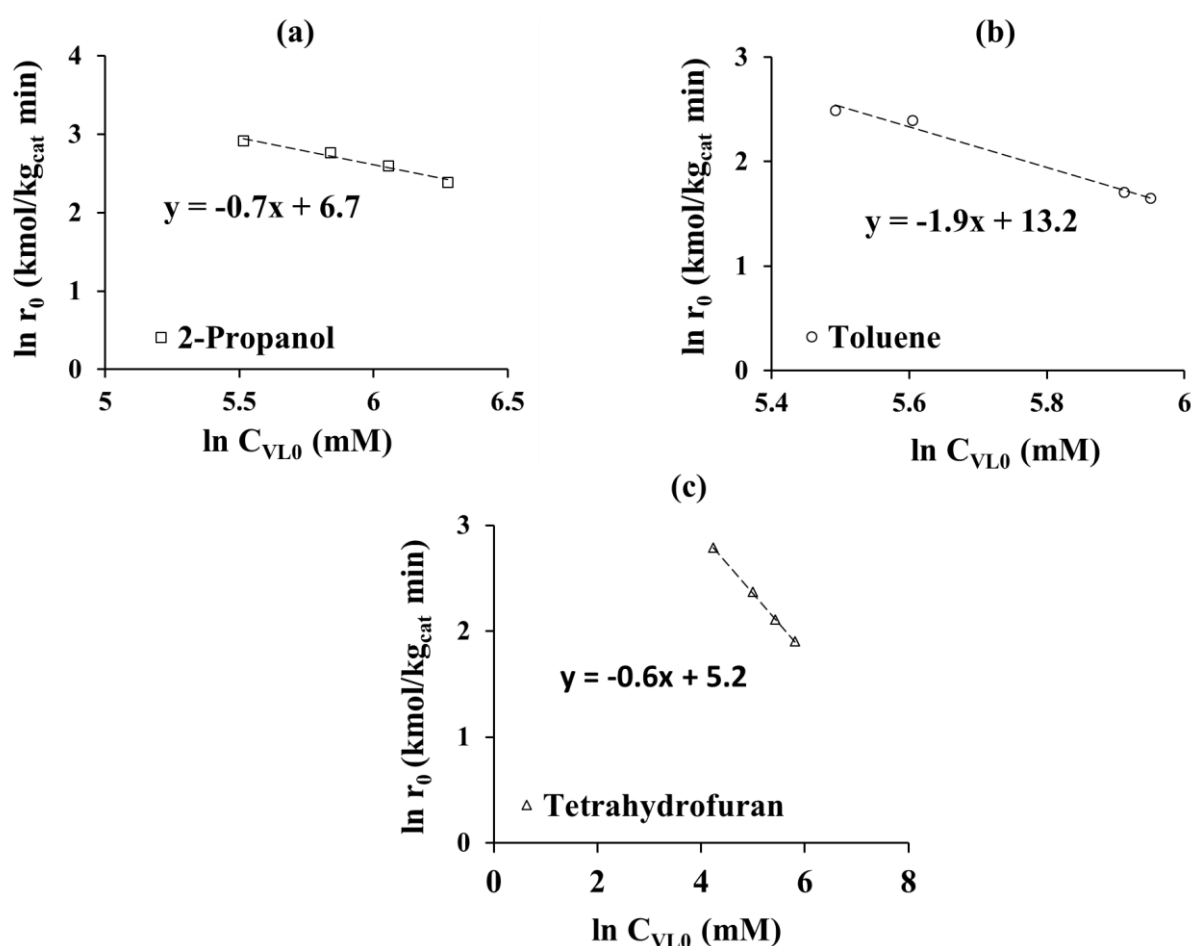
Fig. 6.3B. ln – ln plot of r_0 against C_{VL0} for VL HDO reaction over 6.5 wt % PdRh/Al$_2$O$_3$ catalyst using (a) 2-propanol, (b) Toluene, and (c) Tetrahydrofuran.

As expected the ln – ln plots of r_0 versus C_{VL0} displayed in Figure 6.3B are all linear. From the slope of the ln – ln plots presented in Figures 6.3Ba, 6.3Bb, and 6.3Bc, the order of reaction with respect to VL concentrations found is -0.7 under 2-propanol, -1.9 under toluene, and -0.6 under tetrahydrofuran. Notably, the order of reaction with respect to VL concentration under tetrahydrofuran is identical to the values reported in Section 5.6 of Chapter 5 with ethylacetate as the reaction solvent. Both ethylacetate and tetrahydrofuran are aprotic polar solvents, this possibly explains the similarity in the order of reaction with respect to VL concentration under these solvents. Interestingly in the presence of aprotic apolar solvent such as toluene, distinctly different order of reaction with respect to VL concentration was found. However, surprisingly the order of reaction with respect to VL concentration found in 2-propanol which is a polar protic solvent is identical to those obtained under aprotic polar solvents. From this analysis it can be concluded that the dependence of r_0 on C_{VL0} is the same in polar protic solvents and aprotic polar solvents. However, r_0 depends on C_{VL0} in a different way in aprotic apolar solvents. According to Wan et al.,[232] hydrogenation reactions involving aprotic apolar solvents are not affected by any interactions, while in contrast aprotic polar solvents adsorb strongly to the catalyst active sites. This consequently blocks the active sites of the catalyst from the substrates. The altered solvent – catalyst interaction possibly explains the observed differences in the dependence of r_0 on C_{VL0} in aprotic apolar solvent compared to aprotic polar solvents. According to the literature [232], negative reaction orders suggest substrate inhibition. Hence, the unusual order of reaction found under the various solvents can in general be attributed to substrate inhibition. Earlier in Section 5.6 of chapter 5, it was postulated that as C_{VL0} goes up, the catalyst active sites are blocked by vanillin. As a result of the blocked active sites, the adsorption of hydrogen gas which is the limiting reactant was hindered and this possibly led to reduced catalyst activity at high C_{VL0}.

6.2.3. Effect of Reaction Temperature

The experimental conditions and procedure used to investigate the effect of changes in reaction temperature on vanillin (VL) HDO reaction under the different solvents is provided in Section 3.3.9 of Chapter 3. Figure 6.4A summarises the dependence of VL initial disappearance rate (r_0) on the reaction temperature (T) during VL HDO reaction under the different solvents.
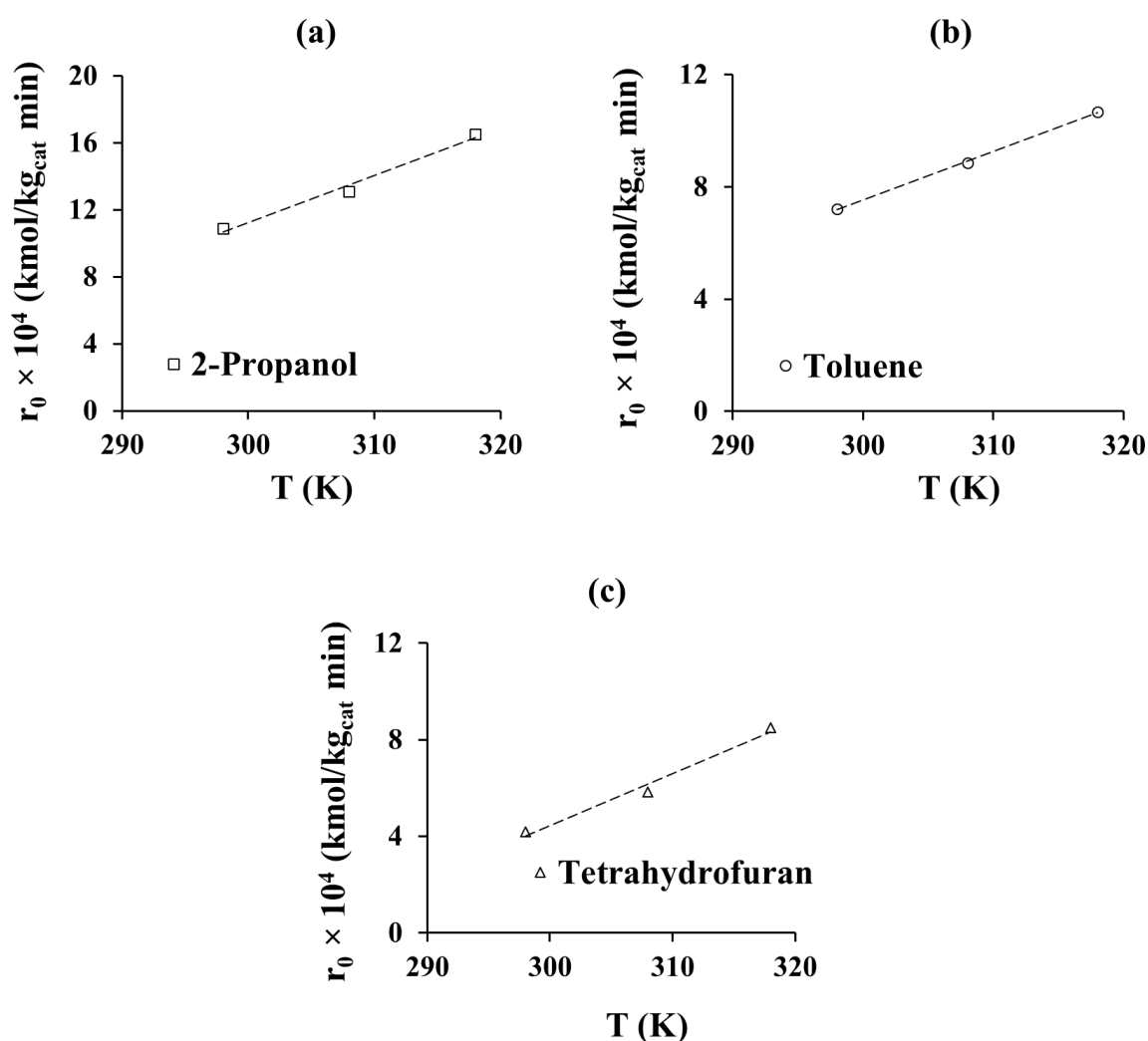
Fig. 6.4A. Influence of reaction temperature (T) on initial rate of VL disappearance (r_0) during VL HDO reaction over PdRh/Al$_2$O$_3$ catalyst in various solvents [(a) 2-Propanol at 1000 rpm, P_H = 2.0 MPa, C_{VL0} = 351.0 mM, and ω = 5.0 kg/m^3, (b) Toluene at 1000 rpm, P_H = 2.0 MPa, C_{VL0} = 272.0 mM, and ω = 5.0 kg/m^3, and (c) Tetrahydrofuran at 1000 rpm, P_H = 2.0 MPa, C_{VL0} = 250.0 mM]. Lines represent best linear fit to the data and shapes represent actual data points.

In conformity with the Arrhenius equation, Figure 6.4A shows that r_0 increases as T increases from 298 K to 318 K under each of the solvents. With 2-propanol as the reaction solvent, Figure 6.4Aa shows that r_0 increases linearly from 10.9×10^{-4} kmol/kg$_{cat}$min to 16.5×10^{-4} kmol/kg$_{cat}$min as T increases from 298 K to 318 K. Likewise, with tetrahydrofuran as the solvent, Figure 6.4Ac shows that r_0 increases linearly from 4.2×10^{-4} kmol/kg$_{cat}$min to 8.5×10^{-4} kmol/kg$_{cat}$min as T increases from 298 K to 318 K. While from Figure 6.4Ab it can be seen that r_0 increases linearly from 7.2×10^{-4} kmol/kg$_{cat}$min to 10.7×10^{-4} kmol/kg$_{cat}$min following increase in T from 298 K to 318 K when toluene is the reaction solvent. The ln – ln plots of catalyst activity against temperature under the different solvents are presented in Figure 6.4B.
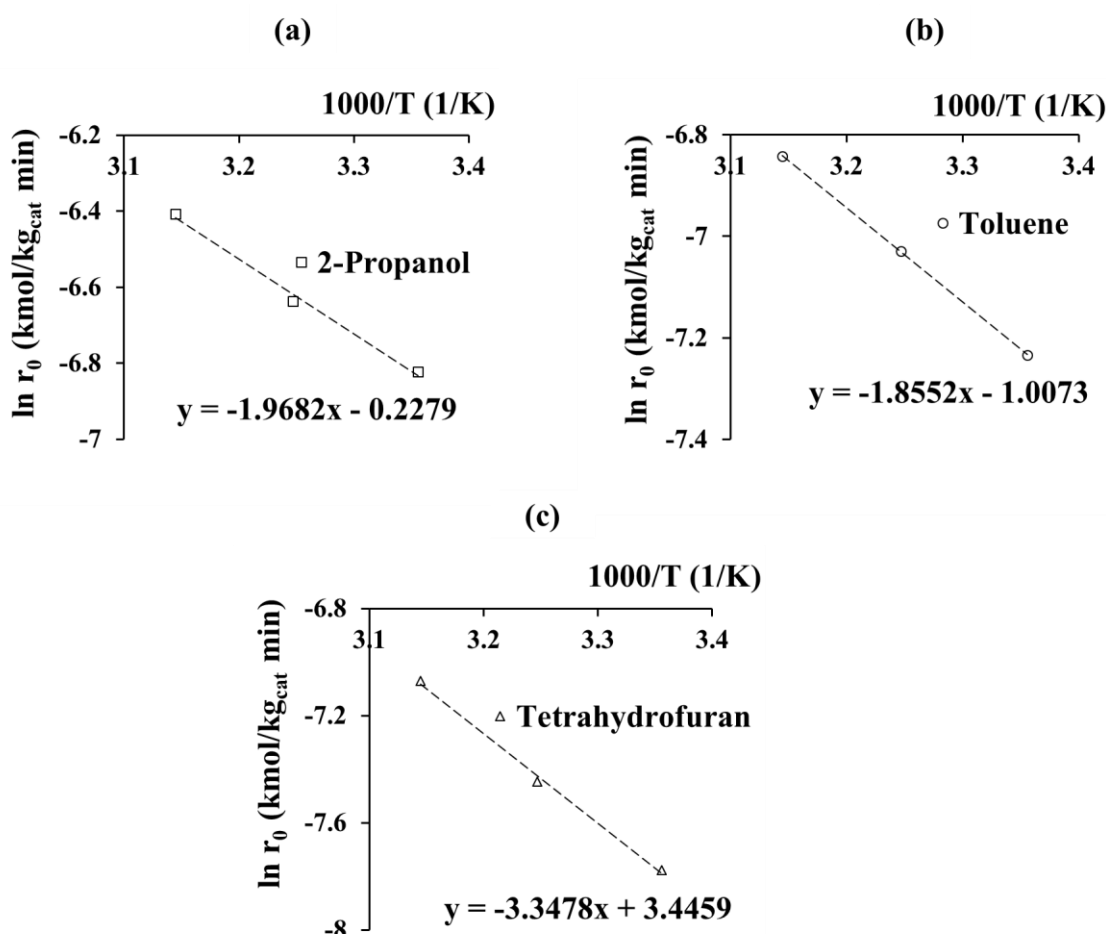
Fig.6.4B. ln – ln plot of PdRh/Al$_2$O$_3$ catalyst activity against reaction temperature for vanillin HDO reaction under (a) 2-Propanol, (b) Toluene, and (c) Tetrahydrofuran. Lines represent best linear fit to the data and shapes represent actual data points.

From the ln – ln plots of catalyst activity against temperature in Figures 6.4Ba, 6.4Bb, and 6.4Bc, the experimental activation energies estimated are (16.3 ± 0.14) kJ/mol in 2-propanol, (16.2 ± 1.16) kJ/mol in toluene, and (27.2 ± 0.17) kJ/mol in tetrahydrofuran. Figures 6.5A and 6.5B summarises changes in selectivity toward vanillyl alcohol and creosol as the reaction progressed under the various solvents at different temperatures.

Fig.6.5A. Vanillyl alcohol selectivity as function of the reaction time and temperature during VL HDO reaction using prepared bimetallic 6.5 wt % PdRh/Al$_2$O$_3$ catalyst under different solvents. (a) 2-Propanol at 1000 rpm, T = 298 K and 318 K, P$_H$ = 2.0 MPa, C$_{VL0}$ = 351.0 mM, and ω = 5.0 kg/m^3, (b) Toluene at 1000 rpm, T = 298 K and 318 K, P$_H$ = 2.0 MPa, C$_{VL0}$ = 272.0 mM, and ω = 5.0 kg/m^3, and (c) Tetrahydrofuran at 1000 rpm, T = 298 K and 318 K, P$_H$ = 2.0 MPa, C$_{VL0}$ = 250.0 mM, and ω = 3.0 kg/m^3 . Lines represent best fit to the data and shapes represent actual data points.

Figure 6.5Aa shows that for VL HDO reaction over the prepared bimetallic PdRh/Al$_2$O$_3$ catalyst using 2-propanol as the solvent, selectivity toward vanillyl alcohol decreases from 55% to 0% after 40 mins at 298 K. Likewise, from Figure 6.5Aa it can be seen that selectivity toward vanillyl alcohol decreases from 31% to 0% at 318 K after 40 mins. Hence, increase in the reaction temperature and time suppresses the selectivity toward vanillyl alcohol when 2-propanol is the reaction solvent for VL HDO over PdRh/Al$_2$O$_3$ catalyst. In contrast, for VL HDO reaction over PdRh/Al$_2$O$_3$ catalyst using toluene as the solvent, Figure 6.5Ab shows that vanillyl alcohol selectivity decreases from 32.9% to 4.1% at 298 K and 45.6% to 9.8% at 318 K after 100 mins. This suggest increase in the reaction temperature improves selectivity toward vanillyl alcohol when VL HDO reaction over PdRh/Al$_2$O$_3$ catalyst is conducted in toluene. Interestingly, the trend in selectivity toward vanillyl alcohol from the reaction is the same under tetrahydrofuran and 2-propanol (see Figure 6.5Ac and 6.5Aa). Figure 6.5Ac shows that from VL HDO reaction under tetrahydrofuran, the selectivity toward vanillyl alcohol dropped to 82.2% at 298 K and 32.5% at 318 K after 100 mins. Hence, increase in the reaction temperature also suppresses the selectivity toward vanillyl alcohol during VL HDO reaction over PdRh/Al$_2$O$_3$ catalyst when the reaction solvent is tetrahydrofuran. As expected for consecutive reactions, Figure 6.5B shows that the trends in selectivity toward creosol from VL HDO reaction under the various solvents are mirror images of the trends displayed in Figure 6.5A. Consequently, in conformity with findings in Section 5.7 of Chapter 5, it was concluded that increase in temperature enhances selectivity toward creosol at the expense of selectivity toward vanillyl alcohol when 2-propanol or tetrahydrofuran is the reaction solvent. While under toluene, increase in temperature marginally enhances selectivity toward vanillyl alcohol at the expense of creosol.

Fig.6.5B. Creosol selectivity as function of the reaction time and temperature during VL HDO reaction using prepared bimetallic 6.5 wt% PdRh/Al$_2$O$_3$ catalyst under different solvents. (a) 2-Propanol at 1000 rpm, T = 298 K and 318 K, P$_H$ = 2.0 MPa, C$_{VL0}$ = 351.0 mM, and ω = 5.0 kg/m^3, (b) Toluene at 1000 rpm, T = 298 K and 318 K, P$_H$ = 2.0 MPa, C$_{VL0}$ = 272.0 mM, and ω = 5.0 kg/m^3, and (c) Tetrahydrofuran at 1000 rpm, T = 298 K and 318 K, P$_H$ = 2.0 MPa, C$_{VL0}$ = 250.0 mM, and ω = 3.0 kg/m^3 . Lines represent best fit to the data and shapes represent actual data points.

6.2.4. Kinetic Modelling of Vanillin HDO Reaction under Different Solvents

The kinetics of vanillin (VL) HDO reaction in ethylacetate was modelled successfully in Section 5.9.2 of Chapter 5 under the assumption of competitive adsorption of dissociatively chemisorbed H$_2$ and VL using nonlinear Generalized Reduced Gradient (GRG) solver function in Microsoft Excel to minimize the residual sum of squares (RSS). As a reminder, equation 6.1

represent the derived rate expression used in Section 5.9.2 of Chapter 5 to model kinetics of VL HDO reaction over the prepared bimetallic PdRh/Al$_2$O catalyst with ethyl acetate as the solvent. Consequently, this rate expression and the described approach in Section 5.9.2 of Chapter 5 is used in this section to model the kinetics of VL HDO reaction over the bimetallic PdRh/Al$_2$O$_3$ catalyst with 2-propanol, tetrahydrofuran, and toluene as the solvent.

$$r = \frac{k_S K_H K_{VL} C_H C_{VL}}{\left(1 + \sqrt{K_H C_H} + K_{VL} C_{VL}\right)^3} \qquad (6.1)$$

Table 6.1, Table 6.2, and Table 6.3 summarises obtained values of the model parameters for VL HDO reaction over the synthesised PdRh/Al$_2$O$_3$ catalyst using 2-propanol, toluene and tetrahydrofuran as the solvent. Under 2-propanol, Table 6.1 shows that at 95% confidence level the rate constant for the reaction increased from 26.62 kmol/kg$_{cat}$min at 298 K to 48.50 kmol/kg$_{cat}$min at 318 K. Likewise, from Table 6.2 it can be seen that at 95% confidence level the rate constant for VL HDO reaction under toluene increased from 12.69 kmol/kg$_{cat}$min at 298 K to 52.80 kmol/kg$_{cat}$min at 318 K. With tetrahydrofuran as the reaction solvent, Table 6.3 shows that at 95% confidence level the rate constant increased from 11.91 kmol/kg$_{cat}$min at 298 K to 29.58 kmol/kg$_{cat}$min at 318 K. Interestingly, the rate constant increased with temperature during VL HDO reaction in each of the solvents considered. As a result, it can be concluded that VL HDO reaction in the different solvents obeys the Arrhenius expression and this explains the described trends in Section 6.2.3. Using the Arrhenius expression, the intrinsic activation energies for VL HDO reaction over PdRh/Al$_2$O$_3$ catalyst in different solvents were determined and presented in Table 6.4. As expected, Table 6.4 shows that at 95% confidence level the intrinsic activation energy for VL HDO reaction over PdRh/Al$_2$O$_3$ catalyst varies with the solvent class from 23.60 kJ/mol in 2-propanol to 56.30 kJ/mol in toluene, and 35.80 kJ/mol in

tetrahydrofuran. On the basis of these activation energies, it can be concluded that VL HDO reaction occurs more readily in 2-propanol followed by tetrahydrofuran and then toluene. Interestingly, this trend is consistent with the order in performance reported in Section 4.5.1 of Chapter 4. As a reminder, it was established in Section 4.5.1 of Chapter 4 that performance in terms of conversion and selectivity toward creosol from VL HDO reaction in different solvents follows the order 2-propanol > tetrahydrofuran > toluene.

Table 6.1. Estimated Values of Model Parameters for VL HDO Reaction over PdRh/Al$_2$O$_3$ Catalyst using 2-propanol as solvent.

Temperature	Model Parameters	95% confidence level
298 K	K_S (kmol/kg$_{cat}$min)	$26.62 \pm 2.21 \times 10^{-1}$
	K_H (m^3/kmol)	$1.00 \times 10^{-1} \pm 9.35 \times 10^{-4}$
	K_{VL} (m^3/kmol)	$1.34 \pm 1.40 \times 10^{-2}$
308 K	K_S (kmol/kg$_{cat}$min)	$35.70 \pm 1.31 \times 10^{-1}$
	K_H (m^3/kmol)	$8.00 \times 10^{-2} \pm 1.40 \times 10^{-3}$
	K_{VL} (m^3/kmol)	$1.13 \pm 4.67 \times 10^{-3}$
318 K	K_S (kmol/kg$_{cat}$min)	$48.50 \pm 2.66 \times 10^{-1}$
	K_H (m^3/kmol)	$7.00 \times 10^{-2} \pm 9.35 \times 10^{-4}$
	K_{VL} (m^3/kmol)	$0.98 \pm 4.67 \times 10^{-3}$

Table 6.2. Estimated Values of Model Parameters for VL HDO Reaction over PdRh/Al$_2$O$_3$ Catalyst using toluene as solvent.

Temperature	Model Parameters	95% confidence level
298 K	K_S (kmol/kg$_{cat}$min)	$12.69 \pm 1.36 \times 10^{-1}$
	K_H (m^3/kmol)	$0.31 \pm 1.87 \times 10^{-3}$
	K_{VL} (m^3/kmol)	$0.35 \pm 4.67 \times 10^{-3}$
308 K	K_S (kmol/kg$_{cat}$min)	$29.61 \pm 1.87 \times 10^{-1}$
	K_H (m^3/kmol)	$0.22 \pm 3.27 \times 10^{-3}$
	K_{VL} (m^3/kmol)	$0.22 \pm 4.67 \times 10^{-3}$
318 K	K_S (kmol/kg$_{cat}$min)	$52.80 \pm 5.94 \times 10^{-1}$
	K_H (m^3/kmol)	$0.18 \pm 4.67 \times 10^{-4}$
	K_{VL} (m^3/kmol)	$0.18 \pm 1.87 \times 10^{-3}$

Table 6.3. Estimated Values of Model Parameters for VL HDO Reaction over PdRh/Al$_2$O$_3$ Catalyst using tetrahydrofuran as solvent.

Temperature	Model Parameters	95% confidence level
	K_S (kmol/kgcat min)	$11.91 \pm 3.74 \times 10^{-2}$
298 K	K_H (m^3/kmol)	$9.20 \times 10^{-2} \pm 1.87 \times 10^{-4}$
	K_{VL} (m^3/kmol)	$1.40 \pm 3.27 \times 10^{-2}$
	K_S (kmol/kgcat min)	$18.72 \pm 1.64 \times 10^{-1}$
308 K	K_H (m^3/kmol)	$8.50 \times 10^{-2} \pm 9.35 \times 10^{-4}$
	K_{VL} (m^3/kmol)	$1.23 \pm 9.35 \times 10^{-3}$
	K_S (kmol/kgcat min)	$29.58 \pm 7.01 \times 10^{-2}$
318 K	K_H (m^3/kmol)	$7.80 \times 10^{-2} \pm 1.40 \times 10^{-3}$
	K_{VL} (m^3/kmol)	$1.08 \pm 4.67 \times 10^{-3}$

Table 6.4. Estimated Values of Kinetic Constants for VL HDO Reaction over PdRh/Al$_2$O$_3$ catalyst using different solvents.

Kinetic Constants	95% Confidence Level		
	2-Propanol	Toluene	Tetrahydrofuran
E_A (kJ/mol)	$23.60 \pm 3.51 \times 10^{-1}$	$56.30 \pm 6.09 \times 10^{-1}$	$35.80 \pm 7.94 \times 10^{-2}$
ΔH_H (kJ/mol)	$-13.20 \pm 1.32 \times 10^{-3}$	$-21.70 \pm 1.93 \times 10^{-3}$	$-6.60 \pm 1.41 \times 10^{-3}$
ΔH_{VL} (kJ/mol)	$-12.30 \pm 1.48 \times 10^{-2}$	$-26.60 \pm 5.03 \times 10^{-3}$	$-6.70 \pm 3.30 \times 10^{-2}$
ΔS_H (kJ/mol k)	$-63.40 \pm 2.68 \times 10^{-2}$	$-82.60 \pm 14.36 \times 10^{-1}$	$-41.90 \pm 7.26 \times 10^{-1}$
ΔS_{VL} (kJ/mol k)	$-38.70 \pm 3.92 \times 10^{-2}$	$-98.30 \pm 16.32 \times 10^{-1}$	$-22.30 \pm 3.87 \times 10^{-1}$

In conformity with findings in Section 5.9.2 of Chapter 5, Tables 6.1, 6.2, and 6.3 shows that the equilibrium adsorption constant for the reactants (i.e. VL and H$_2$) reduces as the reaction temperature increases for VL HDO reaction under 2-propanol, toluene, and tetrahydrofuran. This result reaffirms the conclusion in Section 5.9.2 of Chapter 5 that VL HDO reaction is exothermic and high temperature favours desorption of the reactants from the surface of the

prepared bimetallic PdRh/Al$_2$O$_3$ catalyst. From the Van't Hoff expression in equation 6.2, changes in enthalpy of adsorption and entropy were determined for VL HDO reaction under the different solvents. The results are presented in Table 6.4.

$$\ln K_{ads} = \left(\frac{-\Delta H_{ads}}{RT}\right) + \left(\frac{\Delta S}{R}\right) \qquad (6.2)$$

Herein, K_{ads} is the adsorption equilibrium constant, ΔH_{ads} is the enthalpy change due to adsorption, ΔS is the change in entropy of the system, R is the universal gas constant, and T is the reaction temperature. As expected for a thermodynamically consistent model, the values of enthalpy and entropy changes reported in Table 6.4 are all negative. Hence, values obtained from the model are reasonable. Table 6.4 shows that at 95% confidence level the estimated enthalpy change due to adsorption of hydrogen varies from −6.60 kJ/mol under tetrahydrofuran to −13.20 kJ/mol under 2-propanol and then −21.70 kJ/mol under toluene. Likewise, from Table 4.6 it is clear that change in enthalpy due to adsorption of vanillin at 95% confidence level varies from −6.70 kJ/mol under tetrahydrofuran to −12.30 kJ/mol under 2-propanol and then −26.60 kJ/mol under toluene. Based on this result, it can be concluded that changes in the reaction solvent alters the manner in which the reactants interacts with the prepared bimetallic PdRh/Al$_2$O$_3$ catalyst surface. Looking at the magnitude of the change in enthalpy of adsorption for hydrogen and vanillin under the various solvents, it appears the strength of adsorption of vanillin onto the catalyst surface was marginally stronger than that of hydrogen when the solvent in use is toluene or tetrahydrofuran. This is consistent with the finding reported in Section 5.9.2 of Chapter 5. However, when the reaction solvent is 2-propanol, it appears hydrogen adsorbed slightly stronger than vanillin onto the catalyst surface. In comparison to values of −61.60 kJ/mol for ΔH_H and −39.20 kJ/mol for $\Delta H_{Levoglucosan}$ in the literature,[221] it can be concluded that both vanillin and hydrogen generally adsorbs weakly onto the bimetallic PdRh/Al$_2$O$_3$ catalyst surface. The extent to which the rates predicted from model I matches the

experimental rates from VL HDO reaction under the different solvents was examined through the parity plots presented in Figure 6.6.
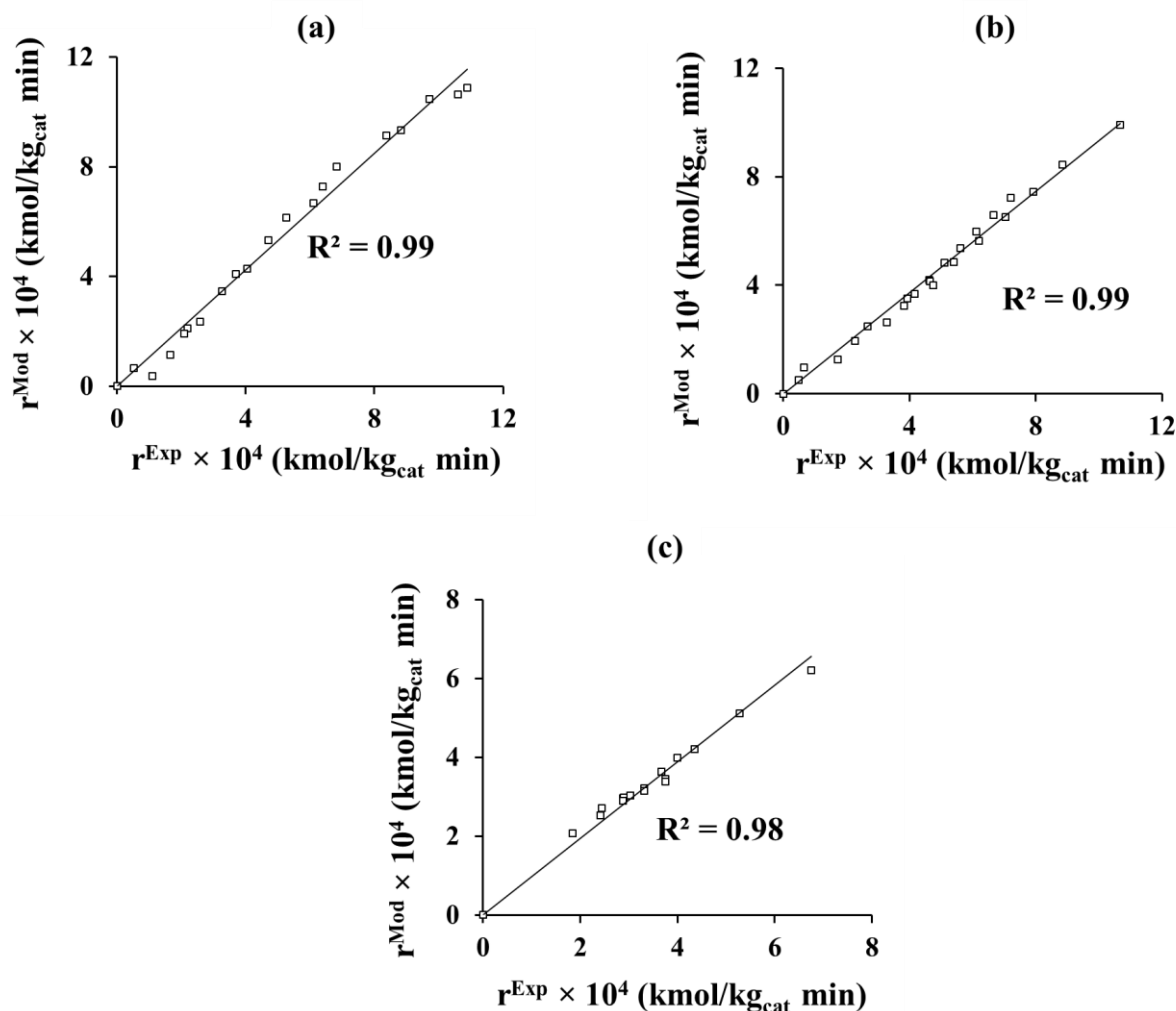
Fig. 6.6. Parity Plot of model I to compare predicted reaction rates and experimental reaction rates under different solvents using the prepared bimetallic 6.5 wt % PdRh/Al$_2$O$_3$ catalyst. (a) 2-Propanol, (b) Toluene, and (c) Tetrahydrofuran. Lines represent best fit to data.

Clearly, with R^2 values greater than or equal to 0.98, model I reliably described the kinetics of VL HDO reaction under the various solvents in a batch reactor. Using equation 6.3, the average absolute percentage error in the estimates of rates predicted from the model compared to the experimental rates was 9.01% with 2-propanol as solvent, 8.12% under toluene, and 4.20% when the solvent is tetrahydrofuran. These values are well below the acceptable limit of 30%

in the literature[223] for kinetics modelling, therefore the proposed model is reliable and acceptable.

$$\text{Error}(\%) = \frac{\Sigma_n\left(\frac{\left|r^{Mod} - r^{Exp}\right|}{r^{Exp}_{AVG}}\right)}{n} \times 100 \qquad (6.3)$$

Herein, r^{Mod} is the rate predicted from the model, r^{Exp} is the experimental rate, r^{Exp}_{AVG} is the average experimental rate, and n is the number of data points. Figures 6.7a to 6.7c further reaffirms the fit of the proposed model to the experimental data because they showed strong agreement between the predicted and experimental VL concentrations at different reaction temperatures under each of the solvents.
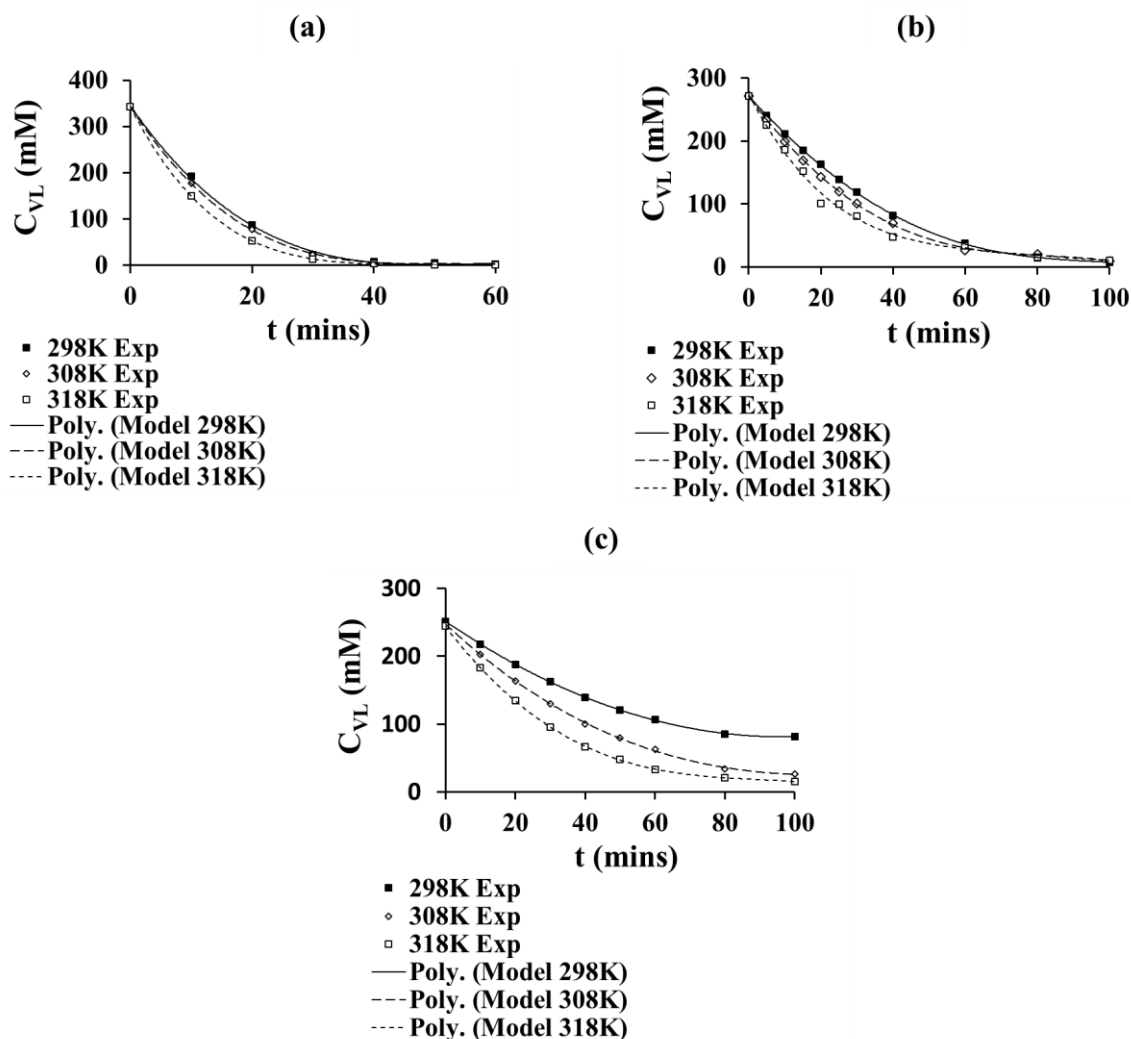
Fig.6.7. Comparison of the changes in predicted and experimental concentrations of vanillin over time during HDO reaction over 6.5 wt $\%PdRh/Al_2O_3$ catalyst in (a) 2-Propanol, (b) Toluene, and (c) Tetrahydrofuran at 298 K, 308 K, and 318 K. Lines represent fit of the proposed kinetic model to the actual experimental data points represented by the shapes.

6.3. Kinetics of Vanillin HDO Reaction in Binary Environments

Preliminary experiments involving HDO reaction of vanillin in the presence of other well-documented compounds found in real bio-oil were conducted through the procedure described in Section 3.4 of Chapter 3 to establish the inhibitory effect of these compounds. Table 3.11 of Section 3.4 in Chapter 3 provides the details on the concentration of vanillin (VL) and other compounds such as furfural, acetaldehyde, guaiacol, and acetic acid selected for this

investigation. The concentration ratios of the selected secondary compounds to vanillin reflects the actual relative proportions of these compounds to vanillin in typical bio-oil.[234] Figure 6.8 represents the influence of additional model compounds on VL conversion; it clearly shows that the rate at which VL changes decreases when the starting reaction mixture contained other compounds. This result confirms the inhibitory effect caused by increased competition for finite number of active sites on the surface of PdRh/Al$_2$O$_3$ catalyst following the addition of a second compound to the starting mixture. On the basis of the data displayed in Figure 6.8, the inhibitory effect of compounds considered follows the order: Furfural > Acetaldehyde > Guaiacol > Acetic Acid. The observed variation in inhibitory effects of these compounds can be attributed to differences in their reactivity relative to vanillin.
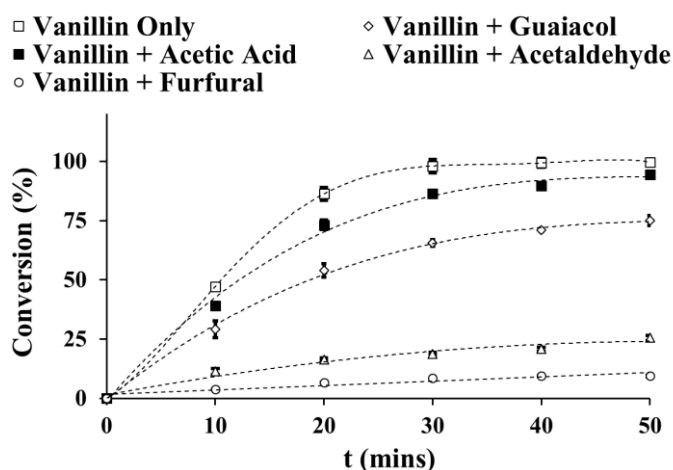
Fig. 6.8. Influence of guaiacol, acetic acid, furfural, and acetaldehyde on rates of VL conversion using the prepared bimetallic 6.5 wt % PdRh/Al$_2$O$_3$ catalyst at 1000 rpm, T = 318 K, P$_H$ = 2.0 MPa and ω = 5.0 kg/m^3. Reaction solvent is ethyl acetate. Lines represent best polynomial fit to data points and shapes represent actual data points.

Interestingly, Huang et al., [71] reported that both furfural and acetaldehyde are more reactive than vanillin. Conversely, hydrogenation reactions of acetic acid and guaiacol reported in the literature were conducted at temperatures significantly higher than 318 K which suggest both compounds are relatively more stable than vanillin.[22, 239,241,292,302] Hence, acetic acid and

guaiacol with greater stability and minimal inhibitory effects are deemed suitable as secondary model compounds in the binary environment for VL HDO reaction kinetics investigation. Moreover, these compounds are known to be major components of real bio-oil.[303–305]

6.3.1. Effect of H$_2$ gas Partial Pressure on VL HDO Reaction in Binary Environment

The effect of changes in hydrogen gas partial pressure (P$_H$) from 1.0 to 4.0 MPa on initial rates of VL disappearance (r$_0$) was investigated in vanillin − acetic acid environment and vanillin − guaiacol environment following the procedure described in Section 3.4 of Chapter 3. Figures 6.9a and 6.9b depict the observed variation in r$_0$ following changes in P$_H$ in both environments. As shown in Figure 6.9a, r$_0$ increases from 5.9×10^{-4} kmol/kg$_{cat}$min to 14.3×10^{-4} kmol/kg$_{cat}$min following changes in P$_H$ from 1.0 to 4.0 MPa in vanillin − acetic acid environment. Likewise, Figure 6.9b clearly indicates that r$_0$ increases from 5.2×10^{-4} kmol/kg$_{cat}$min to 11.4×10^{-4} kmol/kg$_{cat}$min as P$_H$ increases from 1.0 to 4.0 MPa in vanillin − guaiacol mixture. Hence, in both vanillin − acetic acid and vanillin − guaiacol environments increase in P$_H$ enhances the rate of VL disappearance. This conclusion is in line with findings reported in Section 5.5 of Chapter 5 on effect of P$_H$ on r$_0$ in vanillin-only environment. From the slope of the ln − ln plots presented in Figures 6.9c and 6.9d, the order of reaction with respect to P$_H$ in both vanillin − acetic acid and vanillin − guaiacol environments is 0.6. This value is higher than the 0.4 found in vanillin-only environment investigation, however, it shows that VL HDO reaction exhibits nonfirst-order kinetics with respect to P$_H$ in both the pure and binary environments. Despite the similarity in the order of reaction with respect to P$_H$ in the binary environments, further analysis of the data presented in Figures 6.9a and 6.9b shows that r$_0$ is more sensitive to changes in P$_H$ when the reaction occurs in the presence of acetic acid. In the presence of acetic acid, 1 MPa change in P$_H$ is expected to induce a change of 2.7×10^{-4} kmol/kg$_{cat}$min in r$_0$. While in the presence of guaiacol, 1 MPa change in P$_H$ is expected to cause

a corresponding change of 2.1×10^{-4} kmol/kg$_{cat}$min in r_0. The observed variation in response of r_0 to changes in P_H suggest guaiacol and acetic acid inhibits VL HDO reaction differently. Based on the response of r_0 to changes in P_H, it seems guaiacol inhibits VL HDO reaction more strongly than acetic acid. This conclusion is in agreement with the finding in Section 6.3.
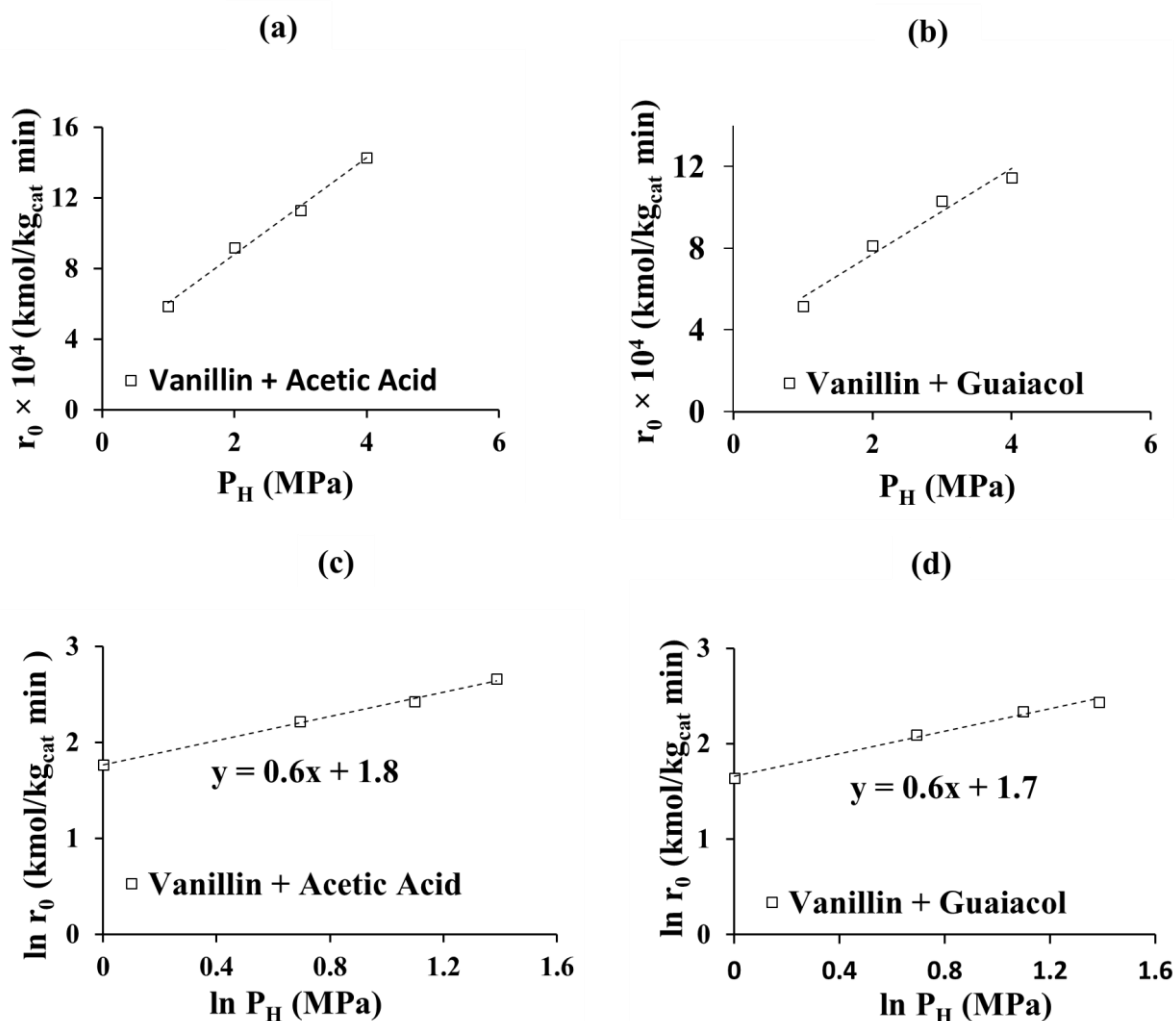
Fig. 6.9. (a) Influence of H_2 gas partial pressure (P_H) on initial rates of VL disappearance (r_0) in vanillin − acetic acid environment at 1000 rpm, T = 318 K, C_{VL0} = 263.0 mM, C_{AA0} = 1166.0 mM and ω = 5.0 kg/m^3, (b) Influence of P_H on r_0 in vanillin − guaiacol environment at 1000 rpm, T = 318 K, C_{VL0} = 263.0 mM, C_{GUA0} = 683.0 mM and ω = 5.0 kg/m^3, (c) ln − ln plots of r_0 against P_H for VL HDO reaction in vanillin – acetic acid environment, and (d) ln − ln plots of r_0 against P_H for VL HDO reaction in vanillin − guaiacol environment. Reaction solvent is ethyl acetate and catalyst is 6.5 wt % PdRh/Al$_2$O$_3$ catalyst. Lines represent best linear fit to the data and shapes represent actual data point.

6.3.2. Effect of Initial Vanillin Concentration on VL HDO Reaction in Binary Environment.

The procedure described in Section 3.4 of Chapter 3 was used to examine the influence of starting VL concentration (C_{VL0}) on the initial rate of VL disappearance (r_0) in the binary environments. Figures 6.10a and 6.10b summarises observed variation in r_0 following changes in C_{VL0}.
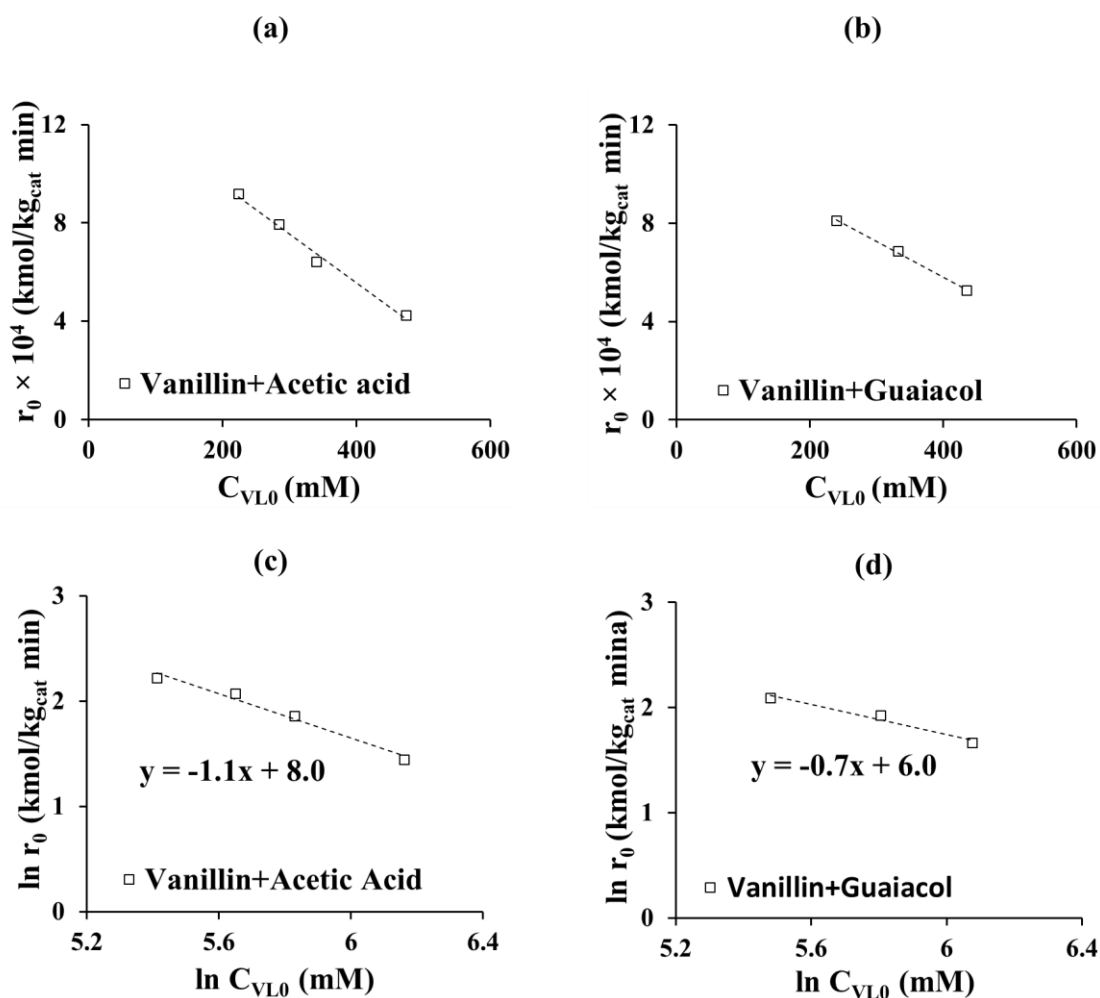
Fig. 6.10. (a) Influence of starting VL concentration (C_{VL0}) on initial rates of VL disappearance (r_0) using the prepared bimetallic 6.5 wt % PdRh/Al$_2$O$_3$ catalyst in vanillin − acetic acid environment at 1000 rpm, T = 318 K, P$_H$ = 2.0 MPa, and ω = 5.0 kg/m^3, (b) Influence of C_{VL0} on r_0 using the prepared bimetallic 6.5 wt % PdRh/Al$_2$O$_3$ catalyst in vanillin − guaiacol environment at 1000 rpm, T = 318 K, P$_H$ = 2.0 MPa, and ω = 5.0 kg/m^3, (c) ln − ln plots of r_0 against C_{VL0} for vanillin – acetic acid environment, and (d) ln − ln plots of r_0 against C_{VL0} for vanillin − guaiacol environment. Reaction solvent is ethyl acetate. Lines represent best linear fit to the data and shapes represent actual data point.

As shown in Figure 6.10a, r_0 decreases from 9.2×10^{-4} kmol/kg$_{cat}$min to 4.2×10^{-4} kmol/kg$_{cat}$min as C_{VL0} increases from 263 mM to 526 mM in vanillin − acetic acid environment. Likewise, Figure 6.10b indicates that r_0 decreases from 8.1×10^{-4} kmol/kg$_{cat}$min to 5.3×10^{-4} kmol/kg$_{cat}$min as C_{VL0} increases from 240 mM to 435 mM in vanillin − guaiacol environment. Notably, these trends are in agreement with findings from the vanillin-only environment study reported in Section 5.6 of Chapter 5. Nonetheless, the dependence of r_0 on C_{VL0} in vanillin − guaiacol environment differs from that in vanillin − acetic acid environment and vanillin-only environment. For every mM increase in C_{VL0}, r_0 decreases by 1.5×10^{-6} kmol/kg$_{cat}$min in vanillin − guaiacol environment and 2.0×10^{-6} kmol/kg$_{cat}$min in vanillin − acetic acid environment and vanillin-only environment. Hence, presence of acetic acid in the starting mixture failed to alter the dependence of r_0 on C_{VL0}. On the contrary, the presence of guaiacol in the starting mixture slightly alter the dependence of r_0 on C_{VL0}. The orders of reaction with respect to VL concentration found from the slope of the ln-ln plots presented in Figures 6.10c and 6.10d are −1.1 in vanillin − acetic acid environment and −0.7 in vanillin − guaiacol environment. These values compare well to the −0.7 reported in Section 5.6 of Chapter 5 as the order of reaction with respect to VL concentration in vanillin-only environment. Consequently, it can be concluded that VL HDO reaction over the prepared bimetallic PdRh/Al$_2$O$_3$ catalyst exhibits nonfirst-order reaction kinetics with respect to the starting vanillin concentration in both pure and binary environments.

6.3.3. Influence of Temperature on Product Distribution from VL HDO Reaction in Binary Environments.

The effect of changes in reaction temperature on product distribution from VL HDO reaction in vanillin − acetic acid and vanillin − guaiacol environments are presented in Figures 6.11a to 6.11d.
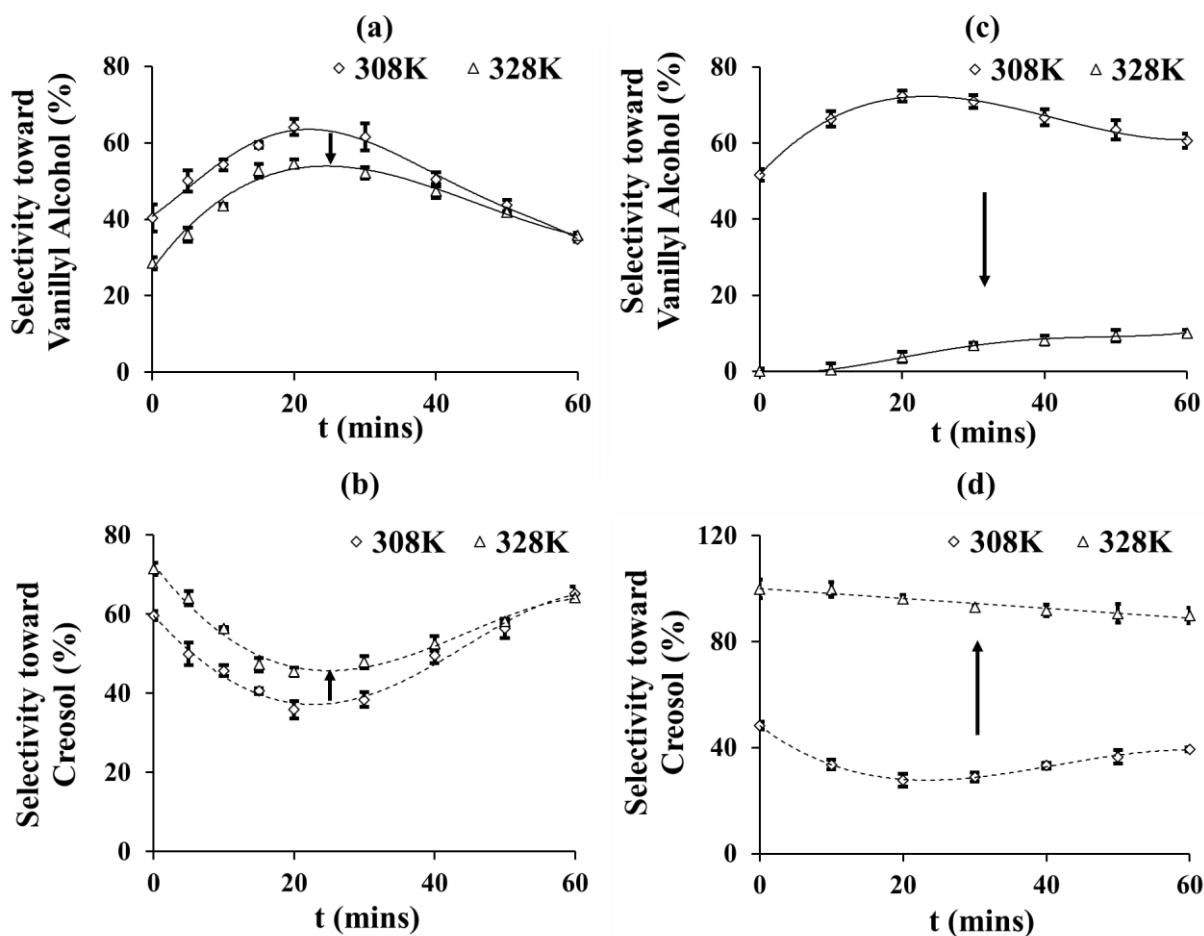
Fig.6.11. Product distribution as function of the reaction time and temperature in binary environment using the prepared bimetallic 6.5 wt % PdRh/Al$_2$O$_3$ catalyst. (a – b) vanillin – acetic acid environment at 1000 rpm, T = 308 K and 328 K, P$_H$ = 2.0 MPa, C$_{VL0}$ = 263.0 mM, C$_{AA0}$ = 1166.0 mM, and ω = 5.0 kg/m^3, (c – d) vanillin – guaiacol environment at 1000 rpm, T = 308 K and 328 K, P$_H$ = 2.0 MPa, C$_{VL0}$ = 263.0 mM, C$_{GUA0}$ = 683.0 mM and ω = 5.0 kg/m^3. Reaction solvent is ethyl acetate. Lines represent best polynomial fit to the data.

Figure 6.11a shows that during VL HDO reaction in vanillin − acetic acid environment, selectivity toward vanillyl alcohol increases from t = 0 mins to t = 20 mins and then decreases from t = 20 mins to t = 60 mins at the different reaction temperatures. Conversely, Figure 6.11b shows that selectivity toward creosol decreases from t = 0 mins to t = 20 mins and then increases from t = 20 mins to t = 60 mins during the reaction in vanillin − acetic acid environment. Figure 6.11c shows that during VL HDO reaction in vanillin − guaiacol environment, the selectivity toward vanillyl alcohol increases from t = 0 mins to t = 20 mins and then decreases from t = 20

mins to t = 60 mins at T = 308 K. In contrast, Figure 6.11d shows that during the same reaction at T = 308 K in vanillin − guaiacol environment, selectivity toward creosol decreases from t = 0 mins to t = 20 mins and then increases from t = 20 mins to t = 60 mins. Hence, it can be concluded that in both vanillin – acetic acid and vanillin − guaiacol environments the trends in selectivity toward vanillyl alcohol over time mirrored the trends in selectivity toward creosol over time. The data displayed in Figures 6.11a and 6.11c indicates that increase in reaction temperature suppresses selectivity toward vanillyl alcohol. Conversely, Figures 6.11b and 6.11d shows that increase in the reaction temperature enhances the selectivity toward creosol. Notably, the trends described here are in line with observations from vanillin HDO reaction in pure environment reported in Section 5.7 of Chapter 5. Hence, it can be concluded that the effect of time and temperature on selectivity toward the products from vanillin HDO reaction in pure and binary environments are the same.

6.3.4. Kinetic Modelling of Vanillin (VL) HDO Reaction in Binary Environment

In order to model the reaction kinetics of VL HDO in binary environment, Langmuir – Hinshelwood – Hougen – Watson (LHHW) approach was used to derive suitable rate expression from the series of elementary steps represented by equations 6.4 to 6.7. The derivation was based on assumption of competitive adsorption of dissociatively chemisorbed H_2, VL, and the secondary model compounds which include acetic acid and guaiacol. Additional information on derivation of the rate expression represented by equation 6.8 is provided in appendix A6.1.

$$VL + S_1 \leftrightarrow VLS_1 \qquad \text{(Fast)} \qquad\qquad (6.4)$$

$$M + S_1 \leftrightarrow MS_1 \qquad \text{(Fast)} \qquad\qquad (6.5)$$

$$H_2 + 2S_1 \leftrightarrow 2HS_1 \qquad \text{(Fast)} \qquad\qquad (6.6)$$

$$2HS_1 + VLS_1 \rightarrow \text{Products} \quad \text{(Slow)} \qquad\qquad (6.7)$$
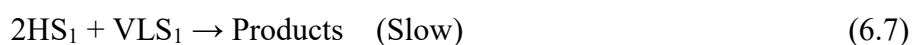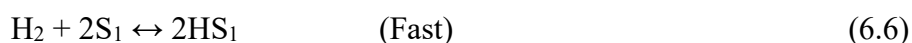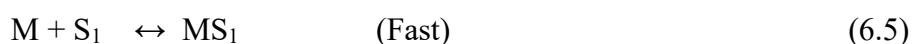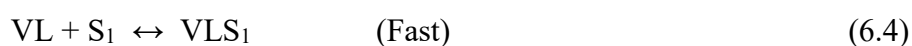
Herein, H_2 denotes molecular hydrogen, H is atomic hydrogen, MS_1 represents adsorbed intermediate species of the secondary model compound, M is the secondary model compound, HS_1 denotes adsorbed atomic hydrogen, VLS_1 stands for adsorbed vanillin intermediate, VL represent vanillin and S_1 denotes the catalyst vacant site.

$$r = \frac{k_S K_H K_{VL} C_H C_{VL}}{\left(1 + K_{VL} C_{VL} + K_M C_M + \sqrt{K_H C_H}\right)^3} \qquad (6.8)$$

Following the approach used to determine the kinetic parameters for vanillin-only environment HDO reaction model in Section 5.9.2 of Chapter 5, the parameters for describing the kinetics of VL HDO reaction in vanillin – acetic acid and vanillin – guaiacol environments were determined and presented in Table 6.5 and Table 6.6.

Table 6.5. Estimated Values of Model Parameters for VL HDO Reaction in Vanillin – Acetic Acid Environment using PdRh/Al$_2$O$_3$ Catalyst.

Temperature	Model Parameters	95% confidence level
308 K	K_S (kmol/kg$_{cat}$ min)	$10.13 \pm 3.74 \times 10^{-2}$
	K_H (m^3/kmol)	$0.20 \pm 1.40 \times 10^{-2}$
	K_{VL} (m^3/kmol)	$0.80 \pm 2.34 \times 10^{-2}$
	K_M (m^3/kmol)	$6.00 \times 10^{-3} \pm 1.87 \times 10^{-4}$
318 K	K_S (kmol/kg$_{cat}$ min)	$24.03 \pm 3.88 \times 10^{-1}$
	K_H (m^3/kmol)	$0.15 \pm 2.34 \times 10^{-3}$
	K_{VL} (m^3/kmol)	$0.70 \pm 5.61 \times 10^{-2}$
	K_M (m^3/kmol)	$1.00 \times 10^{-3} \pm 9.35 \times 10^{-5}$
328 K	K_S (kmol/kg$_{cat}$ min)	$33.99 \pm 7.48 \times 10^{-2}$
	K_H (m^3/kmol)	$9.60 \times 10^{-2} \pm 3.74 \times 10^{-3}$
	K_{VL} (m^3/kmol)	$0.58 \pm 1.40 \times 10^{-2}$
	K_M (m^3/kmol)	$5.00 \times 10^{-4} \pm 3.74 \times 10^{-5}$

Table 6.6. Estimated Values of Model Parameters for VL HDO Reaction in Vanillin – Guaiacol Environment using PdRh/Al$_2$O$_3$ Catalyst.

Temperature	Model Parameters	95% confidence level
308 K	K_S (kmol/kg$_{cat}$ min)	$8.44 \pm 7.48 \times 10^{-2}$
	K_H (m^3/kmol)	$0.19 \pm 4.67 \times 10^{-3}$
	K_{VL} (m^3/kmol)	$0.78 \pm 9.35 \times 10^{-3}$
	K_M (m^3/kmol)	$6.00 \times 10^{-3} \pm 1.40 \times 10^{-4}$
318 K	K_S (kmol/kg$_{cat}$ min)	$13.73 \pm 9.81 \times 10^{-2}$
	K_H (m^3/kmol)	$0.17 \pm 1.87 \times 10^{-3}$
	K_{VL} (m^3/kmol)	$0.64 \pm 1.40 \times 10^{-2}$
	K_M (m^3/kmol)	$4.00 \times 10^{-3} \pm 1.40 \times 10^{-4}$
328 K	K_S (kmol/kg$_{cat}$ min)	$19.00 \pm 1.40 \times 10^{-2}$
	K_H (m^3/kmol)	$0.13 \pm 4.67 \times 10^{-4}$
	K_{VL} (m^3/kmol)	$0.52 \pm 1.40 \times 10^{-3}$
	K_M (m^3/kmol)	$2.00 \times 10^{-3} \pm 4.21 \times 10^{-5}$

Table 6.5 shows that at 95% confidence level, the value of K_S increased from 10.13 kmol/kg$_{cat}$min at 308 K to 33.99 kmol/kg$_{cat}$min at 328 K. Likewise, from Table 6.6 it can be seen that at 95% confidence level, the value of K_S increased from 8.44 kmol/kg$_{cat}$min at 308 K to 19.00 kmol/kg$_{cat}$min at 328 K. Hence, with acetic acid or guaiacol in the starting mixture the rate constant for VL HDO reaction increases with the reaction temperature. This suggest VL HDO reaction in the presence of either acetic acid or guaiacol obeys the Arrhenius expression. Using the Arrhenius expression, the intrinsic activation energies for VL HDO reaction in vanillin – acetic acid and vanillin – guaiacol environments were estimated and presented in Table 6.7. Table 6.7 shows that at 95% confidence level, the intrinsic activation energy for VL HDO reaction in vanillin – acetic acid environment is 51.0 kJ/mol, while in vanillin – guaiacol environment the estimated intrinsic activation energy for VL HDO reaction at 95% confidence level is 34.10 kJ/mol. These values are remarkably different from each other, which suggest

the barrier to VL HDO reaction changes with the type of secondary model compounds present in the starting mixture.

Table 6.7. Estimated Values of Kinetic Constants for VL HDO Reaction in Vanillin – Acetic acid and Vanillin – Guaiacol Environments using PdRh/Al_2O_3 catalyst.

	95% Confidence Limit	
Kinetic Constants	Vanillin – acetic acid environment	Vanillin – guaiacol environment
E_A (kJ/mol)	$51.00 \pm 8.36 \times 10^{-2}$	$34.10 \pm 7.61 \times 10^{-2}$
ΔH_H(kJ/mol)	$-30.80 \pm 1.45 \times 10^{-2}$	$-16.60 \pm 4.70 \times 10^{-3}$
ΔH_{VL}(kJ/mol)	$-13.80 \pm 2.73 \times 10^{-2}$	$-17.50 \pm 9.45 \times 10^{-3}$
ΔH_M(kJ/mol)	$-104.80 \pm 1.91 \times 10^{-4}$	$-47.40 \pm 1.46 \times 10^{-4}$
ΔS_H(kJ/mol)	$-113.00 \pm 4.56 \times 10^{-3}$	$-67.70 \pm 3.18 \times 10^{-3}$
ΔS_{VL}(kJ/mol)	$-46.60 \pm 1.17 \times 10^{-4}$	$-58.80 \pm 6.32 \times 10^{-4}$
ΔS_M(kJ/mol)	$-384.20 \pm 2.45 \times 10^{-4}$	$-196.30 \pm 1.08 \times 10^{-4}$

In comparison to a value of 24.1 kJ/mol reported as the intrinsic activation energy for VL HDO reaction in vanillin-only environment in Section 5.9.2. of Chapter 5, the intrinsic activation energies for the reaction in binary environments are significantly higher. Hence, it can be concluded that the presence of either acetic acid or guaiacol in the starting mixture increases the barrier to VL HDO reaction. This conclusion validates earlier hypothesis in Section 6.1 that the barrier to VL HDO reaction will be higher in real bio-oil environment than the pure environment which contains only vanillin and the solvent. Despite the differences between the activation energy for VL HDO reaction in binary environments and the pure environment, Table 6.5 and 6.6 shows that the adsorption constants for VL and H_2 continue to decrease with increase in the reaction temperature. This indicates that VL HDO reaction remained exothermic, and therefore obeys the classical Van't Hoff expression. Using the Van't Hoff expression in equation 6.2, the changes in enthalpy and entropy of the reactants during VL HDO reaction in vanillin – acetic acid and vanillin – guaiacol environments were estimated and presented in Table 6.7. Notably, all the values are negative and thus confirms thermodynamic consistency

of the model fitted to the experimental data. Table 6.7 shows that change in enthalpy due to VL or H_2 adsorption is remarkably smaller than the change in enthalpy due to acetic acid or guaiacol adsorption. This suggest both acetic acid and guaiacol adsorbs relatively stronger to the bimetallic PdRh/Al$_2$O$_3$ catalyst surface than VL or H_2. The strong interaction between PdRh/Al$_2$O$_3$ catalyst surface and the secondary model compounds (i.e. acetic acid and guaiacol) increases the competition between VL and H_2 for vacant active sites. This possibly explains the increase in barrier to VL HDO reaction in the binary environments compared to vanillin-only environment. The extent to which the rates predicted from the derived model agrees with the experimental data from vanillin – acetic acid and vanillin – guaiacol environments are illustrated by the parity plots in Figures 6.12a and 6.12b. Clearly, with R^2 values greater than or equal to 0.98 in the parity plots for vanillin – acetic acid and vanillin – guaiacol environments, the proposed model reliably described VL HDO reaction in binary environments. Applying equation 6.3, the average percentage error found was 7.27% in the case of VL HDO reaction in vanillin – acetic acid environment and 3.42% for VL HDO reaction in vanillin – guaiacol environment.
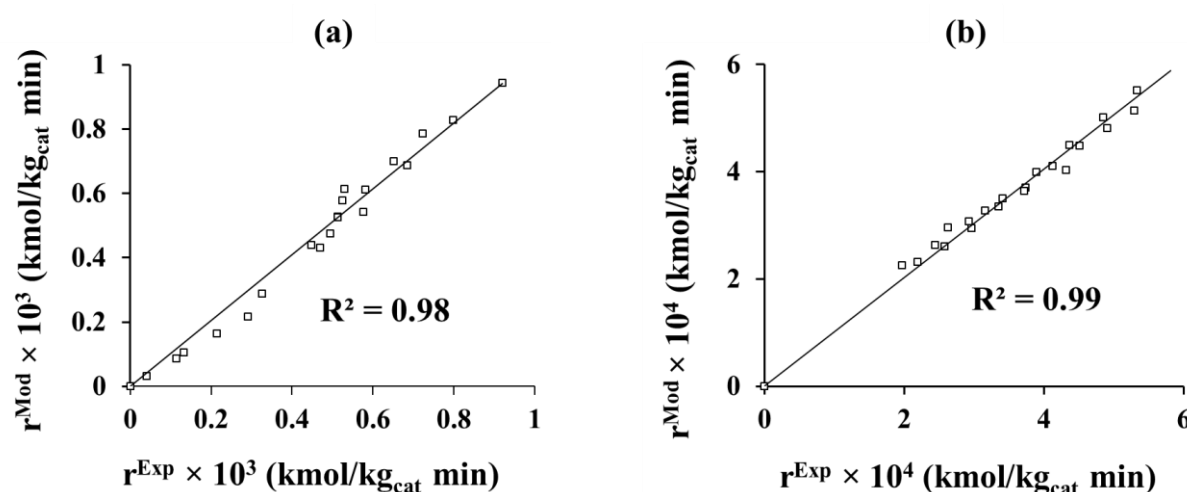
Fig. 6.12. Parity Plots comparing predicted and experimental reaction rates for VL HDO reaction over the prepared bimetallic 6.5 wt% PdRh/Al$_2$O$_3$ catalyst in (a) vanillin – acetic acid, and (b) vanillin – guaiacol environments.

Figures 6.13a and 6.13b further reaffirms the reliability of the proposed model because they showed strong agreement between the experimental and predicted VL concentrations at all the reaction temperatures considered.

(a)

◇ 308K Exp
□ 318K Exp
▵ 328K Exp
--- Poly. (Model 308K)
---- Poly. (Model 318K)
— Poly. (Model 328K)

(b)

◇ 308K Exp
□ 318K Exp
▵ 328K Exp
--- Poly. (Model 308K)
---- Poly. (Model 318K)
— Poly. (Model 328K)
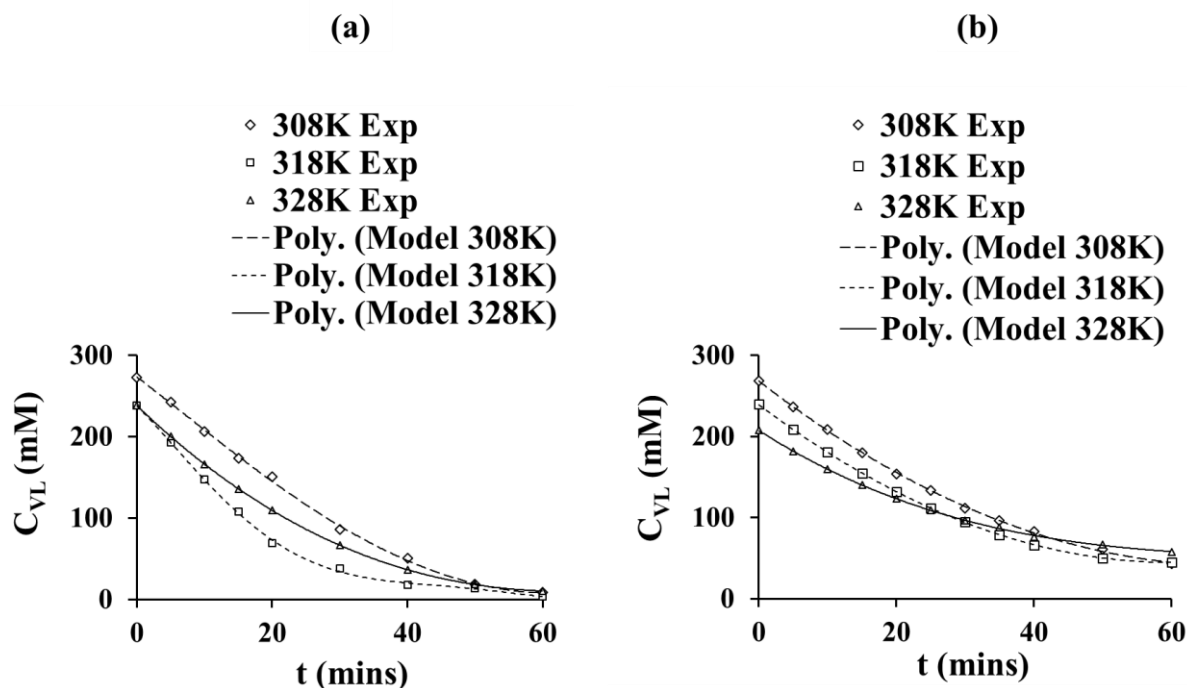
Fig. 6.13. Comparison between predicted and experimental VL concentration from VL HDO reaction using the synthesised 6.5 wt% PdRh/Al$_2$O$_3$ catalyst in (a) vanillin – acetic acid, and (b) vanillin – guaiacol environments.

Table 6.8 summarises changes in fractional coverage of hydrogen gas (θ_H), vanillin (θ_{VL}), acetic acid (θ_A), guaiacol (θ_G) and vacant sites (θ_V) over time in vanillin – acetic acid and vanillin – guaiacol environments at 318 K. It shows that the fractional coverage of vanillin reduces over time, while in contrast the fractional coverage of hydrogen, acetic acid and guaiacol remained relatively unchanged throughout. The negligible change in fractional coverage of guaiacol and acetic acid can be attributed to the difficulty in converting these compounds at the mild reaction temperature used in the study. Likewise, the fixed external H$_2$ gas supply applied during the experiments to maintain constant reaction pressure can be held responsible for the insignificant change in hydrogen gas fractional coverage over time.

Table 6.8. Changes in Fractional Coverage of VL, H_2, Acetic Acid, Guaiacol and Vacant Site over Time at 318K.

	Vanillin – Guaiacol Environment				Vanillin – Acetic Acid Environment			
t	θ_V	θ_{VL}	θ_H	θ_G	θ_V	θ_{VL}	θ_H	θ_A
0	0.844	0.134	0.018	0.004	0.844	0.138	0.017	0.001
10	0.873	0.105	0.019	0.004	0.891	0.090	0.018	0.001
30	0.918	0.058	0.020	0.004	0.955	0.025	0.019	0.001
50	0.944	0.032	0.020	0.004	0.970	0.009	0.019	0.001

6.4. Conclusions

In this chapter the kinetics of vanillin hydrodeoxygenation (HDO) reaction over the prepared bimetallic 6.5 wt % PdRh/Al$_2$O$_3$ catalyst was examined under different solvents which include 2-propanol, tetrahydrofuran, and toluene. The investigation revealed the reaction products are the same under these solvents. However, notable differences were observed in the reaction rates dependence on hydrogen gas partial pressure and starting vanillin concentration. The orders of reaction with respect to hydrogen gas partial pressure found was 0.9 in 2-propanol, 0.3 in tetrahydrofuran, and 0.5 in toluene, while relative to vanillin concentration the orders of reaction found was −0.7 in 2-propanol, −0.6 in tetrahydrofuran, and −1.9 in toluene. Additionally, the intrinsic activation energies and other intrinsic parameters such as adsorption enthalpies for vanillin and hydrogen gas estimated from model I describing the reaction varied significantly following changes in the solvent. The estimated values of intrinsic activation energies for the reaction at 95% confidence level were 23.6 kJ/mol in 2-propanol, 35.8 kJ/mol in tetrahydrofuran, and 56.3 kJ/mol in toluene. As a result, it was concluded that changes in the reaction solvent alters the energy barrier for vanillin hydrodeoxygenation. The second part of this chapter probed the inhibitory effect of other common model compounds such as acetic acid and guaiacol on the kinetics of vanillin hydrodeoxygenation reaction using ethylacetate as

the solvent. It was found that the presence of guaiacol in the starting mixture slightly alter the reaction rate dependence on starting vanillin concentration. In contrast, presence of acetic acid in the starting mixture failed to affect the reaction rate dependence on starting vanillin concentration. The orders of reaction with respect to vanillin concentration found were −1.1 in vanillin – acetic acid environment and −0.7 in vanillin – guaiacol environment. Interestingly, a nonfirst-order reaction kinetics with respect to hydrogen gas partial pressure was found in both vanillin – acetic acid environment and vanillin – guaiacol environment. It was found that the order of reaction with respect to hydrogen gas partial pressure increased from 0.4 in vanillin-only environment to 0.6 in both vanillin – acetic acid and vanillin – guaiacol environments. The reaction kinetics of vanillin hydrodeoxygenation in both vanillin – acetic acid and vanillin – guaiacol environments was then successfully modelled through the Langmuir – Hinshelwood – Hougen – Watson (LHHW) approach under the assumption of competitive adsorption of dissociatively chemisorbed hydrogen and the model compounds. As expected the model parameters which include rate constant, equilibrium adsorption constant for hydrogen, vanillin, guaiacol, and acetic acid varied with the reaction temperature and environment. The estimated values from the model at 95% confidence level for vanillin – acetic acid environment were 51.0 kJ/mol for the intrinsic activation energy, −13.8 kJ/mol for VL adsorption enthalpy, −30.8 kJ/mol for hydrogen gas adsorption enthalpy, and −104.8kJ/mol for acetic acid adsorption enthalpy. Likewise for vanillin hydrodeoxygenation reaction in the presence of guaiacol, the corresponding values at 95% confidence level calculated from the model were 34.2 kJ/mol for the intrinsic activation energy, −17.5 kJ/mol for VL adsorption enthalpy, −16.6 kJ/mol for hydrogen gas adsorption enthalpy, and −47.4 kJ/mol for guaiacol adsorption enthalpy. Hence, the investigation showed that the presence of either acetic acid or guaiacol in the starting

mixture altered the energy barrier for vanillin hydrodeoxygenation reaction and the strength of adsorption of the reactants.

Chapter 7

Conclusions and Recommendations.

The work completed in this thesis explored the role of solvent, processing conditions, catalytic support, and active element on the hydrodeoxygenation reaction using vanillin a less reported compound as the probe molecule. In addition, studies carried out in this thesis probe the kinetics of vanillin hydrodeoxygenation reaction over monometallic and bimetallic Pd-based catalysts. More importantly, valuable information on impact of solvent and other significant model compounds on intrinsic parameters such as rate constant, adsorption constant, and activation energy is reported in this thesis. Past studies on kinetics of model compounds of bio-oil, in particular vanillin were conducted in environments which contain no other compound. However, over 400 compounds are present in real bio-oil environment. This thesis reports the kinetics of vanillin hydrodeoxygenation reaction in the presence of acetic acid and guaiacol. Acetic acid and guaiacol were selected as the secondary compounds for the kinetic investigation of vanillin hydrodeoxygenation in binary environments because of their relative stability compared to vanillin and significant presence in real bio-oil.

7.1. Effect of Catalyst, Solvent, and Operating Condition on Vanillin Upgrading via Hydrodeoxygenation Reaction.

In the completed research work, blank experiments were carried out to investigate non-catalytic and support-only effect on vanillin hydrodeoxygenation reaction. Interestingly, both had negligible impact on the reaction. Conversely, changes in active element of the catalyst significantly altered the conversion and selectivity toward the desired reaction product creosol. To highlight the differences under the various active element, 99% conversion and 71%

selectivity toward creosol was achieved from the reaction using 5 wt % Pd/C catalyst. While in the presence of 5 wt % Pt/C catalyst, 42% conversion and 2% selectivity toward creosol was achieved. In summary, the order in performance of the active elements based on conversion follows Pd > Pt > Rh. However, in terms of selectivity toward creosol the order in performance found is Pd > Rh > Pt. From further investigation, it was concluded that differences in hydrogen consumption and physicochemical properties such as metal dispersion and specific surface area are responsible for the observed changes in performance under the various active elements. Notably, the use of in-house prepared bimetallic PdRh/Al$_2$O$_3$ catalyst improved the selectivity toward creosol from the maximum of 71% under mono-metals to 99% and maintained conversion as high as 98%. The improvement in performance under the prepared bimetallic PdRh/Al$_2$O$_3$ catalyst was attributed to the ligand effect between Pd and Rh on the alumina support. Additional test conducted to examine the stability and reusability of the various catalysts showed that the most and least stable among the commercial mono-metals examined is Pd/C and Pt/SiO$_2$ respectively. The in-house prepared bimetallic catalyst demonstrated excellent stability with conversion above 99% and selectivity toward creosol above 80% after three consecutive cycles. Hence, on the basis of the short and long term results on selectivity toward creosol, it was found that the in-house prepared bimetallic catalyst outperformed the commercial mono-metal catalysts. From the comparative studies on the influence of solvent on vanillin hydrodeoxygenation reaction, it was established that changes in solvent class significantly affects both the distribution of products and conversion. Among the solvents considered, water emerged as the most efficient medium for the reaction with the highest ratio of vanillin converted and creosol formed per moles of hydrogen consumed. However, activity of the prepared bimetallic catalyst was remarkably low in water compared to the other reaction media because of losses in the catalytic support. The lowest conversion and selectivity toward

creosol of 70% and 3% respectively was achieved using toluene as the reaction solvent. Likewise, significantly high amount of hydrogen was consumed to convert vanillin to creosol under toluene. Hence, it was concluded that among the solvents examined, toluene is the least efficient medium for vanillin hydrodeoxygenation reaction. On the basis of results obtained from experiments conducted under the conditions established by Taguchi method of experimental design, it was found that changes in processing condition significantly influences conversion and product selectivity from vanillin hydrodeoxygenation. Over the operational range of 318 K to 338 K reaction temperature, 1.0 MPa to 3.0 MPa hydrogen gas pressure, 0.1 to 0.5 kg/m^3 catalyst loading, and 500 rpm to 900 rpm agitation speed; the condition which maximises the selectivity toward creosol and conversion was found to be 338 K, 3.0 MPa, 0.5 kg/m^3, and 500 rpm. Among the processing parameters considered, catalyst loading emerged as the most influential parameter accounting for 77% of variation in performance. While in contrast, agitation speed was responsible for less than 1% of the variation in performance and therefore emerged as the least influential parameter.

7.2.   Kinetics of Vanillin Hydrodeoxygenation Reaction Using Monometallic and Bimetallic Pd-Based Catalysts.

In order to probe further the observed differences in vanillin hydrodeoxygenation reaction over different catalysts, experiments were conducted at mild conditions in the kinetically controlled regime using mono-metal and bi-metal Pd-based catalysts which include Pd/C, Pd/Al_2O_3, and $PdRh/Al_2O_3$ in a batch reactor with ethylacetate as the solvent. The experiments shows that nonfirst-order reaction kinetics with respect to vanillin concentration and hydrogen gas partial pressure fit best to the reaction rate data under the various catalysts considered. To be precise the estimated order of reaction with respect to vanillin concentration ranges from −1.2 to −0.6, while relative to hydrogen gas partial pressure the order lies in the range of 0.3 to

0.7. The nonfirst-order dependence suggest inhibitory effects possibly as a result of strong adsorption of vanillin onto the catalysts active sites which consequently prevented the adsorption of hydrogen gas. From transport limitation analysis, hydrogen gas was established to be the limiting reactant in the system. Hence, the decline in adsorption of hydrogen gas possibly explains the decrease in activity of the catalysts as concentration of vanillin increases. In addition, from the kinetic measurements it was found that increase in the reaction temperature enhances selectivity toward creosol provided the reaction is catalysed by Pd/C or PdRh/Al$_2$O$_3$ particles. While in the presence of Pd/Al$_2$O$_3$ particles, increase in the reaction temperature marginally increase selectivity toward vanillyl alcohol at the expense of creosol. The experimental data obtained from the kinetic studies was successfully modelled using a Langmuir – Hinshelwood – Hougen – Watson (LHHW) expression derived under the assumption of competitive adsorption of vanillin and dissociative hydrogen. With values of the measured coefficient of determination (R^2) $\geq$ 99.5%, the developed model reliably predicts the actual rate of reaction under the various catalysts. It was found that the intrinsic kinetic parameters for the reaction varied remarkably with the type of catalyst in use. Thus, explains the observed significant variation in performance following changes in the catalyst for the reaction. At 95% confidence level, the estimated intrinsic kinetic parameters for the reaction under Pd/C catalyst were 50.6 kJ/mol for the intrinsic activation energy, $-$28.9 kJ/mol for the adsorption enthalpy of H$_2$ gas, and $-$32.5 kJ/mol for the adsorption enthalpy of vanillin. However, for reactions conducted using Pd/Al$_2$O$_3$ catalyst, the obtained values for intrinsic kinetic parameters at 95% confidence level include 64.1 kJ/mol for the activation energy, $-$10.4 kJ/mol for the adsorption enthalpy of H$_2$ gas, and $-$10.9 kJ/mol for the adsorption enthalpy of vanillin. In the case of reactions catalysed by bimetallic PdRh/Al$_2$O$_3$ particles, the value obtained at 95% confidence level for the intrinsic kinetic parameters include intrinsic activation

energy of 24.1 kJ/mol, −7.8 kJ/mol for the adsorption enthalpy of H_2 gas, and −13.4 kJ/mol for the adsorption enthalpy of vanillin. On the basis of the estimated intrinsic activation energies for the reaction under the various catalysts, it can be concluded that barrier to the reaction was significantly higher under the monometallic catalysts compared to the prepared bimetallic PdRh/Al_2O_3 catalyst. In addition, the estimated enthalpy of adsorption for the reactants showed remarkable variation in the strength of interactions of the reactants with the surface of alumina and activated carbon supported catalysts. The values obtained indicates the reactants which include hydrogen and vanillin adsorbed more strongly to the surface of activated carbon supported catalyst than alumina supported catalysts.

7.3. Kinetics of Vanillin Hydrodeoxygenation Reaction Using Different Solvents.

In an attempt to provide additional reasons for the observed differences in conversion and distribution of products from vanillin (VL) hydrodeoxygenation (HDO) reaction under different solvents, VL HDO experiments were conducted under kinetically controlled regime using the in-house prepared bimetallic PdRh/Al_2O_3 catalyst and different classes of solvents. Nonfirst-order reaction kinetics with respect to hydrogen gas partial pressure and starting vanillin concentration was found under each of the solvents. Nonetheless, notable differences was observed in the estimated reaction orders. With respect to hydrogen gas partial pressure, the calculated orders of reaction include 0.9 under 2-propanol, 0.3 under tetrahydrofuran, and 0.5 under toluene. While relative to the starting vanillin concentration, the estimated reaction orders are −0.7 under 2-propanol, −0.6 under tetrahydrofuran, and −1.9 under toluene. In addition, modelling of the reaction kinetics data obtained from experiments under different solvents showed remarkable changes in values of intrinsic parameters such as activation energies and adsorption enthalpies of the reactants. With 2-propanol as the solvent, the estimated values of intrinsic parameters at 95% confidence level found include 23.6 kJ/mol for the intrinsic

activation energy, −13.2 kJ/mol for the adsorption enthalpy of H_2 gas, and −12.3 kJ/mol for the adsorption enthalpy of vanillin. While under tetrahydrofuran, the intrinsic parameters calculated values at 95% confidence level are 35.8 kJ/mol for the intrinsic activation energy, −6.6 kJ/mol for the adsorption enthalpy of H_2 gas, and −6.7 kJ/mol for the adsorption enthalpy of vanillin. For reactions conducted using toluene as the solvent, the estimated values of intrinsic parameters at 95% confidence level are 56.3 kJ/mol for the intrinsic activation energy, −21.7 kJ/mol for the adsorption enthalpy of H_2 gas, and −26.6 kJ/mol for the adsorption enthalpy of vanillin. Hence, changes in intrinsic parameters and reaction rate dependence on the two reactants possibly explain the observed variation in product distribution and conversion following changes in the reaction solvent.

7.4. Kinetics of Vanillin Hydrodeoxygenation Reaction in Binary Environments.

In order to understand the effect of prominent compounds present in bio-oil on rate of vanillin (VL) hydrodeoxygenation (HDO), HDO experiments were conducted in the kinetically controlled regime using reaction mixtures containing VL as the primary compound and either acetic acid or guaiacol as the secondary compound. The results obtained from the investigation showed that the relationship between the rate of vanillin disappearance and starting vanillin concentration is affected slightly by the presence of guaiacol in the reaction environment. Interestingly, nonfirst-order reaction kinetics with respect to vanillin concentration was found in both vanillin – acetic acid and vanillin – guaiacol environments. It was found that the order of reaction with respect to hydrogen gas partial pressure increases from 0.4 in pure environment to 0.6 in the binary environments. The kinetics of VL HDO reaction in both vanillin – acetic acid and vanillin – guaiacol environments were successfully modelled through a modified Langmuir – Hinshelwood – Hougen – Watson (LHHW) method. Notably, the presence of acetic acid or guaiacol in the reaction environment altered the intrinsic kinetic parameters. The

estimated values of the intrinsic kinetic parameters for VL HDO reaction in vanillin – acetic acid environment at 95% confidence level were 51.0 kJ/mol for the intrinsic activation energy, −13.8 kJ/mol for VL adsorption enthalpy, −30.8 kJ/mol for hydrogen gas adsorption enthalpy, and −104.8 kJ/mol for acetic acid adsorption enthalpy. While in vanillin – guaiacol environment, values of the intrinsic kinetic parameters for VL HDO reaction estimated from the model at 95% confidence level are 34.2 kJ/mol for reaction activation energy, −17.5 kJ/mol for VL adsorption enthalpy, −16.6 kJ/mol for hydrogen gas adsorption enthalpy, and −47.4 kJ/mol for guaiacol adsorption enthalpy. On the basis of results presented, the presence of acetic acid or guaiacol in the reaction environment increases the adsorption enthalpies for the reactants and the intrinsic activation energy for VL HDO reaction.

7.5. Recommendations.

In conformity with past studies on bio-oil and model compounds upgrading, the present work successfully used a probe molecule vanillin to demonstrate the importance of catalyst, solvent, and operating condition in hydrodeoxygenation reaction. Nonetheless, shortcomings of this work present opportunities for further research studies. The present work utilised noble metal catalysts which are known to be expensive. Although, limitations on resources available for catalyst characterisation ultimately confined the present work to commercial catalysts, experimenting with cheap alternative catalysts is highly desirable to improve the process economics. Amorphous catalysts such as Ni–Mo–B, Co–Ni–Mo–B etc. represent attractive alternatives to noble metal catalysts. However, highly sophisticated characterisation tools will be required to relate their properties to catalytic performance. Likewise, metal loadings of the catalysts employed in the present work could be reduced to lessen economic concern around their use. This could be achieved by conducting additional experiments to evaluate performance under catalysts with different metal loadings. In addition, it is unusual to design

a bimetallic containing two noble metals such as Pd and Rh, often the second metal is a non-noble metal such as Fe, Cu, Ag, Zn, Sn e.t.c. Therefore, additional experiments using non-noble metal catalysts will provide in-depth information on activity of non-noble metals for vanillin hydrodeoxygenation and facilitate improvement in the bimetallic catalyst utilised in the present work. In particular, bimetallic alloy catalysts such as Ni–Co, Ni–Mo, Ni–Re, Ni–W e.t.c that have shown promising hydrogenating performance in past studies on hydrodeoxygenation could be synthesised and tested to completely eliminate the need for Pd–Rh combination. Undoubtedly, the hydrothermal stability of the bimetallic catalyst employed in the present work needs improvement because its activity diminished significantly when water was the reaction solvent. Improvement in the hydrothermal stability of the bimetallic catalyst synthesised could be achieved through additional screening experiments on promising alternative supports such as Zirconia (ZrO_2), Titania (TiO_2), and Ceria (CeO_2). As expected the screening experiments together with the kinetic studies conducted in this work clearly showcase the superiority of the prepared bimetallic $PdRh/Al_2O_3$ catalyst over the contemporary commercial mono-metal catalysts. However, insufficient characterisation made it extremely challenging to explain the observed differences in performance under the mono-metal catalysts and bimetallic catalyst. This problem illustrate the importance of characterisation in understanding the chemistry of heterogeneous reactions. For instance, performing additional characterisation experiments such as X-ray photoelectron spectroscopy (XPS), Ammonia Temperature-Programmed Desorption (NH_3-TPD), Temperature-Programmed Reduction (TPR), CO chemisorption, and Extended X-ray absorption fine structure (EXAFS) will certainly improve the existing knowledge on changes in the precursor commercial Rh/Al_2O_3 catalyst following addition of the Pd dopant. Likewise, from these experiments valuable supplementary data on the various catalysts examined in Section 4.4 of Chapter 4 could be

deduce and use to interpret observed differences in performance. The X-ray diffraction (XRD) and Scanning Electron Microscopy (SEM)-Energy Dispersive X-ray (EDX) techniques employed in the present work to examine the surface morphologies of the catalysts post reaction are sufficient. However, to ascertain any possible changes in surface properties of the catalysts post reaction, thermogravimetric analysis (TGA) and Brunauer – Emmett – Teller (BET) analysis could be employed in conjunction with the techniques used in the present work. The kinetic studies completed in this research work benefits the industry because it shed light on ways in which the choice of solvent, catalyst, and other processing parameters affects upgrading of oxygenates present in bio-oil during hydrodeoxygenation reaction under mild conditions. Likewise, findings from these studies are valuable to the industry because they can be used to guide the selection of processing parameters to ensure high rates and selectivity toward the deoxygenated product. The framework employed in this work can be adopted in other academic environment to probe the kinetics of liquid-phase catalytic reaction. At the same time, findings from the kinetic studies conducted add to existing knowledge on the upgrading of vanillin via hydrodeoxygenation reaction. Hence, both the industry and the academic sector can benefit from the findings reported in this thesis. In general, the kinetic studies conducted can be improved by repeating the investigation for different catalysts, solvents and binary environment under the same conditions. Likewise, the work on kinetics over different catalysts could be improved by performing additional experiments using the precursor commercial Rh/Al_2O_3 catalyst. This way it would be easier to completely understand the role of the Pd dopant in the reaction. To enhance understanding of the steps involve in vanillin hydrodeoxygenation reaction, additional experiments could be performed with vanillyl alcohol as the starting material using different catalysts and solvents. This will shed more light on the influence of solvent and catalyst in the reaction steps and improve knowledge on the rate determining step

during vanillin hydrodeoxygenation reaction over different catalysts and under different solvents. Of course with a clearer knowledge of the rate determining step, modelling of the reaction can be improved. Ideally, the effect of changes in catalyst loading should be examined following changes in the solvent and shift in the kinetic studies from pure system to binary system. This way it would be possible to confirm the absence of mass transfer limitation in the subsequent studies rather than inferring it from previous experiments under pure environment. Likewise, the present work could have benefited from using catalysts with identical metal loading rather than adjusting for the differences. For this reason, it is highly recommended in future studies to utilise synthesised catalysts with the same metal loadings for the investigation on vanillin hydrodeoxygenation reaction over different catalysts. It is worth highlighting that continuous operations are often preferred in the industry to batch processes. Therefore, the relevance of work completed in this thesis could be improved through additional experiments with a continuous reactor. This idea was removed from the initial project plan because of the challenges encountered in the process of recommissioning the fixed bed reactor available in the laboratory used to conduct this research work. Finally, it is recommended to conduct a series of adsorption experiments using different solvents to shed light on possible changes in adsorption affinity of the reactant, intermediate, and the desired product.

References

1. Lai, Q., Zhang, C., Holles, J.H., (2016). Hydrodeoxygenation of guaiacol over Ni@Pd and Ni@Pt bimetallic overlayer catalysts, Appl Catal A Gen., 528, 1 – 13.

2. Raj, B., Singh, O., (2012). Global Trends of Fossil Fuel Reserves and Climate Change in the 21st Century, Foss Fuel Environ., 168 – 192.

3. Lugo-José, Y.K., Monnier, J.R., Williams, C.T., (2014). Gas-phase catalytic hydrodeoxygenation of propanoic acid over supported group VIII noble metals: Metal and Support Effects, Appl Catal A Gen., 469, 410 – 418.

4. Luis, J., Mora, C., (2018). Hydrodeoxygenation of acetic acid using monometallic and bimetallic catalysts supported on carbon, PhD Thesis. University of South Carolina.

5. Patel, M., Kumar, A., (2016). Production of renewable diesel through the hydroprocessing of lignocellulosic biomass-derived bio-oil: A review, Renew Sustain Energy Rev., 58, 1293 – 1307.

6. Lu, M., Du, H., Wei, B., Zhu, J., Li, M., Shan, Y., (2017). Catalytic hydrodeoxygenation of guaiacol over palladium catalyst on different Titania supports, Energy Fuels., 31, 10858 – 10865.

7. Ghampson, I.T., Sepúlveda, C., Garcia, R., Frederick, B.G., Wheeler, M.C., Escalona, N., (2012). Guaiacol transformation over unsupported molybdenum-based nitride catalysts, Appl Catal A Gen., 413 – 414.

8. Newell, R.G., Raimi, D., Aldana, G., (2019). Global energy outlook 2019: The next generation of energy, report 19-06., Resources for the Future: Washington D.C.

9. Huber, G.W., Iborra, S., Corma, A., (2006). Synthesis of transportation fuels from biomass: chemistry, catalysts, and engineering, Chem Rev., 106, 4044 – 4098.

10. Chheda, J.N., Huber, G.W., Dumesic, J.A., (2007). Liquid-phase catalytic processing of biomass-derived oxygenated hydrocarbons to fuels and chemicals, Angew Chemie-Int Ed., 46, 7164 – 7183.

11. Huber, G.W., Corma, A., (2007). Synergies between bio- and oil refineries for the production of fuels from biomass, Angew Chemie-Int Ed., 46, 7184 – 7201.

12. Carlos Serrano-Ruiz, J., Dumesic, J.A., (2011). Catalytic routes for the conversion of biomass into liquid hydrocarbon transportation fuels, Energy Environ. Sci., 4, 83.

13. Xiu, S., Shahbazi, A., (2012). Bio-oil production and upgrading research: a review, Renew Sustain Energy Rev., 16, 4406 – 4414.

14. Zhang, Q., Chang, J., Wang, T., Xu, Y., (2007). Review of biomass pyrolysis oil properties and upgrading research, Energy Convers Manag., 48, 87 – 92.

15. Nigam, P.S., Singh, A., (2011). Production of liquid biofuels from renewable resources, Prog Energy Combust Sci., 37, 52 – 68.

16. Fatih, Demirbas.M., (2009). Biorefineries for biofuel upgrading: a critical review, Appl Energy., 86, 151 – 161.

17. Thamsiriroj, T., Murphy, J.D., (2008). Is it better to import palm oil from Thailand to produce biodiesel in Ireland than to produce biodiesel from indigenous Irish rape seed, Appl Energy., 86, 595 – 604.

18. Patil, V., Tran, K.Q., Giselrød, H.R., (2008). Towards sustainable production of biofuels from microalgae, Int J Mol Sci., 9, 1188 – 1195.

19. Lee, C.R., Yoon, J.S., Suh, Y.W., Choi, J.W., Ha, J.M., Suh, D.J., (2012). Catalytic roles of metals and supports on hydrodeoxygenation of lignin monomer guaiacol, Catal Commun., 17, 54 – 58.

20. Mohan, D., Pittman, C.U., Steele, P.H., (2006). Pyrolysis of wood/biomass for bio-oil: a critical review, Energy Fuels., 20, 848 – 889.

21. Dellomonaco, C., Clomburg, J.M., Miller, E.N., Gonzalez, R., (2011). Engineered reversal of the [bgr]-oxidation cycle for the synthesis of fuels and chemicals, Nature., 476, 355 – 359.

22. Zhang, X., Long, J., Kong, W., Zhang, Q., Chen, L., Wang, T., (2014). Catalytic upgrading of bio-oil over Ni-based catalysts supported on mixed oxides, Energy Fuels., 28, 2562 – 2570.

23. Echeandia, S., Pawelec, B., Barrio, V.L., Arias, P.L., Cambra, J.F., Loricera, C.V., (2014). Enhancement of phenol hydrodeoxygenation over Pd catalysts supported on mixed HY zeolite and Al_2O_3. An approach to O-removal from bio-oils, Fuel., 117, 1061 – 1073.

24. Boullosa-Eiras, S., Lødeng, R., Bergem, H., Stöcker, M., Hannevold, L., Blekkan, E.A., (2014). Catalytic hydrodeoxygenation of phenol over supported molybdenum carbide, nitride, phosphide, and oxide catalysts, Catal Today., 223, 44 – 53.

25. Jae, J., Tompsett, G.A., Foster, A.J., Hammond, K.D., Auerbach, S.M., Lobo, R.F., (2011). Investigation into the shape selectivity of zeolite catalysts for biomass conversion, J Catal., 279, 257 – 268.

26. Li, K., Wang, R., Chen, J., (2011). Hydrodeoxygenation of anisole over silica supported Ni_2P, MoP, and NiMoP catalysts, Energy Fuels., 25, 854 – 863.

27. Mortensen, P.M., Grunwaldt, J.D., Jensen, P.A., Knudsen, K.G., Jensen, A.D., (2011). A review of catalytic upgrading of bio-oil to engine fuels, Appl Catal A Gen., 407, 1 – 19.

28. Bridgwater, A.V., (2012). Review of fast pyrolysis of biomass and product upgrading, Biomass and Bioenergy., 38, 68 – 94.

29. Oasmaa, A., Czernik, S., (1999). Fuel oil quality of biomass pyrolysis oils: state of the art for the end users, Energy Fuels., 13, 914 – 921.

30. Solantausta, Y., Oasmaa, A., Sipilä, K., Lindfors, C., Lehto, J., Autio, J., (2012). Bio-oil production from biomass: steps toward demonstration, Energy Fuels., 26, 233 – 240.

31. Cheng, S., Wei, L., Zhao, X., Kadis, E., Cao, Y., Julson, J., (2016). Hydrodeoxygenation of prairie cordgrass bio-oil over Ni-based activated carbon synergistic catalysts combined with different metals, N Biotechnol., 33, 440 – 448.

32. Czernik, S., Bridgwater, A.V., (2004). Overview of applications of biomass fast pyrolysis oil, Energy Fuels., 18, 590 – 598.

33. Khromova, S.A., Smirnov, A.A., Bulavchenko, O.A., Saraev, A.A., Kaichev, V.V., Reshetnikov, S.I., (2014). Anisole hydrodeoxygenation over Ni – Cu bimetallic catalysts: The effect of Ni/Cu ratio on selectivity, Appl Catal A Gen., 470, 261 – 270.

34. Roldugina, E.A., Naranov, E.R., Maximov, A.L., Karakhanov, E.A., (2018). Hydrodeoxygenation of guaiacol as a model compound of bio-oil in methanol over mesoporous noble metal catalysts, Appl Catal A Gen., 553, 24 – 35.

35. Zacher, A., Olarte, M., Santosa, D., (2014). A review and perspective of recent bio-oil hydrotreating research, Green Chem., 16, 491.

36. He, Z., Wang, X., (2012). Hydrodeoxygenation of model compounds and catalytic systems for pyrolysis bio-oils upgrading, Catal Sustain Energy., 1, 28 – 52.

37. Zhang, L., Liu, R., Yin, R., Mei, Y., (2013). Upgrading of bio-oil from biomass fast pyrolysis in China: A review, Renew Sustain Energy Rev., 24, 66 – 72.

38. Ahmad, M.M., Nordin, MFR., Azizan, M.T., (2010). Upgrading of bio-oil into high-value hydrocarbons via hydrodeoxygenation, Department of Chemical Engineering, University Technology PETRONAS, Am J Appl Sci., 7, 746 – 755.

39. Basu, P., (2018). Production of synthetic fuels and chemicals from biomass. In: Biomass Gasification, Pyrolysis, and Torrefaction, 375 – 404.

40. Elliot, D.C., (2007). Historical developments in hydroprocessing bio-oils, Energy Fuels., 21, 1792 – 1815.

41. Wildschut, J., Arentz, J., Rasrendra, C.B., Venderbosch, R.H., Heeres, H.J., (2009). Catalytic hydrotreatment of fast pyrolysis oil: Model studies on reaction pathways for the carbohydrate fraction, Environ Prog Sustain Energy., 28, 450 – 460.

42. Gao, D., Schweitzer, C., Hwang, H.T., Varma, A., (2014). Conversion of guaiacol on noble metal catalysts: Reaction performance and deactivation studies, Ind Eng Chem Res., 53, 18658 – 18667.

43. Bridgwater, A.V., (1996). Production of high grade fuels and chemicals from catalytic pyrolysis of biomass, Catal Today., 29, 285 – 295.

44. Bridgwater, A.V., (1994). Catalysis in thermal biomass conversion, Appl Catal A Gen., 116, 5 – 47.

45. Boucher, M.E., Chaala, A., Pakdel, H., Roy, C., (2000). Bio-oils obtained by vacuum pyrolysis of softwood bark as a liquid fuel for gas turbines. Part II: Stability and ageing of bio-oil and its blends with methanol and a pyrolytic aqueous phase, Biomass and Bioenergy., 19, 351 – 361.

46. Vispute, T.P., Huber, G.W., (2009). Production of hydrogen, alkanes, and polyols by aqueous phase processing of wood-derived pyrolysis oils, Green Chem., 11, 1433 – 1445.

47. Klass, D., (1998). Thermal conversion: Pyrolysis and Liquefaction, Biomass Renew Energy Fuels Chem., 651.

48. Ruddy, D.A., Schaidle, J.A., Ferrell, J.R., Wang, J., Moens, L., Hensley, J.E., (2014). Recent advances in heterogeneous catalysts for bio-oil upgrading via "ex situ catalytic fast pyrolysis": catalyst development through the study of model compounds, Green Chem., 16, 454 – 490.

49. Mu, W., Ben, H., Ragauskas, A., Deng, Y., (2013). Lignin pyrolysis components and upgrading technology review, Bioenergy Res., 6, 1183 – 1204.

50. Zhang, X., Zhang, Q., Wang, T., Ma, L., Yu, Y., Chen, L., (2013). Hydrodeoxygenation of lignin derived phenolic compounds to hydrocarbons over $Ni/SiO_2–ZrO_2$ catalysts, Bioresour Technol., 134, 73 – 80.

51. Maggi, R., Delmon, B., (1993). Characterization of Bio-oils produced by pyrolysis. In: Advances in thermochemical biomass conversion, Springer Netherlands., 1086 – 1094.

52. Hosoya, T., Kawamoto, H., Saka, S., (2009). Solid/liquid and vapor-phase interactions between cellulose and lignin derived pyrolysis products, J Anal Appl Pyrolysis., 85, 237 – 246.

53. Lou, R., Wu, S.Bin., Lv, G.J., (2010). Effect of conditions on fast pyrolysis of bamboo lignin, J Anal Appl Pyrolysis., 89, 191 – 196.

54. Lou, R., Wu, S.Bin., Lv, G.J., Guo, D.L., (2010). Pyrolytic products from rice straw and enzymatic mild acidolysis lignin, Bioresour., 5, 2184 – 2194.

55. Mullen, C.A., Boateng, A.A., (2010). Catalytic pyrolysis GC/MS of lignin from several sources, Fuel Process Technol., 91, 1446 – 1458.

56. Yang, Q., Wu, S., Lou, R., Lv, G., (2010). Analysis of wheat straw lignin by thermogravimetry and pyrolysis gas chromatography/ mass spectrometry, J Anal Appl Pyrolysis., 87, 65 – 69.

57. Fache, M., Boutevin, B., Caillol, S., (2015). Vanillin production from lignin and its use as a renewable chemical, ACS Sustainable Chem Eng., 4, 35 – 46.

58. Guitierrez, A., Kaila, R.K., Honkela, M.L., Slioor, R., Krause, AO.I., (2009). Hydrodeoxygenation of guaiacol on noble metal catalysts, Catal Today., 147, 239 – 246.

59. Furimsky, E., Mikhlin, J.A., Jone, D.Q., Adley, T., Baikowitz, H., (1986). On the mechanism of hydrodeoxygenation of ortho substituted phenols, Can J Chem Eng., 64, 982 – 985.

60. Huuskas, M.K., (1986). Effect of catalyst composition on the hydrogenolysis of anisole, Polyhedron., 5, 233 – 236.

61. Jongerius, A.L., Gosselink, R.W., Dijkstra, J., Bitter, J.H., Bruijnincx, PCA., Weckhuysen, B.M., (2013). Carbon nanofiber supported transition-metal carbide catalysts for the hydrodeoxygenation of guaiacol, ChemCatChem., 5, 2964 – 2972.

62. Cheng, S., Wei, L., Zhao, X., Julson, J., (2016). Application, Deactivation, and Regenration of Heterogeneous Catalysts in bio-oil upgrading, Catalysts., 6, 195.

63. He, L., Qin, Y., Lou, H., Chen, P., (2015). Highly dispersed molybdenum carbide nanoparticles supported on activated carbon as an efficient catalyst for the hydrodeoxygenation of vanillin, RSC Adv., 5, 43141 – 43147.

64. Nie, R., Yang, H., Zhang, H., Yu, X., Lu, X., Zhou, D., (2017). Mild temperature hydrodeoxygenation of vanillin over porous nitrogen-doped carbon black supported nickel nanoparticles, Green Chem., 19, 3126 – 3134.

65. Bu, Q., Lei, H., Zacher, A.H., Wang, L., Ren, S., Liang, J., (2012). A review of catalytic hydrodeoxygenation of lignin derived phenols from biomass pyrolysis, Bioresource Technol., 124, 470 – 477.

66. Elliot, D.C., Hart, T.R., (2009). Catalytic hydroprocessing of chemical models for bio-oil, Energy Fuels., 23, 631 – 637.

67. Bui, V.N., Toussaint, G., Laurenti, D., Mirodatos, C., Geantet, C., (2009). Co-processing of pyrolysis bio-oils and gas oil for new generation of bio-fuels: Hydrodeoxygenation of guaiacol and SRGO mixed feed, Catal Today., 143, 172 – 178.

68. Elliot, D.C., (2015). Biofuel from fast pyrolysis and catalytic hydrodeoxygenation, Curr Opin Chem eng., 9, 59 – 65.

69. Bindwal, A.B., Vaidya, P.D., (2014). Reaction kinetics of vanillin hydrogenation in aqueous solution using a Ru/C catalyst, Energy Fuels., 28, 3357 – 3362.

70. Mahfud, F.H., Ghijsen, F., Heeres, H.J., (2007). Hydrogenation of fast pyrolysis oil and model compounds in a two-phase aqueous organic system using homogeneous ruthenium catalysts, J Mol Catal A Chem., 264, 227 – 236.

71. Huang, F., Li, W., Lu, Q., Zhu, X., (2010). Homogeneous catalytic hydrogenation of bio-oil and related model aldehyde with $RuCl_2(PPh_3)_3$, Chem Eng Technol., 33, 2082 – 2088.

72. Busetto, L., Fabbri, D., Mazzoni, R., Salmi, M., Torri, C., Zanotti, V., (2011). Application of the shvo catalyst in homogeneous hydrogenation of bio-oil obtained from pyrolysis of white poplar: new mild upgrading conditions, Fuel., 90, 1197 – 1207.

73. Shit, S.C., Singuru, R., Pollastri, S., Joseph, B., Rao, B.S., Lingaiah,N., (2018). Cu–Pd bimetallic nanoalloy anchored on a N-rich porous organic polymer for high performance hydrodeoxygenation of biomass-derived vanillin, Catal Sci Technol., 8, 2195 – 2210.

74. Santos, J.L., Alda-Onggar, M., Fedorov, V., Peurla, M., Eränen, K., Mäki-Arvela, P., (2018). Hydrodeoxygenation of vanillin over carbon supported metal catalysts, Appl Catal A Gen., 561, 137 – 149.

75. Sulman, A., Mäki-Arvela, P., Bomont, L., Fedorov, V., Alda-Onggar, M., Smeds, A., (2018). Vanillin hydrodeoxygenation: Kinetic modelling and solvent effect, Catal Letters., 148, 1 – 13.

76. Hao, P., Schwartz, D.K., Medlin, J.W., (2018). Effect of surface hydrophobicity of Pd/Al_2O_3 on vanillin hydrodeoxygenation in a water/oil system, ACS Catal., 8, 11165 – 11173.

77. Statistics | World Total Primary Energy Supply (TPES) by source, available at https://www.iea.org/statistics/ , accessed 16-06-19.

78. BP methodological changes, available at https://www.bp.com/content/dam/bp/business-sites/en/global/corporate/pdfs/energy-economics/statistical-review/bp-stats-review-2018-full-report.pdf , accessed 16-06-19.

79. Rios, E.C.S., Moretti, A.S., Velasco, I.T., Souza, H.P., Abatepaulo, F., Soriano, F., (2011). World energy outlook report, 66, 469 – 476.

80. Duminda, A., Sandun, D., (2013). Methods and applications of deoxygenation for the conversion of biomass to petrochemical products, web of science., 274 – 298.

81. European Commission Renewable Energy Progress Report, (2019). 1 – 16.

82. DECC national renewable energy action plan for the United Kingdom, available at https://assets.publishing.service.gov.uk/goverment/uploads/system/uploads/attachment_data/file/47871/25-nat-ren-energy-action-plan.pdf, accessed 25-11-19.

83. UK risks missing clean energy targets, despite recent renewables growth | Greentech Media, available at https://www.greentechmedia.com/articles/read/uk-risks-mising-clean-energy-targets-despite-recent-renewables-growth, accessed 17-11-19.

84. Snell, R., (2012). Carbon-Carbon bond forming reactions for bio-oil upgrading: heterogeneous catalyst and model compound studies, PhD Thesis. Iowa State University.

85. Alonso, D.M., Bond, J.Q., Dumesic, J.A., (2010). Catalytic conversion of biomass to biofuels, Green Chem., 12, 1493 – 1513.

86. Huber, G.W., Sara, I., Corma, A., (2006). Synthesis of transportation fuels from biomass, Chem Rev., 2, 4044 – 4098.

87. Demirbas, A., (2008). Biofuels sources, biofuel policy, biofuel economy, and global biofuel projections, Energy Convers Manag., 49, 2106 – 2116.

88. Bridgwater, A.V., Meier, D., Radlein, D., (1999). An overview of fast pyrolysis of biomass, Org Geochem., 30, 1479 – 1493.

89. Demirbas, M.F., Balat, M., (2006). Recent advances on the production and utilization trends of biofuels: a global perspective, Energy Convers Manag., 47, 2371 – 2381.

90. Demirbas, A., (2011). Competitive liquid biofuels from biomass, Appl Energy., 88, 17 – 28.

91. Zhou, C.H., Xia, X., Lin, C.X., Tong, D.S., Beltramini, J.,(2011). Catalytic conversion of lignocellulosic biomass to fine chemicals and fuels, Chem Soc Rev., 40, 5588 – 5617.

92. Isikgor, F.H., Remzi, B.C., (2015). Lignocellulosic biomass: a sustainable platform for the production of bio-based chemicals and polymers, Polym Chem., 6, 4497.

93. Wang, H., Male, J., Wang, Y., (2013). Recent advances in hydrotreating of pyrolysis bio-oil and its oxygen-containing model compounds, ACS Catal., 3, 1047 – 1070.

94. Van De, V.S., Geboers, J., Jacobs, P.A., Sels, B.F., (2011). Recent advances in the catalytic conversion of cellulose, ChemCatChem., 3, 82 – 94.

95. Shen, D.K., Gu, S., (2009). The mechanism for thermal decomposition of cellulose and its main products, Bioresour Technol., 100, 6496 – 6504.

96. Detroy, R.W., (2019). Bioconversion of agricultural biomass to organic chemicals, Department of wood and paper science, North Carolina State University.

97. Biomass Feedstocks | Department of Energy, available at https://www.energy.gov/eere/bioenergy/biomass-feedstocks, accessed 20-12-19.

98. Callum, A.S., (2006). Wood Modification: Chemical, thermal, and other processes, 1 – 217.

99. Lignocellulose: A complex biomaterial, available at https://cen.acs.org/articles/86/i49/Lignocellulose-complex-biomaterial.html, accessed 25-01-20.

100. Chakar, F.S., Ragauskas, A.J., (2004). Review of current and future softwood kraft lignin process chemistry, Ind Crops Prod., 20, 131 – 141.

101. Pandey, M.P., Kim, C.S., (2011). Lignin depolymerisation and conversion: a review of thermochemical methods, Chem Eng Technol., 34, 29 – 41.

102. Tijmensen, M.J., Faaij, A.P., Hamelinck, C.N., Van Hardeveld, M.R., (2002). Exploration of the possibilities for production of Fischer Tropsch liquids and power via biomass gasification, Biomass and Bioenergy., 23, 129 – 152.

103. Li, H., Yuan, X., Zeng, G., Tong, J., Yan, Y., Cao, H., (2008). Liquefaction of rice straw in sub and supercritical 1,4-dioxane–water mixture, Fuel Process Technol., 90, 657 – 663.

104. Kleinert, M., Gasson, J.R., Barth, T., (2009). Optimizing solvolysis conditions for integrated depolymerisation and hydrodeoxygenation of lignin to produce liquid biofuel, J Anal Appl Pyrolysis., 85, 108 – 117.

105. Brownsort, P.A., (2009). Biomass pyrolysis processes: review of scope, control, and variability, UK Biochar Research Centre, working paper 5.

106. Duan, J., Han, J., Sun, H., Chen, P., Lou, H., Zheng, X., (2012). Diesel-like hydrocarbons obtained by direct hydrodeoxygenation of sunflower oil over Pd/Al-SBA-15 catlysts, CATCOM., 17, 76 – 80.

107. Bridgwater, A.V., Peacocke, GVC., (1999). Fast pyrolysis processes for biomas, Renew Sustain Energy Rev.,4, 1 – 73.

108. Diebold, J.P., (1999). A review of the chemical and physical mechanisms of the storage stability of fast pyrolysis bio-oils, National Renewable Energy Laboratory (NREL) subcontractor report, Colarado.

109. Elkasabi, Y., Mullen, C.A., Pighinelli, A., Boateng, A.A., (2014). Hydrodeoxygenation of fast pyrolysis bio-oils from various feedstocks using carbon supported catalysts, Fuel Process Technol., 123, 11 – 18.

110. Oasmaa,A., Meier, D., (2005). Norms and standards for fast pyrolysis liquids, J Anal Appl Pyrolysis., 73, 323 – 334.

111. Oasmaa, A., Kuoppala, E., (2003). Fast pyrolysis of forest residue. 3. Storage stability of liquid fuel, Energy Fuels., 17, 1075 – 1084.

112. Venderbosch, R.H., Prins, W., (2010). Fast pyrolysis technology development, Biofuels., 4, 178 – 208.

113. Mullen, C.A., Boateng, A.A., Goldberg, N.M., Lima, I.M., Laird, D.A., Hicks, K.B., (2010). Bio-oil and bio-char production from corn cobs and stover by fast pyrolysis, Biomass and Bioenergy., 34, 67 – 74.

114.Snell, R.,(2012). Carbon-Carbon bond forming reactions for bio-oil upgrading: heterogeneous catalyst and model compound studies, PhD Thesis. Iowa State University.

115. Cheng, S., Wei, L., Zhao, X., Julson, J., (2016). Application, Deactivation, and Regeneration of Heterogeneous Catalysts in Bio-Oil Upgrading, Catalysts., 6, 195.

116. Xiu, S., Shahbazi, A., (2012). Bio-oil production and upgrading research: a review, Renew Sustain Energy Rev., 16, 4406 – 4414.

117. Lødeng, R., Hnnevold, L., Bergem, H., Stöcker, M., (2013). Catalytic hydrotreatment of bio-oils for high quality fuel production, Catal Sustain Prod Bio fuels., 351– 396.

118. Mu, W., Ben, H., Ragauskas, A., Deng, Y., (2013). Lignin pyrolysis components and upgrading technology review, Bioenergy Res., 6, 1183 – 1204.

119. Qin, F., Cui, H., Yi, W., Wang, C., (2014). Upgrading the water soluble fraction of bio-oil by simultaneous esterification and acetalation with online extraction, Energy Fuels., 28, 2544 – 2553.

120. Branca, C., Giudicianni, P., Blasi, C.D., (2003). GC/MS characterization of liquids generated from low temperature pyrolysis of wood , Ind Eng Chem Res., 14, 3190 – 3202.

121. Thangalazhy, G.S., Adhikari, S., Ravindran, H., Gupta, R.B., Fasina, O., Tu, M., (2010). Physicochemical properties of bio-oil produced at various temperatures from pine wood using an auger reactor, Bioresour Technol., 101, 8389 – 8395.

122. Sipila, È .K., Kuoppala, E., Fagerna, ELS., Oasmaa, A., (1998). Characterization of biomass-based flash pyrolysis oils, Biomass and Bioenergy., 14, 103 – 113.

123. Oasmaa, A., Solantausta, Y.O., Arpiainen, V., Knoppala, E., Sipil€, K., (2010). Fast pyrolysis bio-oils from wood and agricultural residues, Energy Fuels., 24, 1380 – 1388.

124. Czernik, S., Johnson, D.K., Black, S., (1994). Stability of wood fast pyrolysis oil, Biomass and Bioenergy., 7, 187 – 192.

125. Ruddy, D.A., Schaidle, J.A., Ferrell, J.R., Wang, J., Moens, L., Hensley, J.E., (2014). Recent advances in heterogeneous catalysts for bio-oil upgrading via "ex situ catalytic fast pyrolysis": catalyst development through the study of model compounds, Green Chem., 16, 454 – 490.

126. Bridgwater, A.V., (2012). Review of fast pyrolysis of biomass and product upgrading, Biomass and Bioenergy., 38, 68 – 94.

127. Ji-lu, Z., (2007). Bio-oil from fast pyrolysis of rice husk: Yields and related properties and improvement of the pyrolysis system, J Anal Appl Pyrolysis., 80, 30 – 35.

128. Guo, X., Wang, S., Wang, Q., Guo, Z., Luo, Z., (2011). Properties of bio-oil from fast pyrolysis of rice husk, Chinese J Chem Eng., 19, 116 – 121.

129. Zacher, A.H., Olarte, M.V., Santosa, D.M., Elliot, D.C., Jones, S.B., (2014). A review and perspective of recent bio-oil hydrotreating research, Green Chem., 16, 491.

130. Mortensen, P.M., Grunwaldt, J.D., Jensen, P.A.,Knudsen, K.G., Jensen, A.D., (2011). A review of catalytic upgrading of bio-oil to engine fuels, Appl Catal A Gen., 407, 1 – 19.

131. Bridgwater, A.V., (1996). Production of high grade fuels and chemicals from catalytic pyrolysis of biomass, Catal Today., 29, 285 – 295.

132. Hoekstra, E., A Hogendoorn, K.J., Wang, X., M Westerhof, R.J., A Kersten, S.R., M Van Swaaij W.P., (2009). Fast pyrolysis of biomass in a fluidized bed reactor: In situ filtering of the vapors, Ind Chem Res., 48, 4744 – 4756.

133. Patwardhan, P.R., Satrio, J.A., Brown, R.C., Shanks, B.H., (2010). Influence of inorganic salts on the primary pyrolysis products of cellulose, Bioresour Technol., 101, 4646 – 4655.

134. Wang, Y., He, T., Liu, K., Wu, J., Fang, Y., (2012). From biomass to advanced bio-fuel by catalytic pyrolysis/hydro-processing: Hydrodeoxygenation of bio-oil derived from biomass catalytic pyrolysis, Bioresour Technol., 108, 280 – 284.

135. Wildschut, J., Iqbal, M., Mahfud, F.H., Cabera, I.M., Venderbosch, R.H., Heeres, H.J., (2010). Insights in the hydrotreatment of fast pyrolysis oil using a ruthenium on carbon catalyst, Energy Environ Sci., 3, 962 – 970.

136. Taarning, E., Osmundsen,C.M., Yang, X., Voss, B., Andersen, S.I., Christensen, C.H., (2011). Zeolite catalyzed biomass conversion to fuels and chemicals, Energy Environ Sci., 4, 793 – 804.

137. De, F., Mercader, M., Groeneveld, M.J., Kersten, S.R.A., Geantet, C., Toussaint, G., (2011). Hydrodeoxygenation of pyrolysis oil fractions: process understanding and quality assessment through co-processing in refinery units, Energy Environ Sci., 4, 985.

138. Li, N., Huber, G.W., (2010). Aqueous-phase hydrodeoxygenation of sorbitol with Pt/SiO$_2$–Al$_2$O$_3$, J Catal., 270, 48 – 59.

139. Chiaramonti, D., Bonini, M., Fratini, E., Tondi, G., Gartner, K., Bridgwater, A.V., (2003). Development of emulsions from biomass pyrolysis liquid and diesel and their use in engines Part 1: emulsion production, Biomass and Bioenergy., 25, 85 – 99.

140. Chiaramonti, D., Bonini, M., Fratini, E., Tondi, G., Gartner, K., Bridgwater, A.V., (2003). Development of emulsions from biomass pyrolysis liquid and diesel and their use in engines Part 2: tests in diesel engines, Biomass and Bioenergy., 25, 101 – 111.

141. Ikura, M., Stanciulescu, M., Hogan, E., (2003). Emulsification of pyrolysis derived bio-oil in diesel fuel, Biomass and Bioenergy., 24, 221 – 232.

142. Stephanidis, S., Nitsos, C., Kalogiannis, K., Iliopoulou, E.F., Lappas, A.A., Triantafy llidis, K.S., (2011). Catalytic upgrading of lignocellulosic biomass pyrolysis vapours: Effect of hydrothermal pre-treatment of biomass, Catal Today., 167, 37 – 45.

143. Pütun, E., Uzin, B.B., Pütun, A.E., (2009). Rapid pyrolysis of olive residue: effect of catalytic upgrading of pyrolysis vapors in a two-stage fixed bed reactor, Energy Fuels., 23, 2248 – 2258.

144. Peng, J., Chen, P., Lou, H., Zheng, X., (2009). Catalytic upgrading of bio-oil by HZSM-5 in sub and supercritical ethanol, Bioresour Technol., 100, 3415 – 3418.

145. Vitolo, S., Seggiani, M., Frediani, P., Ambrosini, G., Politi, L., (1999). Catalytic upgrading of pyrolytic oils to fuel over different zeolites, Fuel., 78, 1147 – 1159.

146. Samolada, M.C., Baldauf, W., Vasalos, I.A., (1998). Production of a bio-gasoline by upgrading biomass flash pyrolysis liquids via hydrogen processing and catalytic cracking, Fuel., 77, 1667 – 1675.

147. Furimsky, E., (2000). Catalytic hydrodeoxygenation, Appl Catal A Gen., 199, 147 – 190.

148. Adjaye, J.D., Bakhshi, N.N., (1995). Production of hydrocarbons by catalytic upgrading of a fast pyrolysis bio-oil Part 1: Conversion over various catalysts, Fuel Processing Technol., 45, 161 – 183.

149. Wang, Y., Fang, Y., He, T., Hu, H., Wu, J., (2011). Hydrodeoxygenation of dibenzofuran over noble metal supported on mesoporous zeolite, CATCOM., 12, 1201 – 1205.

150. Gayubo, A.G., Aguayo, A.T., Atutxa, A., Aguado, R., Bilbao, J., (2004). Transformation of oxygenate components of biomass pyrolysis oil on a HZSM-5 Zeolite: Alcohols and Phenols, Ind Eng Chem Res., 43, 2610 – 2618.

151. Zhu, X., Mallinson, R.G., Resasco, D.E., (2010). Role of transalkylation reactions in the conversion of anisole over HZSM-5, Appl Catal A Gen., 379, 172 – 181.

152. Chantal, P.D., Kaliaguine, S., Grandmaison, J.L., (1985). Reactions of phenolic compounds over HZSM-5, Appl Catal., 18, 133 – 145.

153. Elliot, D.C., Beckman, D., Bridgwater, A.V., Diebold, J.P., Gevert, S.B., Solantausta, Y., (1991). Developments in direct thermochemical liquefaction of biomass, Energy Fuels., 5, 399 – 410.

154. Luo, Y., Guda, V.K., Hassan, E.B., Steele, P.H., Mitchell, B., Yu, F., (2016). Hydrodeoxygenation of oxidised distilled bio-oil for the production of gasoline fuel type, Energy Convers Manag., 112, 319 – 327.

155. He, Z., Wang, X., (2012). Hydrodeoxygenation of model compounds and catalytic systems for pyrolysis bio-oils upgrading, Catal Sustain Energy., 1, 28 – 52.

156. Elliot, D.C., Todd, R.H., Neuenschwander, G.G., Rotness, L.J., Zacher, A.H., (2009). Catalytic hydroprocessing of biomass fast pyrolysis bio-oil to produce hydrocarbon products, Environ Prog Sustain Energy., 28, 1 – 10.

157. Mahfud, F.H., (1975). Exploratory studies on fast pyrolysis oil upgrading, PhD Thesis. University of Groningen.

158. Högskolan, T., Lke Şenol, O. A B., Teknillinen, K., (2007). Hydrodeoxygenation of aliphatic and aromatic oxygenates on sulphided catalysts for production of second generation biofuels, PhD Thesis. Helsinki University of Technology.

159. Venderbosch, R.H., Ardiyanti, A.R., Wildschut, J., Oasmaa, A., Heeres, H.J., (2010). Stabilization of biomass derived pyrolysis oils, J Chem Technol Biotechnol., 85, 674 – 686.

160. Bindwal, A.B., Vaidya, P.D., (2014). Reaction kinetics of vanillin hydrogenation in aqueous solutions using a Ru/C catalyst, Energy Fuels., 28, 3357 – 3362.

161. Jiang, G., Nowakowski, D.J., Bridgwater, A.V., (2010). Effect of the temperature on the composition of lignin pyrolysis products, Energy Fuels., 24, 4470 – 4475.

162. Bocchini, P., Galletti, G.C., Camarero, S., Martinez, A.T., (1997). Absolute quantitation of lignin pyrolysis products using an internal standard, J Chromatogr., 773, 227 – 232.

163. Greenwood, P.F., van Heemst, J.D.H., Guthrie, E.A., Hatcher, P.G., (2002). Laser micropyrolysis GC–MS of lignin, J Anal Appl Pyrolysis., 62, 365 – 373.

164. Ingram, L., Mohan, D., Bricka, M., Steele, P., Strobel, D., Crocker, D., (2008). Pyrolysis of wood and bark in an auger reactor: physical properties and chemical analysis of the produced bio-oils, Energy Fuels., 22, 614 – 625.

165. Jegers, H.E., Klein, M.T., (1985). Primary and secondary lignin pyrolysis reaction pathways, Ind Eng Chem Process Des Dev., 24, 173 – 183.

166. Nowakowski, D.J., Bridgwater, A.V., Elliot, D.C., Meier, D., De Wild, P., (2010). Lignin fast pyrolysis: results from an international collaboration, J Anal Appl pyrolysis., 88, 53 – 72.

167. Scholze, B., Meier, D., (2001). Characterization of the water insoluble fraction from pyrolysis oil (pyrolytic lignin). Part I. PY GC/MS FTIR and functional groups, J Anal Appl pyrolysis., 60, 41 – 54.

168. Popov, A., Kondratieva, E., Goupil, J.M., Mariey, L., Bazin, P., Gilson, J.P., (2010). Bio-oils hydrodeoxygenation: adsorption of phenolic molecules on oxidic catalyst supports, J Phys Chem C., 114, 15661 – 15670.

169. Silva, E.A., Zabkova, M., Araújo, J.D., Cateto, C.A., Barreiro, M.F., Belgacem, M.N., (2009). An integrated process to produce vanillin and lignin based polyurethanes from kraft lignin, Chem Eng Res Des., 87, 1276 – 1292.

170. Holladay, J.E., Bozell, J.J., White, J.F., Johnson, D., (2007). Top value added chemicals from biomass. Volume II: Results of screening for potential candidates from biorefinery lignin.

171. Following many routes to naturally derived vanillin | chemical and engineering news, available at https://cen.acs.org/articles/92/i6/following-routes-naturally-derived-vanillin.html, accessed 30-01-20.

172. Yang, X., Liang, Y., Zhao, X., Song, Y., Hu, L., Wang, X., (2014). Au/CNTs catalyst for highly selective hydrodeoxygenation of vanillin at the water/oil interface, RSC Adv., 4, 31932 – 31936.

173. Jiang, H., Yu, X., Peng, X., Zhang, H., Nie, R., Lu, X., (2016). Efficient aqueous hydrodeoxygenation of vanillin over a mesoporous carbon nitride modified Pd nanocatalyst, RSC Adv., 6, 69045 – 69051.

174. Zhang, X., Tang, W., Zhang, Q., Wang, T., Ma, L., (2017). Hydrocarbons production from lignin derived phenolic compounds over Ni/SiO$_2$ catalyst, Energy Procedia., 105, 518 – 523.

175. Jongerius, A.L., Jastrzebski, R., Bruijnincx, P.C.A., Weckhuysen, B.M., (2012). CoMo sulfide catalyzed hydrodeoxygenation of lignin model compounds: an extended reaction network for the conversion of monomeric and dimeric substrates, J Catal., 285, 315 – 323.

176. Mahfud, F.H., Bussemaker, S., Kooi, B.J., Ten Brink, G.H., Heeres, H.J., (2007). The application of water soluble ruthenium catalysts for the hydrogenation of the dichloromethane soluble fraction of fast pyrolysis oil and related model compounds in a two phase aqueous organic system, J Mol Catal A Chem.,277, 127 – 136.

177. Yang, H., Nie, R., Xia, W., Yu, X., Jin, D., Lu, X., (2017). Co embedded within biomass derived mesoporous N-doped carbon as an acid resistant and chemoselective catalyst for transfer hydrodeoxygenation of biomass with formic acid, Green Chem., 19, 5714 – 5722.

178. Zhu, Z., Tan, H., Wang, J., Yu, S., Zhou, K., (2014). Hydrodeoxygenation of vanillin as a bio-oil model over carbonaceous microspheres supported Pd catalysts in the aqueous phase and pickering emulsions, Green Chem., 16, 2636 – 2643.

179. Yang, X., Liang, Y., Cheng, Y., Song, W., Wang, X., Wang, Z., (2014). Hydrodeoxygenation of vanillin over carbon nanotube supported Ru catalysts assembled at the interfaces of emulsion droplets, CATCOM, 47, 28 – 31.

180. Mukherjee, D., Singuru, R., Venkataswamy, P., Damma, D., Reddy, B.M., (2019). Ceria promoted Cu –Ni/SiO$_2$ catalyst for selective hydrodeoxygenation of vanillin, ACS Omega., 4, 4770 – 4778.

181. Shit, S.C., Koley, P., Joseph, B., Marini, C., Nakka, L., Tardio, J., (2019). Porous organic polymer driven evolution of high performance cobalt phosphide hybrid nanosheets as vanillin hydrodeoxygenation catalyst, ACS Appl Mater Interfaces., 11, 24140 – 24153.

182. Dyson, P.J., Jessop, P.G., (2016). Solvent effects in catalysis: rational improvements of catalysts via manipulation of solvent interactions, Catal Sci Technol., 6, 3302 – 2216.

183. Augustine, R.L., (1976). The stereochemistry of hydrogenation of α,β-unsaturated ketones, Adv Catal., 25, 56 – 80.

184. Blaser, H.U., Jalett, H.P., Wiehl, J., (1991). Enantioselective hydrogenation of α-ketoesters with cinchona-modified platinum catalysts: effect of acidic and basic solvents and additives, J Mol Catal., 68, 215 – 222.

185. Wehrli, J.T., Baiker, A., Monti, D.M., Blaser, H.U., Jalett, H.P., (1989). Enantioselective hydrogenation of α-ketoesters: influence of reaction medium and conversion, J Mol Catal., 245 – 257.

186. Gilbert, L., Mercier, C., (1993). Solvent effects in heterogeneous catalysis: application to the synthesis of fine chemicals, Stud Surf Sci Catal., 78, 51 – 66.

187. Koopman, P.G.J., Buurmans, H.M.A., Kieboom, A.P.G., van Bekkum, H., (2010). Solvent reactant support interactions in liquid phase hydrogenation, Recl des Trav Chim des Pays Bas., 100, 156 – 161.

188. Augustine, R.L., Techasauvapak, P., (1994). Heterogenous catalysis in organic synthesis. Part 9: specific site solvent effects in catalytic hydrogenation, J Mol Catal., 87, 95 – 105.

189. He, J., Zhao, C., Lercher, J.A., (2014). Impact of solvent for individual steps of phenol hydrodeoxygenation with Pd/C and HZSM-5 as catalysts, J Catal., 309, 362 – 375.

190. Dumesic, J.A., Huber, G.W., Boudart, M., (2014). Principles of heterogeneous catalysis, chemical engineering: catalyst science and technology NPTEL, 1 – 15.

191. Furimsky, E.,(1983). Chemistry of catalytic hydrodeoxygenation, Catal Rev., 25, 421 – 458.

192. Speight, J., Topsoe, H., Clausen, B.S., Massoth, F.E., (1996). A review of hydrotreating catalysis science and technology, Fuel Sci Technol Int., 14, 1465.

193. Laurent, E., Delmon, B., (1994). A study of the hydrodeoxygenation of carbonyl, carboxylic and guaiacyl groups over sulfided CoMo/Al₂O₃ and NiMo/Al₂O₃ catalysts I: Catalytic reaction schemes, Appl Catal A Gen., 109, 77 – 96.

194. Viljava, T.R., Komulainen, R.S., Krause, A.O.I., (2000). Effect of H2S on the stability of CoMo/Al₂O₃ catalyst during hydrodeoxygenation, Catal Today., 60, 83 – 92.

195. Furimsky, E., Massoth, F.E., (1999). Deactivation of hydroprocessing catalysts, Catal Today., 52, 381 – 495.

196. Laurent, E., Delmon, B., (1994). Influence of water in the deactivation of a sulfided NiMo γ-Al₂O₃ catalyst during hydrodeoxygenation, J Catal., 146, 281 – 291.

197. Centeno, A., Laurent, E., Delmon, B., (1995). Influence of the support of CoMo sulfide catalysts and of the addition of potassium and platinum on the catalytic performances for the hydrodeoxygenation of carbonyl, carboxyl, and guaiacol type molecules, J Catal., 154, 288 – 298.

198. Tang, T., Yin, C., Wang, Li., Ji, Y., Xaio, F.S., (2007). Superior performance in deep saturation of bulky aromatic pyrene over acidic mesoporous Beta zeolite supported palladium catalyst, J Catal., 249, 111 – 115.

199. Niquille-Rothlisberger, A., Prins, R., (2006). Hydrodesulfurization of 4,6-dimethyldibenzothiophene and dibenzothiophene over alumina-supported Pt, Pd, and Pt–Pd catalysts, J Catal., 242, 207 – 216.

200. Wildschut, J., Mahfud, F.H., Venderbosch, R.H., Heeres, H.J., Hydrotreatment of fast pyrolysis oil using heterogeneeous noble metal catalysts, Ind Eng Chem Res., 48, 10324 – 10334.

201. Ardiyanti, A.R., Gutierrez, A., Honkela, M.L., Krause, A.O.L., Heeres, H.J., (2011). Hydrotreatment of wood based pyrolysis oil using zirconia supported mono- and bimetallic (Pt, Pd, Rh) catalysts, Appl Catal A Gen., 407, 56 – 66.

202. Mendes, M.J., Santos, O.A.A., Jordao, E., Silva, A.M., (2001). Hydrogenation of oleic acid over ruthenium catalysts, Appl Catal A Gen., 217, 253 – 262.

203. Pestman, R., Koster, R.M., Pieterse, J.A.Z., Ponec, V., (1997). Reactions of carboxylic acids on oxides: 1. Selective hydrogenation of acetic acid to acetaldehyde, J Catal., 168, 255 – 264.

204. Mars, P., van Krevelen, D.W., (1954). Oxidations carried out by means of vanadium oxide catalysts, Chem Eng Sci., 3, 41 – 59.

205. Figueiredo, J.L., Pereira, M.F.R., (2010). The role of surface chemistry in catalysis with carbons, Catal Today., 150, 2 – 7.

206. Ardiyanti, A.R., Khromova, S.A., Venderbosch, R.H., Yakovlev, V.A., Melián-Cabrera, I.V., Heeres, H.J., (2012). Catalytic hydrotreatment of fast pyrolysis oil using bimetallic Ni–Cu catalysts on various supports, Appl Catal A Gen., 449, 121 – 130.

207. Leng, S., Wang, X., He, X., Liu, L., Liu, Y., Zhong, X., (2013). NiFe/γ-Al2O3: A universal catalyst for the hydrodeoxygenation of bio-oil and its model compounds, CATCOM., 41, 34 – 37.

208. Robinson, A.M., Hensley, J.E., Will Medlin, J., (2016). Solvent effects in catalysis: rational improvements of catalysts via manipulation of solvent interactions, Catal Sci Technol., 6, 3302.

209. Nowicka, E., Sankar, M., (2018). Designing Pd-based supported bimetallic catalysts for environmental application, Univ-Sci A (Appl Phys & Eng)., 19, 5 – 20.

210. Prins, R., Bussell, M.E., (2012). Metal phosphides: preparation, characterization, and catalytic reactivity, Catal letters., 142, 1413 – 1436.

211. Whiffen, V.M.L., Smith, K.J., (2010). Hydrodeoxygenation of 4-methylphenol over unsupported MoP, MoS2, and MoO catalysts, Energy Fuels., 24, 4728 – 4737.

212. Zhao, H.Y., Li, D., Bui, P., Oyama, S.T., (2011). Hydrodeoxygenation of guaiacol as model compound for pyrolysis oil on transition metal phospide hydroprocessing catalysts, Appl Catal A Gen., 391, 305 – 310.

213. Si, Z., Zhang, X., Wang, C., Ma, L., Dong, R., (2017). An overview on catalytic hydrodeoxygenation of pyrolysis oil and its model compounds, Catalysts., 7, 169.

214. Lee, W.S., Wang, Z., Wu, R.J., Bhan, A., (2014). Selective vapor-phase hydrodeoxygenation of anisole to benzene on molybdenum carbide catalysts, J Catal., 319, 44 – 53.

215. Lu, Q., Chen, C.J., Luc, W., Chen, J.G., Bhan, A., Jiao, F., (2016). Ordered mesoporous metal carbides with enhanced anisole hydrodeoxygenation selectivity, ACS Catal., 6, 3506 – 3514.

216. Wang, W., Yang, Y., Luo, H., Liu, W., (2010). Characterization and hydrodeoxygenation properties of Co promoted Ni–Mo–B amorphous catalysts: influence of Co content, React Kinet Mech Catal., 101, 105 – 115.

217. Wang, W., Yang, Y., Luo, H., Hu, T., Lin, W., (2011). Amorpohous Co–Mo–B catalyst with high activity for the hydrodeoxygenation of bio-oil, CATCOM., 12, 436 – 440.

218. Gao, D., Schweitzer, C., Hwang, H.T., Varma, A., (2014). Conversion of guaiacol on noble metal catalysts: reaction performance and deactivation studies, Ind Eng Chem Res., 53, 18658 – 18667.

219. Lee, H., Kim, Y.M., Lee, I.G., Jeon, J.K., Jung, S.C., Chung, J.D., (2016). Recent advances in the catalytic hydrodeoxygenation of bio-oil, Korean J Chem Eng., 33, 3299 – 3315.

220. Iino, A., Cho, A., Takagaki, A., Kikuchi, R., Ted, O.S., (2014). Kinetic studies of hydrodeoxygenation of 2-methyltetrahydrofuran on a Ni2P/SiO2 catalyst at medium pressure, J Catal., 311, 17 – 27.

221. Bindwal, A.B., Vaidya, P.D., (2013). Kinetics of aqueous-phase hydrogenation of levoglucosan over Ru/C catalyst, Ind Eng Chem Res., 52, 17781 – 17789.

222. Nie, L., Resasco, D.E., (2014). Kinetics and mechanism of m-cresol hydrodeoxygenation on a Pt/SiO2 catalyst, J Catal., 317, 22 – 29.

223. Chen, Y., Miller, D.J., Jackson, J.E., (2007). Kinetics of aqueous-phase hydrogenation of organic acids and their mixtures over carbon supported ruthenium catalyst, Ind Eng Chem Res., 46, 3334 – 3340.

224. Zhou, L., Lawal, A., (2017). Kinetic study of hydrodeoxygenation of palmitic acid as a model compound for microalgaeover Pt / γ -Al$_2$O$_3$, Appl Catal A Gen., 532, 40 – 49.

225. Jain, A.B., Vaidya, P.D., (2015). Kinetics of aqueous-phase hydrogenation of model bio-oil compounds over a Ru/C catalyst, Energy Fuels., 29, 361 – 368.

226. Bykova, M.V., Zavarukhin, S.G., Trusov, L.I., Yakovlev, V.A., (2013). Guaiacol hydrodeoxygenation kinetics with catalyst deactivation taken into consideration, Kinet Catal., 54, 40 – 48.

227. Sheu, Y.H.E., Anthony, R.G., Soltes, E.J., (1988). Kinetic studies of upgrading pine pyrolytic oil by hydrotreatment, Fuel Process Technol., 19, 31 – 50.

228. Su-Ping, Z., (2003). Study of hydrodeoxygenation of bio-oil from the fast pyrolysis of biomass, Energy sources., 25, 57 – 65.

229. Zhang, S., Yan, Y., Li, T., Ren, Z., (2009). Lumping kinetic model for hydrotreating of bio-oil from the fast pyrolysis of biomass, Energy sources, 31, 639 – 645.

230. Ardiyanti, A.R., Khromova, S.A., Venderbosch, R.H., Yakovlev, V.A., Heeres, H.J., (2012). Catalytic hydrotreatment of fast pyrolysis oil using non sulfided bimetallic Ni–Cu catalysts on a δ-Al_2O_3 support, Appl Catal B Environ., 117, 105 – 117.

231. Gamliel, D.P., Karakalos, S., Valla, J.A., (2018). Liquid phase hydrodeoxygenation of anisole, 4-ethylphenol, and benzofuran using Ni, Ru, and Pd supported on USY zeolite, Appl Catal A Gen., 559, 20 – 29.

232. Wan, H., Vitter, A., Chaudhari, R.V., Subramaniam, B., (2014). Kinetic investigations of unusual solvent effects during Ru/C catalyzed hydrogenation of model oxygenates, J Catal., 309, 174 – 184.

233. Athreya, S., Venkatesh, Y.D., (2012). Application of Taguchi method for optimization of process parameters in improving the surface roughness of lathe facing operation, Int Ref J Eng Sci., 1, 13 – 19.

234. Fisk, C.A., Morgan, T., Ji, Y., Crocker, M., Crofcheck, C., Lewis, S.A., (2009). Bio-oil upgrading over platinum catalysts using in situ generated hydrogen, Appl Catal A Gen., 358, 150 – 156.

235. Thommes, M., Kaneko, K., Neimark, A.V., Olivier, J.P., Rodriguez-Reinoso, F., Rouquerol, J., (2015). Phsysisorption of gases with special reference to the evaluation of surface area and pore size distribution (IUPAC Technical Report), Pure Appl Chem., 87, 1051 – 1069.

236. Hart, A., (2014). Advanced studies of catalytic upgrading of heavy oils, PhD Thesis. University of Birmingham, UK.

237. Paul, A.W., (2001). An introduction to the physical characterization of materials by mercury intrusion porosimetry with emphasis on reduction and presentation of experimental data, 1 – 23.

238. Westermack, S., (2000). Use of mercury porosimetry and nitrogen adsorption in characterization of the pore structure of mannitol and microcrystalline cellulose powders, granules, and tablets, PhD Thesis. University of Helsinki, Finland.

239. Lu, M., Du, H., Wei, B., Zhu, J., Li, M., Shan, Y., (2017). Catalytic hydrodeoxygenation of guaiacol over palladium catalyst on different titania supports, Energy Fuels., 31, 10858 – 10865.

240. Diao, X., Ji, N., Zheng, M., Liu, Q., Song, C., Huang, Y., (2018). MgFe hydrotalcites derived layered structure iron molybdenum sulfide catalysts for eugenol hydrodeoxygenation to produce phenolic chemicals, J Energy Chem., 27, 600 – 610.

241. Lin, Y.C., Li, C.L., Wan, H.P., Lee, H.T., Liu, C.F., (2011). Catalytic hydrodeoxygenation of guaiacol on Rh-based and sulfided CoMo and NiMo catalysts, Energy Fuels., 25, 890 – 896.

242. De, M., (2014). Lecture 5 solid catalysts. NPTEL Chem Eng Catal Sci Technol Lect., 1 – 53.

243. Bruker advanced x-ray solutions: Introduction to x-ray fluorescence, guide to XRF basics, Bruker AXS GmbH, (2006).

244. Ida, H., (2005). X-ray fluorescence analysis with portable instruments, Japan Anal., 54, 1021 – 1022.

245. Utpalendu, K., (2013). Measurement and interpretation of porosity and pore size distribution in mudrocks the hole story of shales, PhD Thesis. Colarado School of Mines.

246. Wacharasindhu, S., Likitmaskul, S., Punnakanta, L., Chaichanwatanakul, K., Angsusingha, K., Tuchinda, C., (1985). Reporting physisorption data for gas/solid systems with special reference to the determination of surface area and porosity, Pure Appl Chem., 57, 603 – 619.

247. Liu, J., Huang, F., Liao, X., Shi, B., (2013). Synthesis of thermally stable mesoporous alumina by using bayberry tannin as template in aqueous system, Bull Korean Chem Soc., 34, 2650 – 2656.

248. Gobora, H.M., Mohamed, R.S., Khalil, F.H., El-Shall, M.S., Hassan, S.A., (2014). Various characteristics of Ni and Pt/Al_2O_3 nanocatalysts prepared by microwave method to be applied in some petrochemical processes, Egypt J Pet., 23, 105 – 118.

249. Rouquerol, J., Llewellyn, P., Rouquerol, F., (2007). Is the BET equation applicable to microporous adsorbents, Stud Surf Sci Catal., 160, 49 – 56.

250. Strem A., (2017). Information on heterogeneous catalyst from strem chemicals manual.

251. Lowell, S., Shields, J.E., Thomas, M.A., Thommes, M.,(2004). Characterization of porous solids and powders: surface area, pore size, and density, Kluwer Academic., 42, 5288.

252. Gao, D., Xiao, Y., Varma, A., (2015). Guaiacol hydrodeoxygenation over platinum catalyst: reaction pathways and kinetics, Ind Eng Chem Res., 54, 10638 – 10644.

253. Dai, C., Li, Y., Ning, C., Zhang, W., Wang, X., Zhang, C., (2017). The influence of alumina phases on the performance of Pd/Al_2O_3 catalyst in selective hydrogenation of benzonitrile to benzylamine, Appl Catal A Gen., 545, 97 – 103.

254. Persson, K., Pfefferle, L.D., Schwartz, W., Ersson, A., Järås, S.G., (2007). Stability of palladium-based catalysts during catalytic combustion of methane: the influence of water, Appl Catal B Environ., 74, 242 – 250.

255. Narayan, R., Nayak, U.Y., Raichur, A.M., Garg, S., (2018). Mesoporous silica nanoparticles: a comprehensive review ons synthesis and recent advances, Pharmaceutics., 10, 1 – 50.

256. He, Z., Wang, X., (2014). Highly selective catalytic hydrodeoxygenation of guaiacol to cyclohexane over Pt/TiO_2 and $NiMo/Al_2O_3$ catalysts, Front Chem Sci Eng., 8, 369 – 377.

257. Bond, G.C., (1975). Small particles of the platinum metals, Platin Met Rev., 19, 126 – 134.

258. Gharibshahi, E., Saion, E., (2012). Influence of dose on particle size and optical properties of colloidal platinum nanoparticles, Int J Mol Sci., 13, 14723 – 14741.

259. Khdary, N.H., Ghanem, M.A., (2014). Highly dispersed platinum nanoparticles supported on silica as catalyst for hydrogen production, RSC Adv., 4, 50114 – 50122.

260. Viet, T.T., Lee, J.H., Ma, F., Kim, G.R., Ahn, I.S., Lee, C.H., (2013). Hydrocracking of petroleum vacuum residue with activated carbon and metal additives in a supercritical m-xylene solvent, Fuel., 103, 553 – 561.

261. Viet, T.T., Lee, J.H., Ryu, J.W., Ahn, I.S., Lee, C.H., (2012). Hydrocracking of vacuum residue with activated carbon in supercritical hydrocarbon solvents, Fuel., 94, 556 – 562.

262. Dockner,T., (1988). Reduction and hydrogenation with the system hydrocarbon/carbon: New synthetic methods, Angew Chemie Int Ed., 27, 679 –682.

263. Lan, L., Liu, Y., Liu, S., Ma, X., Li, X., Dong, Z., (2019). Effect of the supports on catalytic activity of Pd catalysts for liquid phase hydrodechlorination/ hydrogenation reaction, Environ Technol., 40, 1615 – 1623.

264. Deepa, A.K., Dhepe, P.L., (2014). Function of metals and supports on the hydrodeoxygenation of phenolic compounds, Chempluschem., 79, 1573 – 1583.

265. Skoplyak, O., Barteau, M.A., Chen, J.G., (2009). Comparison of H_2 production from ethanol and ethylene glycol on M/Pt(111) (M = Ni, Fe, Ti)bimetallic surfaces, Catal Today., 147, 150 – 157.

266. Do, P.T.M., Foster, A.J., Chen, J., Lobo, R.F., (2012). Bimetallic effects in the hydrodeoxygenation of meta cresol on γ-Al_2O_3 supported Pt–Ni and Pt–Co catalysts, Green Chem., 14, 1388 – 1397.

267. Resende, K.A., Teles, C.A., Jacobs, G., Davis, B.H., Cronauer, D.C., Jeremy, K.A., (2018). Hydrodeoxygenation of phenol over zirconia supported Pd bimetallic catalysts: The effect of second metal on catalyst performance, Appl Catal B Environ., 232, 213 – 231.

268. Iwasa, N., Takizawa, M., Arai, M., (2005). Palladium based alloy and monometallic catalysts for gas phase hydrogenation of crotonaldelyde: Effects of alloying and alloy crystallite size, Appl Catal A Gen., 283, 255 – 263.

269. Reichardt, C., (1984). Solvent effects in organic chemistry, 21 – 40.

270. Kosower, E.M., (1958). The effect of solvent on spectra III. The use of Z-values in connection with kinetic data, J Am Chem Soc., 80, 3267 – 3270.

271. Zhang, X., Long, J., Kong, W., Zhang, Q., Chen, L., Wang, T., (2014). Catalytic upgrading of bio-oil over Ni-based catalysts supported on mixed oxides, Energy Fuels., 28, 2562 – 2570.

272. McManus, I., Daly, H., Thompson, J.M., Connor, E., Hardacre, C., Wilkinson, S.K., (2015). Effect of solvent on the hydrogenation of 4-phenyl-2-butanone over Pt based catalysts, J Catal., 330, 344 – 353.

273. Young, C.L., (1981). IUPAC solubility data series: hydrogen and deuterium, IUPAC solubility data series: hydrogen and deuterium, 5.

274. Akpa, B.S., D'agostino, C., Gladden, L.F., Hindle, K., Manyar, H., Mcgregor, J., (2012). Solvent effects in the hydrogenation of 2-butanone, J Catal., 289, 30 – 41.

275. Wilkinson, S.K., McManus, I., Daly, H., Thompson, J.M., Hardacre, C., Sedaie Bonab, N., (2015). A kinetic analysis methodology to elucidate the roles of metal, support, and solvent for the hydrogenation of 4-phenyl-2-butanone over Pt/TiO$_2$, J Catal., 330, 362 – 373.

276. Al-Marshed, A., Hart, A., Leeke, G., Greeves, M., Wood, J., (2015). Optimization of heavy oil upgrading using dispersed nanoparticles iron oxide as a catalyst, Energy Fuels., 29, 6306 – 6316.

277. Perego, C., (2002). Experimental methods in catalytic kinetics, Catal Today., 52, 133 – 145.

278. Boullosa-Eiras, S., Lødeng, R., Bergem, H., Stöcker, M., Hannevold, L., Blekkan, E.A., (2014). Catalytic hydrodeoxygenation (HDO) of phenol over supported molybdenum carbide, nitride, phosphide, and oxide catalysts, Catal Today., 223, 44 – 53.

279. Wildschut, J., Melián-Cabrera, I., Heeres, H.J., (2010). Catalyst studies on the hydrotreatment of fast pyrolysis oil, Appl Catal B Environ., 99, 298 – 306.

280. Santos, J.L., Maki-Arvela, P., Warna, J., Monzon, A., Centeno, M.A., (2019). Hydrodeoxygenation of vanillin over noble metal catalyst supported on biochars:Part II: Catalytic behaviour, Appl Catal B Environ., 118425 – 118500.

281. Wijayasekara, D.B., (2007). Minimum agitation speed for solid suspension and mixing time in a torispherical bottomed pharmaceutical stirred tank under different baffling conditions, MSc Thesis. New Jersey Science and Technology University.

282. Zhang, Z., Jackson, J.E., Miller, D.J., (2002). Kinetics of aqueous phase hydrogenation of lactic acid to propylene glycol, Ind Eng Chem Res., 41, 691 – 696.

283. Kuusisto, J., Mikkola, J.P., Sparv, M., Warna, J., Karhu, H., Salmi, T., (2008). Kinetics of the catalytic hydrogenation of d-lactose on a carbon supported ruthenium catalyst, Chem Eng J., 139, 69 – 77.

284. Singh, U.K., Vannice, M.A., Kinetics of liquid phase hydrogenation reactions over supported metal catalysts: A review, Appl Catal A Gen ., 213, 1 – 24.

285. Maccarrone, M.J., Torres, G.C., Lederhos, C., Betti, C., Badano, J.M., Quiroga, M., (2012). Kinetic study of the partial hydrogenation of 1-heptyne over Ni and Pd supported on alumina, Intech., 159 – 184.

286. C.R.W, P.C., (1955). Correlation of diffusion coefficients in dilute solutions, AIChE J., 1, 264 – 270.

287. Pintar, A., Berčič, G., Levec, J., (1998). Catalytic liquid phase nitrite reduction: kinetics and catalyst deactivation, AIChE J., 44, 2280 – 2292.

288. Perego,C., (2002). Experimental methods in catalytic kinetics, Catal Today., 52, 133 – 145.

289. Crezee, E., Hoffer, B.W., Berger, R.J., Makkee, M., Kapteijn, F., Moulijn, J.A., (2003). Appl Catal A Gen., 251, 1 – 17.

290. D6champ, N., Gamez, A., Perrard, A., Gallezot, P., (1995). Kinetics of glucose hydrogenation in a trickle bed reactor, Catal Today., 24, 29.

291. De Bellefon, C., Tanchoux, N., Caravieilhes, S., (1998). New reactors and methods for the investigation of homogeneous catalysis, Journal of organometallic chemistry., 567, 143.

292. Rachmady, W., Vannice, M.A., (2000). Acetic acid hydrogenation over supported platinum catalysts, J Catal., 192, 322 – 334.

293. Mukherjee, S., Vannice, M.A., (2006). Solvent effects in liquid phase reactions. I. Activity and selectivity during citral hydrogenation on Pt/SiO_2 and evaluation of mass transfer effects, J Catal., 243, 108 – 130.

294. Mukherjee, S., Vannice, M.A., (2006). Solvent effects in liquid phase reactions. II. Kinetic modeling for citral hydrogenation, J Catal., 243, 131 – 148.

295. Hu, B., Fishwick, R.P., Pacek, A.W., Winterbottom, J.M., Wood, J., Stitt, E.H., (2007). Simultaneous measurement of in situ bubble size and reaction rates with a heterogeneous catalytic hydrogenation reaction, Chem Eng Sci., 62, 5392 – 5396.

296. Nitta, Y., Kubota, T., Okamoto, Y., (2004). Solvent effect on the structure sensitivity in enantioselective hydrogenation of α, β-unsaturated acids with modified palladium catalysts, J Mol Catal A Chem., 212, 155 – 159.

297. Toukoniitty, E., Mäiki-Arvela, P., Kuusisto, J., Nieminen, V., Päivärinta, J., Hotokka, M., (2003). Solvent effects in enantioselective hydrogenation of 1-phenyl-1,2-propanedione, J Mol Catal A Chem., 192, 135 – 151.

298. Masson, J., Cividino, P., Court, J., (1997). Selective hydrogenation of acetophenone on chromium promoted raney nickel catalysts. III. The influence of the nature of the solvent, Appl Catal A Gen., 161, 191 – 197.

299. Aramendia, M.A., Borau, V., Gomez, J.F., Herrera, A., Jimenez, C., Marinas, J.M., (1993). Reduction of acetophenone over Pd/AlPO4 catalysts. Linear free energy relationship (LFER), J Catal., 140, 335 – 343.

300. Carey, F.A., Sundberg, R.J., (2007). Advanced organic chemistry Part A: Structure and mechanisms, advanced organic chemistry, 1171.

301. Bertero, N.M., Trasarti, A.F., Apesteguia, C.R., Marchi, A.J., (2011). General solvent effect in the liquid phase hydrogenation of acetophenone over Ni/SiO_2: a comprehensive study of the phenomenon, Appl Catal A Gen., 394, 228 – 238.

302. Wan, H., Chaudhari, R.V., Subramaniam, B., (2013). Aqueous phase hydrogenation of acetic acid and its promotional effect on p-cresol hydrodeoxygenation, Energy Fuels., 27, 487 – 493.

303. Oyebanji, J.A., Okekunle, P.O., Lasode, O.A., Oyedepo, S.O., (2018). Chemical composition of bio-oils produced by fast pyrolysis of two energy biomass, Biofuels., 9, 479 – 487.

304. Oasmaa, A., Sipilä, K., Solantausta, Y., Kuoppala, E., (2005). Quality improvement of pyrolysis liquid: Effect of light volatiles on the stability of pyrolysis liquids, Energy Fuels., 19, 2556 – 2561.

305. Zhang, Z., Wang, Q., Tripathi, P., Pittman, C.U., (2011). Catalytic upgrading of bio-oil using 1-octene, and 1-butanol over sulfonic acid resin catalysts, Green Chem., 13, 940 – 949.

BET PLOTS AND SAMPLE CALCULATION
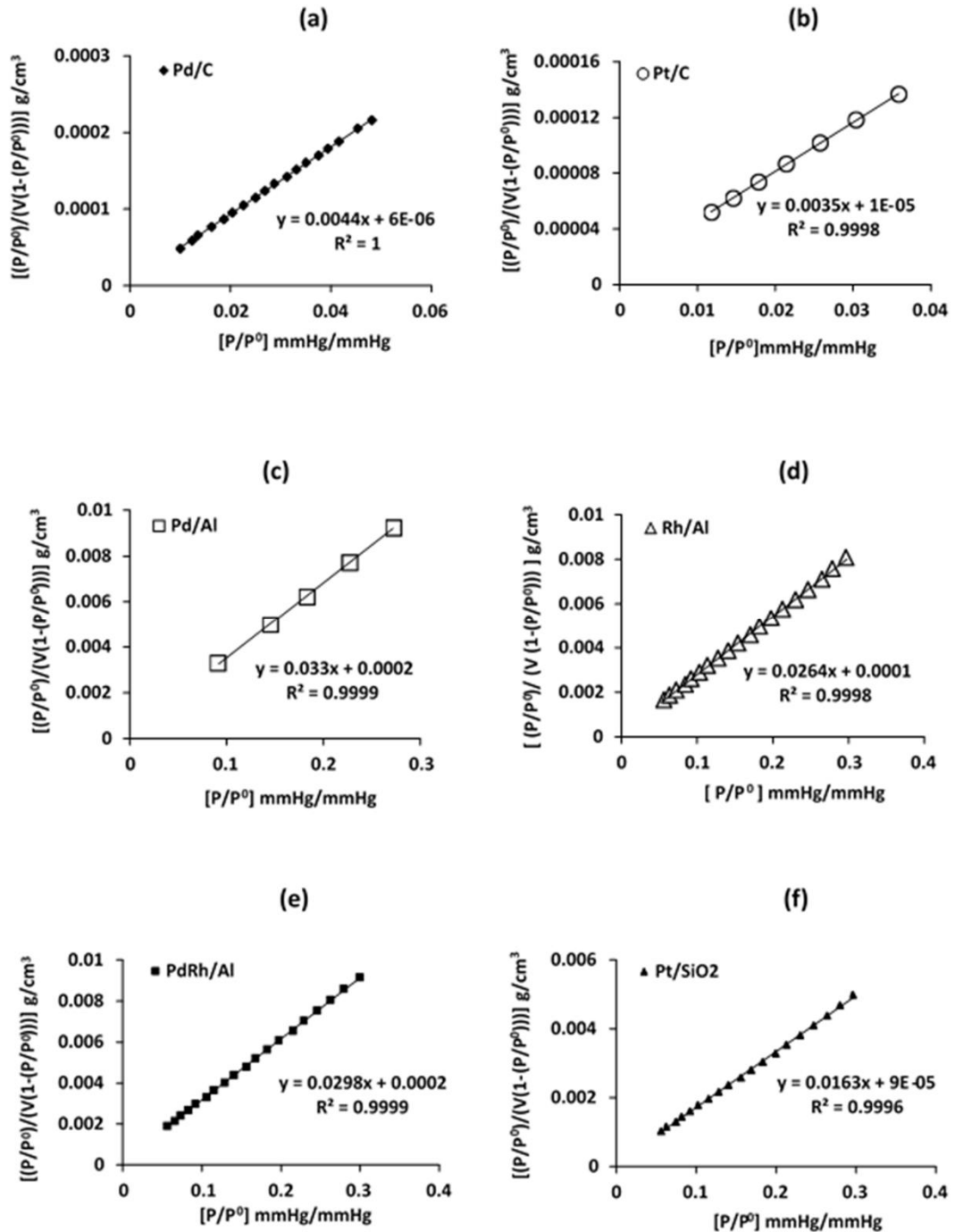
Fig. A3.1. BET Plot for (a) Pd/C catalyst, (b) Pt/C catalyst, (c) Pd/Al$_2$O$_3$ catalyst, (d) Rh/Al$_2$O$_3$ catalyst, (e) PdRh/Al$_2$O$_3$ catalyst, and (f) Pt/SiO$_2$ catalyst.

A3.1. SAMPLE CALCULATION OF SPECIFIC SURFACE AREA, AVERAGE PORE SIZE, AND PORE VOLUME FROM BET PLOT.

Using the BET Plot for Pd/C catalyst, the following approach illustrates the technique used to obtain the specific surface area (S_{BET}), average pore size (d_{AVG}), and the total specific pore volume (V) from the different plots presented in Figure A3.1. From Figure A3.1a, the slope of the line (s) representing BET plot of Pd/C catalyst is 0.0044 and the intercept (i) is 6×10^{-6}. As explained in Section 3.4, i is related to the monolayer volume (V_m) and BET constant (C) through equation 3.7 and s relates to both V_m and C through equation 3.6.

$$s = \frac{(C-1)}{V_m C} \qquad\qquad (3.6)$$

$$i = \frac{1}{V_m C} \qquad\qquad (3.7)$$

It follows that V_m can be calculated from equation 3.8 and C from equation 3.9.

$$V_m = \frac{1}{s+i} \qquad\qquad (3.8)$$

$$C = \frac{s}{i} + 1 \qquad\qquad (3.9)$$

Substituting the value of 0.0044 for s and 6×10^{-6} for i in equation 3.8 and 3.9 yield corresponding values of 227 cm³/g for V_m and 734 for C. Consequently, substituting values of 227 cm³/g for V_m, 6.022×10^{23} molecules/mol for n_a, 0.162 nm² for a_m and 0.0224 m³/mol for m_V in equation 3.10 lead to a S_{BET} value of 989 m²/g for Pd/C catalyst.

$$S_{BET} = \frac{V_m n_a a_m}{m_V} \qquad\qquad (3.10)$$

From equation 3.11, substituting 34.6×10^{-6} m³/mol for V_N and 430.7 cm³/g for V_{gas} yield a value of 0.659 cm³/g as the total specific pore volume of Pd/C catalyst.

$$V = V_{liq} = \frac{V_{gas} \times V_N}{m_V} \qquad\qquad (3.11)$$

The average pore size (d_{AVG}) was estimated from equation 3.12 to be 2.67 nm by substituting 0.659×10^{-6} m^3/g for V and 989 m^2/g for S_{BET} in equation 3.12.

$$d_{AVG} = \frac{4V}{S_{BET}}$$ (3.12)

CALIBRATION CURVES

Fig. A3.2. Calibration Curves for (a) Vanillin, (b) Vanillyl Alcohol, (c) Creosol, and (d) Guaiacol.

SCANNING ELECTRON MICROSCOPY (SEM)-ENERGY DISPERSIVE X-RAY (EDX) ANALYSIS.
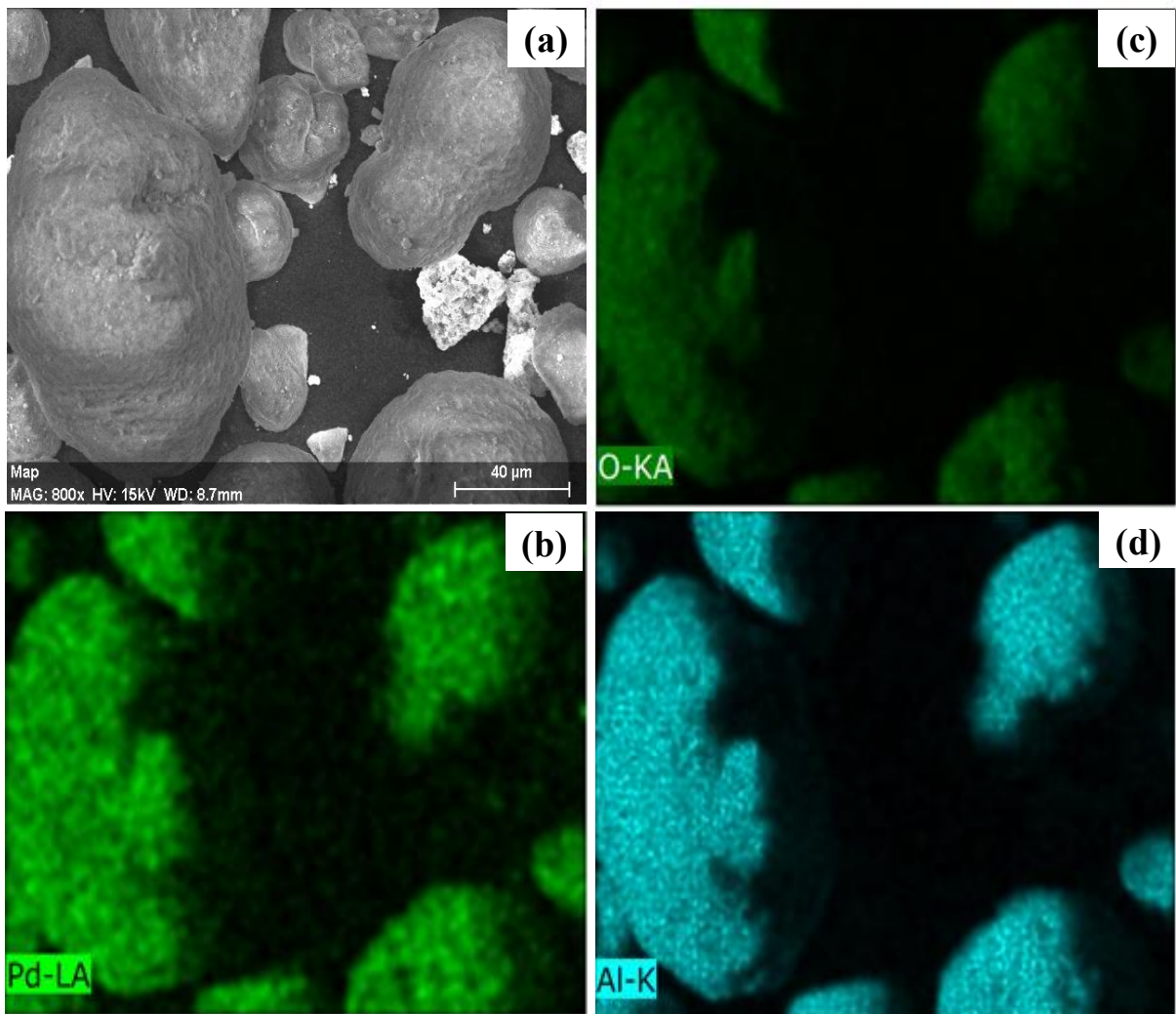
Fig. A4.1. SEM image and elemental mapping of Fresh 5 wt % Pd/Al$_2$O$_3$ catalyst [(a) SEM micrograph, (b) Pd mapping, (c) O mapping, and (d) Al mapping].
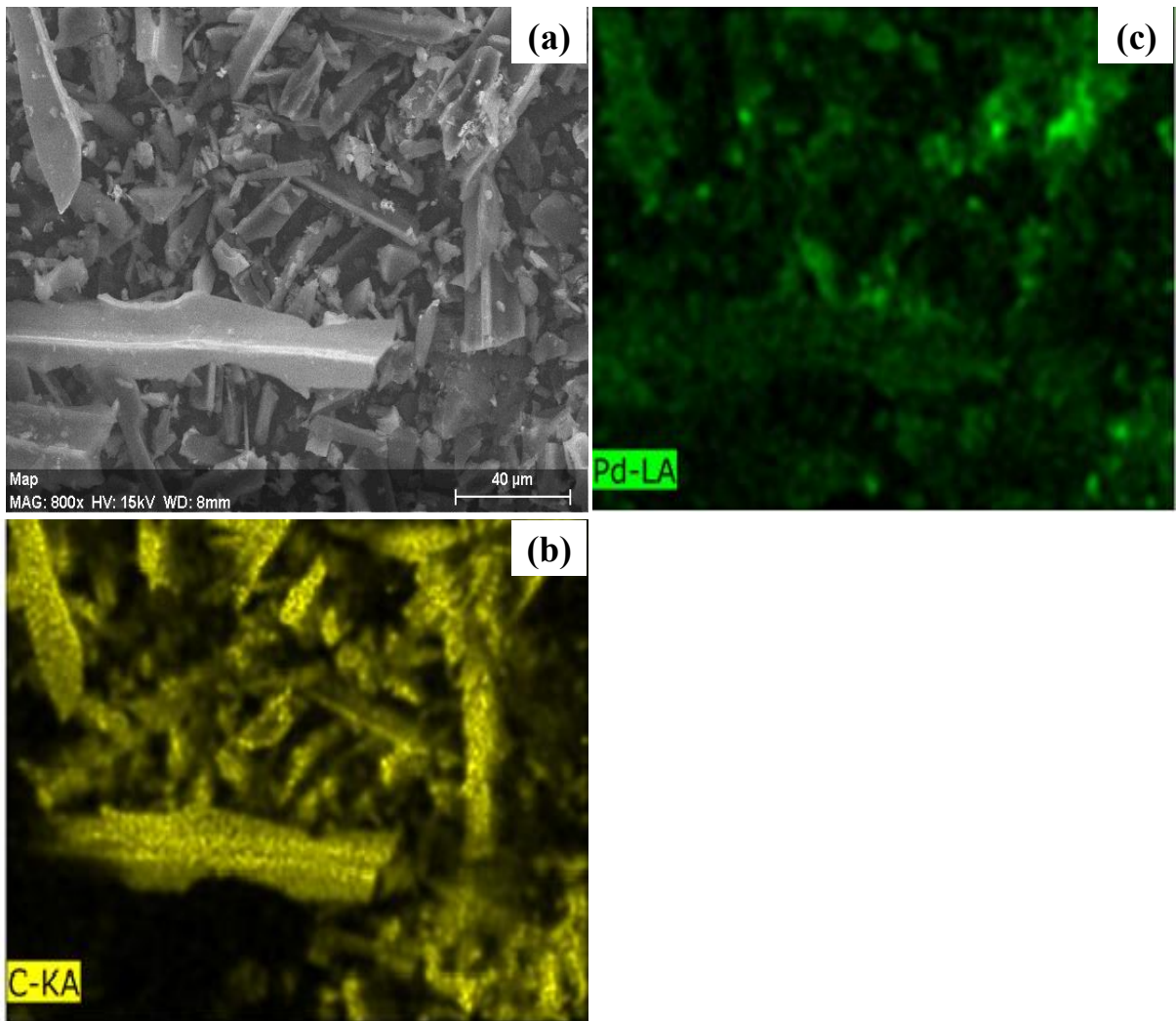
Fig. A4.2. SEM image and elemental mapping of Fresh 5 wt % Pd/C catalyst [(a) SEM micrograph, (b) C mapping, and (c) Pd mapping].
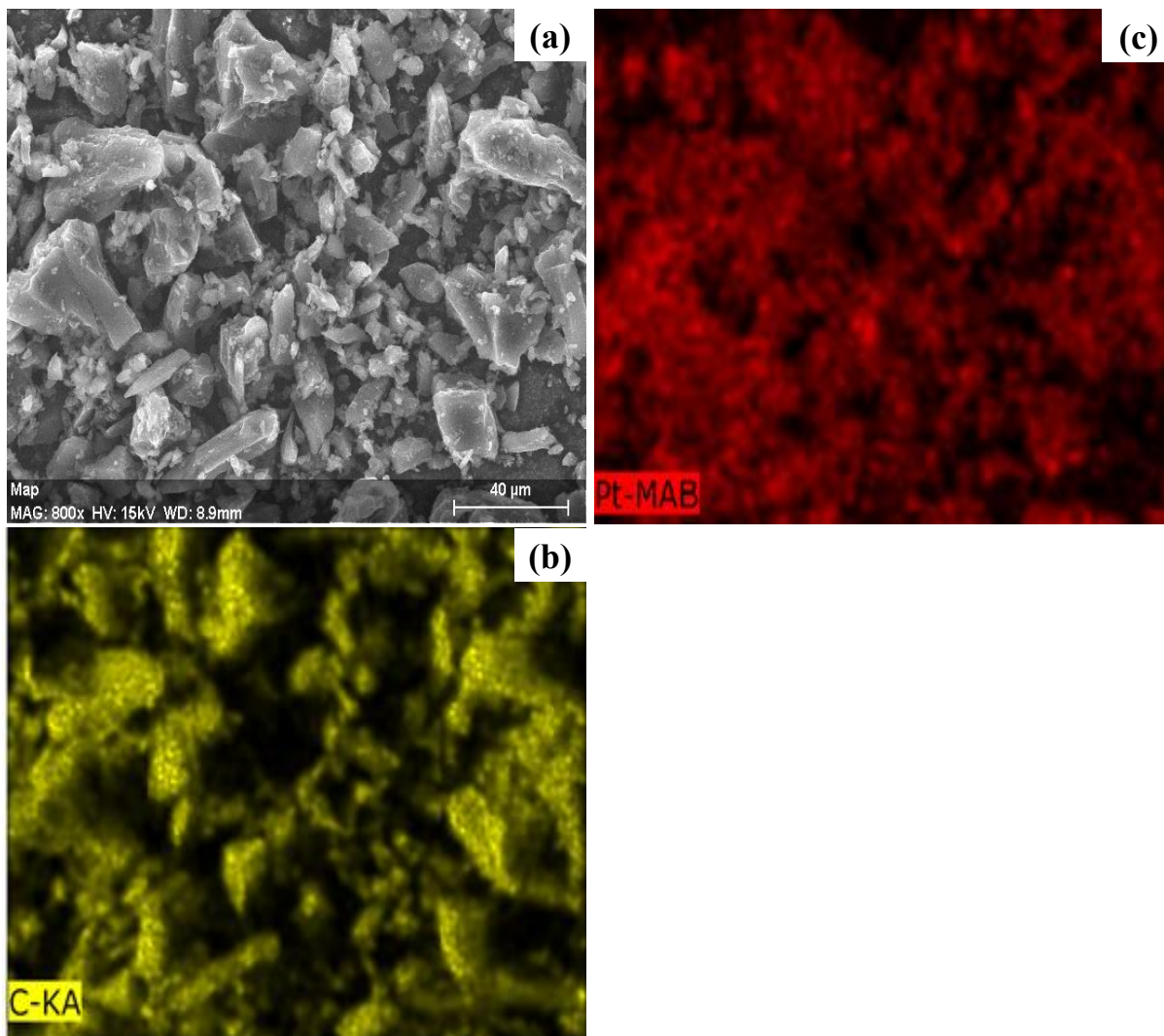
Fig. A4.3. SEM image and elemental mapping of Fresh 5 wt % Pt/C catalyst [(a) SEM micrograph, (b) C mapping, and (c) Pt mapping].
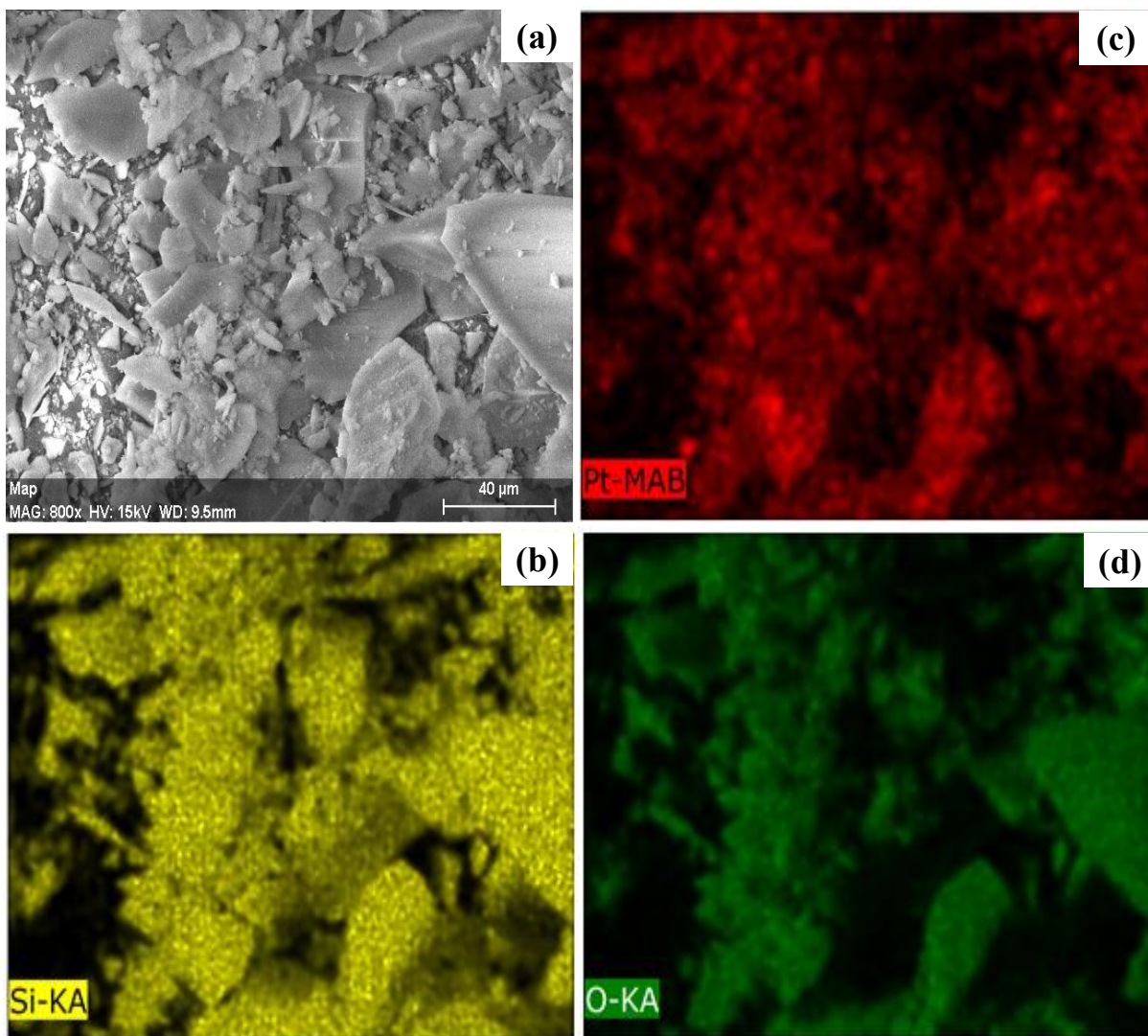
Fig. A4.4. SEM image and elemental mapping of Fresh 5 wt % Pt/SiO$_2$ catalyst [(a) SEM micrograph, (b) Si mapping, (c) Pt mapping, and (d) O mapping].

Table A4.1. Summary of degree of deoxygenation, signal to noise ratio and square of deviations.

Run	T(K)	P(bar)	CL(kg/m³)	Agitation Speed(RPM)	DOD	S/N	(n-m)²
1	318	10	0.5	500	14.77793856	23.3922771	7.56884585
2	318	20	0.3	700	7.528932051	17.5346676	9.65006907
3	318	30	0.1	900	6.548225742	16.3224729	18.6507441
4	328	10	0.3	900	8.282689367	18.3634275	5.18789955
5	328	20	0.1	500	5.759798993	15.2081466	29.5172394
6	328	30	0.5	700	19.64801363	25.866373	27.3032316
7	338	10	0.1	700	8.121297774	18.1925087	5.99571489
8	338	20	0.5	900	22.37536166	26.9954013	40.376845
9	338	30	0.3	500	15.65820177	23.8948377	10.5866556
						Total	154.837245

Note: T is the reaction temperature, P is the hydrogen gas pressure, CL is the catalyst loading measured as weight of catalyst in kg per unit volume of solvent in m^3, DOD is the degree of deoxygenation, S/N is the signal to noise ratio and $(n-m)^2$ is square of the difference between individual (n) and mean (m) signal to noise ratio.

The mean signal to noise ratio (m) was calculated as follows:

$$m = \frac{(23.3922771+17.5346676+\cdots+23.8948377)}{9} = 20.6411$$

The total sum of squares deviation (SS_T) was computed using equation A4.1.

$$SS_T = \sum_{i=1}^{9}(n - m)^2 \tag{A4.1}$$

Calculation of Average S/N ratios per level for parameters e.g. temperature at Level 1:

$$m_{T1} = \frac{(23.3922771+17.5346676+16.3224729)}{3} = 19.0831$$

Calculation of the standard deviation of S/N ratios per level for parameters e.g. temperature at

Level 1:

SD_{T1}

$$= \sqrt{\frac{(23.3923 - 19.0831)^2 + (17.5247 - 19.0831)^2 + (23.3923 - 19.0831)^2}{3}}$$

$$= 3.7807$$

Table A4.2: Summary of the average and standard deviations of S/N ratios per level for all the parameters.

Levels	Temperature		Pressure		Catalyst loading		Agitation Speed	
	m_{ij}	SD_{ij}	m_{ij}	SD_{ij}	m_{ij}	SD_{ij}	m_{ij}	SD_{ij}
1	19.08	3.78	19.98	2.95	25.42	1.84	20.83	4.88
2	19.81	5.47	19.91	6.24	19.93	3.46	20.53	4.63
3	23.03	4.47	22.03	5.03	16.57	1.51	20.56	5.67

Note: m_{ij} represents average of signal to noise ratio for specific parameter i at level j, and SDij represents standard deviation of signal to noise ratio for specific parameter i at level j.

Calculation of sum of square deviations and mean variance for specific parameter e.g. Temperature is as follows:

$(SS)_{Temp} = 3(19.08 - 20.64)^2 + 3(19.81 - 20.64)^2 + 3(23.03 - 20.64)^2 = 26.4$

Degree of freedom = n -1 = 3 – 1 = 2

Mean variance $= \frac{(SS)_{Temp}}{2} = 13.2$

The percentage contribution (P %) of the parameters e.g. Temperature is as follows:

$P\% = \frac{13.2}{77.4} \times 100 = 17.1\%$

$(SS)_{Error} = (SS)_{Temp} + (SS)_{Press} + (SS)_{Catalyst} + (SS)_{Agitation} - SS_T = 0$

APPENDIX A5.1.

ZWIETERING CORRELATION AND REACTOR DATA.

The Zwietering Correlation used to estimate the minimum agitation speed is represented below in equation A5.1.

$$N_{js} = s' \cdot \frac{\nu^{0.1} \, d_p^{0.5} \left(\frac{g\Delta\rho}{\rho_L}\right)^{0.45} X^{0.13}}{D^{0.85}} \qquad (A5.1)$$

Herein, N_{js} represent just suspended agitation speed, d_p denotes characteristic length of the particle, ν represent the kinematic viscosity of the solvent, g represent acceleration due to gravity, $\Delta\rho$ denotes difference between the catalyst and solvent densities, ρ_L represent the solvent density, X denotes the solid loading, D represent diameter of the stirrer, and s' is the system configuration constant calculated from equation A5.2.

$$s' = 2\left(\frac{D_I}{D}\right)^{1.33} \qquad (A5.2)$$

Where D_I is the internal diameter of the reactor. The reactor data include 3.30 cm for D_I and 2.06 cm for D. While the solvent density is 0.902 g/ml and kinematic viscosity is 0.00428 cm^2/s.

CALCULATION OF INITIAL REACTION RATE FROM CONVERSION-TIME PLOT.

Figure A5.2 represent the conversion-time plot obtained from vanillin HDO reaction over the prepared bimetallic PdRh/Al$_2$O$_3$ catalyst with the agitation speed fixed at 900 rpm. As shown in Figure A5.2, a third order polynomial with R^2 value of 0.999 reliably fit the experimental conversion-time data. Consequently, the third order polynomial expression was differentiated with respect to time to determine suitable expression for the rate at which vanillin is converted. The initial reaction rate was then estimated from the derived vanillin conversion rate expression by substituting t = 0.

The equation shown on the plot: $y = 0.002x^3 - 0.244x^2 + 8.615x + 0.510$, $R^2 = 0.999$
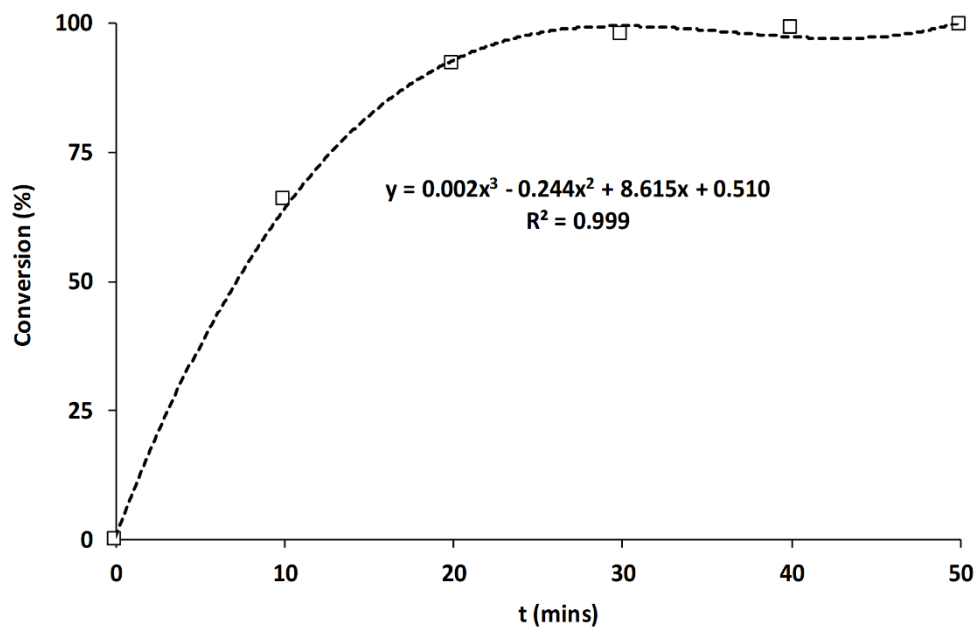
Fig. A5.2. Conversion-Time plot at T = 318 K, P$_H$ = 2.0 MPa, ω = 3.4 kg/m^3, agitation speed = 900rpm, and C$_{VL, 0}$ = 263.0 mM.

SAMPLE CALCULATION OF INITIAL TURN OVER FREQUENCY.

The initial turn over frequency (TOF) was estimated from equation A5.3. It requires information about the metal dispersion (D), initial reaction rate (r_0), and the molecular weight of the metal (M_{metal}). For the monometallic catalysts, the molecular weight of Pd which is 106.42 kg/kmol was used, while average molecular weight of 102.11 kg/kmol was used for the bimetallic catalyst.

$$TOF = \left(\frac{r_0 M_{metal}}{D}\right) \qquad (A5.3)$$

For instance, substituting values of 0.281 for D, 106.42 kg/kmol for M_{metal}, and 304.4 kmol/kg min for r_0 produces the maximum initial TOF of 12 per min under Pd/C catalyst.

RATE EXPRESSIONS DERIVATION AND TEST.

Competitive dissociative chemisorbed H_2 and VL Derivation (Model I)

$$VL + S_1 \leftrightarrow VL\ S_1 \tag{1}$$

$$H_2 + 2S_1 \leftrightarrow 2HS_1 \tag{2}$$

$$VLS_1 + 2HS_1 \rightarrow P \tag{3}$$

Let r_i denote the overall reaction rate for step i where i = 1…3.

Assuming the adsorption steps occurred rapidly so that step 3 is the rate determining step (RDS) and only irreversible step in the mechanism.

From equation 1:
$$k_1 C_{VL}\theta_V - k_{-1}\theta_{VL} = 0 \tag{4}$$

$$\leftrightarrow\ \theta_{VL} = K_{VL}C_{VL}\theta_V \tag{5}$$

From equation 2:
$$k_2 C_H \theta_V^2 - k_{-2}\theta_H^2 = 0 \tag{6}$$

$$\leftrightarrow\ \theta_H = \sqrt{K_H C_H}\ \theta_V \tag{7}$$

From equation 3:
$$r_S = K_S\theta_{VL}\theta_H^2 \tag{8}$$

Site Balance:
$$\theta_V + \theta_{VL} + \theta_H = 1 \tag{9}$$

Replacing Θ_{VL} by the expression in equation 5 and Θ_H by the expression in equation 7 gives:

$$\theta_V = \frac{1}{1 + K_{VL}C_{VL} + \sqrt{K_H C_H}} \tag{10}$$

Substitute eq. 10 into eq.7 to get:

$$\theta_H = \frac{\sqrt{K_H\ C_H}}{1 + K_{VL}C_{VL} + \sqrt{K_H C_H}} \tag{11}$$

Substitute eq. 11 and eq. 5 into eq.8 to get:

$$r_S = \frac{K_S K_H K_{VL}\ C_{VL}C_H}{\left[1 + K_{VL}C_{VL} + \sqrt{K_H C_H}\ \right]^3} \tag{12}$$

Non-Competitive dissociative chemisorbed H_2 and VL Derivation (Model II)

$$VL + S_1 \leftrightarrow VL\,S_1 \tag{13}$$

$$H_2 + 2S_2 \leftrightarrow 2HS_2 \tag{14}$$

$$VLS_1 + 2HS_2 \rightarrow P \tag{15}$$

Assuming the RDS is again step 3 and the only irreversible step in the mechanism.

From equation 13: $\quad k_1 C_{VL}\theta_v - k_{-1}\theta_{VL} = 0 \tag{16}$

$$\leftrightarrow \quad \theta_{VL} = K_{VL}C_{VL}\theta_{V1} \tag{17}$$

From equation 14: $\quad k_2 C_H \theta_V{}^2 - k_{-2}\theta_H{}^2 = 0 \tag{18}$

$$\leftrightarrow \quad \theta_H = \sqrt{K_H C_H}\,\theta_V \tag{19}$$

From equation 15: $\quad r_S = K_S \theta_{VL}\theta_H{}^2 \tag{20}$

Site 1 Balance: $\qquad \theta_{V1} + \theta_{VL} = 1 \tag{21}$

Site 2 Balance: $\qquad \theta_{V2} + \theta_H = 1 \tag{22}$

Substitute eq. 17 into eq. 21 to get:

$$\theta_{V1} = \frac{1}{1+K_{VL}C_{VL}} \tag{23}$$

Substitute eq. 19 into eq. 22 to get:

$$\theta_H = \frac{1}{1+\sqrt{K_H C_H}} \tag{24}$$

Substitute eq. 23 into eq. 17 to get:

$$\theta_{VL} = \frac{K_{VL}C_{VL}}{1+K_{VL}C_{VL}} \tag{25}$$

Substitute eq. 25 and eq. 24 into eq. 20 to get:

$$r_S = \frac{K_S K_H K_{VL}\, C_{VL}C_H}{\left[1 + \sqrt{K_H C_H}\,\right]^2 [1 + K_{VL}C_{VL}]} \tag{26}$$

Competitive dissociative chemisorbed H_2 and VL (Hydrogen adsorption as RDS) Derivation
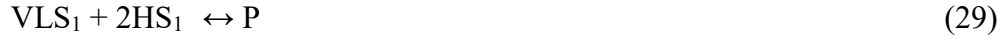
$$VL + S_1 \leftrightarrow VL\ S_1 \tag{27}$$

$$H_2 + 2S_1 \rightarrow 2HS_1 \tag{28}$$

$$VLS_1 + 2HS_1 \leftrightarrow P \tag{29}$$

Assuming step 2 is the rate determining step (RDS) and only irreversible step in the mechanism.

From equation 27: $\quad k_1 C_{VL}\theta_v - k_{-1}\theta_{VL} = 0 \tag{30}$

$$\theta_{VL} = K_{VL}C_{VL}\theta_V \tag{31}$$

From equation 28: $\quad r_H = k_H C_H \theta_V{}^2 \tag{32}$

From equation 29: $\quad k_3\theta_H{}^2\theta_{VL} - k_{-3}C_p = 0 \tag{33}$

$$\theta_H{}^2 = \frac{C_p}{k_s\theta_{VL}} \tag{34}$$

Site Balance: $\quad\quad\quad \theta_V + \theta_{VL} + \theta_H = 1 \tag{35}$

$$\theta_V = \frac{\left[1 - \frac{C_p}{(k_s\theta_{VL})^2}\right]}{1 + k_{VL}C_{VL}} \tag{36}$$

Assuming $(K_s\theta_{VL})^2 >>>> C_p$ then

$$\theta_V = \frac{1}{1 + k_{VL}C_{VL}} \tag{37}$$

$$\theta_V{}^2 = \frac{1}{(1 + k_{VL}C_{VL})^2} \tag{38}$$

Substituting eq. 38 into eq. 32 lead to:

$$r_H = \frac{k_H C_H}{[1 + k_{VL}C_{VL}]^2} \tag{39}$$

Competitive dissociative chemisorbed H_2 and VL (VL adsorption as RDS) Derivation

$$VL + S_1 \rightarrow VL\ S_1 \tag{40}$$

$$H_2 + 2S_1 \leftrightarrow 2HS_1 \tag{41}$$

$$VLS_1 + 2HS_1 \leftrightarrow P \tag{42}$$

Assuming step 1 is the rate determining step (RDS) and only irreversible step in the mechanism.

From equation 40: $\quad r_{VL} = k_{VL} C_{VL} \theta_V$ $\hspace{3cm}$ (43)

From equation 41: $\quad \theta_H = \sqrt{k_H C_H} \theta_V$ $\hspace{3cm}$ (44)

From equation 42: $\quad k_3 \theta_H{}^2 \theta_{VL} - k_{-3} C_p = 0$ $\hspace{2cm}$ (45)

$$\theta_{VL} = \frac{C_p}{k_s k_H C_H \theta_V{}^2}$$ $\hspace{5cm}$ (46)

Site Balance: $\hspace{2cm} \theta_V + \theta_{VL} + \theta_H = 1$ $\hspace{2.5cm}$ (47)

$$\theta_V = \frac{1 - \dfrac{C_p}{k_s k_H C_H \theta_V{}^2}}{1 + \sqrt{k_H C_H}}$$ $\hspace{4cm}$ (48)

Assuming $k_s k_H C_H \theta_V{}^2 >>>> C_p$ then

$$\theta_V = \frac{1}{1 + \sqrt{k_H C_H}}$$ $\hspace{5cm}$ (49)

Substitute eq. 49 into eq. 43 to get:

$$r_{VL} = \frac{k_{VL} C_{VL}}{1 + \sqrt{k_H C_H}}$$ $\hspace{5cm}$ (50)

Non - Competitive dissociative chemisorbed H_2 and VL (VL adsorption as RDS) Derivation

$VL + S_1 \rightarrow VL\ S_1$ $\hspace{6cm}$ (51)

$H_2 + 2S_1 \leftrightarrow 2HS_1$ $\hspace{6cm}$ (52)

$VLS_1 + 2HS_1 \leftrightarrow P$ $\hspace{6cm}$ (53)

Assuming step 1 is the rate determining step (RDS) and only irreversible step in the mechanism.

From equation 51: $\quad r_{VL} = k_{VL} C_{VL} \theta_{V1}$ $\hspace{3cm}$ (54)

From equation 52: $\quad k_2 C_H \theta_{V2}{}^2 - k_{-2} \theta_H{}^2 = 0$ $\hspace{2cm}$ (55)

$\theta_H = \sqrt{k_H C_H} \theta_{V2}$ $\hspace{5cm}$ (56)

From equation 53: $\quad \theta_{VL} = \dfrac{C_p}{k_s \theta_H{}^2}$ $\hspace{3cm}$ (57)

Site 1 balance: $\qquad \theta_{V1} + \theta_{VL} = 1$ (58)

$$\theta_{V1} = 1 - \frac{C_p}{k_s \theta_H{}^2}$$ (60)

Assuming $(K_s \theta_H{}^2) >>>> C_p$ then $\theta_{V1} \sim 1$, therefore eq. 54 reduces to:

$$r_{VL} = k_{VL} C_{VL}$$ (61)

Non-Competitive dissociative chemisorbed H_2 and VL (Hydrogen adsorption as RDS) Derivation

$VL + S_1 \leftrightarrow VL\ S_1$ (62)

$H_2 + 2S_1 \rightarrow 2HS_1$ (63)

$VLS_1 + 2HS_1 \leftrightarrow P$ (64)

Assuming step 2 is the rate determining step (RDS) and only irreversible step in the mechanism.

From equation 62: $\qquad \theta_{VL} = k_{VL} C_{VL} \theta_{V1}$ (65)

From equation 63: $\qquad r_H = k_H C_H \theta_{V2}{}^2$ (66)

From equation 64: $\qquad \theta_H = \dfrac{C_p^{\frac{1}{2}}}{\sqrt{k_s \theta_{VL}}}$ (67)

Site balance 1: $\qquad \theta_{V1} + \theta_{VL} = 1$ (68)

$$\theta_{V1} = \frac{1}{1 + k_{VL} C_{VL}}$$ (69)

Site balance 2: $\qquad \theta_{V2} + \theta_H = 1$ (70)

$$\theta_{V2} = 1 - \frac{C_p^{\frac{1}{2}}}{\sqrt{k_s \theta_{VL}}}$$ (71)

Assuming $(k_s \theta_{VL})^{1/2} >>>> C_p^{1/2}$ then $\theta_{V2} \sim 1$, therefore eq. 66 reduces to:

$$r_H = k_H C_H$$ (72)
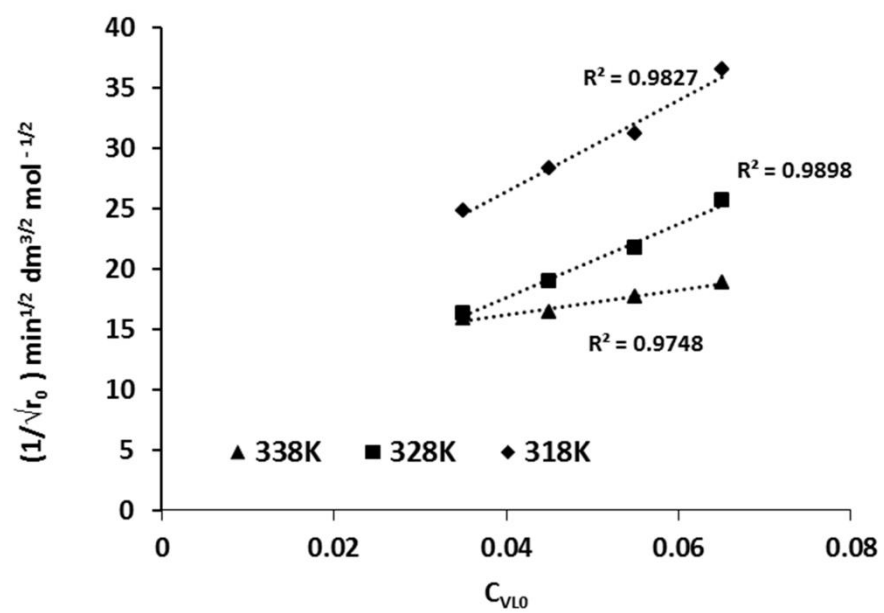
Fig. A5.3. Plot of $1/\sqrt{r_0}$ against C_{VL0} at 318 K, 328 K and 338 K.

APPENDIX A6.1.

BINARY ENVIRONMENT RATE EXPRESSION DERIVATION.

Competitive dissociative chemisorbed H_2 , VL, and M Derivation

$$VL + S \leftrightarrow VL\ S \quad \text{(fast)} \tag{73}$$

$$M + S \leftrightarrow AA\ S \quad \text{(fast)} \tag{74}$$

$$H_2 + 2S \leftrightarrow 2HS \quad \text{(fast)} \tag{75}$$

$$2HS + VLS \rightarrow P \quad \text{(slow)} \tag{76}$$

Let r_i denote the overall reaction rate for step i where $i = 1\ldots4$.

Assuming the adsorption steps occurred rapidly so that step 4 is the rate determining step (RDS) and only irreversible step in the mechanism.

From equation 73: $\quad k_1 C_{VL}\theta_v - k_{-1}\theta_{VL} = 0 \tag{77}$

$$\leftrightarrow \quad \theta_{VL} = K_{VL}C_{VL}\theta_V \tag{78}$$

From equation 74: $\quad k_2 C_M\theta_v - k_{-2}\theta_M = 0 \tag{79}$

$$\leftrightarrow \quad \theta_M = K_M C_M\theta_V \tag{80}$$

From equation 75: $\quad k_3 C_H\theta_V{}^2 - k_{-3}\theta_H{}^2 = 0 \tag{81}$

$$\leftrightarrow \quad \theta_H = \sqrt{K_H C_H}\ \theta_V \tag{82}$$

From equation 76: $\quad r_s = K_S\theta_{VL}\theta_H{}^2 \tag{83}$

Site Balance: $\qquad \theta_V + \theta_{VL} + \theta_H + \theta_M = 1 \tag{84}$

Replacing Θ_{VL} by the expression in equation 78, Θ_H by the expression in equation 82, and Θ_M by the expression in equation 80 gives:

$$\theta_V = \frac{1}{1 + K_{VL}C_{VL} + \sqrt{K_H C_H} + K_M C_M} \tag{85}$$

Substitute eq. 85 into eq.82 to get:

$$\theta_H = \frac{\sqrt{K_H\,C_H}}{1 + K_{VL}C_{VL} + \sqrt{K_H C_H} + K_M C_M} \tag{86}$$

Substitute eq. 86 and eq. 78 into eq.83 to get:

$$r_S = \frac{K_S K_H K_{VL}\,C_{VL}C_H}{\left[1 + K_{VL}C_{VL} + \sqrt{K_H C_H} + K_M C_M\,\right]^3} \tag{87}$$